Versuchsanstalt für Wasserbau,
Hydrologie und Glaziologie
der Eidgenössischen
Technischen Hochschule Zürich

Mitteilungen 105

Weakly nonlinear unidirectional shallow water waves generated by a moving boundary

Johannes Sander

Zürich, 1990

Herausgeber: Prof. Dr. D. Vischer

Vorwort

An unserer Versuchsanstalt läuft seit längerer Zeit ein Forschungsprogramm zur Erfassung der Folgen von Uferinstabilitäten in Seen und Stauseen. Letztlich geht es darum, die Wellen zu bestimmen, die von Lawinen, Gletscherabbrüchen, Murgängen, Bergstürzen und Hangrutschen erzeugt werden und die am Gegenufer auflaufen oder allenfalls über die Talsperre schwappen. Solche Wellen haben schon an verschiedenen Orten, so auch an mehreren Schweizer Seeufern, zu Verheerungen geführt.

Die Problematik lässt sich in drei Fragen aufgliedern: Wie wird die Sturzenergie der Ufer in Wellenenergie umgewandelt? Wie breiten sich die Wellen aus? Wie weit laufen sie an den betroffenen Ufern auf, oder wie stark schlagen sie über ein Hindernis? Dabei ist zu vermerken, dass diese Wellen eine enge Verwandtschaft zu den berüchtigten, erbebenbedingten Tsunamis auf den Meeren haben.

In der vorliegenden Schrift widmet sich Dr. Johannes Sander der Frage der Wellenerzeugung und der Wellenausbreitung bei verhältnismässig langsamen Uferbewegungen. Im Sinne einer Abstraktion approximiert er dabei den See durch einen rechteckigen Kanal und behandelt in seinen Experimenten und Rechnungen die darin entstehenden und hin- und herlaufenden solitären Kanalwellen.

Wir hoffen mit dieser Arbeit einen willkommenen Beitrag zur erwähnten Problematik zu leisten. Das entsprechende Forschungsprojekt wurde in erste Linie von Professor Dr. Kolumban Hutter, Technische Hochschule Darmstadt, betreut, dem wir hiermit für seinen unermüdlichen Einsatz danken. Wir erwähnen hier auch gerne die fruchtbare Zusammenarbeit mit Professor Dr. Stuart Savage und seinem Masterstudenten Marc Villeneuve von der McGill Universität Montreal, Kanada.

Professor Dr. Daniel Vischer

Contents

Zusammenfassung

Die historische Entwicklung der Theorie einer kanalisierten Welle wird ausgiebig dargestellt. Ausgangspunkte sind die experimentellen Untersuchungen von Russell und die mathematischen Betrachtungen von Gerstner und Airy. Die Entwicklung der mathematischen Theorien von Wellen in flachen Gewässern wird vom Beginn des 19. Jahrhunderts an verfolgt. Die wichtigsten Aufsätze sind dargestellt und erläutert. Die Hauptergebnisse sind für das Folgende die Grundlage. Es wird eine Übersicht über hydraulische und numerische Untersuchungen zu Wellen, die durch Lawinen entstehen, gegeben. Dieser Teil endet mit den Gleichungen von Wu und Villeneuve & Savage. Ihre Gleichungen sind vom Boussinesq Typ wobei sie Bewegungen des Kanalbodens mit einbeziehen. Insofern stellen sie das vollständigste, bekannte Flachwassermodell dar. Das dazugehörige numerische Lösungsverfahren von Villeneuve wird mit eigenen Experimenten getestet. Die Rechnungen stehen dabei in gutem Einklang mit den experimentellen Resultaten. Zusätzlich werden die Anwendungsgrenzen des numerischen Modells dargestellt.

Einige neue Ergebnisse zu Wellen, die durch verschiedene Geometrien des Wellengenerators erzeugt wurden, werden aus einer Methode zur Lösung der Korteweg-de Vries Gleichung erzielt. Es wird gezeigt, dass im Falle eines keilförmigen Erregungsmechanismus eine typische maximale Wellenlänge und eine typische maximale Wellenamplitude von der Froudezahl, die aus der Geschwindigkeit des Wellengenerators berechnet wird, abhängen. Dies führt zu einem Zusammenhang zwischen der Anzahl von Solitonen in die sich die Welle aufspaltet, oder einer speziell zu wählenden Ursellzahl, und einer modifizierten Froudezahl. Alle diese typischen Grössen sind dabei von der Neigung des Keils unabhängig.

Im letzten Teil werden Wellen betrachtet, die durch poröse Körper erzeugt wurden. Ein neues mathematische Modell, das auf den Flachwasserapproximationen basiert, wurde entwickelt und mit den experimentellen Resultaten verglichen. Dabei wurde eine gute Übereinstimmung festgestellt.

Summary

This thesis provides the reader with a historical review of the evolution of the mathematical theory of channelized waves. The starting points are the experimental observations of Russell and the mathematical theories of Gerstner and Airy. The evolution of the mathematical theory of waves in shallow water is presented from the beginning in the 19th century to present. The main results of these theories are needed to follow the more specific subject of waves which are generated by landslides. A state of the art leads to a review of hydraulic and numerical investigations dealing with landslide induced waves. This section will be closed with a set of equations obtained by Wu and later by Villeneuve & Savage. Their equations are of the Boussinesq type and include spatial and temporal variations of the channel bottom. Therefore it is the most complete model of motions in shallow water. The inferences deduced from the numerical model of Villeneuve will be compared with own experimental results. The model is found to be able to satisfactorily reproduce the experiments. Limitations of the validity of the numerical computations are equally given.

Some new results of waves obtained by several different generation mechanisms are obtained with the aid of the solution technique of the Korteweg-de Vries equation. It is shown that for a wedge type piston generator a typical maximum wavelength and a typical maximum waveheight are related to the piston Froude number. Moreover, this suggests a relation between the number of solitons (a special Ursell number) into which the wave will disperse with a modified piston-Froude number. All these characteristic numbers are independent of the angle of inclination of the wedge that was used as wave generator.

The last part describes waves which are generated by a porous body. A new mathematical model based on the shallow water assumption is developed. Comparisons with experiments show, that the model is able to reproduce the transfer of momentum from a moving porous body into the surrounding water with fair to sufficient accuracy.

Résumé

Le développement historique de la théorie des ondes dans les canaux est rappelé. Les recherches expérimentales de Russell et les considérations mathématiques de Gerstner et Airy en sont à l'origine. L'élaboration des théories mathématiques concernant les ondes en eau peu profonde a été recherchée rétrospectivement jusqu'au début du 19ème siècle. Les contributions les plus importantes à ce sujet sont décrites et discutées. Les principaux résultats obtenus constituent la base du présent travail. Un aperçu des investigations hydrauliques et numériques traitant des ondes dues aux avalanches est donné. Les équations de Wu et de Villeneuve & Savage sont traitées à la fin de cette première partie. Ces équations, du type de celles de Boussinesq, prennent en compte les mouvements du fond du canal. De ce fait, elles décrivent le modèle le plus complet connu dans un milieu en eau peu profonde. Le procédé de résolution numérique y relatif dû à Villeneuve, a été testé à partir des essais réalisés dans le cadre de cette étudé. Une bonne concordance existe entre les résultats fournis par le calcul et par l'essai. De plus, les limites d'application du modèle numérique sont présentées.

Quelques résultats nouveaux, relatifs aux ondes engendrées par différentes géométries du générateur, ont été obtenus par l'application de l'équation de Korteweg-de Vries. On montre que, dans le cas d'un mécanisme générateur d'onde présentant une forme en coin, la longueur et l'amplitude maximales de l'onde dépendent du nombre de Froude rapporté à la vitesse du générateur. Ceci conduit à une relation entre le nombre d'ondes solitaires en lesquelles l'onde primitive se subdivise, ou un nombre d'Ursell particulier à choisir, et un nombre de Froude modifié. Tous ces paramètres typiques ne dépendent pas de l'inclinaison du coin.

Dans la dernière partie, des ondes engendrées par des corps poreux sont prises en considération. Un nouveau modèle mathématique, basé sur les approximations de la situation en eau peu profonde, a été développé. Les résultats qu'il fournit sont en bon accord avec les résultats expérimentaux.

List of Figures

List of Tables

Notations

As far as the notation is not explained inside the text, one should interprete symbols as follows

Chapter 1

c	Wave velocity
c_0	Velocity of the wave, linear theory
$\mathbf{e}_i$	Unit vector of coordinate i
g	Acceleration due to gravity
h	Undisturbed water depth
H	Height of elevation of cnoidal wave
k	Wave number
K	Depth of depression of cnoidal wave
p	Pressure
p_0	Atmospheric pressure
P	Non hydrostatic pressure
q	Volume of the wave elevation
Q	Total volume of the wave elevation
t	Time coordinate
T	Surface tension
u	Horizontal velocity of the water particles
u_0	Horizontal velocity of the water particles at the bottom of the channel
U	Mean horizontal velocity
v	Vertical velocity of the water particles
W_n	Weighting function
x	Horizontal coordinate
x^1, x^2	Coordinates in 1-direction and 2-direction
y	Vertical coordinate
ϵ	Expansion parameter
ζ	Vertical coordinate of trajectory
η	Wave elevation
η_{max}	Maximum wave amplitude
η_0	Constant, similar to maximum wave amplitude
ϑ	Limiting value for surface tension effects: $\vartheta \leq 0$ negative solitary waves are possible
κ	Maximum curvature of surface
λ	Wavelength
ξ	Horizontal coordinate of trajectory
ρ	Density
σ	Expansion parameter
ϕ	Velocity potential
ϕ_0	Velocity potential at the bottom of the channel
ψ	Streamfunction

Chapter 2

c	Wave velocity
c_0	Velocity of the wave, linear theory
d	Distance the wave generator is moved
Fr	Piston Froude number: $Fr = max\{v(t)\}/\sqrt{gh}$
Fr_c	Wave Froude number: $Fr = c/\sqrt{gh}$
g	Acceleration due to gravity
h	Undisturbed water depth
Re	Reynolds number
s	Final slope of rotating plate
t	Time coordinate
Ur	Ursell number
$\widetilde{Ur}$	Modified Ursell number: $Ur/(d/h)$
$v(t)$	Velocity of the wave generator: horizontal direction in cases of piston type generator; vertical direction in case of rotating plate
V	Displaced volume of the wave generator during motion
x	Horizontal coordinate
y	Vertical coordinate starting from the undisturbed free surface
α	Final angle of rotating plate $s = \tan\alpha$
η	Wave elevation
η_{max}	Maximum wave amplitude in one experiment
η_∞	Upper bound for wave amplitude in a set of experiments
λ	Wavelength
λ_{max}	Maximum wavelength in one experiment
λ_∞	Upper bound for wavelength in a set of experiments
μ	Kinematic viscosity
ρ	Density
$\dot{\varphi}$	Angular velocity of gear box

Chapter 3

$a(k;t)$	Transmission coefficient
$b(k;t)$	Reflexion coefficient
$c(t)$	Coefficient for the discrete eigenvalues
d	Distance the wave generator is moved
Fr	Piston Froude number
h	Undisturbed water depth
k	Positive eigenvalues of the discrete spectrum
K_n	Negative eigenvalues of the discrete spectrum
l_1, l_2	Wave length of the potentials q_1, q_2
N, N^o	Number of discrete eigenvalues, number of solitons
$q(x)$	Initial potential
q_1, q_2	Square well potentials
Q_1, Q_2	Maximum of q_1, q_2

Q_3	Minimum of q_2
t	Time coordinate
t_0	Time of initial condition
x	Horizontal coordinate
x_0	Coordinate of initial condition
η	Wave elevation
λ	Eigenvalue of the wave function
ψ	Wave function

Chapter 4

A	Parameter of the linear transference of momentum
B	Parameter of the nonlinear transference of momentum
D	Flux parameter
d	Distance the wave generator is moved
F	Pressure distribution factor
Fr	Piston Froude number
h	Undisturbed water depth
H	Total depth of the water
n	Porosity
p	Pressure
p_{-h}, p_η	Pressure at the bottom of the channel and on the free surface
R	Radius of the cylinders of the porous wedge
u	Horizontal velocity of the water particles
u_{-h}, u_η	Horizontal velocity of the water particles at the bottom of the channel and on the free surface
u_{sk}	Horizontal velocity of the porous body
v	Vertical velocity of the water particles
v_{-h}, v_η	Vertical velocity of the water particles at the bottom of the channel and on the free surface
v_{sk}	Vertical velocity of the porous body
x	Horizontal coordinate
y	Vertical coordinate starting from the undisturbed free surace
ϵ	Vertical scaling factor
ν	Vertical velocity relative to the porous body
σ	Horizontal scaling factor
ω	Horizontal velocity relative to the porous body

1 On the development of the theory of waves

1.1 A historical essay

The history of mechanics of water waves commences with the discovery of the laws of a wave which was among those that fascinated human beings most: the *tidal wave*. For its discovery it was necessary that HUYGENS [34], in his book *Horologium oscillatorium*, published in 1673, was able to formulate the law of attraction between two massive bodies, thereby essentially creating the physics of dynamics, i. e. the physics of motion caused by forces, see SPEISER [33]. Shortly afterwards and influenced by him, NEWTON [61] achieved the necessary philosophical anchorage of this new physics. His *Philosphiae Naturalis Principia Mathematica*, of which the first edition appeared in 1687, does not lay the mathematical foundation of the new contemplation. Rather, NEWTON is the first who subjects the natural phenomena *to an all embracing, axiomatic and mathematical description.* His concept of force and its effect on bodies (of arbitrary kind, not necessarily equipped with mass and of arbitrary whence also e. g. vanishing extent) corresponds to the postulation of an universal law according to which the separation of the mechanics of the firmament from that of the earthy phenomena is subdued. NEWTON's considerations of the mechanical motion are still restricted to systems with only one degree of freedom. In the physics of that time the mathematical notion of a three-dimensional space had not yet arisen. In his writings about tidal motion, NEWTON essentially does not go beyond statical equilibrium conditions which can be solved geometrically, see AITON [3]. However, the new knowledge of the theoretical basis of gravitation permitted several authors to contemplate about the occurrences of tides as the outcome of a force balance between Earth, Moon and the Sun. The first dynamical theory of tidal waves on an Earth covering ocean with constant depth is due to LAPLACE [48] and was published in 1775.

By formulating the conservation law of momentum for a mass point, and by applying it in integrated form to a fluid continuum, EULER [17] laied in 1750 the foundation of the modern, analytical theory of fluids. It was him who perceived NEWTON's third law of translatoric motion as a law pertinent to mass points subject to attracting and repelling forces and who formulated it for the first time as a law appropriate to a continuum. EULER first considers an infinitesimally small body M subjected to forces P, Q and R in the $x-$, $y-$, and $z-$ directions of the coordinates (*Soit un corps infiniment petit, ou dont toute la masse soit réunie dans un seul point, cette masse étant* $= M$ ... [17], §20) and writes

$$2Mddx = Pdt^2, \tag{1.1}$$

$$2Mddy = Qdt^2, \tag{1.2}$$

$$2Mddz = Rdt^2. \tag{1.3}$$

The factor 2 results from the definitions of units with which EULER calculates. (More detailed explanations are given by TRUESDELL in his explanatory remarks

to [87] *Prolog, Part VI.*) EULER's equations read in modern vectorial notation

$$\mathbf{K} = \frac{d(m\mathbf{v})}{dt}. \tag{1.4}$$

a) Lagrange

Research concerning the velocity of sound led to the first differential wave equation, whose earliest publication in 1759 must be credited to LAGRANGE [43] [1]. It culminates in the presentation of the differential equation of the oscillating cord, an equation entirely equivalent to that of the one-dimensional propagation of sound. This is why LAGRANGE finds it by considering a chain of mass points which are connected by springs first[2],

$$\frac{d^2\phi}{dt^2} = gh\frac{d^2\phi}{dx^2}. \tag{1.5}$$

In his major memoir [44] LAGRANGE describes the speed of sound to be twice as large as the speed of free fall. In the same work he also quotes an identical formula for the propagation of an infinitesimally small wave in a horizontal channel of depth h.

b) Gerstner

A first complete solution to a wave theory in an infinitely deep channel is published by GERSTNER [24] in 1809. In his theory he regards a wave as the motion of particles of the water. The fluid is perceived to consist of planes of equal pressure, surfaces which consist throughout time of the same fluid particles. The shape of the surfaces is obtained from a force balance between hydrostatic pressure, gravity and centrifugal forces, which apply at the water particles. The free surface is an example of such a surface. Because all water particles belong to such a surface, there exist simultaneously an arbitrary number of wave surfaces. Therefore, the actual free surface of a water body can only be determined by observation. As trajectories of the water particles GERSTNER computes, by way of the above mentioned force balance, *trochoids*; these are circular motions, on which a uniform horizontal speed is superposed. As a result, the fluid motion is not irrotational, (see [46] §251). The diameter of the circles diminishes with depth, whereas the superimposed horizontal motion remains constant for all particles. The maximum wave height is given by the (acute) cycloid for which the circumferential speed equals the horizontal speed. When the circumferential velocities are larger the cycloids are prolonged and show double points with negative velocities of the water particles. According to GERSTNER this phenomenon arises, when the water at the wave crests becomes foamy. Breaking waves are, however, explicitly excluded by this theory. The time of a wave, that is the time, in which the water moves from the crest of one wave to the next is $\pi\sqrt{2a/g}$. The radius of the circle by which the cycloid was formed is denoted by

[1] LAGRANGE must be mentioned first, because he applies the mathematical formalism of the vibrating cord to the particles of air. In the same year, EULER [18] publishes a much more mature version, which, however, contains an error (see also [87] pp. CXIX - CXXI).

[2] The symbol ∂, indicative of a partial derivative goes back to KARL GUSTAV JACOB JACOBI, 1804 - 1851, which he used in a paper on elliptic functions. Here the notations used by the different authors will be used.

a. Figure 1 reproduces the graphs of this wave theory.

GERSTNER's wave must be regarded as the classical example of an exact solution of a wave subjected to the action of gravitation, whereby the fluid particles are moving along closed trajectories. Further references of such and similar approaches can be found in THACKER [85].

With this work a complete theoretical wave theory was at the disposal, however, it could experimentally not be reproduced. The work of the WEBER brothers [92] on waves was complementary to this, as it contains a large number of experiments, partly by themselves, partly by others; in addition it contains a summary of the theoretical treatises known at that time and thus may serve as a rich source of information.

c) Russell

The starting point of todays wave theory is set by RUSSELL with his systematic series of experiments published in the years 1838 and 1845. His first report [70] is based on experiments, which were conducted in the mouths of the rivers Dee and Clyde (West Scotland), as well as experiments which allowed clearer inferences from an artificial channel. In his second report [71] he introduces and explains in detail a classification of waves. The main result of the two reports is the discovery and experimental verification of the *Great Primary Wave of Translation*, which he characterizes as a ***solitary wave***. This wave is not oscillatory. The speed of a solitary wave in a flat channel with depth h depends on the total waveheight $h + \eta$ and is given by

$$c = \sqrt{g(h + \eta)}. \tag{1.6}$$

RUSSELL lists the following properties of this wave:

- The solitary wave is reflected at a vertical wall and moving in the opposite direction without changing its form.
- Under collision the solitary waves maintain their shape.
- The form of a solitary wave is that of a trochoid.
- The height of a solitary wave remains unchanged during motion. Only because of *adhesion of water to the sides* of the channel and because of imperfect fluidity (i. e. viscosity) does it decrease with time.
- In a channel with decreasing depth the waves break if the waveheight exceeds the water depth.

Similarly to GERSTNER, RUSSELL describes wave breaking as the result of too high wave crests. In this case the wave form corresponds to a prolonged cycloid. In his second report in the paragraph *'The nature of waves and their varieties'* RUSSELL remarks that the *motion of transmission* (= motion of the wave) must be differentiated from the *motion of migration* (= motion of the water) in which the

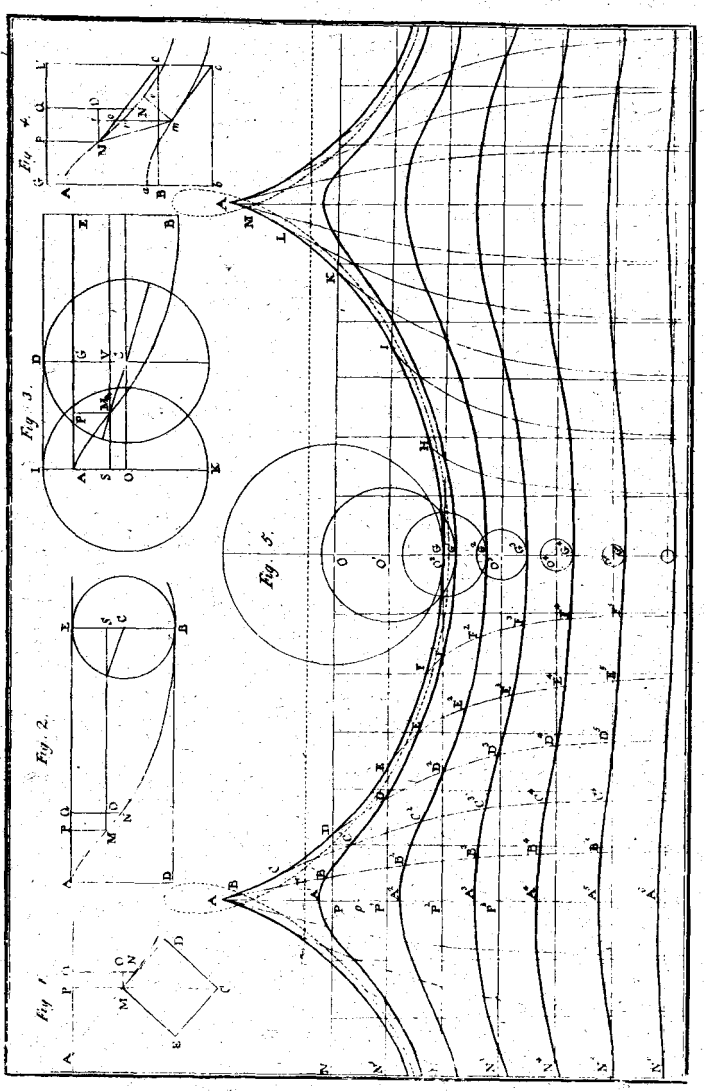

Figure 1: GERSTNER*'s wave theory. Reproduction from Annalen der Physik, Volume 32, 1809. Figures 1 – 4 serve* GERSTNER *as explanations when deriving his equations. Figure 5 shows the resulting isobaric surfaces on which the water particles move. The wave motion corresponds to this movement. The dotted line of a stretched cycloid with a double point is regarded as indicator of wave breaking.*

wave is moving. *'Wave motion is therefore a transcendental motion; ... the motion of motion – the transference of motion without the transference of the matter, of form without the substance, of force without the agent'* ([71], p. 315). With these words RUSSELL speaks out very clearly the essential property of wave motion. After this fundamental essay about the essence of a wave he continues to divide water waves into the following four classes:

Wave of first order. The wave of translation. The wave of first order is characterized by the fact that the total fluid mass is moved from one place to another and then rests there. The motion of the fluid does not correspond to the motion of the wave. Its shape is a single (solitary) hump above the still water surface or a single (solitary) trough completely beneath the water line. The wave moves with a uniform velocity.

RUSSELL experiments with various mechanisms in order to generate this wave in a channel. Figure 2 shows an engraving illustrating this. In his five upper figures on the left a vertical plate is moved forward and shown in various positions. In the next three figures RUSSELL illustrates, how a wave is developing, when a vertical plate holds water back at a higher level and then, upon sudden lifting the plate, the different water levels are equalized and a wave is formed. In the two upper graphs on the right RUSSELL shows a body falling vertically into the channel and forming a wave.

Further observations and attempts of explanations are reproduced in the remaining figures. On the upper right (*Fig. 4*) the reflection of a wave is shown, below it (*Fig. 5*) the simultaneous motion of water particles along the *entire length of the wave* (first graph) and the complete trajectory of four particles during the passage of the wave are shown (second graph). The third graph of the same figure reproduces the motion of the wave. The infinitesimal water columns $a\,b\,\beta\,\alpha$, $b\,c\,\gamma\,\beta$ etc. suffer an excess pressure and change thereby their forms. The pressure they experience at their vertical faces is transmitted to the neighbouring cells; therefore, a transfer of momentum generates the wave motion. *The wave is thus a receptacle of moving power*; it transmits energy. The lower most graph of the series illustrates the streamlines of the wave. The formation and development of two positive waves and that of a positive and a negative wave is shown in the two lower most graphs. RUSSELL further argues that the formation of a negative wave, sitting completely below the water line ought to be achievable under reverse conditions. However, under such circumstances he always observes an oscillating wave train which follows the negative wave. As regards the wave generating mechanism RUSSELL argues that the volume of the water displaced by the wave should be approximately equal to the volume that was added or removed by the wave generating mechanism. In particular, the height of the added volume is about the same as that of the forming wave. If one selects a overly long initial volume (second to the last graph), then a main solitary wave is formed followed by other waves. The various waves that are formed move independently of each other with a speed corresponding to their

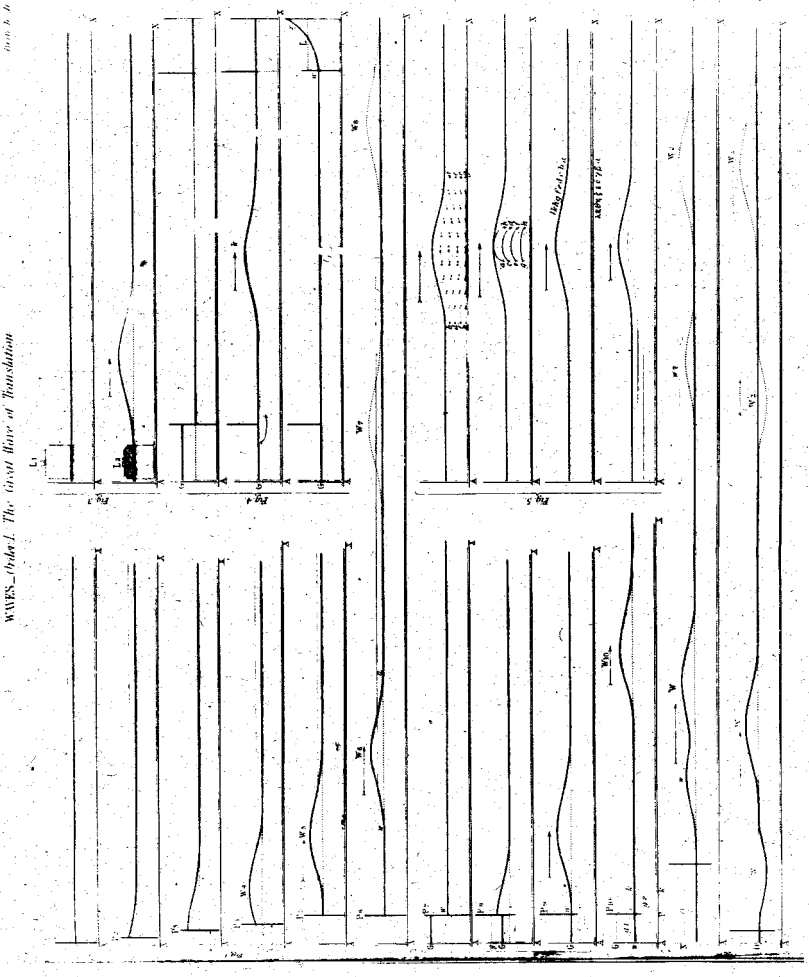

Figure 2: *Reproduction of the mechanisms that generate solitary waves. From: Report of the 7th Meeting of the British Association for the Advancement of Science, Liverpool 1838, plate 47.*

waveheights. An initial volume that is excessively small (lower most graph) implies that the subsequent wave has negative height.

Waves of second order. Oscillating waves. The wave of second order lies partly above and partly underneath the still-water line with a trough corresponding to each crest. These waves always occur in groups, and standing as well as travelling waves are possible.

Waves of the third order. Capillary waves. In these waves the water is only excited in a very thin layer. Thereby capillary forces due to surface tension arise. Figure 3 shows such a wave, it is generated by a pin that moves in the direction of the indicated arrow.

Waves of fourth order. Corpuscular waves. These waves are formed when sound propagates in a fluid. They are not visible, since movements by which the wave is carried further are too small to be detectable by the eye. RUSSELL therefore muses that either the molecules of the fluid will change their formes, or the density of the fluid will change or an instantaneous and infinitesimal change in the intermolecular distance will arise. He quotes the equation for the speed of sound of compressible gases which POISSON [65] had been able to derive in 1823 already, and he also mentions the measurements of the speed of sound in Lac Léman that were performed by COLLADON & STURM [10] in 1838.

d) Airy

Shortly before RUSSELL's second report went to press there appeared in 1845 the memoir *'On waves'* by AIRY [2]. Principal aim of this work is to establish a theory of tides for fiords and channels with access to the sea. The largest chapter is concerned with the theory of waves in a straight channel. For the case of small particle excursions a continuity equation is derived and a force balance, called the *equation of equal pressure* is deduced. Both equations are derived in a coordinate system moving with the observer. The pressure balance corresponds to EULER's momentum balance, whence no assumption of the distribution on the pressure is made

$$\frac{d^2y}{dt^2} = -g - \frac{dp}{dy}. \tag{1.7}$$

By restricting the motion of the water particles to oscillations with generally different movements of the particles in the vertical and horizontal directions ([2] §160 ff.) AIRY deduces the speed c of the oscillating wave in an uniform channel in the form

$$c^2 = \frac{g}{k}\tanh(h\,k) \tag{1.8}$$

with the wave length

$$\lambda = \frac{2\pi}{k}. \tag{1.9}$$

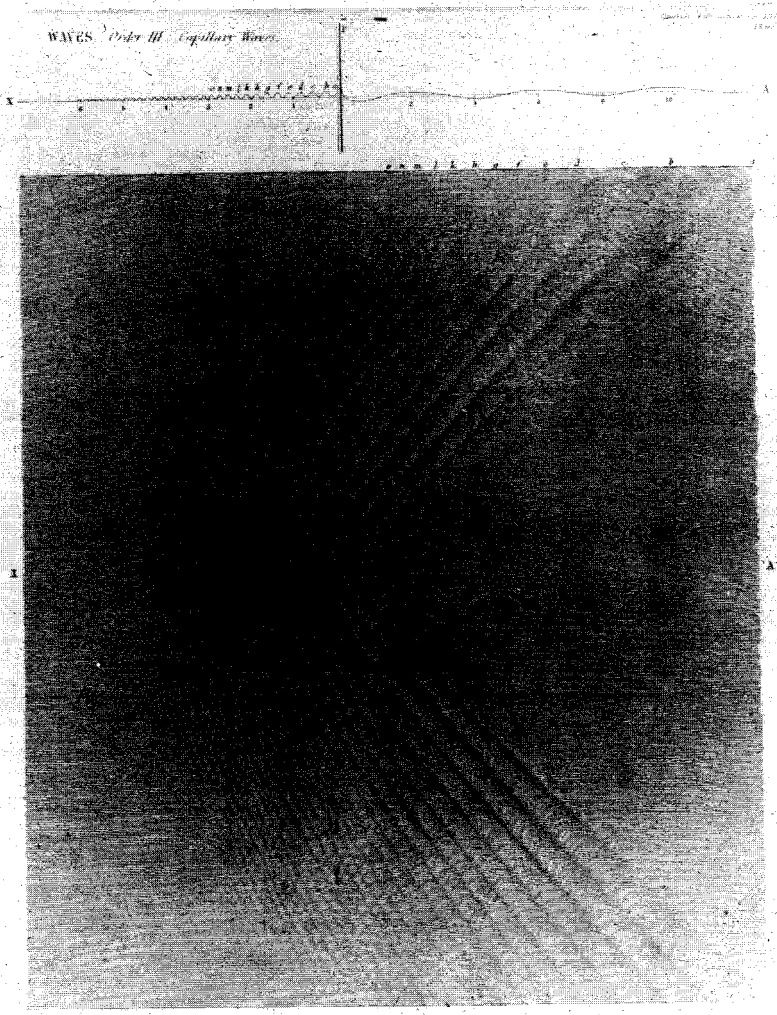

Figure 3: *Reproduction of a capillary wave. From: Report of the 7th Meeting of the British Association for the Advancement of Science, Liverpool 1838, Plate 57. The pin in the middle of the print has a diameter of* 1/16 *inch.*

Hence, the wave speed depends on both water depth and wavelength. Two limiting cases are distinguished, namely

$$c^2 \approx \begin{cases} \dfrac{g\lambda}{2\pi}, & \text{for } \lambda < h, \\ gh, & \text{for } \lambda > 1000\,h. \end{cases} \tag{1.10}$$

The particles of waves with short wavelength move in circles, if the point of consideration is distant from the bottom. For long waves the circles are stretched to ellipses. For the latter, the horizontal movement of particles positioned along a vertical is about the same.

For long waves ([2] §192 ff.), with small particle motions AIRY assumes that the horizontal component of the acceleration can be ignored; as a result, the horizontal movement of the particles in a vertical line is uniform. Furthermore, a hydrostatic pressure distribution is assumed. In comparison to the channel depth the wave-height can, however, be large.

In moving coordinates $x+X(x,t)$ the governing equations are obtained as follows: Particles in water of depth h which are located between two parallel vertical lines at x and $x+b$ will be moved to the positions $x+X$ and $x+X+b+dX/dx \cdot b$ after a time t will have elapsed with a new water depth $h+\eta$. Because the volume must be conserved, the continuity equation

$$bh = b\left(1+\frac{dX}{dx}\right)(h+\eta) \tag{1.11}$$

is obtained, from which

$$h+\eta = \frac{h}{1+\dfrac{dX}{dx}} \tag{1.12}$$

is deduced. In a similar way, AIRY obtains the *equation of equal pressure*: The pressure exerted on a particle with coordinates $x+X$ and y corresponds to the length of the water column $l-y$ above it, with $l=h+\eta$. Once the particle has reached the position given by $x+X+b+dX/dx \cdot b$ and y, it experiences a pressure of $l+dl/dx \cdot b - y$. Since the pressure is the same in all directions, the horizontal pressure by which a column of water is moved through the distance $b(1+dX/dx)$, equals the weight of the column of which the length is changed by the amount of $-dl/dx \cdot b$. A particle, belonging to that column is accelerated in the horizontal direction by this pressure difference. The balance of acceleration and pressure force thus yields

$$\frac{d^2(x+X)}{dt^2} = -g\frac{dl}{dx}\frac{1}{1+\dfrac{dX}{dx}}. \tag{1.13}$$

Because x and t are independent variables the equation of long waves of a moving

particle

$$\frac{d^2X}{dt^2} = gh\frac{\frac{d^2X}{dx^2}}{\left(1+\frac{dX}{dx}\right)^3} \tag{1.14}$$

is obtained in which (1.12) was used. Expanding the right hand side for small dX/dx yields

$$\frac{d^2X}{dt^2} - gh\frac{d^2X}{dx^2} = gh\frac{d^2X}{dx^2}\left(-3\frac{dX}{dx} + 6\left(\frac{dX}{dx}\right)^2 + \cdots\right), \tag{1.15}$$

which suggests AIRY's first approximation

$$\frac{d^2X}{dt^2} - gh\frac{d^2X}{dx^2} = 0 \tag{1.16}$$

with the solution

$$X = f_1(ct - x) + f_2(ct + x). \tag{1.17}$$

The periodic behaviour of a tidal wave is assumed as a harmonic wave moving along from the left boundary; so

$$X = a\cos(ct - x) \tag{1.18}$$

is obtained. By substituting this result into the right hand side of equation (1.15) and taking into account the first term only, AIRY computes to second order the speed of a wave crest relative to a fixed system, i. e. the channel, and finds ([2] §208 ff.)

$$c = \sqrt{gh}\left(1 + \frac{3}{2}\frac{\eta}{h}\right) \approx \sqrt{gh\left(1 + 3\frac{\eta}{h}\right)}. \tag{1.19}$$

An account of this can be found in LAMB [46] §175: The speed of the wave relative to the fluid particles in its immediate neighbourhood is given by $c^2 = gh$. When the elevation η, though small compared with the wave-length, is not regarded as infinitely small, a closer approximation to the wave-velocity is secured if, in $c^2 = gh$, h is replaced by $h + \eta$. This gives a wave celerity $c^2 = g(h + \eta)$ or $c = \sqrt{gh}(1 + \eta/(2h))$, relative to the fluid in the immediate neighbourhood. Since this fluid has itself an velocity $\sqrt{gh}\,\eta/h$, the velocity of propagation in space is approximately $c = \sqrt{gh}(1 + 3\eta/(2h))$, a result substantially due to AIRY.

AIRY remarks that on the basis of the dependence of the wave speed on wave-height, the wave front must become steeper in the course of time, whereas its rear must become flatter. A solitary wave, which he classifies as a long wave, therefore cannot be of permanent form.

e) Earnshaw

AIRY's work had already been printed when EARNSHAW [16] presented in 1849 a mathematical theory of two solitary waves in a horizontal channel. His theory differentiates between a positive and a negative wave. Motivated by RUSSELL's

experiments he assumes a priori a uniform wave speed and a horizontal particle velocity that is independent of the vertical position: $u = u(x,t)$. Interesting is the way in which he expresses partial derivatives. From EULER's equations he obtains

$$d_x p = -d_t u - u d_x u \,, \tag{1.20}$$

$$d_y p = -g - d_t v - u d_x v - v d_y v \tag{1.21}$$

and he writes continuity in the form

$$0 = d_x u + d_y v \,. \tag{1.22}$$

From his assumption of uniform wave velocity he concludes without further explanation

$$0 = d_t u + c d_x u \,. \tag{1.23}$$

EARNSHAW does not impose any restriction upon the vorticity of the fluid. He solves the continuity equation for v and substitutes the resulting expression into equation (1.21) with the result

$$d_y p = -g + \left(d_t d_x u + u d_x^2 u - (d_x u)^2 \right) y \,. \tag{1.24}$$

Since u was assumed independent of y the same must be true also for $d_x p$ owing to equation (1.20). With

$$0 = d_y d_x p = d_x d_y p \tag{1.25}$$

he thus infers that $d_y p$ is equally independent of x. EARNSHAW further concludes that because of (1.23) the term in parenthesis on the right of equation (1.24) must also be independent of t; thus it is independent of x, y and t and must be constant. (This last conclusion is not correct, but poses an additional assumption on the pressure which ought to satisfy a relation analogous to equation (1.23)). A wave thus satisfies the equations

$$n^2 = d_t d_x u + u d_x^2 u - (d_x u)^2 \,, \tag{1.26}$$

$$\delta_t^2 y = -n^2 y \,, \tag{1.27}$$

where $n^2 = const.$ and δ has been introduced as the symbol expressing total differentiation.

The force, which, by the last two equations, determines the vertical motion, thus varies with the distance from the channel bottom, but possesses always the same sign. For a positive wave the force is acting in a direction such that the particles are drawn back to their equilibrium positions; the constant n^2 must therefore be positive. A negative wave is correspondingly characterized by a negative constant $-n^2$. Integration of the last two equations yields for $n^2 > 0$ the wave speed of a positive wave,

$$c^2 = \frac{\dfrac{2g(h+\eta)^2}{2h+\eta}}{1 + \dfrac{4h^2}{\lambda^2}\left(\log_e\left(\tan\left(\dfrac{\pi}{4} + \dfrac{1}{2}\cos^{-1}\dfrac{h}{h+\eta}\right)\right)\right)^2}$$

$$\overset{h+\eta \approx h}{\approx} \sqrt{g(h+\eta)} \,, \tag{1.28}$$

whereas for $n^2 < 0$ that of a negative wave is obtained,

$$c^2 = \frac{\frac{2g(h+\eta)^2}{2h+\eta}}{1 - \frac{4h^2}{\lambda}\left(\cos^{-1}\frac{h+\eta}{h}\right)^2}. \tag{1.29}$$

The solution of the equations of motion, however, contains a jump in pressure between the fluid at rest and the frontal position of the wave of finite length. Due to this discontinuity EARNSHAW concludes that RUSSELL's assumption of an uniform wave speed must be wrong, and consequently the decay of the amplitude of RUSSELL's wave cannot be due to wave friction and viscosity of the fluid.

f) Stokes

In 1847 STOKES [80] presents a theory of oscillating waves. His investigation supposes a homogeneous, incompressible fluid in a channel of uniform depth. The goal is the derivation of wave equations of various orders, whereby the wave should be form invariant and propagate with constant speed, so that

$$\eta = f(x - ct). \tag{1.30}$$

On the basis of BERNOULLI's equation the velocity potential ϕ satisfies the equation

$$p = g\rho y - \rho\frac{d\phi}{dt} - \frac{\rho}{2}\left(\left(\frac{d\phi}{dx}\right)^2 + \left(\frac{d\phi}{dy}\right)^2\right) \tag{1.31}$$

and for an incompressible irrotational flow must obey the LAPLACE equation

$$\frac{d^2\phi}{dx^2} + \frac{d^2\phi}{dy^2} = 0. \tag{1.32}$$

At the channel bottom $y = 0$ one must further have [3]

$$\frac{d\phi}{dy} = 0 \tag{1.33}$$

and at the free surface $y = h + \eta$ where the atmospheric pressure is constant,

$$\frac{dp}{dt} + \frac{d\phi}{dx}\frac{dp}{dx} + \frac{d\phi}{dy}\frac{dp}{dy} = 0. \tag{1.34}$$

STOKES further assumes that u, v and p are functions of $(x - ct, y)$, in which case the velocity potential ϕ must have the form

$$\phi = \phi(x - ct, y) - (gl)t \tag{1.35}$$

[3] For simplicity the origin of the vertical coordinate y is taken to be at the channel bottom as was done by STOKES in his memoir, so $y = 0$ corresponds to the bottom and $y = h$ to the water surface at rest.

in which $-gl$ is an arbitrary constant. Substituting it into equation (1.31) yields

$$p = g\rho(y+l) + c\rho\frac{d\phi}{dx} - \frac{\rho}{2}\left(\left(\frac{d\phi}{dx}\right)^2 + \left(\frac{d\phi}{dy}\right)^2\right). \tag{1.36}$$

On the other hand (1.34) becomes at the free surface

$$\left(\frac{d\phi}{dx} - c\right)\frac{dp}{dx} + \frac{d\phi}{dy}\frac{dp}{dy} = 0. \tag{1.37}$$

STOKES now eliminates the pressure p between (1.36) and (1.37) and obtains

$$\begin{aligned} &g\frac{d\phi}{dy} - c^2\frac{d^2\phi}{dx^2} + 2c\left(\frac{d\phi}{dx}\frac{d^2\phi}{dx^2} + \frac{d\phi}{dy}\frac{d^2\phi}{dxdy}\right) \\ &- \left(\frac{d\phi}{dx}\right)^2\frac{d^2\phi}{dx^2} - 2\frac{d\phi}{dx}\frac{d\phi}{dy}\frac{d^2\phi}{dxdy} - \left(\frac{d\phi}{dy}\right)^2\frac{d^2\phi}{dy^2} = 0. \end{aligned} \tag{1.38}$$

This equation and equation (1.36) are exact. For a second order approximation the three last terms of (1.38) are neglected. The velocity potential is now expanded about $y = 0$. The free surface is expressed by the lowest order approximation of equation (1.36), viz.

$$y = -l - \frac{c}{g}\frac{d\phi}{dx} + \frac{c}{g}\frac{d^2\phi}{dxdy}\left(l + \frac{c}{g}\frac{d\phi}{dx}\right) + \frac{1}{2g}\left(\left(\frac{d\phi}{dx}\right)^2 + \left(\frac{d\phi}{dy}\right)^2\right), \tag{1.39}$$

and in the first two terms of (1.38) the second approximation (consisting of the first two terms of the expansion of ϕ up to terms of order y) is substituted, while the next two terms are approximated by one order less. When terms smaller than order $(d\phi)^2$ or $d^2\phi$ are ignored, this process yields

$$\begin{aligned} &g\frac{d\phi}{dy} - c^2\frac{d^2\phi}{dx^2} - \left(g\frac{d^2\phi}{dy^2} - c^2\frac{d^3\phi}{dx^2dy}\right)\left(l + \frac{c}{g}\frac{d\phi}{dx}\right) \\ &+ 2c\left(\frac{d\phi}{dx}\frac{d^2\phi}{dx^2} + \frac{d\phi}{dy}\frac{d^2\phi}{dxdy}\right) = 0. \end{aligned} \tag{1.40}$$

This is the equation of the free surface to second order. Omitting terms that are small yields the first order equation

$$g\frac{d\phi}{dy} - c^2\frac{d^2\phi}{dx^2} = 0. \tag{1.41}$$

To construct a solution to the problem, ϕ must now satisfy equation (1.32) subject to the boundary conditions (1.33) and (1.40). The general solution reads

$$\phi = \sum Ae^{m(x-ct)+ny} + C(x-ct) + \hat{C} + Dy + \hat{D} \tag{1.42}$$

with real or imaginary m and n satisfying

$$m^2 + n^2 = 0. \tag{1.43}$$

In the limit as $x - ct \to \pm\infty$, ϕ must remain finite. This is why m must be purely imaginary. $\hat{C}$ and $\hat{D}$ can be ignored, and on the basis of the boundary condition (1.33) $D = 0$. Hence (1.42) simplifies and can be written with real positive k as

$$\phi = C(x - ct) + \sum \left(e^{k(h-y)} + e^{-k(h-y)} \right) \eta_{max} \sin(k(x - ct)) . \tag{1.44}$$

The term $C(x - ct)$ corresponds to an arbitrary uniform flow and can be eliminated by the choice of an appropriate frame of reference, as will be shown later.

The first approximation (1.41) must be satisfied for all x. This is certainly the case if the speed c of an oscillatory wave is chosen according to

$$c^2 = \frac{g\lambda}{2\pi} \tanh\left(\frac{2\pi h}{\lambda}\right) , \tag{1.45}$$

with the wavelength λ

$$\lambda = \frac{2\pi}{k} . \tag{1.46}$$

Thus for a given wavelength there is only one value k and, apart from the undetermined function $C(x - ct)$, there is only one oscillating solution, namely

$$\phi = \eta_{max} \left(e^{k(h-y)} + e^{-k(h-y)} \right) \sin(k(x - ct)) \tag{1.47}$$

with the following approximation for the free surface

$$\eta = -\frac{k\eta_{max}c}{g} \left(e^{kh} + e^{-kh} \right) \cos(k(x - ct)) . \tag{1.48}$$

The amplitude η_{max} and the wavelength λ can be chosen arbitrarily. The velocity c of the wave is independent of the waveheight, for which reasons STOKES rejects the existence of waves of permanent form. He concludes that the decay of the waveheight as described by RUSSELL must therefore be regarded as a property of the wave and cannot be ascribed to the properties of the fluid.

In the first approximation (1.48) he sets $l = 0$ (compare equation (1.36)) because the mean value of η must vanish. To obtain the second order approximation, equation (1.47) is substituted into (1.40). With the general solution (1.44) STOKES is able to obtain the solution of the second order of which the free surface equation reads

$$\eta = \eta_{max} \cos(k(x - ct)) - K\eta_{max}^2 \cos(2k(x - ct)) , \tag{1.49}$$

$$K = \frac{\left(e^{kh} + e^{-kh} \right) \left(e^{2kh} + e^{-2kh} + 4 \right)}{2 \left(e^{kh} - e^{-kh} \right)^3} , \tag{1.50}$$

where K is positive. The crests and troughs of these waves are differently large. The maximum waveheight is given by $\eta_{max} + K\eta_{max}^2$, whereas the largest trough

is given by $\eta_{max} - K\eta_{max}^2$. These solutions hold for arbitrary h/λ and sufficiently small η/h. Furthermore, if one assumes h/λ to be small, the second order formula for the free surface becomes

$$\eta = \eta_{max}\cos(k(x-ct)) - \frac{3\eta_{max}^2}{4k^2h^3}\cos(2k(x-ct))\,. \tag{1.51}$$

The coefficient of the first term which stems from the first approximation must be large in comparison to the coefficient of the second term, which is of second order, whence

$$\eta_{max} \gg \frac{\eta_{max}^2}{k^2h^3}\,, \tag{1.52}$$

from which he deduces

$$\frac{\lambda^2\eta_{max}}{h^3} \ll 1\,. \tag{1.53}$$

STOKES concludes that

$$\frac{\eta_{max}}{h} < \left(\frac{h}{\lambda}\right)^2\,, \tag{1.54}$$

must hold. Alternatively, AIRY's results implied

$$\frac{\eta_{max}}{h} > \left(\frac{h}{\lambda}\right)^2\,. \tag{1.55}$$

Therefore, the results of STOKES and AIRY are valid under different physical conditions.

By letting $h \to \infty$ STOKES obtains the equations of second order for deep water, namely

$$\phi = -\eta_{max}c\,e^{-ky}\sin(k(x-ct))\,, \tag{1.56}$$

$$\eta = \eta_{max}\cos(k(x-ct)) - \frac{1}{2}k\eta_{max}^2\cos(2k(x-ct))\,, \tag{1.57}$$

$$k = \frac{2\pi}{\lambda}\,, \tag{1.58}$$

$$c^2 = \frac{g\lambda}{2\pi}\,. \tag{1.59}$$

For infinitely deep water STOKES also derives the *equation of the third order*. Starting with equation (1.38), the same procedure as outlined above for the second order equations is employed. By taking into account the results of the first and second order he obtains

$$\eta = \eta_{max}\cos(k(x-ct)) - \frac{1}{2}k\eta_{max}^2\cos(2k(x-ct)) + \frac{3}{8}k^2\eta_{max}^3\cos(3k(x-ct))\,, \tag{1.60}$$

$$k = \frac{2\pi}{\lambda}\,, \tag{1.61}$$

$$c^2 = \frac{g\lambda}{2\pi}\left(1 + \frac{2\pi\eta_{max}^2}{\lambda^2}\right)^2\,. \tag{1.62}$$

As already mentioned, the velocity by which the wave profile is moving in the channel, can be determined only to within an arbitrary constant. By adding an uniform counter flow one can make the wave as fast as one wishes. To obtain a unique definition, STOKES proposes to select this wave velocity as the wave speed c which is obtained when the mean horizontal velocity of the particle u is made to vanish.

STOKES mentions two possibilities for averaging the particle velocity. They were considered by WEHAUSEN & LAITONE [93].

1. If one averages velocities over the entire space exposed to the wave, one obtains for the wave speed c

$$\lim_{\substack{a\to\infty\\ b\to\infty}} \frac{1}{b-a}\int_a^b \int_0^{h+\eta} u(x,y) - c \; dy\, dx = 0\,. \tag{1.63}$$

In the case of periodic waves this equation simplifies to

$$\frac{1}{\lambda}\int_0^{\lambda} \int_0^{h+\eta} u(x,y) - c \; dy\, dx = 0\,. \tag{1.64}$$

If one chooses a mean depth

$$\bar{h} = \frac{1}{\lambda}\int_0^{\lambda} \eta + h \; dx\,, \tag{1.65}$$

one can see that this velocity defines the mean volume flux per unit width

$$Q = \frac{1}{\lambda}\int_0^{\lambda} \int_h^{h+\eta} u \; dy\, dx\,, \tag{1.66}$$

so that

$$Q = c\bar{h}\,. \tag{1.67}$$

In a moving coordinate system $x' = x - ct$ the mean volume flux vanishes; the wave speed c corresponds to the velocity of the centre of gravity of the entire fluid (or the fluid between two parallel lines which are a wavelength apart).

2. If one averages over time t, then one obtains

$$c = \lim_{t\to\infty} \frac{1}{t}\int_0^t u(x+ct, y)\; dt \;=\; \lim_{t\to\infty} \frac{1}{ct}\int_{x'}^{x'+ct} u(x,y)\; dx \tag{1.68}$$

and for periodic waves

$$c = \frac{1}{\lambda}\int_{x'}^{x'+\lambda} u \; dx\,. \tag{1.69}$$

With the assumption that u and v are bounded and the motion is irrotational, $u_y = v_x$, it follows that $\partial c/\partial y = 0$. The two definitions are therefore independent of the vertical coordinate and yield, in infinitely deep water, the same results.

STOKES published in 1880 [81] in his collected papers an appendix of his article of 1849, where he shows that a wave with maximum amplitude possesses at it crest

a tip angle of 120^0. This statement will be significant, when the question of the highest amplitude of the wave of permanent form is posed.

g) Boussinesq

It is BOUSSINESQ [8] who, in 1872, introduces a new procedure of approximating the wave equations [4]. Starting with EULER's equations

$$\frac{1}{\rho}\frac{dp}{dx} = -\left(\frac{du}{dt}\right), \tag{1.70}$$

$$\frac{1}{\rho}\frac{dp}{dy} = -g - \left(\frac{dv}{dt}\right), \tag{1.71}$$

with

$$\left(\frac{du}{dt}\right) = \frac{du}{dt} + u\frac{du}{dx} + v\frac{du}{dy}, \; etc. \tag{1.72}$$

and the continuity equation [5]

$$\frac{d\rho}{dt} + \frac{d.\rho u}{dx} + \frac{d.\rho v}{dy} = 0 \tag{1.73}$$

he introduces the velocity potential ϕ for an irrotational, incompressible ideal fluid, but restricts himself to planar motion in a vertical plane. By integrating the continuity equation (expressed in terms of the velocity potential)

$$\frac{d^2\phi}{dx^2} + \frac{d^2\phi}{dy^2} = 0 \tag{1.74}$$

he obtains

$$\phi = \phi_0 - \int_0^y dy \int_0^y \frac{d^2\phi}{dx^2}\, dy, \tag{1.75}$$

where ϕ_0 satisfies the boundary condition $v(x, y = 0) = 0$ [6]. BOUSSINESQ further assumes that the horizontal velocity u differs only slightly from the velocity u_0 at the bottom. The potential ϕ then can be replaced by its value at the bottom ϕ_0. Replacing therefore in the integral term of (1.75) ϕ by ϕ_0, he obtains

$$\phi = \phi_0 - \frac{y^2}{2}\frac{d^2\phi_0}{dx^2}. \tag{1.76}$$

If this expression is once again substituted into the right hand side of equation (1.75) and if this procedure is arbitrarily continued, a successive approximation for ϕ is obtained:

$$\phi = \phi_0 - \frac{y^2}{1\cdot 2}\frac{d^2\phi_0}{dx^2} + \frac{y^4}{1\cdot 2\cdot 3\cdot 4}\frac{d^4\phi_0}{dx^4} - \frac{y^6}{1\cdot 2\cdot 3\cdot 4\cdot 5\cdot 6}\frac{d^6\phi_0}{dx^6} + \cdots \tag{1.77}$$

[4] The main results were already published a year before. The velocity of the solitary wave is developed in [7], the differential equation of second order in [6].

[5] At the time of printing a dot is inserted into the first derivative whenever more than one symbols follow e. g. $d.abc/dx$.

[6] See footnote on page 28.

Since parallel motions at infinity are not taken into account, he imposes the boundary conditions there $u_0 = \phi_0 = 0$. With these implementations he obtains

$$\phi_0 = -\int_x^\infty \frac{d\phi_0}{dx}\,dx = -\int_x^\infty u_0\,dx\,. \tag{1.78}$$

BOUSSINESQ determines the pressure by requesting vanishing atmospheric pressure and writes

$$p = \rho g(h + \eta - y) + P\,. \tag{1.79}$$

The term P contains all non-hydrostatic contributions; it is essentially proportional to the curvature of the free surface. According to BERNOULLI's equation it is thus given by

$$\frac{p}{\rho} = -gy - \frac{d\phi}{dt} - \frac{1}{2}\left(\frac{d^2\phi}{dx^2} + \frac{d\phi}{dy^2}\right) + \textit{une fonction arbitraire de } t\,. \tag{1.80}$$

Together with equation (1.79) and the condition that for points x far away from the wave disturbance one has $\eta = 0$, $\phi = 0$ and $P = 0$, he concludes that the arbitrary function must also vanish. In this way BOUSSINESQ obtains the non-hydrostatic part in the form

$$P = -\rho\left(g\eta + \frac{d\phi}{dt} + \frac{1}{2}\left(\frac{d^2\phi}{dx^2} + \frac{d^2\phi}{dy^2}\right)\right)\,. \tag{1.81}$$

The surface is determined by the requirement that

$$P = 0\,, \tag{1.82}$$

and the condition that no fluid particle can leave the surface by the condition

$$v = \frac{d\eta}{dt} + u\frac{d.h\eta}{dx}\,. \tag{1.83}$$

In the next step he replaces in equation (1.77) ϕ by the bottom velocity u_0 as given in (1.78). Moreover, in the boundary conditions (1.81) and (1.83) ϕ is replaced by its expansion (1.77) and evaluated at the free surface $y = h+\eta$. When performing these operations integration and differentiation are arbitrarily interchanged. BOUSSINESQ obtains series expansions in terms of η and u_0. These are small quantities and its derivatives with respect to x must increasingly be smaller with growing degree of differentiation in order that the series of ϕ converges. The first approximation is obtained if only the linear terms η, u_0 and du_0/dx are taken into account; it reads

$$\left.\begin{aligned} \int_x^\infty \frac{du_0}{dt}\,dx &= g\eta \\ \frac{d\eta}{dt} &= -h\frac{du_0}{dx} \end{aligned}\right\} \Leftrightarrow \frac{d^2\eta}{dt^2} = gh\frac{d^2\eta}{dx^2}\,, \tag{1.84}$$

a result that was already given by LAGRANGE. BOUSSINESQ finds the velocity u_0 by solving the equation on the right of (1.84) and subsequent integration of the first

equation on the left. In addition he focuses his attention to waves moving in the positive x-direction, so that

$$\eta = f(x - t\sqrt{gh}), \tag{1.85}$$

$$u_0 = \eta\sqrt{\frac{g}{h}}. \tag{1.86}$$

In a second approximation the smallest, quadratic terms are also taken into account, by substituting into them the velocity as obtained from the first approximation. In this way he obtains the relations

$$\left.\begin{aligned} \int_x^\infty \frac{du_0}{dt}\,dx &= g\eta + \frac{g}{2}\left(\frac{\eta^2}{h} + h^2\frac{d^2\eta}{dx^2}\right) \\ \frac{d\eta}{dt} &= -h\frac{du_0}{dx} - \sqrt{gh}\frac{d}{dx}\left(\frac{\eta^2}{h} - \frac{h^2}{6}\frac{d^2\eta}{dx^2}\right) \end{aligned}\right\}$$

$$\Leftrightarrow \frac{d^2\eta}{dt^2} = gh\frac{d^2\eta}{dx^2} + gh\frac{d^2}{dx^2}\left(\frac{3\eta^2}{2h} + \frac{h^2}{3}\frac{d^2\eta}{dx^2}\right). \tag{1.87}$$

The speed of the wave, c is obtained from the integrated continuity equation

$$\frac{d\eta}{dt} + \frac{d.\eta c}{dx} = 0. \tag{1.88}$$

(which BOUSSINESQ does not identify as such). By integrating it with respect to x and differentiating the result with respect to t he obtains, upon using (1.87) and imposing the boundary condition $\eta = 0$, as $x \to \infty$

$$\frac{d.\eta c}{dt} + gh\frac{d}{dx}\left(\frac{3\eta^2}{2h} + \frac{h^2}{3}\frac{d^2\eta}{dx^2}\right) = 0. \tag{1.89}$$

This equation possesses solutions of the form $\chi = \chi(x + \sqrt{gh}\,t)$ with

$$\chi = \eta\,(c - \sqrt{gh}\,t) - \frac{\sqrt{gh}}{2}\left(\frac{3\eta^2}{2h} + \frac{h^2}{3}\frac{d^2\eta}{dx^2}\right), \tag{1.90}$$

as can be corroborated by differentiating the result with respect to t. χ must vanish if a suitable coordinate system travelling with the wave is chosen and waves which propagate in the positive x-direction are considered. The velocity c of a wave is therefore given by

$$c = \sqrt{gh}\left(1 + \frac{3}{4}\frac{\eta}{h} + \frac{h^2}{6\eta}\frac{d^2\eta}{dx^2}\right), \tag{1.91}$$

or in squared form by

$$c^2 = g\left(h + \frac{3}{2}\eta + \frac{h^3}{3\eta}\frac{d^2\eta}{dx^2}\right). \tag{1.92}$$

This speed corresponds to a velocity of a vertical plane at x_0 which has always the same volume $Q = \int_{x_0}^\infty \eta\,dx$ ahead of it. Indeed, a volume element $\eta\,dx$ can be envisaged between two planes normal to x and a distance dx apart. The fluid volume between these planes is kept constant through time. The planes move with a

celerity c the wave possesses when passing theses planes. This velocity c is obtained from the volume of the wave $q = \int_x^\infty \eta\, dx$ and that at a later time $t + dt$, when the lower limit x of the interval is given by $x + c\, dt$. Since the integral preserves its value through time BOUSSINESQ obtains $-\eta c + \int_x^\infty d\eta/dt\, dx = 0$. Differentiating this with respect to x yields the continuity equation (1.88).

Some further results will now also be quoted.

- The volume of the wave is constant

$$Q = \int_{x_0}^{\infty} \eta\, dx\,. \tag{1.93}$$

- The energy of the wave is constant

$$E = \int_{x_0}^{\infty} \eta^2\, dx\,. \tag{1.94}$$

  It follows from this that the vertical coordinate of the centre of gravity of the wave is constant.

- As a third invariant integral BOUSSINESQ finds [7]

$$M = \int_{x_0}^{\infty} \frac{d\eta^2}{dx^2} - 3\frac{\eta^3}{h^3}\, dx\,. \tag{1.95}$$

  which he calls *Momeni d'instabilité*.

Using M and the velocity of the form invariant *l'onde solitaire* BOUSSINESQ computes the wave profile. By assuming

$$c = g\,(h + \eta_{max})\,, \tag{1.96}$$

in which η_{max} is at first arbitrary but constant, equation (1.91) can be integrated. Imposing the motion u_0 at infinity he obtains the two solutions [8]

$$\frac{\eta_{max}}{\eta} = \begin{cases} \text{coshyp}^2\left(\frac{1}{2}\sqrt{\frac{3}{h^3}\eta_{max}}\,(x - u_0)\right) \\ \text{-sinhyp}^2\left(\frac{1}{2}\sqrt{\frac{3}{h^3}\eta_{max}}\,(x - u_0)\right) \end{cases} \tag{1.97}$$

For a given wave energy E and a given volume Q the amplitude of the wave η_{max} becomes as $x_0 \to -\infty$

$$\eta_{max} = \frac{3}{16}\frac{Q^2}{h^3} = \frac{3}{4}\frac{\sqrt[3]{E^2}}{4h}\,, \tag{1.98}$$

where the energy and the volume of the solitary wave are connected by

$$E = \frac{Q^3}{8h} \tag{1.99}$$

[7] BOUSSINESQ writes $d\eta^2/dx^2$ and means $(d\eta/dx)^2$.

[8] coshyp and sinhyp are hyperbolic functions, same as cosh or sinh

in which h is the water depth.

h) Lord Rayleigh

J. W. STRUTT (known as LORD RAYLEIGH) asked himself in 1876 [52] whether a wave could exist in a channel that is long and flat in comparison to the water depth and is also maintaining its form. To this end he assumed a counter flow with the same velocity with which the wave was moving. The wave is thus stationary at a fixed place. RAYLEIGH shows that the wave speed c cannot equal $\sqrt{gh}$, since pressure fluctuations would arise at the free surface which would induce a motion thus contradicting stationarity. A development of the velocity components [9] u and v in the form

$$\begin{aligned} u &= \cos\left(y\frac{d}{dx}\right) f(x) = f(x) - \frac{y^2}{1\cdot 2} f''(x) + \cdots, \\ -v &= \sin\left(y\frac{d}{dx}\right) f(x) = yf'(x) - \frac{y^3}{1\cdot 2\cdot 3} f'''(x) + \cdots \end{aligned} \tag{1.100}$$

satisfies the LAPLACE equation

$$\frac{d^2u}{dx^2} + \frac{d^2v}{dy^2} = 0 \tag{1.101}$$

of an irrotational incompressible fluid. Furthermore, the stream function ψ that obeys the relations

$$u = \frac{d\psi}{dy}, \tag{1.102}$$

$$v = -\frac{d\psi}{dx}, \tag{1.103}$$

must then have the form

$$\psi = yf - \frac{y^3}{1\cdot 2\cdot 3} f'' + \frac{y^5}{1\cdot 2\cdot 3\cdot 4\cdot 5} f^{IV} - \cdots \tag{1.104}$$

The function $f(x)$ describes the velocity at the bottom

$$u(x,0,t) = f(x), \tag{1.105}$$

and the pressure P at the free surface must fulfil the equation

$$-2\frac{p-P}{\rho} = 2g\eta + u^2 + v^2, \tag{1.106}$$

with

$$P = \text{const.} \tag{1.107}$$

Given these relations it is RAYLEIGH's intention to try to make the expression $p - P$ constant by accordingly choosing η. If the expressions (1.100) are substituted into (1.106), and $u^2 + v^2 = (1 + y'^2)u^2$ is accounted for, an equation is obtained which

[9] See footnote on page 28.

permits successive elimination of f from it and from expression (1.104) for the streamfunction ψ. What emerges is the representation

$$\psi\left(1-\frac{\eta^2}{3}\left(\frac{1}{\eta}\right)''-\frac{\eta^5}{45}\left(\frac{1}{\eta}\right)^{IV}-\cdots\right)=\sqrt{\frac{\bar{\omega}\eta^2-2g\eta^3}{1+\eta'^2}}, \tag{1.108}$$

with

$$\bar{\omega}=-2\frac{p-P}{\rho}. \tag{1.109}$$

Squareing and neglecting terms of order four yields

$$\psi^2\left(1-\frac{1}{3}\eta'^2+\frac{2}{3}\eta\eta''\right)=\bar{\omega}\eta^2-2g\eta^3, \tag{1.110}$$

which can now be integrated subject to the boundary conditions at the undisturbed water level ($x\to\infty$)

$$\psi = u_0 h, \tag{1.111}$$

$$\bar{\omega} = u_0^2+2gh. \tag{1.112}$$

Via this integration RAYLEIGH obtains an expression for the wave speed $u_0=c$,

$$c^2=g(h+\eta), \tag{1.113}$$

and the free surface elevation η with amplitude η_{max} [10]

$$\left(\frac{d\eta}{dx}\right)^2+\frac{3}{h^2(h+\eta_{max})}(\eta-h)^2(\eta-(h+\eta_{max}))=0. \tag{1.114}$$

This equation contains the following general informations:

1. η possesses two extrema, a minimum at $\eta=h$ and a maximum at $\eta=h+\eta_{max}$.
2. To each maximum waveheight there exists one and only one wave.
3. There is no negative solitary wave.
4. The free surface $\eta(x)$ is symmetric with respect to $x=0$. Integration of (1.114) yields

$$\pm x = \sqrt{\frac{h^2(h+\eta_{max})}{3\eta_{max}}} \times\ln\left(\frac{2\eta_{max}}{\eta-h}-1+2\sqrt{\frac{\eta_{max}^2}{(\eta-h)^2}-\frac{\eta_{max}}{\eta-h}}\right). \tag{1.115}$$

[10] An equation of the same form was also obtained and solved by BOUSSINESQ, see (1.97), so that the solution can be written in the form

$$\eta=\eta_{max}\,\mathrm{sech}^2\left(\frac{1}{2}\sqrt{\frac{3\eta_{max}}{h^2(h+\eta_{max})}}x\right).$$

5. The solitary wave is infinitely long i. e. the waveheight decreases continuously, but never reaches the undisturbed water level exactly.

6. The wave breaks if the particle velocity (of the stationary wave) reaches the wave speed c.

In order to arrive at a finite wavelength RAYLEIGH takes the length between points where the amplitude ratio $(\eta - h)/\eta_{max}$ is given by a prescribed value. This length x he calls *effective wavelength* and computes it to be

$$\frac{\eta - h}{\eta_{max}} = \frac{1}{10} \Rightarrow \frac{x}{h} = 2.1\sqrt{1 + \frac{h}{\eta_{max}}}. \tag{1.116}$$

i) De Saint-Venant

DE SAINT-VENANT [14] considers in 1885 an infinitely long horizontal channel. He starts from the volume conservation law of a rectangular fluid element

$$\frac{du}{dx} + \frac{dv}{dy} = 0, \tag{1.117}$$

and its dynamical equilibrium

$$\frac{1}{\rho}\frac{dp}{dx} = -u', \tag{1.118}$$

$$\frac{1}{\rho}\frac{dp}{dy} = -g - v', \tag{1.119}$$

in which the primed quantities are given by

$$u' = \frac{du}{dt} + u\frac{du}{dx} + v\frac{du}{dy}, \; etc. \tag{1.120}$$

and denote the total derivatives. At the fluid boundaries one has [11] .

$$\left.\begin{array}{rcl} v &=& \dfrac{d\eta}{dt} + u\dfrac{d\eta}{dx}, \\ p &=& 0, \end{array}\right\} \quad \text{for} \quad y = h + \eta, \qquad \begin{array}{rcl} v &=& 0, \end{array} \quad \text{for} \quad y = 0. \tag{1.121}$$

With the definition of a mean velocity in the direction of the channel

$$U = \frac{1}{h + \eta}\int_0^{h+\eta} u\, dy. \tag{1.122}$$

The equation of conservation of volume can also be deduced by means of the following considerations: During a time increment dt the volume $(h + \eta)\, dx$ between the places x and $x + dx$ is changed by

$$\frac{d(h + \eta)}{dt}\, dx\, dt. \tag{1.123}$$

[11] See footnote on page 28.

This increase in volume equals the change in volume flux $(h+\eta)\,U\,dt$ between x and $x+dx$

$$\left((h+\eta)U + \frac{d(h+\eta)U}{dx}dx\right)\,dt\,. \tag{1.124}$$

Because h is constant, he obtains from equations (1.123) and (1.124)

$$\frac{d\eta}{dt} + \frac{d(h+\eta)U}{dx} = 0\,. \tag{1.125}$$

DE SAINT-VENANT assumes now that η is small in comparison to h and that u differs only slightly from U. Then, the following equation holds

$$\frac{d\eta}{dt} + h\frac{dU}{dx} = 0\,. \tag{1.126}$$

By integrating the continuity equation in which $u = U$ and by satisfying the boundary condition at the free surface, the vertical velocity distribution

$$v = \frac{d\eta}{dt}\frac{y}{h} \tag{1.127}$$

is obtained which is a linear function of the distance from the bottom. By ignoring quadratic terms involving η and $d\eta$ he deduces the relation

$$v' = \frac{dv}{dt} = \frac{d^2\eta}{dt^2}\frac{y}{h}\,. \tag{1.128}$$

Substituting this into (1.119) yields an expression for dp/dy which can be integrated to yield (to the same order of approximation) the pressure distribution

$$\frac{p}{\rho} = g(h+\eta-y) + \frac{d^2\eta}{dt^2}\frac{h^2-y^2}{2h}\,. \tag{1.129}$$

In much the same way as in (1.128) DE SAINT-VENANT deduces

$$u' = \frac{dU}{dt} + U\frac{dU}{dx}\,, \tag{1.130}$$

and derives with the aid of (1.129) and (1.118), again by dropping second order terms,

$$\frac{dU}{dt} + U\frac{dU}{dx} + g\frac{d\eta}{dx} + \frac{h}{3}\frac{d^3\eta}{dt^2dx} = 0\,. \tag{1.131}$$

Assuming the representation $\eta = \eta(x-ct)$ and $U = U(x-ct)$, which are appropriate for waves of permanent form, and substituting these expressions into (1.125) and (1.131) he obtains for the wave speed the expression

$$c^2 = gh\left(1 + \frac{3}{2}\frac{\eta}{h} + \frac{h^2}{3\eta}\frac{d^2\eta}{dx^2}\right)\,. \tag{1.132}$$

He assumes the relation

$$c^2 = g(h+\eta_{max})\,, \tag{1.133}$$

with the as yet undetermined constant η_{max}, which *a posteriori* will be shown to be the maximum waveheight of the solitary wave. An integration of (1.132) yields

$$\left(\frac{d\eta}{dx}\right)^2 = \frac{3\eta^2(\eta_{max}-\eta)}{h^3}, \tag{1.134}$$

$$\Rightarrow \frac{\eta_{max}}{\eta} - \frac{1}{2} = \frac{1}{2}\cosh\left(\sqrt{\frac{3\eta_{max}}{h^3}}(x-ct)\right), \tag{1.135}$$

whence the same solution as found previously by BOUSSINESQ. The solitary wave is therefore symmetric about its maximum η_{max}.

Next DE SAINT-VENANT considers the volume of a solitary wave

$$q = \int_x^\infty \eta\, dx. \tag{1.136}$$

From it he deduces

$$\frac{dq}{dx} = -\eta \;\Rightarrow\; \frac{d\eta}{dx} = \frac{d\eta}{dq}\frac{dq}{dx} = -\eta\frac{d\eta}{dq}, \tag{1.137}$$

and with (1.134) it follows that

$$\frac{d\eta}{dq} = \sqrt{\frac{3}{h^3}}\sqrt{\eta_{max}-\eta} \;\Rightarrow\; \sqrt{\eta_{max}} - \sqrt{\eta_{max}-\eta} = \frac{1}{2}\sqrt{\frac{3}{h^3}}\,q. \tag{1.138}$$

Owing to the symmetry properties the entire volume of the wave is then,

$$Q = \int_{-\infty}^{\infty}\eta\, dx = 2\int_{x_0}^{\infty}\eta\, dx \tag{1.139}$$

in which x_0 is the coordinate where the maximum η_{max} arises. Thus,

$$\sqrt{\eta} = \frac{1}{2}\sqrt{\frac{3}{h^3}}\frac{Q}{2} \;\Rightarrow\; \eta_{max} = \frac{3}{16}\frac{Q^2}{h^3}, \tag{1.140}$$

and consequently,

$$\eta = \frac{3}{4h^3}q(Q-q). \tag{1.141}$$

DE SAINT-VENANT determines the particle trajectories by considering the positions of a water particle underneath the surface at time $t = -\infty$, when the particle is in front of the wave and at a later time, when it has been displaced by the action of the wave. When the wave passes the molecule it is transported a horizontal distance of magnitude ξ. Because the horizontal velocity is assumed constant over the entire depth h, a volume $h\xi$ is 'displaced' which must manifest itself as a wave hump. Therefore

$$q = h\xi. \tag{1.142}$$

Together with relation (1.141) it is seen that the trajectory of a particle sitting on the free surface traces a parabola. With this equation, DE SAINT-VENANT gives

the trajectory of a molecule on the free surface only; at lower depths one may easily deduce from (1.127) and $\int v\,dt = \zeta$, that in a moving system $\zeta = \eta y/h$, implying that trajectories at lower depths become more shallow and degenerate at the channel bottom $y = 0$ to straight lines.

j) McCowan

STOKES' critique that the decay of the height of a solitary wave cannot be traced back to wall friction and viscosity is responded by MCCOWAN [53] in 1891 with a renewed attempt of a wave theory. Stream function ψ and velocity potential ϕ can be written in complex form

$$\psi + \imath\phi = -c\cdot(y + \imath x) + f(y + \imath x)\ . \tag{1.143}$$

where c is the wave speed. A solitary wave cannot be periodic in x, it must be continuous and possess a finite waveheight in the entire fluid and a vanishing or finite amplitude as $x \to \pm\infty$, which is independent of x and y. The function

$$f(y + \imath x) = \sum_{i=0}^{i=\infty} a_{2i+1} \tan^{2i+1}\left(\frac{1}{2}k(y + \imath x)\right)\ , \tag{1.144}$$

in which $ky < \pi$ fulfils these conditions. MCCOWAN studies the lowest order approximation, in which only the first term of the above expansion is taken into account and finds with $a_1 = a$

$$\psi + \imath\phi = -c(y + \imath x) + ca\tan\left(\frac{1}{2}k(y + \imath x)\right)\ , \tag{1.145}$$

with the imaginary part

$$\phi = -cx + ca\frac{\sinh kx}{\cos ky + \cosh kx}, \tag{1.146}$$

and the real part

$$\psi = -cy + ca\frac{\sin ky}{\cos ky + \cosh kx}\ . \tag{1.147}$$

At the mean water depth $y = h$ which equals the depth for $x \to \infty$ he obtains the condition

$$\psi = -ch\,, \tag{1.148}$$

and for an elevated water level η above the mean level, he obtains

$$\psi + cy = c\eta\,. \tag{1.149}$$

Altogether, the equation of the free surface η obtains

$$\eta = a\frac{\sin k(h+\eta)}{\cos k(h+\eta) + \cosh kx}\,, \tag{1.150}$$

with the maximum of the wave $\eta = \eta_{max}$ at $x = 0$. With the aid of (1.146), (1.147) and by considering (1.150) MCCOWAN then computes the total velocity $u^2 + v^2$. With the condition

$$u^2 + v^2 = c^2 - 2g\eta \tag{1.151}$$

valid at the free surface, he obtains to within terms of order $O(\eta^3)$

$$c^2 = \frac{g}{k}\tan kh\,, \tag{1.152}$$

$$ka = \frac{2}{3}\sin^2 k(h+\frac{2}{3}\eta_{max})\,. \tag{1.153}$$

Since the right hand side of equation (1.153) is positive, no negative solitary wave can exist.

In a communication, STOKES [82] and LAMB [46] §252, will show that the velocity of the solitary wave

$$c^2 = \frac{g}{k}\tan kh \tag{1.154}$$

is an exact equation. To show this they assume a form of the velocity potential at a position x in front of the wave (i. e. a boundary condition at $x \to \infty$), see also (1.47) for a wave travelling only in the positive x-direction

$$\phi = A\,e^{-k(x-ct)}\cos ky\,. \tag{1.155}$$

This assumption satisfies the equation of the fluid $\nabla^2\phi = 0$ and the condition on the free surface $y = h$

$$\frac{d^2\phi}{dt^2} + g\frac{d\phi}{dy} = 0 \tag{1.156}$$

provided the condition (1.154) holds.

In MCCOWAN's approximation the pressure distribution at the free surface is not constant. But his solution is improved because the pressure is constant at the maximum and at the boundaries. The amendment was reached with the improved value $k(h+\frac{2}{3}\eta_{max})$ in equation (1.153) instead of kh. The free surface is determined by three parameters a, k, η_{max}, two of which can be eliminated, if kh is assumed so small that higher order terms in kh can be ignored. In equation (1.150) and (1.153) MCCOWAN thus expands the right hand sides in terms of powers of kh and, on dropping terms of higher than linear order, obtains

$$\eta = \eta_{max}\mathrm{sech}^2\left(\frac{1}{2}kx\right)\,, \tag{1.157}$$

$$k^2 = \frac{3\eta_{max}}{h^3}\,, \tag{1.158}$$

which agrees with the solution (1.97) found by BOUSSINESQ. RAYLEIGH obtained

$$k^2 = \frac{3\eta_{max}}{h^2(h+\eta_{max})}\,, \tag{1.159}$$

see footnote on page 38. MCCOWAN finds as the next approximation of equation (1.153) accurate to order $O(k^2h^2)$

$$\eta = \eta_{max}\mathrm{sech}^2\frac{1}{2}kx\,, \tag{1.160}$$

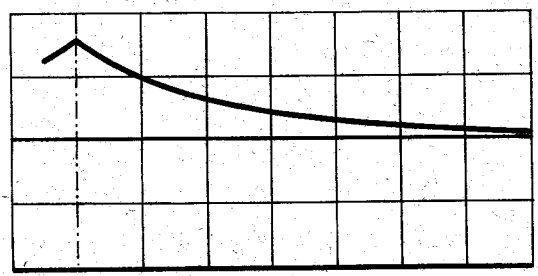

Figure 4: *Form of the wave according to* McCowan *[54]. The wave is symmetric relative to its crest. There the tangents to the surface intersect at* 120^0. *The heavier line represents the channel bottom; the mean water depth is that line which is approached asymptotically by the wave. The maximum wave height is* $0.78h$.

$$k^2 = \frac{3\eta_{max}}{h^2\left(h+\frac{19}{12}\eta_{max}\right)}, \tag{1.161}$$

$$c^2 = gh\left(1+\frac{1}{3}k^2h^2\right). \tag{1.162}$$

and regards it *natural to take for the wave-length*

$$\lambda = \frac{2\pi}{k} \Rightarrow \lambda = 2\pi\sqrt{\frac{h^2}{3\eta_{max}}\left(h+\frac{19}{12}\eta_{max}\right)}. \tag{1.163}$$

The wave starts to break, when $\lambda = 2\pi/k = 2\pi h$, whence $kh = 1$. With regard to the motion of the fluid particles McCowan remarks that the horizontal component of the particle velocity is nearly constant for all particles which are situated on a vertical line, whereas the vertical component is approximately linearly growing with the distance from the bottom. Therefore, the particle trajectories are nearly parabolic. A particle at a distance y_0 from the bottom moves approximately along the trajectory

$$(x-a)^2 + 2ay\cot ky_0 = a^2. \tag{1.164}$$

In a further article [54] McCowan searches for the maximum reachable wave-height of a solitary wave. First he shows that at the crest the tangents to the free surface cross at an angle of 120^0 (see figure 4). The highest amplitude that can be reached is

$$\eta_{max} = 0.78h. \tag{1.165}$$

In summary we may state: The method to force the solitary wave into a stationary configuration by indroducing a counter flow, did not permit with all certainty the inference of the existence of a wave with invariant form. One had not yet succeeded to determine the counter flow in such a way that the pressure at the free surface was everywhere constant.

k) Korteweg & de Vries

KORTEWEG & DE VRIES [40] circumvent this problem also by considering a counter flow but not requiring that the wave is perfectly still in this moving coordinate system. With the expansion (1.100) that was already used by RAYLEIGH, an irrotational, incompressible fluid is analysed and the expansion of the velocity components are studied. With regard to the boundary conditions they request at *each* order of approximation that the pressure variations are minimal. On the free surface they also incoporate a surface tension T [12]

$$p = p_0 - T\frac{\partial^2 \eta}{\partial x^2}, \tag{1.166}$$

where p_0 is the atmospheric pressure and

$$\frac{p}{\rho} = \chi(t) - \frac{\partial \phi}{\partial t}\frac{1}{2}\left(u^2 + v^2\right) - g\eta, \tag{1.167}$$

where $\chi(t)$ is an arbitrary function left undetermined. Obviously the kinematic surface condition

$$-u\frac{\partial \eta}{\partial x} + v - \frac{\partial \eta}{\partial t} = 0 \tag{1.168}$$

must also be satisfied. A successive approximation is now performed, and as a first approximation the relations

$$\eta = C_1 + \eta_0, \tag{1.169}$$
$$f = C_2 + f_0, \tag{1.170}$$

are assumed, in which $C_1 = h$, $C_2 = \sqrt{gh}$ are constant and $\eta_0(x,t)$, $f_0(x,t)$ are assumed to be sufficiently small. With the series (1.100) for u and v it follows from equations (1.167) and (1.168) to lowest order that

$$\sqrt{gh}\frac{\partial f_0}{\partial x} + \frac{\partial f_0}{\partial t} + g\frac{\partial \eta_0}{\partial x} = 0, \tag{1.171}$$
$$\sqrt{gh}\frac{\partial \eta_0}{\partial x} + \frac{\partial \eta_0}{\partial t} + h\frac{\partial f_0}{\partial x} = 0. \tag{1.172}$$

Stationary solutions must obey the relations

$$\frac{d\eta_0}{dt} = \frac{df_0}{dt} = 0, \tag{1.173}$$

and is selected in the form

$$f_0 = -\frac{\sqrt{gh}}{h}(\eta + \alpha), \tag{1.174}$$

with $\alpha = const.$ and small. A variation of α will result in a variation of the velocity. This solution corresponds to a long wave with uniform horizontal and vanishing vertical fluid velocity. With a horizontal counter flow of the same magnitude, f_0,

[12] For the partial derivative these authors use the symbol ∂. This way of writing partial derivatives was already used by MCCOWAN in 1894.

the wave is kept stationary at a fixed position. In other words, only waves are considered which are moving with the same velocity and in one direction only.

If in lieu of the first approximation for f the next higher approximation is chosen,

$$f = C_2 + f_0 + f_1 = \sqrt{gh} - \sqrt{\frac{g}{h}}(\eta + \alpha + \gamma), \tag{1.175}$$

in which necessarily $\eta > \alpha > \gamma$, KORTEWEG and DE VRIES deduce on using equations (1.169) and (1.175), the equations of the second approximation. By eliminating γ among the resulting equations, they obtain (instead of η_0 we write for simplicity η)

$$\frac{\partial \eta}{\partial t} = \frac{3}{2}\sqrt{\frac{g}{h}}\frac{\partial\left(\frac{1}{2}\eta^2 + \frac{2}{3}\alpha\eta + \frac{1}{3}\vartheta\frac{\partial^2\eta}{\partial x^2}\right)}{\partial x}, \tag{1.176}$$

$$\vartheta = \frac{h^3}{3} - \frac{Th}{\rho g}. \tag{1.177}$$

Stationary solutions of equation (1.176) for which the left hand side must vanish are obtained by integrating its right hand side, this results in a positive solitary wave. In this process they choose $2\alpha = -\eta_{max}$ and impose the boundary conditions $\eta = \partial\eta/\partial x = \partial^2\eta/\partial x^2 = 0$, as $x \to \infty$. Performing this integration yields

$$\eta = \eta_{max}\mathrm{sech}^2\left(x\sqrt{\frac{\eta_{max}}{4\vartheta}}\right). \tag{1.178}$$

For $2\alpha = \eta_{max}$ KORTEWEG & DE VRIES obtain a negative wave

$$\eta = -\eta_{max}\mathrm{sech}^2\left(x\sqrt{\frac{\eta_{max}}{-4\vartheta}}\right). \tag{1.179}$$

In view of (1.177) such a solitary wave is only possible if

$$h < \sqrt{\frac{3T}{\rho g}} \tag{1.180}$$

is satisfied. This limit depth of stationary water waves is $0.47cm$ ($T = 0.072N/m$ at 20^0C).

KORTEWEG & DE VRIES obtain periodic *cnoidal* waves [13] by imposing the boundary conditions in a wave trough, $\partial\eta/\partial x = 0$, instead at the undisturbed water level. With these altered boundary conditions they obtain

$$\eta = H\mathrm{cn}^2\left(x\sqrt{\frac{H+K}{4\vartheta}}\right), \tag{1.181}$$

[13] cn denotes the JACOBI elliptic function which possesses a single zero in c and a simple pole in n. The values c and n follow from ARGAND's [1] diagram.

in which H is the maximum amplitude (wave-height above the water line) and $K > h$ corresponds to a wave trough. When $K = 0$ and $H = \eta_{max}$ the solitary wave is obtained.

From the equations of the second approximation which are not stated here, γ can be determined. With it, f is fully known. The particle velocity of a cnoidal wave is then given by

$$\begin{aligned} u &= \sqrt{gh} - \sqrt{\frac{g}{h}}\left\{\eta + \frac{K-H}{2} - \frac{\eta^2}{4(h-K)}\right. \\ &\quad \left. + \left(\frac{1}{h-K} + \frac{T}{2\rho g\vartheta}\right)\left((H-K)\eta + \frac{HK}{2} - \frac{3}{2}\eta^2\right)\right\} \\ &\quad + \frac{1}{2\vartheta}\sqrt{\frac{g}{h-K}}\left((H-K)\eta + \frac{HK}{2} - \frac{3}{2}\eta^2\right)y^2 + \cdots, \end{aligned} \tag{1.182}$$

$$v = \sqrt{\frac{g\eta(H-\eta)(K+\eta)}{(h-K)\vartheta}}\,y. \tag{1.183}$$

The wave speed of the solitary wave corresponds to the velocity at the boundary as $x \to \infty$

$$c = \sqrt{gh}\left(1 + \frac{\eta_{max}}{2h}\right). \tag{1.184}$$

If according to STOKES the speed of the wave is given as that speed c for which the horizontal momentum vanishes (see equation (1.64)), KORTEWEG & DE VRIES obtain for a cnoidal wave

$$c = \sqrt{\frac{g}{h-K}}\left(\eta + K - \sqrt{2(K+H)\vartheta}\,\frac{E(K)}{\lambda}\right). \tag{1.185}$$

This equation contains three parameters K, H and λ by which the cnoidal wave is determined. $E(K)$ denotes the complete elliptic integral of the second kind.

Neglecting surface tension a successive approximation up to third order yields for the wave speed of the solitary wave

$$c^2 = g(h-K)\left(1 + \frac{H-K}{h-K} - \frac{1}{20}\frac{(H-K)^2}{(h-K)^2} - \frac{33}{40}\frac{HK}{(h-K)^2}\right), \tag{1.186}$$

or

$$c = \sqrt{g(h-K)}\left(1 + \frac{H-K}{h-K} - \frac{3}{20}\frac{(H-K)^2}{(h-K)^2} - \frac{33}{40}\frac{HK}{(h-K)^2}\right), \tag{1.187}$$

and the form of the free surface is given by

$$\eta = \left(1 - \frac{3(H-K)}{4(h-K)}\right)\eta_1 + \frac{3}{4(h-K)}\eta_1^2, \tag{1.188}$$

$$\eta_1 = H\mathrm{cn}^2\left(\frac{1}{2}\left(1 - \frac{5(H-K)}{8(h-K)}\right)x\sqrt{\frac{3(H+K)}{(h-K)^3}}\right) \tag{1.189}$$

which for the case of a solitary wave (with $K = 0$ and $H = \eta_{max}$) reduces to

$$\eta = \left(1 - \frac{3\eta_{max}}{4h}\right)\eta_1 + \frac{3}{4h}\eta_1^2, \tag{1.190}$$

$$\eta_1 = \eta_{max}\mathrm{sech}^2\left(\frac{1}{2}\left(1 - \frac{5\eta_{max}}{8h}\right)x\sqrt{\frac{3\eta_{max}}{h^3}}\right). \tag{1.191}$$

With this article by KORTEWEG & DE VRIES the century of wave theory in channels terminates. The analyses are continued with questions concentrating on how higher order approximations can be obtained, and one also searches for a mathematical proof of the existence of a wave with permanent form; more specifically, attempts are made to clarify the question whether an exact solution of a stationary wave of constant form does at all exist for the equations of an irrotational ideal fluid.

l) Friedrichs

An important contribution, introducing a ***systematic*** approximation procedure is given by FRIEDRICHS [21] in 1948. Starting with EULER's equations he obtains via a pertubation expansion the ***shallow water equations***. The computations are performed with stretched dimensionless variables (denoted by a hat $\hat{}$)

$$\begin{aligned} \hat{x} &= \sqrt{\frac{\kappa}{h}}x, & u &= \sqrt{gh}\,\hat{u}, \\ \hat{y} &= \frac{y}{h}, & v &= \sqrt{\frac{gh}{\kappa h}}\,\hat{v}, \\ \hat{t} &= \sqrt{gh}\sqrt{\frac{\kappa}{h}}t, & \eta &= h\hat{\eta}, \\ & & p &= \rho g h\hat{p}, \end{aligned} \tag{1.192}$$

subject to the conditions

$$\begin{aligned} \hat{\eta}(0,\hat{t}) &= 1, \\ \hat{\eta}_{\hat{x}}(0,\hat{t}) &= 0, \\ -1 \leq \hat{\eta}_{\hat{x}\hat{x}}(0,\hat{t}) &< 0\,. \end{aligned} \tag{1.193}$$

The following procedure is essentially a development in terms of the parameter $\sigma = \kappa h$, where κ is the maximum initial curvature of the free surface $\kappa = \eta_{xx}(0,0)$.

FRIEDRICHS employs the pertubation expansions

$$\hat{u} = \hat{u}^{(0)} + \sigma\hat{u}^{(1)} + \sigma^2\hat{u}^{(2)} + \cdots, \tag{1.194}$$

$$\hat{v} = \hat{v}^{(0)} + \sigma\hat{v}^{(1)} + \sigma^2\hat{v}^{(2)} + \cdots, \tag{1.195}$$

$$\hat{p} = \hat{p}^{(0)} + \sigma\hat{p}^{(1)} + \sigma^2\hat{p}^{(2)} + \cdots, \tag{1.196}$$

$$\hat{\eta} = \hat{\eta}^{(0)} + \sigma\hat{\eta}^{(1)} + \sigma^2\hat{\eta}^{(2)} + \cdots, \tag{1.197}$$

and constructs the lowest order solution (σ^0). The continuity equation

$$\hat{v}_{\hat{y}} = -\sigma\hat{u}_{\hat{x}} \tag{1.198}$$

yields to lowest order

$$\hat{v}_{\hat{y}}^{(0)} = 0 \Rightarrow \hat{v}^{(0)}, \tag{1.199}$$

and the equation of irrotational flow

$$\hat{u}_{\hat{y}} - \hat{v}_{\hat{x}} = 0 \tag{1.200}$$

leads to

$$\hat{u}_{\hat{y}}^{(0)} = 0 \Rightarrow \hat{u}^{(0)} = \hat{u}^{(0)}(\hat{x}). \tag{1.201}$$

The balance equations of momentum

$$\hat{v}\hat{u}_{\hat{y}} = -\sigma\left(\hat{u}_{\hat{t}} + \hat{u}\hat{u}_{\hat{x}} + \hat{p}_{\hat{x}}\right), \tag{1.202}$$

$$\hat{v}\hat{v}_{\hat{y}} = -\sigma\left(\hat{v}_{\hat{t}} + \hat{u}\hat{v}_{\hat{x}} + \hat{p}_{\hat{y}} + 1\right), \tag{1.203}$$

imply a hydrostatic pressure distribution in the form

$$\hat{p}_{\hat{y}}^{(0)} = -1 \Rightarrow \hat{p}^{(0)} = \hat{\eta}^{(0)}(\hat{x}, \hat{t}) - \hat{y}, \tag{1.204}$$

where the zero pressure is assumed at the free surface $\hat{y} = \hat{\eta}(\hat{x}, \hat{t})$. The kinematic boundary condition

$$\hat{v} = \sigma(\hat{\eta}_{\hat{t}} + \hat{u}\hat{\eta}_{\hat{x}}), \tag{1.205}$$

becomes in the lowest approximation

$$\hat{v}^{(1)} = \hat{\eta}_{\hat{t}}^{(0)} + \hat{u}^{(0)}\hat{\eta}_{\hat{x}}^{(0)}. \tag{1.206}$$

Hence $\hat{v}^{(1)}$ cannot be dropped because it is determined by quantities of lowest order as can be seen from the first order terms in the continuity equation

$$\hat{v}_{\hat{y}}^{(1)} = -\hat{u}_{\hat{x}}^{(0)} \Rightarrow \hat{v}^{(1)} = -\hat{y}\hat{u}_{\hat{x}}^{(0)}. \tag{1.207}$$

Thus, the lowest order version of the free surface equation is given by

$$\hat{\eta}_{\hat{t}}^{(0)} + (\hat{u}^{(0)}\hat{\eta}^{(0)})_{\hat{x}} = 0. \tag{1.208}$$

All in all, when reverting to the original coordinates, the shallow water equations for long waves read

$$\eta_t + (u\eta)_x = 0, \tag{1.209}$$

$$u_t + uu_x^{\cdot} + g\eta_x = 0, \tag{1.210}$$

$$p = \rho g(\eta - y). \tag{1.211}$$

This method can dispense us with any physical assumptions except that σ must be small. FRIEDRICHS is convinced that with his method also higher approximations can be deduced, but he does not go any further. STOKER [79] shows that the parameter σ can equally be defined as the ratio of a typical vertical length h and a typical horizontal length λ: $\sigma = h^2/\lambda^2$. The physical interpretation, however, corresponds to that of FRIEDRICHS.

m) Waves of order $O((\eta_0/h)^n)$

In the same year KELLER [38] obtains the next higher approximation, linear in σ. The solution of the governing equation yields cnoidal and solitary waves. Thereby the solitary wave is characterized as a wave with an infinitely long wave length,

$$\eta = h + \eta_0 \text{sech}^2\left(\frac{\sqrt{3}x}{2h}\left(\frac{\eta_0}{h}\right)^{\frac{1}{2}}\right), \tag{1.212}$$

in which

$$p = \rho g(\eta + h - y), \tag{1.213}$$

$$v = 0, \tag{1.214}$$

$$\frac{u}{\sqrt{gh}} = \frac{1}{2}(\eta_0 + 2h) - \eta_0 \text{sech}^2\left(\frac{\sqrt{3}x}{2h}\left(\frac{\eta_0}{h}\right)^{\frac{1}{2}}\right), \tag{1.215}$$

$$\lambda = \infty. \tag{1.216}$$

η_0 denotes a characteristic length which here is set equal to η_{max}; henceforth it will no longer equal the wave amplitude but still be indicative of its order of magnitude.

To lowest order the solution of permanent form is thus independent of σ and piecewise constant (representing a shock wave, or a bore).

The next higher approximation is obtained by LAITONE [45]. Meanwhile, in this process of systematic approximation, the differential equations have become so long that we shall refrain from stating them. Also for the first time, the pressure distribution in the fluid is no longer hydrostatic:

$$\frac{p}{\rho g h} = \frac{\eta - y}{h} - \frac{3}{4}\left(\frac{\eta_0}{h}\right)^2\left(2\frac{y}{h} + \frac{y^2}{h^2}\right)(2\text{sech}^2 A - 3\text{sech}^4 A) + O\left(\frac{\eta_0}{h}\right)^3 \tag{1.217}$$

The form of the solitary wave and its speed are given by

$$\frac{\eta}{h} = 1 + \frac{\eta_0}{h}\text{sech}^2 A - \frac{3}{4}\left(\frac{\eta_0}{h}\right)^2 \text{sech}^2 A \cdot (1 - \text{sech}^2 A) + O\left(\frac{\eta_0}{h}\right)^3, \tag{1.218}$$

$$A = \frac{x}{h}\sqrt{\frac{3}{4}\frac{\eta_0}{h}}\left(1 - \frac{5}{8}\frac{\eta_0}{h}\right) + O\left(\frac{\eta_0}{h}\right)^{\frac{5}{2}}, \tag{1.219}$$

$$c = \sqrt{gh}\left(1 + \frac{1}{2}\frac{\eta_0}{h} - \frac{3}{20}\left(\frac{\eta_0}{h}\right)^2\right) + O\left(\frac{\eta_0}{h}\right)^3. \tag{1.220}$$

The speed c corresponds to the particle velocity at infinity $c = u(\infty)$. The wave speed, but no longer the form of the solitary wave agrees with that of KORTEWEG & DE VRIES. The highest solitary wave has an amplitude

$$\begin{aligned} \left(\frac{\eta_0}{h}\right)_{max} &= \frac{5}{7} = 0.714, \quad \text{for} \quad O\left(\frac{\eta_0}{h}\right)^2 \text{approximations,} \\ \left(\frac{\eta_0}{h}\right)_{max} &= \frac{8}{11} = 0.727, \quad \text{for} \quad O\left(\frac{\eta_0}{h}\right)^{\frac{5}{2}} \text{approximations.} \end{aligned} \tag{1.221}$$

$$
\begin{aligned}
\frac{\eta}{h} &= \overbrace{\frac{\eta_0}{h}\operatorname{sech}^2 A}^{Boussinesq[8]} \\
&\quad \overbrace{-\frac{3}{4}\left(\frac{\eta_0}{h}\right)^2 \operatorname{sech}^2 A \tanh A}^{Laitone[45]} \\
&\quad \overbrace{+\left(\frac{\eta_0}{h}\right)^3 \left(\frac{5}{8}\operatorname{sech}^2 A \tanh^2 A - \frac{101}{80}\operatorname{sech}^4 A \tanh^4 A\right)}^{Grimshaw[29]} + \cdots \\
A &= \frac{x}{h}\sqrt{\frac{3}{4}\frac{\eta_0}{h}\left(\overbrace{1}^{[8]} \overbrace{-\frac{5}{3}\frac{\eta_0}{h}}^{[45]} \overbrace{+\frac{71}{128}\left(\frac{\eta_0}{h}\right)^2}^{[29]} + \cdots\right)} \\
c &= \sqrt{gh}\left(\overbrace{1}^{[8]} + \overbrace{\frac{1}{2}\frac{\eta_0}{h}}^{[45]} \overbrace{-\frac{3}{20}\left(\frac{\eta_0}{h}\right)^2}^{[29]} + \frac{3}{56}\left(\frac{\eta_0}{h}\right)^3 + \cdots\right)
\end{aligned}
$$

Table 1: ***Shape and velocity of solitary water waves for various theories up to order three.***

This value describes the limit, above which the vertical velocity component does no longer monotonically increase. LAITONE remarks that in his experiments he could not observe waves with sharp crests of which tangents to the free surface were intersecting at an angle of 120^0. When the mentioned maximum wave heights are reached, the waves break unsymmetrically instead with a rounded wave crest.

Cnoidal waves reach the same maximum height as do the solitary waves. In this case the parameter η_0 in equation (1.221) is the total waveheight from the wave trough to the wave crest.

The same class of approximate solutions is also given by GRIMSHAW [29] who in 1971 constructs the solution up to third order $O((\eta_0/h)^3)$. (A clearer description of it can be found in [30].) A solution of ninth order $O((\eta_0/h)^9)$ was then computed by FENTON [20] 1972 and that of order 14 by LONGUET-HIGGINS & FENTON [51] in 1974. For the latter two solutions a computerized algebraic manipulation procedure (symbolic manipulation system) had to be employed. In Tables 1 and 2 the wave heights and wave speeds of the theories of the first, second, third and ninth order are listed.

With such approximate formulas, however the existence of a mathematical solitary wave solution is by no means demonstrated, and neither is an answer given to

Table 2: *Shape and velocity of the solitary wave of ninth order according to* FENTON *[20].*

$$\frac{\eta}{h} = 1 + \sum_{i=1}^{9} \sum_{j=1}^{i} \left(\frac{\eta_0}{h}\right)^{2i} b_{ij} \operatorname{sech}^{2i} Ax + O\left(\frac{\eta_0}{h}\right)^{10}$$

b_{ij}

$i =$	1	2	3	4	5	6	7	8	9
$j = 1$	1.000	−0.7500	0.6250	−1.36817	1.86057	−2.57413	3.4672	−4.6849	6.191
2	–	0.75	−1.8875	3.88033	−7.45136	13.2865	−22.782	37.670	−60.57
3	–	–	1.2625	−4.68304	12.7637	−31.1191	68.258	−139.28	269.84
4	–	–	–	2.17088	−11.4199	40.1068	−116.974	301.442	−712.125
5	–	–	–	–	4.24687	−28.4272	120.490	−411.416	1217.98
6	–	–	–	–	–	8.7280	−71.057	355.069	−1384.37
7	–	–	–	–	–	–	18.608	−180.212	1023.07
8	–	–	–	–	–	–	–	41.412	−450.29
9	–	–	–	–	–	–	–	–	90.279

$$A = \frac{x}{h}\sqrt{\frac{3}{4}\frac{\eta_0}{h}}\left(1 + \sum_{i=1}^{8} c_i \left(\frac{\eta_0}{h}\right)^{i}\right)$$

c_i

$i =$	1	2	3	4	5	6	7	8	9
	−0.625000	0.554688	−0.561535	0.567095	−0.602969	−0.624914	0.670850	0.700371	–

$$c^2 = gh\left(1 + \sum_{i=1}^{9} d_i \left(\frac{\eta_0}{h}\right)^{i}\right)$$

d_i

$i =$	1	2	3	4	5	6	7	8	9
	1.000000	−0.050000	−0.042857	−0.0342857	−0.0315195	−0.029278	0.026845	−0.030263	−0.021935

the question whether these expansions converge in any way to a true solution.

n) Existence proofs

The first proof of existence of a *periodic wave* in a fluid of finite depth goes back to STRUIK [83]. For cnoidal and solitary waves LAVRENT'EV [49] formulated existence conditions in 1954, and in the same year FRIEDRICHS & HYERS [22] did the same. Their proof rests on an iterative procedure. Starting from the CAUCHY-RIEMANN equations of an incompressible irrotational fluid they deduce an integral equation containing a parameter a which is essentially gh/c^2. Proof of the convergence of the solution is only achieved in case the independent horizontal variable ϕ is stretched with a and the vertical variable ψ is left unchanged. The independent variables are the velocity potential ϕ and the stream function ψ:

$$u = a u_1(a\phi, \psi) + a^2 u_2(a\phi, \psi) + \cdots \tag{1.222}$$

$$v = a v_1(a\phi, \psi) + a^2 v_2(a\phi, \psi) + \cdots \tag{1.223}$$

If a is sufficiently close to 1, but smaller than 1, then a symmetric solitary wave exists.

The connection between the exact wave equation and the equation of BOUSSINESQ and KORTEWEG-DE VRIES is brought by CRAIG [11] in 1985. He studies waves with typical amplitudes $\eta \ll h$ and typical wave lengths $\lambda \gg h$, for which $\eta\lambda^2/h = 1$, i. e. $\eta/h = (h/\lambda)^2 = \epsilon$. If the solution of the wave equation (CAUCHY-RIEMANN equations) for an irrotational incompressible fluid

$$\frac{\partial u}{\partial x} = -\frac{\partial v}{\partial y}, \tag{1.224}$$

$$\frac{\partial u}{\partial y} = \frac{\partial v}{\partial x}, \tag{1.225}$$

is substituted into the BOUSSINESQ equation, a small error proportional to ϵ^2 is encountered whose size depends on the particle motion. However, the initial values of these solutions need to be elements of the SOBOLEV space H^r, $r > 7$ [14]. Unfortunately with this nothing is said about the existence of exact solutions of the BOUSSINESQ equation which seems to approximate the CAUCHY-RIEMANN equations. In addition the BOUSSINESQ equation is ill posed, as typical solutions, like the cnoidal functions for the KORTEWEG-DE VRIES equation, do not exist.

On the other hand, the KORTEWEG-DE VRIES equation is a well posed problem. A solution of the CAUCHY-RIEMANN wave equations converges to a solution of the

[14] For a function f of a SOBOLEV space H^r, one has

$$f \in H^r : \|f(x)\|_{H,r}^2 \overset{\text{def}}{=} \sum_{|\alpha|<r} \int \left| \frac{\partial^\alpha f(x)}{\partial x^\alpha} \right|^2 dx < \infty$$

$$\Leftrightarrow \int \left(1 + |x|^2\right)^r |f(x)|\, dx < \infty,$$

that is, all derivatives up to and including order r exist and are r-fold quadratic integrable.

KORTEWEG-DE VRIES equation with an error of order ϵ^2, if the initial data also satisfy the KORTEWEG-DE VRIES equation, i. e. if the wave travels only in one direction.

With the aid of the theory of complex variables, CRAIG corroborates that the BOUSSINESQ equation forms an approximation of the CAUCHY-RIEMANN equations to order ϵ^2 and with the further reduction

$$\frac{\partial}{\partial t} \to \frac{\partial}{\partial t} - \frac{\partial}{\partial x} \tag{1.226}$$

it leads to the KORTEWEG-DE VRIES equation.

The connection between the BOUSSINESQ equation and the KORTEWEG-DE VRIES equation is made explicit in a review article by MIURA [60]. A similar transformation is also given by MILES [56]; unfortunately his starting equations are fraught with an error. Ensuing developments follow MIURA.

From the BOUSSINESQ equations (note the plural) (1.87)

$$u_t = -g\eta_x - \frac{1}{2}g\frac{\partial}{\partial x}\left(\frac{\eta^2}{h} + h^2\eta_{xx}\right), \tag{1.227}$$

$$\eta_t = -hu_x - c_0\frac{\partial}{\partial x}\left(\frac{\eta^2}{h} - \frac{h^2}{6}\eta_{xx}\right), \tag{1.228}$$

with $c_0 = \sqrt{gh}$, we eliminate u to obtain

$$\eta_{tt} - c_0^2\eta_{xx} = \frac{1}{2}\frac{\partial^2}{\partial x^2}\left(\frac{\eta^2}{h} + h^2\eta_{xx}\right) - c_0\frac{\partial^2}{\partial x \partial t}\left(\frac{\eta^2}{h} - \frac{h^2}{6}\eta_{xx}\right). \tag{1.229}$$

This equation is now restricted to solutions for which

$$\partial_x = -c_0\partial_t \tag{1.230}$$

holds, whence waves which only propagate in the positive x-direction. Substituting this into the right hand side one obtains the BOUSSINESQ equation (note the singular)

$$\eta_{tt} - c_0^2\eta_{xx} \stackrel{!}{=} c_0^2\frac{\partial^2}{\partial x^2}\left(\frac{3}{2}\frac{\eta^2}{h} + \frac{h^2}{3}\eta_{xx}\right). \tag{1.231}$$

If the same reduction is performed with the operator on the left hand side of the equation,

$$\partial_x^2 - c_0\partial_t^2 = (\partial_x + c_0\partial_t)(\partial_x - c_0\partial_t) = (\partial_x + c_0\partial_t)2\partial_x, \tag{1.232}$$

the dimensional version of the wave equation of the KORTEWEG-DE VRIES type is obtained

$$\eta_t + c_0\eta_x + \frac{3}{2}\frac{c_0}{h}\eta\eta_x + c_0\frac{h^2}{6}\eta_{xxx} = 0. \tag{1.233}$$

With the substitutions

$$\hat{t} = -\frac{1}{2}\sqrt{\frac{g}{h}}\sqrt{\frac{3}{h^3}}\,t, \tag{1.234}$$

$$\hat{x} = -\sqrt{\frac{3}{h^3}}\,x, \tag{1.235}$$

$$\hat{\eta} = \frac{1}{2}\eta + \frac{1}{3}h, \tag{1.236}$$

it transforms into

$$\hat{\eta}_{\hat{t}} + 6\hat{\eta}\hat{\eta}_{\hat{x}} + \hat{\eta}_{\hat{x}\hat{x}\hat{x}} = 0. \tag{1.237}$$

The KORTEWEG-DE VRIES equation (1.176), which was established for waves which propagate in the opposite (negative) direction reads

$$\eta_t = \frac{3}{2}\sqrt{\frac{g}{h}}\frac{\partial}{\partial x}\left(\frac{1}{2}\eta^2 + \frac{2}{3}\alpha\eta + \frac{1}{3}\vartheta\eta_{xx}\right), \tag{1.238}$$

and is transformed into the standard form (1.237) by using the substitutions

$$\hat{t} = -\frac{1}{2}\sqrt{\frac{g}{h}}\frac{1}{\sqrt{\vartheta}}\,t, \tag{1.239}$$

$$\hat{x} = \frac{x}{\sqrt{\vartheta}}, \tag{1.240}$$

$$\hat{\eta} = \frac{1}{2}\eta + \frac{1}{3}\alpha. \tag{1.241}$$

Let us return to the question how the various theories of long waves in shallow water are connected. Whereas AIRY postulated steepening waves, BOUSSINESQ found waves of permanent form. Both theories contain the linear wave theory as a limit theory for small amplitudes. The decisive contribution towards a clarification of this connection was brought by URSELL [88] in 1953. The prerequisites are

$$\begin{aligned} \frac{\eta}{h} &\ll 1, \quad O\left(\frac{\eta}{h}\right) = \sigma, \\ \frac{h^2}{\lambda^2} &\ll 1, \quad O\left(\frac{h^2}{\lambda^2}\right) = \epsilon. \end{aligned} \tag{1.242}$$

URSELL shows that the value of the ratio of ϵ and σ will decide upon to which theory an approximation of the equation of continuity and irrotationality will lead. In the limit as $\epsilon \to 0$, $\sigma \to 0$ one obtains the linear wave theory. When $\sigma \ll \epsilon$ a linear dispersive theory is obtained which does not admit any stationary solution other than periodic wave trains. In case $\sigma = \epsilon$ BOUSSINESQ's theory is obtained and when $\sigma \gg \epsilon$ AIRY's theory emerges (see figure 5). URSELL therefore calls the BOUSSINESQ equation the more general wave equation. The ratio

$$\frac{\sigma}{\epsilon} = \frac{\eta\lambda^2}{h^3} \tag{1.243}$$

is called URSELL number.

Figure 5: *Connection between the theories of* BOUSSINESQ, AIRY *and dispersive waves. Depending on the ratio of ϵ and σ the wave motion can be approximated by different theories.*

Up to this point two essential methods of approximating the differential equation for long and shallow waves were distinguished. The first method introduces two dimensionless parameters $\eta/h = \sigma$ and $h/\lambda = \epsilon$. Then an expansion of the velocity or the corresponding potential is performed up to a certain order. The equations of BOUSSINESQ, FRIEDRICHS, KELLER, LAITONE, GRIMSHAW and FENTON have been derived this way. In the second method a sinusoidal series is chosen as a solution. The coefficient of the first term η_0 and the wave number k must thereby be subjected to certain constraints. This method was developed by STOKES and used by RAYLEIGH and MCCOWAN.

An entirely different approach is taken by GREEN & NAGHDI [28] in 1976. They apply a variational principle to the continuity and EULER equations. SHIELDS & WEBSTER [77] deduce with it the equation of long waves in shallow water. The region occupied by the fluid (x^1, x^2, x^3) with arbitrary bottom contour $h(x^1, x^2, t)$ and free surface $\eta(x^1, x^2, t)$ is mapped onto a region between two parallel lines (x^1, x^2, s) with

$$-1 \leq s \leq +1\,, \tag{1.244}$$

$$s = 2\frac{x^3 - 0.5(h+\eta)}{\eta - h}\,. \tag{1.245}$$

Then it is assumed that the velocity field can be represented by

$$\mathbf{v}(x^1, x^2, x^3, t) = \sum_{n=0}^{m} \mathbf{W}_n(x^1, x^2, t) s^n\,. \tag{1.246}$$

However, this representation cannot simultaneously satisfy the continuity equation, the kinematic boundary conditions and the conservation of momentum. Therefore an integral is formed for the EULER equation (momentum balance) such that momentum is conserved in an averaged sense:

$$\begin{aligned} \int_h^\eta \left(\mathbf{v}_{,t} + v^i \mathbf{v}_{,i}\right) s^n \, dx^3 &= -\frac{1}{\rho}\int_h^\eta \left(p_{,i}\,\mathbf{e}_i + \rho g \mathbf{e}_3\right) s^n \, dx^3\,, \\ n &= 1, \ldots, m\,. \end{aligned} \tag{1.247}$$

This way SHIELDS and WEBSTER obtain a so call weak solution. This variational procedure goes back to KANTOROVICH. Depending on the choice of the counting index m one obtains m different systems of equations which must be solved numerically.

The solution is not necessarily irrotational. In addition the method makes no assumption on any parameter as is always the case if a pertubation approach is taken. An error estimate is, however, hard to obtain.

The method that leads to the complete solution of the nonlinear wave equation of the KORTEWEG-DE VRIES type, has been introduced by GARDNER, GREEN, KRUSKAL & MIURA [23] in 1967. They solve the KORTEWEG-DE VRIES equation to given initial data by transforming the original equation to a SCHRÖDINGER equation and searching for an inverse solution of this problem. This procedure is known

as *inverse scattering method* and will be introduced in chapter 4.

Finally, let us point the reader's attention to a few articles of the last few years, which provide a review to particular aspects of the illustrated problems. All articles quote a rich number of relevant literature.

The properties of the KORTEWEG-DE VRIES equation and the methods of its solution are summarized by MIURA [60]. A historical report about the work of BOUSSINESQ, KORTEWEG-DE VRIES and the method of inverse scattering, as well as some extensions of this equation are given by MILES [57]. The behaviour of solitary waves is studied by GRIMSHAW [30] and MILES [56]. GRIMSHAW describes in addition solitary waves in stratified fluids. A review about the various solution procedures of the wave equation is given by SCHWARTZ & FENTON [75]. They summarize results for deep and shallow water and provide a brief account of numerical methods.

1.2 Physical and mathematical models for the description of water waves induced by landslides

Two methods are common to describe the prediction of water waves induced by landslides. The first comprises a mathematical deductive procedure that is based on physical laws of mechanics. In its development essential mathematical and physical assumptions are involved through which a simple model law is obtained. The other, empirical method starts from the physical properties that are needed in a description of the processes of interest. By means of a dimensional analysis the minimum number of independent 'properties' is determined which is necessary owing to reasons of physical dimensionality to find the relevant functional relationships experimentally.

1.2.1 Physical models

a) Wiegel

A first empirical assessment is provided by TAKAHASHI [84] and JOHNSON & BERMEL [36]. WIEGEL [94] intends to simulate tsunamis (under water earthquakes) by under water landslides. To this end he makes various blocks (of triangular and cubic shape) to slide along an inclined (45^0) plane into a channel. The blocks possess the same width as does the channel. In a second series of experiments blocks of various weights are used which are vertically plunging into the channel. The initial position of the blocks was always chosen such that they were just immersing or kept at a prescribed depth underneath the water.

For the vertically falling blocks, WIEGEL finds that the wavelength of the induced wave is independent of the waterdepth, the initial depth of submergence of the body and the weight of the body. As regards the form of the generated wave he observes that directly above the body a wave trough is initially formed followed

by a wave hump of approximately the same height. Following the crest, the surface rapidly resumed its still-water position. At the first station ($x/h = 0.73 - 0.41$) immediately after the location of excitement ($x/h = 0$) a wave hump first forms followed by a trough and a second hump as well as a continuing wave tail. This wave is already dispersed at the second station ($x/h = 3.21 - 1.81$).

The waveform changes entirely if the body is extended by sidewalls such that they reach far above the water surface. In this case a single wave-hump and a single wave-trough were formed which travelled as a unity along the channel without dispersion. In other words, the wave is formed by both, the displaced water underneath the body and the confluent water masses above the body.

In all studied cases the wave speed depends on the wavelength and water depth. If in place of the body a plate of lead that is much thinner than the water is deep is plunging vertically into the water, then the wave speed $\sqrt{gh}$ of long waves is obtained. The Ursell number $\eta\lambda^2/(2h^3)$ of the first wave of the entire generated wave train is about 30. The waves are therefore of the AIRY type.

The wave-height depends primarily upon the weight of the submerged body, its depth of submergence and the water depth. The wavelength is independent of these parameters; it varies with the length of the employed body and the angle of inclination along which it slides into the water. Only a small fraction of about 1% of its potential energy in its initial position is transferred into wave energy. The rest is apparently dissipated in turbulence.

b) Prins

PRINS [66,67] shows that the ratios H/h and L/h of an initial dam-up or lowering of the water by the amount H over a length L decides in a channel, of which character the generated wave will be. PRINS differentiates among four wave types. The leading part of the forming wave train possesses the following properties (see also figure 6):

1. Oscillatory wave characteristics. The leading wave is part of a dispersive wave pattern. The waves are the same for an initial elevation as for an initial depression, except for the sign. The first wave is not the largest.

2. Solitary wave characteristics followed by a trough connecting it with the dispersive wave pattern.

3. A single solitary wave separated from the dispersive wave tail by a more or less flat part at the still water level.

4. A complex form, which, while travelling outward, breaks up into a few solitary waves separated from the dispersive wave pattern.

The domains H/h, L/h for which the various wave types arise are shown in figure 7.

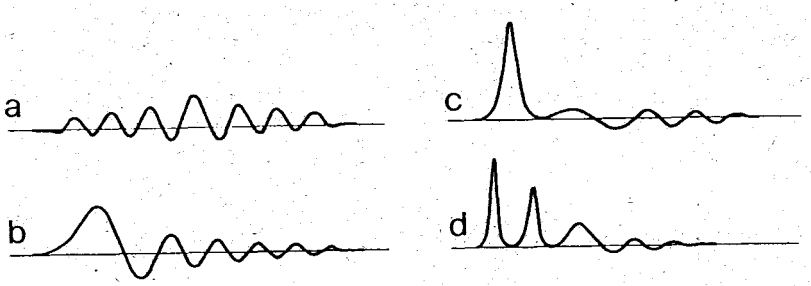

Figure 6: *Characteristic wave systems, generated by an initial elevation, according to* PRINS.
a) An oscillatory wave; b) a solitary wave, followed by a trough and a dispersive wave; c) a single solitary wave separated from the wave tail; d) multiple solitary waves.

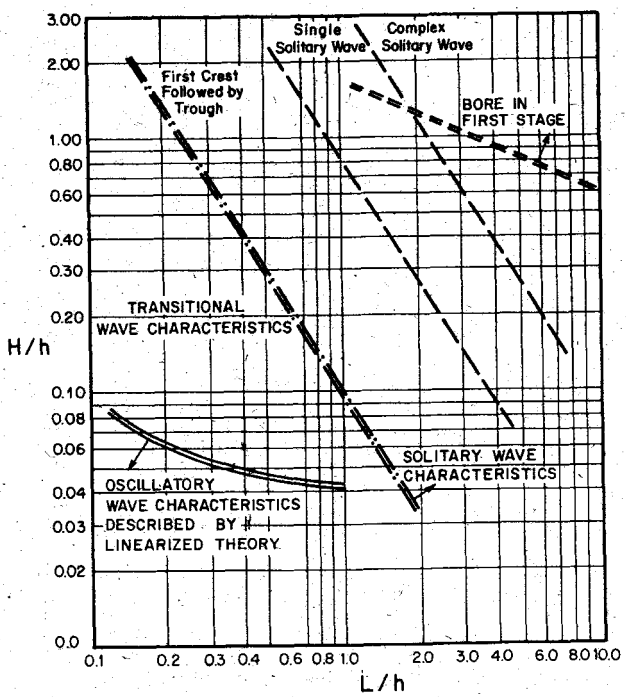

Figure 7: *Characteristics of the wave system for an initially elevated water surface and relation of the length L/h and height H/h of the elevation. Modified from* PRINS *[66].*

c) Miller

MILLER [58,59] studies the behaviour of a wave which is generated by a moving vertical plate in a horizontal channel. The plate is moved forward by a distance d ($0.3 \leq d/h \leq 8.0$) with a FROUDE number $Fr = v/\sqrt{gh}$ (v = speed of the plate) between $0.03 \leq Fr \leq 0.8$. MILLER quotes the following ranges of d/h and Fr to be relevant for natural phenomena:

Landslide	$d/h \approx 8.0$	$Fr > 40$
Submarine overthrust	$d/h < 1.0$	$Fr < 0.3$
	$d/h < 9.0$	$Fr > 1.0$
	same wave-length	
	various amplitudes e. g.	
	$0.025 < d/h < 8.0$	$0.03 < Fr < 0.8$
No studies	$d/h < 1.0$	$Fr > 1.0$

MILLER determines the velocities of his waves between two gauges that are $0.1m$ apart and repeats the procedure with gauges that are $2.5m$ apart; results agreed fairly well. The wave breaks at a FROUDE number with a wave speed $Fr = c/\sqrt{gh}$ of approximately $Fr = 1.26$.

If waves other than of the solitary-type are generated these waves (of sinusoidal and bore type) pass several stages and form solitary waves. The forming wave train may consist of several solitary waves and a tailing sinusoidal wave train. As an example, MILLER mentions the development of a bore into its components:
'Bore → undular bore → lead undulation becomes solitary + trailing undular bore consisting of remaining undulations → lead undulation solitary + second undulation becomes solitary → in several runs three successive solitary forms have emerged from the preceding undular form.'

d) Kamphuis & Bowering

KAMPHUIS & BOWERING [37] work with an inclined track equipped with rollers and let cubes glide into a channel of $1m$ width and different water depths ($0.23m$ – $0.46m$). Wave trains are formed which, at $x/h \approx 80$, have reached a stable wave height, i. e. beyond this point the wave-height does no longer decrease appreciably. Except for the case of a vertical track (free fall) the first wave of the wave train is the highest. A dimensional analysis and the conducted experiments show the following results:

1. The maximum wave height essentially depends upon the volume per unit width of the plunging cubes ($l \times b \times w$: length × width × height) and upon the FROUDE number $Fr = v_E/\sqrt{gh}$ formed with the velocity v_E of the body at the instance of submergence into the channel. For angles of submergence $> 30^0$ and aspect ratios $w/h \geq 0.5$ and $q = lw/h^2$ in the interval $0.05 \leq q \leq 1.0$ a sufficient approximation for the maximum waveheight η_{stable} at $x/h \approx 37$ is

given by

$$\frac{\eta_{stable}}{h} = Fr^{0.7}(0.31 + 0.2\log q)\,. \tag{1.248}$$

2. For $10 \le x/h \le 48$, $0.1 \le q \le 1.0$ the wave height decreases according to the law

$$\frac{\eta}{h} = \frac{\eta_{stable}}{h} + 0.35\exp\left(-0.08\frac{\overline{x}}{h}\right)\,. \tag{1.249}$$

3. The transfer of kinetic energy of the impinging body into wave energy is below 50% and drops below 25% for higher velocities of the body, depending on the FROUDE number. For cubes in free fall only about 10% – 20% of the kinetic energy is transferred into wave energy. Thereby the energies have to be considered in appropriate dimensionless form. For the kinetic energy the authors choose

$$K = \frac{1}{2}\frac{\rho_{rock}}{\rho}\frac{l}{h}\frac{w}{h}\frac{v_E^2}{gh}\,, \tag{1.250}$$

with the density ρ_{rock} of the falling material. The wave energy is used in the form $E/(\rho g h^3)$ with the wave amplitude η_{max} and the theoretical value of the wave energy

$$E = \begin{cases} \rho g c \int \eta^2 dt & \text{in deep water,} \\ \dfrac{8}{3\sqrt{3}}\left(\dfrac{\eta_{max}}{h}\right)^{\frac{3}{2}} & \text{for solitary waves.} \end{cases} \tag{1.251}$$

4. To within $\pm 1\%$ the wave speed is

$$c = \sqrt{gh}\left(1 + \frac{1}{2}\frac{\eta_{max}}{h}\right)\,. \tag{1.252}$$

5. The wave length L or the period T of the leading wave decreases according to

$$T = \sqrt{\frac{h}{g}}\left(11 + 0.225\frac{x}{h}\right)\,, \tag{1.253}$$

where $2\pi L = T$.

e) Huber

HUBER [32] models rockfalls by a finite volume of gravel. His masses of granular material slide along an inclined plane into a channel. He generates and observes the same wave types (solitary, sinusoidal, bore-type) as PRINS has done before. His results may be summarized as follows:

1. Irrespective of the kind of wave generation the following results hold in $5 \le x/h \le 100$ for the leading wave:

   - The length of the wave λ increases with distance from the source:

$$\frac{\lambda}{h} = a\left(\frac{x}{h}\right)^{0.45}\,, \quad 2.06 < a < 4.64\,, \quad \bar{a} = 3.00\,. \tag{1.254}$$

- The following formula holds for the wave period T

$$T = \sqrt{\frac{h}{g}}\, a \left(\frac{x}{h}\right)^{0.45}, \quad 1.88 \le a \le 4.30, \quad \bar{a} = 2.85. \tag{1.255}$$

- The ratio of maximum wave height η_{max} to wave length is given by

$$\frac{\eta_{max}}{\lambda} = a \left(\frac{x}{h}\right)^{-0.82}, \quad 0.07 < a < 0.41, \quad \bar{a} = 0.17. \tag{1.256}$$

The indicated values of a denote the largest and the smallest deviation; mean values are denoted by $\bar{a}$.

2. HUBER states that the URSELL number depends both upon the type of the wave and the inclination of the slide board. It changes with the progressive wave.

3. For each inclination angle of the slide board the wave speed is given by a regression line. The differences must, however, be regarded as small. A typical result is e. g.

$$c^2 = gh\left(0.9 + 1.0\frac{\eta_{max}}{h}\right). \tag{1.257}$$

4. The wave height is connected to the volume of the gravel mass per unit width by the power law of the form

$$\frac{\eta_{max}}{h} = a\left(\frac{V}{h^2}\right)^b, \quad 0.125 \le a \le 0.676, \quad 0.268 \le b \le 0.760. \tag{1.258}$$

The parameters a and b depend upon the inclination of the side board and the distance travelled by the wave.

5. The transfer of kinetic energy from the moving gravel mass to the wave decreases with increasing impinging velocity. The following estimates were found

$$\begin{aligned} \frac{K}{E} &\approx 30\% \quad \text{for} \quad \mathrm{Fr} < 1, \\ \frac{K}{E} &< 5\% \quad \text{for} \quad \mathrm{Fr} = 2.5. \end{aligned} \tag{1.259}$$

The rate of transfer is independent of the rock mass, but depends on the angle of the slide board. HUBER explains this by the fact that the avalanche is moving farther into the channel, and thus more energy can be converted into turbulence when slopes are steep.

f) Scheidegger

Using observations of natural avalanches SCHEIDEGGER [73] finds a relation between the volume V of a rock fall in m^3 and the bed friction coefficient

$$f = 0.62419\, V^{-0.1566}. \tag{1.260}$$

With this equation by employing MOHR's circle arguments he finds the maximum distance an avalanche or rockfall can travel.

g) Slingerland & Voight

SLINGERLAND & VOIGHT [78] make sacks filled with gravel slide into a wide water reservoir. The maximum amplitude of the forming circular waves at a distance $x/h \approx 4$ can be computed by means of the formula

$$\frac{\eta_{max}}{h} = K^{0.71} e^{-1.25} . \tag{1.261}$$

Here K denotes the dimensionless kinetic energy which is evaluated for the maximum velocity v_{max} of the falling sacks with volume V and according to (1.250) given by

$$K = \frac{1}{2} \frac{\rho_{rock}}{\rho} \frac{V}{h^3} \frac{v_{max}^2}{gh} . \tag{1.262}$$

The maximum velocity is computed with the aid of MOHR's circle for an avalanche that travelled a distance s on a slope of inclination α

$$v_{max}^2 = 2gs(\sin\alpha - f\cos\alpha) . \tag{1.263}$$

SLINGERLAND & VOIGHT give some data for stones. The friction angle is $f \approx 0.25$ and the density of the rocks is $\rho_{rock} \approx 2.7 kg/dm^3$, as usual. With this an example analysis is given for observed waves, with accurate re-prediction of the wave height.

A review article [78] also lists some of the works discussed here.

1.2.2 Mathematical models

h) Wiegel, Noda, Kuba, Gee & Tornberg

WIEGEL, NODA, KUBA, GEE and TORNBERG [95] are among the first to perform a comparison of linear wave theory [42] with results from experiments that are performed in a similar way as those of PRINS [66,67]. Instead of initially damming-up the water WIEGEL ET AL. make blocks of height H and length L fall vertically into the channel. They corroborate the experimental results of PRINS and are able to reproduce the behaviour of the wave amplitude $\eta/H \sim h^{-2/3}$ and $\eta/H \sim L/h$, which is predicted by the linear wave theory. Thereby, the FROUDE number (built with the velocity of the immersing body) and the weight affect the waves only marginally.

i) Noda

The same experiments are used by NODA [62] to test an extended linear theory. He develops a solution to the linear wave theory for a uniformly falling box of length L of which the height is so large, that it is always above the water line. Furthermore he constructs a solution for a vertical wall that is moved horizontally in the direction of the channel. Basis of his analysis is the general solution the linear equations for an incompressible, irrotational fluid obtained by KENNARD [39], who found a solution

in integral form for an arbitrary boundary condition $F(y,t) = 0$ at $x = 0$, that must be described by the velocity potential ϕ via

$$\frac{\partial \phi}{\partial x} = F(x,t)\,. \tag{1.264}$$

NODA describes a method how the boundary condition must be formulated in order to simulate a vertically falling rectangular block. The uniform motion of a vertical wall can directly be incorporated into KENNARD's solution. The solution integral is approximated by numerical procedures. NODA is able to verify his computations with the experiments of WIEGEL ET AL. [95]. In addition he finds that the maximum wave height η_{max} for the case of a horizontally moving wall depends upon the FROUDE number,

$$\frac{\eta_{max}}{h} = 1.32\,Fr\,. \tag{1.265}$$

In a further article NODA [63] used the same method to construct the linear wave solution to the experiments of PRINS [66,67] and finds that the first wave is always the highest provided $L/h > 0.6$, and if $x/h = 5$. At smaller L/h-values dispersive waves are formed.

j) Das & Wiegel

The range of validity of conditions for the theoretical analysis of the moving wall computations performed by NODA is determined by DAS & WIEGEL [12]. The theory assumes that the displacement of the wall is small compared to the water depth and the acceleration of the wall motion is small compared to the gravitational acceleration, and further that the speed of the wall is small compared to the shallow water wave speed $\sqrt{gh}$. They find the best agreement between observations and theory at position $x/h = 5$, in experiments for which dimensionless distances L/h by which the wall had been displaced were not too small (within the range $0.1 < L/h < 1.6$). At large distances, $x/h \geq 15$, deviations were considerable. The computed amplitude η/h for small L/h was first overestimated; at $L/h \approx 0.4 - 0.6$ the theoretical values agreed well with those from the experiments, for larger values of L/h the linear theory underestimated the wave heights.

k) Davidson & McCartney, Raney & Butler

A hydraulic model investigation was conducted for potential landslides in a reproduced area by DAVIDSON & MCCARTNEY [13]. Three different materials were used to simulate the landslide: rock-filled bags, gravel and square concrete cubes. The material slides down on rollers an inclined V-shaped slope. A numerical model for this model area was constructed by RANEY & BUTLER [69]. For an incompressible, irrotational fluid, the vertical component of the velocity is neglected and the governing equations are integrated over the water depth, resulting in the momentum equations

$$\frac{\partial u}{\partial t} + u\frac{\partial u}{\partial x} + v\frac{\partial u}{\partial y} + g\frac{\partial \eta}{\partial x} = R_x + L_x\,, \tag{1.266}$$

$$\frac{\partial v}{\partial t} + u\frac{\partial v}{\partial x} + v\frac{\partial v}{\partial y} + g\frac{\partial \eta}{\partial y} = R_y + L_y\,, \tag{1.267}$$

and the continuity equation

$$\frac{\partial \eta}{\partial t} - \frac{\partial h}{\partial t} + \frac{\partial}{\partial x}((h+\eta)u) + \frac{\partial}{\partial y}((h+\eta)v) = 0\,, \tag{1.268}$$

where

$$R_x = g\frac{(V_x-u)\left((V_x-u)^2+(V_y-v)^2\right)^{1/2}}{C^2(h+\eta)}, \tag{1.269}$$

$$R_y = g\frac{(V_y-v)\left((V_x-u)^2+(V_y-v)^2\right)^{1/2}}{C^2(h+\eta)}, \tag{1.270}$$

$$L_x = \beta(V_x-u)\left((V_x-u)^2+(V_y-v)^2\right)^{1/2}, \tag{1.271}$$

$$L_y = \beta(V_y-v)\left((V_x-u)^2+(V_y-v)^2\right)^{1/2}, \tag{1.272}$$

$$\beta = \frac{C_D}{2h}\frac{A_z}{A_c}. \tag{1.273}$$

Here h is the reservoir depth including vertical deformations which are created by the landslide material, R_x, R_y represent the bottom friction, and L_x, L_y are acceleration terms affecting the fluid through contact friction with the impinging avalanche. C is CHEZY's coefficient, C_D the pressure drag coefficient, V_x, V_y are the components of the landslide velocity, A_z the vertical cross-sectional area of the slide and A_c the size of a grid cell introduced in the numerical computations.

Bottom friction coefficients are represented in terms of the CHEZY coefficient. The force per unit mass which the water experiences consists of a pressure drag exerted on the water by the front of the moving landslide.

A finite difference approximation of the equations and an implicit-explicit alternating direction technique is employed to solve the equations. The landslide characteristics are the volume, the average velocity at which it moves, its path through the water, the general shape of its leading face and the final position of the slide in the reservoir. All these data were available from physical experiments. Agreement between the numerical results and the observational data of the wave height is satisfactory. The average difference between the observed and computed height of the first wave crest was about 25%. Numerical results are compared with those of the physical model only until the first wave crest is obtained. Once the crest passed, the numerical model predictions are poor. This may be due to a significant amount of wave runup that occurs at the reservoir boundaries. A map with the final position of an experimentally generated landslide and the position of the gauge is shown in figure 8. Numerical and physical data of the wave height can be found in figure 9.

l) Kouitas

A finite element approach to landslide induced waves is presented by KOUITAS [41]. The mathematical model is based on the SAINT-VENANT equation of unidirectional

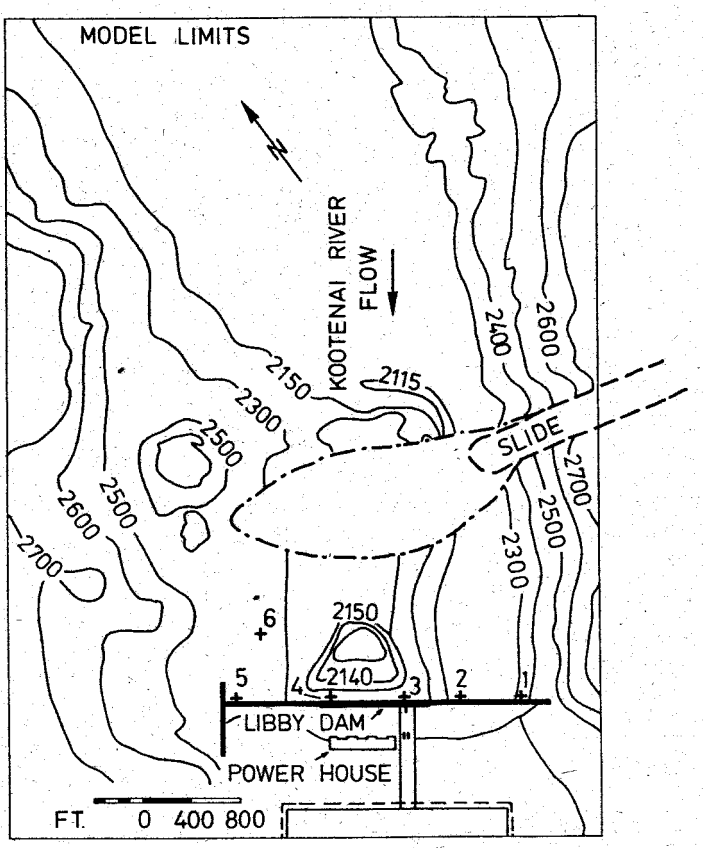

Figure 8: *Model area for physical and numerical experiments from* DAVIDSON & MCCARTNEY *[13] and* RANEY & BUTLER *[69].*

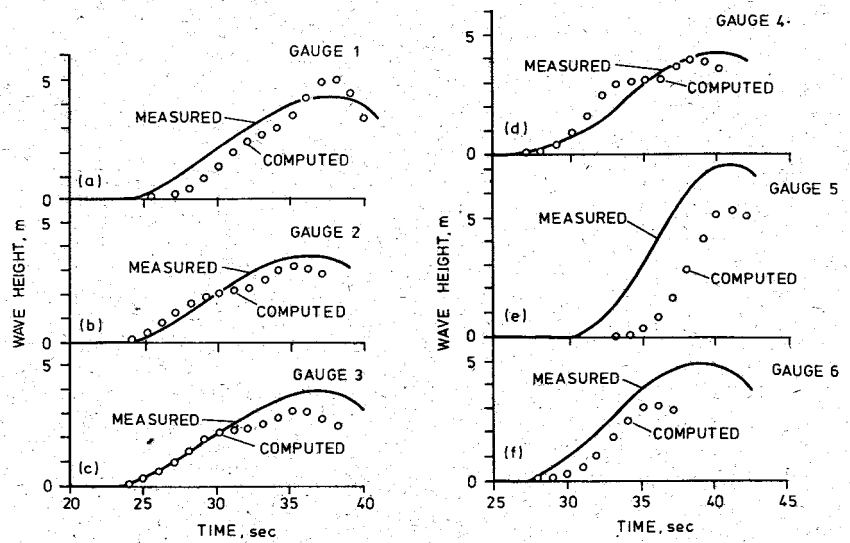

Figure 9: *Comparison of numerical and experimental results from* RANEY & BUTLER *[69]. The position of the gauges is indicated in figure 8.*

flow in a channel of arbitrary width $\tau(y,t)$. The effect of the landslide is introduced into the continuity equation, which has the form

$$\frac{\partial \eta}{\partial t} + \frac{A}{T}\frac{\partial U}{\partial x} + U\frac{\partial h+\eta}{\partial x} + \frac{1}{T}\int_0^{h+\eta}\frac{\partial \tau}{\partial t}\,dy = 0\,; \tag{1.274}$$

U is the cross sectional mean velocity, A the channel cross section and T the free surface width. The momentum equation becomes

$$\frac{\partial U}{\partial t} + U\frac{\partial U}{\partial x} = -g\frac{\partial \eta}{\partial x} - gS_f\,. \tag{1.275}$$

The slope of the energy grade line is denoted by S_f. A MANNING type formula is used for its approximation. The flow field is discretized by one-dimensional finite elements with linear shape functions. The functions η and U are linearly approximated with the same functions. Therefore, a GALERKIN method can be applied. A standard approach is used for the integration of the time derivatives by the use of an EULER forward difference, and a linearization of the nonlinear convective term according to

$$U\frac{\partial U}{\partial x} \approx U^{n-1}\frac{\partial U^n}{\partial x} \tag{1.276}$$

is used. These procedures result in a set of algebraic equations which were solved. No experimental results are quoted to show the validity of the numerical calculations.

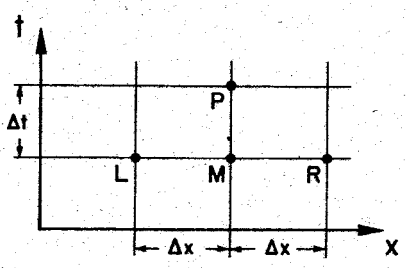

Figure 10: *Notation for diffusive scheme, in an x-t grid. The width of the mesh is Δx, the time step Δt.*

m) Chaudhry, Mercer & Cass

CHAUDHRY, MERCER & CASS [9] build a river model into which sandbags are sliding from the side. Different slide materials like loose gravel, individual bags of a certain volume, individual bags contained within a single impervious wrapping of plastic film to eliminate porosity effects were used but did not affect the size of the generated waves. A likely reason for this may have been the gentle nature of the slide movement that minimizes the impact effects. It was found that the height of the generated waves was independent of the slide velocity but increased with the slide travel distance.

The mathematical model is based on the SAINT-VENANT equation (see (1.275)). Continuity is chosen in the form

$$\frac{\partial Q}{\partial x} + T\frac{\partial \eta}{\partial t} = 0\,, \tag{1.277}$$

with discharge Q. LAX's diffusive scheme based on the explicit finite difference method was selected to solve the equations and resulted in the finite difference representation

$$\begin{aligned} U_P &= U_M + \frac{1}{2}\frac{\Delta t}{\Delta x}U_M\left((U_L - U_R) + g(\eta_L - \eta_R)\right) \\ &\quad + g\,\Delta t\frac{1}{2}(S_L + S_R)\,, \end{aligned} \tag{1.278}$$

$$\eta_P = \eta_M + \frac{1}{2}\frac{\Delta t}{\Delta x}\frac{1}{T_M}(Q_L - Q_R)\,. \tag{1.279}$$

Indices are indicated in figure 10. The boundary conditions are as follows: At the upstream end the water level variation with time was available from physical models, at the downstream end a weir was installed which allows overtopping of higher water levels. The numerical model cannot calculate wave run up. The results of measured and computed waveheight time series are shown in figure 11. The input data for the numerical calculations are obtained from the waveheight measured nearby the

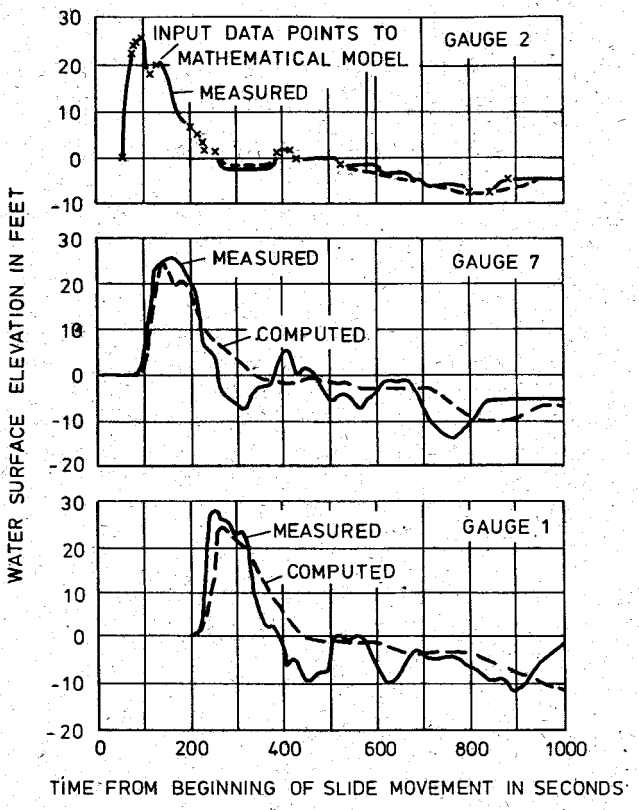

Figure 11: *Comparison of numerical and experimental results from* CHAUDHRY ET AL. *[9] for a river model. The numerical model requires input data for the initial waveheight. The location of Gauge 7 and of gauge 1 is upstream from gauge 2.*

landslide.

n) Pugh & Chiang

PUGH & CHIANG [68] consider a three dimensional canyon model. They presume that the displacement of the water is the major factor creating the wave as long as the landslide velocity is less than the wave celerity of the water. For the same reason the exact landslide geometry is not considered necessary. The landslide is therefore simulated by using a simple wedge shaped piston.

The authors find an empirical relation for the maximum stable waveheight η_{max} (stable in a sense that the wave decay is the same in all directions in the basin) in terms of the distance L the landslide of volume V has moved:

$$\frac{\eta_{max}}{h} = \frac{0.14\left(\frac{V}{h^3}\right)^{1/2}}{10^{\frac{L/h}{58}}}, \tag{1.280}$$

valid in the range $1.0 < L/h < 4.0$. For slide FROUDE numbers above 0.6 an increase of the velocity of the landslide produced only a minor growth of wave heights.

The numerical model introduced by RANEY & BUTLER is extended by them to three dimensions. The effects of bottom friction and pressure drag due to the landslide is expressed by a MANNING type formula

$$S_f = R_x + L_x = n^2 g u \left(u^2 + v^2\right)^{1/2} \frac{1}{1.486^2 (h+\eta)^{4/3}}, \tag{1.281}$$

outside the landslide area, and

$$S_f = R_x + L_x = -\frac{1}{2}\frac{Fr^2}{(h+\eta)A} C_D \cos\alpha, \tag{1.282}$$

at the location covered by the moving landslide, with the slide cross section A, roughness n, the horizontal slide FROUDE number $Fr = V_x/\sqrt{gh}$, the angle α between slide and the horizontal and the pressure and viscous drag coefficient C_D. The equations are solved with an explicite central difference scheme. The presented example of calculated data shows that the first peak of the wave height and also that of its reflection agree very well with experimental data. The wave tails, which in the irregular bathymetry of the canyon, underly multiple reflections and refractions, are poorly represented in the calculations.

o) Townson & Kaya

TOWNSON & KAYA [86] attempt a comparison between numerical and observational data for a three dimensional reservoir. They model an impervious landslide with an air proof bag which is slowly filled from above with air. A wire mesh that is fixed at the bottom of the basin determines the final form of the air filled bag. The position of the slide front was recorded on film. A numerical model was used which is based on depth averaged equations and rearranged according to the method of

characteristics. The same landslide forcing terms as used by RANEY & BUTLER [69] are included. These terms had little effect on the waveheight. The deformation of the lake bottom due to the landslide is taken from the physical model. In general the numerical scheme underestimated the maximum waveheight. Numerical wave forms are much more smoothed than are the physical data. The numerical model was only able to reproduce the principal wave. The reasons are:

1. Discretization errors: the coarseness of the grid in the slide-generation compared with the large propagation zone, then the lower resolution of transverse than of longitudinal waves.

2. Numerical dispersion in those shallower areas (with strongly variable depth) of the lake where numerical propagation rate greatly exceeds the real wave celerity.

p) Gozali & Hunt

GOZALI & HUNT [26] give a purely numerical approach for nonlinear, nondispersive long waves generated in a straight channel by a moving piston. They show that waves are nondispersive when the characteristic dimensionless horizontal distance of the wave (i. e. the nondimensional distance the piston is moved) is larger than ten water depths. The equations of continuity and horizontal momentum applicable to nondispersive waves are

$$\frac{\partial h+\eta}{\partial t}+\frac{\partial u(h+\eta)}{\partial x} = 0, \tag{1.283}$$

$$\frac{\partial u}{\partial t}+u\frac{\partial u}{\partial x} = -g\frac{\partial h+\eta}{\partial x}. \tag{1.284}$$

Now, equation (1.283) is multiplied by c and equation (1.284) is added to obtain

$$\left(c(h+\eta)\frac{\partial u}{\partial x}+\frac{\partial u}{\partial t}\right)+c\left(\frac{(c\,u+g)}{c}\frac{\partial(h+\eta)}{\partial x}+\frac{\partial(h+\eta)}{\partial t}\right)=0. \tag{1.285}$$

Let then

$$\frac{dx}{dt}=c(h+\eta)+u=\frac{c\,u+g}{c}, \tag{1.286}$$

which possesses the solution

$$c=\pm\sqrt{\frac{g}{h+\eta}}. \tag{1.287}$$

Then, we obtain the characteristics

$$\frac{dx}{dt}=u\pm\sqrt{g(h+\eta)}=u\pm c. \tag{1.288}$$

Inserting equation (1.288) in (1.285) and integrating yields four ordinary differential equations instead of the two partial differential equations (1.283) and (1.284):

$$u\pm 2c=const. \quad \text{along} \quad \frac{dx}{dt}=u\pm c. \tag{1.289}$$

GOZALI & HUNT chose the following boundary conditions to describe the motion of the vertical wall

$$\left.\begin{array}{rcl} u(x,0) & = & 0 \\ c(x,0) & = & c_0 \end{array}\right\} \quad \text{for} \quad 0 \le x \le \infty \tag{1.290}$$

with $c_0 = \sqrt{gh}$. The velocity of the left boundary, at the vertical plate, is assumed to be parabolic in time with a maximum speed u_{max}, at t_0 when the plate is stopped:

$$\begin{array}{ll} u(0,t) = 4u_{max}\left(1 - \dfrac{t}{t_0}\right)\dfrac{t}{t_0}, & \text{for} \quad 0 \le t \le t_0, \\ u(0,t) = 0, & \text{for} \quad t_0 \le t \le \infty. \end{array} \tag{1.291}$$

In this way a flux condition is described instead of the piston motion. Due to the nondispersive character of the equations a shock front (bore) always forms in the one dimensional solution. The equations along the characteristics (1.289) are solved with a HARTREE method to obtain the velocity u and the free surface η from $c = \sqrt{g(h+\eta)}$. Results show, that for increasing velocity u_{max} of the piston, the maximum height of the wave also increases. The solutions appear to approach a common asymptote as either time or distance increase. The results will be discussed in greater detail in chapter 4.

q) Villeneuve, Savage

The incorporation of an unsteady bed into the equation of BOUSSINESQ is given by VILLENEUVE & SAVAGE [90,89]. Their equations correspond to those given earlier by WU [96]. The resulting equations are solved numerically using a finite difference scheme in which a flux correction method (FCT) is used. This scheme is used in our calculations, and results will be compared with physical data in chapter 4. We will see that the numerical solution predicts the wave form for all time, short and large, including a proper representation of the wave tail, whereby no experimental input-data is necessary. All we have to know is the history of the motion of the landslide. Further, the equations are valid for weakly nonlinear waves and must be restricted to small waveheights, and the computed data will show satisfactory agreement with experiments even for waveheights up to about $0.6h$.

Two classical methods to develop the equations are used by VILLENEUVE [89]. First, depth averaging and scaling reduce the momentum and continuity equations to BOUSSINESQ type equations, when higher order terms are neglected. Second, an expansion scheme according to FRIEDRICHS [21] and KELLER [38] results in the same set of equations.

The procedure of expansion used by PEREGRINE [64], who obtained equations for a slowly variable bed $h(x)$, is extended by including a bed which changes in space and time. The free surface $\eta(x,t)$ and the motion of the bottom of the channel $h(x,t)$ are determined by employing the kinematic and dynamic conditions at the

free surface and the kinematic condition along the bed:

$$\left.\begin{aligned} v &= \frac{\partial \eta}{\partial t} + u\frac{\partial u}{\partial x} \\ p &= 0 \end{aligned}\right\} \quad \text{at} \quad y = \eta(x,t), \qquad (1.292)$$
$$v = -\frac{\partial h}{\partial t} - u\frac{\partial h}{\partial x} \quad \text{at} \quad y = -h(x,t).$$

If we now integrate the (nondimensional) equation of continuity and use the above boundary conditions we obtain the volume balance law

$$\frac{\partial \eta}{\partial t} + \frac{\partial Q}{\partial x} = \frac{\partial h}{\partial t}, \qquad (1.293)$$

with the discharge Q

$$Q = \int_{-h}^{\eta} u \, dy. \qquad (1.294)$$

Furthermore, the (nondimensional) equations of momentum read

$$\frac{\partial u}{\partial t} + u\frac{\partial u}{\partial x} + v\frac{\partial u}{\partial y} = \frac{\partial p}{\partial x}, \qquad (1.295)$$

$$\frac{\partial v}{\partial t} + u\frac{\partial v}{\partial x} + v\frac{\partial v}{\partial y} = \frac{\partial p}{\partial y}, \qquad (1.296)$$

and the condition of irrotationality is

$$\frac{\partial u}{\partial y} + \frac{\partial v}{\partial x} = 0. \qquad (1.297)$$

The variables η, u, p and Q are now expanded in terms of the parameter ϵ

$$\eta = \eta_0 + \epsilon\eta_1 + \epsilon^2\eta^2 + \cdots, \qquad (1.298)$$
$$u = u_0 + \epsilon u_1 + \epsilon^2 u^2 + \cdots, \qquad (1.299)$$
$$p = p_0 + \epsilon p_1 + \epsilon^2 p^2 + \cdots, \qquad (1.300)$$
$$Q = Q_0 + \epsilon Q_1 + \epsilon^2 Q^2 + \cdots \qquad (1.301)$$

so that the variables $\eta_0, \eta_1, \ldots, u_0, u_1, \ldots$ etc. and their derivatives are of order $O(1)$. The independent variables x and t are scaled with the parameter σ, so that the scaled coordinates $(\hat{x}, y, \hat{t})$ are of order $O(1)$:

$$\left(\frac{\partial}{\partial x}, \frac{\partial}{\partial t}\right) = \frac{1}{\sigma}\left(\frac{\partial}{\partial \hat{x}}, \frac{\partial}{\partial \hat{t}}\right). \qquad (1.302)$$

The parameters ϵ and σ are small. One of their physical interpretation is that ϵ describes the shallowness of the wave compared to the water depth, and σ relates the length of the wave to the water depth:

$$\sigma \sim \frac{\eta}{h}, \qquad (1.303)$$
$$\epsilon \sim \frac{h}{\lambda}. \qquad (1.304)$$

From continuity follows that

$$v = \sigma(v_0 + \epsilon v_1 + \cdots). \tag{1.305}$$

We also assume

$$\frac{\partial h}{\partial t} = \left(\frac{\partial h}{\partial t}\right)_0 + \epsilon\left(\frac{\partial h}{\partial t}\right)_1 + \epsilon^2\left(\frac{\partial h}{\partial t}\right)_2 + \cdots \tag{1.306}$$

At zero order ($\epsilon = \sigma = 0$) the solution *is taken* to be still water so that

$$\eta_0 = u_0 = v_0 = Q_0 = \left(\frac{\partial h}{\partial t}\right)_0 = \text{const.} = 0\,, \tag{1.307}$$

with a stress free boundary and a linear pressure distribution

$$p_0 = -y. \tag{1.308}$$

Actually the zero-order equations turn out to be the finite-amplitude shallow water equations of AIRY's type, viz.

$$\frac{\partial \eta_0}{\partial \hat{t}} + \frac{\partial}{\partial \hat{x}}((h+\eta_0)u_0) = -\left(\frac{\partial h}{\partial t}\right)_0, \tag{1.309}$$

$$\frac{\partial u_0}{\partial \hat{t}} + u_0\frac{u_0}{\partial \hat{x}} + \frac{\partial \eta_0}{\partial \hat{x}} = 0. \tag{1.310}$$

The first order solution will be derived now. With (1.307) and the assumption $O(\epsilon) = O(\sigma^2)$ irrotationality becomes, see equation (1.305),

$$\frac{\partial u_1}{\partial y} = 0 \Rightarrow \begin{cases} u_1 = u_1(x,t), \\ Q_1 = hu_1. \end{cases} \tag{1.311}$$

From the boundary condition

$$p_0 + \epsilon p_1 = 0\,, \quad \text{at} \quad y = \eta_0 + \epsilon\eta_1 \tag{1.312}$$

there follows

$$p_1 = \eta_1\,. \tag{1.313}$$

Substituting the expansions (1.298) – (1.300) into equations (1.293), (1.295) and (1.296) and accounting for the lowest order solution constructed above, yields the first order equations

$$\frac{\partial \eta_1}{\partial \hat{t}} + \frac{\partial hu_1}{\partial \hat{x}} = -\left(\frac{\partial h}{\partial t}\right)_1, \tag{1.314}$$

$$\frac{\partial u_1}{\partial \hat{t}} + \frac{\partial \eta_1}{\partial \hat{x}} = 0\,, \tag{1.315}$$

which are the linearized long wave equations. The vertical velocity is obtained by integrating the continuity equation and with respect to the kinematic boundary condition we obtain to first order

$$v_1 = -\left(\frac{\partial h}{\partial t}\right)_1 - \frac{\partial hu_1}{\partial \hat{x}} - y\frac{\partial u_1}{\partial \hat{x}}\,. \tag{1.316}$$

To second order, $O(\epsilon^2) = O(\epsilon\sigma^2)$, and owing to (1.311) irrotationality gives

$$\frac{\partial u_2}{\partial y} = \frac{v_1}{\partial \hat{x}} . \tag{1.317}$$

Integration and substitution of equation (1.316) leads to

$$u_2 = U_2(\hat{x},\hat{t}) - y\frac{\partial}{\partial \hat{x}}\left(\frac{\partial h}{\partial t}\right)_1 - y\frac{\partial^2 h u_1}{\partial \hat{x}^2} - \frac{y^2}{2}\frac{\partial^2 u_1}{\partial \hat{x}^2} , \tag{1.318}$$

with an arbitrary function $U_2(\hat{x},\hat{t})$. The second order vertical momentum equation (deducible from equation (1.296)) includes now a vertical acceleration

$$\frac{\partial v_1}{\partial \hat{t}} = -\frac{\partial p_2}{\partial y} . \tag{1.319}$$

With the boundary condition

$$p_0 + \epsilon p_1 + \epsilon^2 p_2 = 0 , \quad \text{at} \quad y = \eta_0 + \epsilon\eta_1 + \epsilon^2\eta_2 \tag{1.320}$$

and equation (1.316) the pressure distribution (1.319) becomes

$$p_2 = \eta_2 + y\frac{\partial}{\partial \hat{t}}\left(\frac{\partial h}{\partial t}\right)_1 + y\frac{\partial^2 h u_1}{\partial \hat{t}\partial \hat{x}} + \frac{y^2}{2}\frac{\partial^2 u_1}{\partial \hat{t}\partial \hat{x}} . \tag{1.321}$$

To obtain the second order continuity equation an expansion for Q is needed. To this end we substitute equations (1.298) and (1.299) into the definition (1.294) of Q and rearrange the integrals in order of ϵ; then we obtain to second order in ϵ

$$\begin{aligned} \epsilon^2 Q_2 &= \int_{\epsilon\eta_1}^{\epsilon^2\eta_2} u_0\, dy + \int_{\eta_0}^{\epsilon\eta_1} \epsilon u_1\, dy + \int_{-h}^{\eta_0} \epsilon^2 u_2\, dy \\ &= \int_0^{\epsilon\eta_1} \epsilon u_1\, dy + \int_{-h}^{0} \epsilon^2 u_2\, dy , \end{aligned} \tag{1.322}$$

with the aid of which equation (1.318) can be rewritten as

$$Q_2 = \eta_1 u_1 + hU + \frac{h^2}{2}\frac{\partial}{\partial \hat{x}}\left(\left(\frac{\partial h}{\partial t}\right)_1 + \frac{\partial h u_1}{\partial \hat{x}}\right) - \frac{h^3}{6}\frac{\partial^2 u_1}{\partial \hat{x}^2} . \tag{1.323}$$

This leads to the second order equations

$$\frac{\partial \eta_2}{\partial \hat{t}} + \frac{\partial Q_2}{\partial \hat{x}} + \left(\frac{\partial h}{\partial t}\right)_2 = 0 , \tag{1.324}$$

$$\frac{\partial U}{\partial \hat{t}} + u_1\frac{u_1}{\partial \hat{x}} + \frac{\eta_2}{\partial \hat{x}} = 0 . \tag{1.325}$$

PEREGRINE [64] states that 'the second-order terms have first-order effects over moderate times. To include these (second order) effects first-order variables incorporating the second-order terms are used'. For the amplitude and bottom motion the obvious variable is

$$\eta = \epsilon\eta_1 + \epsilon^2\eta_2 , \tag{1.326}$$

$$\frac{\partial h}{\partial t} = \epsilon\left(\frac{\partial h}{\partial t}\right)_1 + \epsilon^2\left(\frac{\partial h}{\partial t}\right)_2 . \tag{1.327}$$

For the velocity several possibilities exist. For each a different equation will result. For example:

1. The mean velocity

$$\bar{u} = \frac{1}{h+\eta}\left(\epsilon Q_1 + \epsilon^2 Q_2\right), \tag{1.328}$$

which will be used here.

2. The velocity at the bottom $y = -h(x)$ (see MEI & LE MÉHAUTE [55]).

3. The velocity at the still water level $y = 0$ (see PEREGRINE [64]).

$$\tilde{u} = u(x,0,t) = \epsilon u_1 + \epsilon^2 U. \tag{1.329}$$

With the depth averaged velocity $\bar{u}$ the first order equations (1.314), (1.315) are introduced into the second order equations (1.324), (1.325) via (1.326) – (1.328). Finally VILLENEUVE obtains

$$\frac{\partial \eta}{\partial t} + \frac{\partial}{\partial x}((h+\eta)\bar{u}) = -\frac{\partial h}{\partial t} \tag{1.330}$$

$$\frac{\partial \bar{u}}{\partial t} + \bar{u}\frac{\bar{u}}{\partial x} + \frac{\partial \eta}{\partial x} = \frac{h}{2}\frac{\partial^2}{\partial t \partial x}\left(\frac{\partial h}{\partial t} + \frac{\partial h\bar{u}}{\partial x}\right) - \frac{h^2}{6}\frac{\partial^3 \bar{u}}{\partial t \partial x^2}. \tag{1.331}$$

The continuity equation (1.330) is exact, while the momentum equation (1.331) is of order $O(\epsilon^2\sigma^3)$.

2 Experimental Procedure

The purpose of this study is the experimental investigation of rockslide-generated water waves in a confined reservoir. This requires the study of 1) the avalanching motion of the rock mass down the mountain side, 2) the impact mechanism of the rocks when impinging on the water and the related generation of momentum and dissipation of energy by turbulence and 3) the wave motion that sets in within the reservoir as a result of the interactions. In this initial study we wish to emphasize the wave motion aspects; to this end, idealizations are called for. We shall replace the reservoir by a straight channel and the interaction between the rockslide and the water by a wave-generating device. The purpose is to establish a correspondence between initial conditions at the location of the wave generator and the wave that is set in motion. More specifically, the subject of our interest is the study of the behaviour of nonlinear shallow water waves generated by moving boundaries. Our focus will be on

- wave heights
- vertical velocity profiles over water depths.

2.1 Experimental Set-Up

The set-up consists of a $16m$ long channel with a cross section $0.3m$ wide and $0.3m$ high (see figure 12). The bottom and the back wall are made from dark gray $1cm$ thick PVC sheets, and the front is made from a $1cm$ thick sheet of perspex to permit direct observation of the wave inside the channel. The bottom is horizontal to within a variation of $\pm 1mm$ due to the accuracy of the thickness of the PVC sheet. The channel is filled with water through a hose from a valve connected to the community water system, and two valves, built into the bottom at each end, allow it to empty within 15 to 20 minutes. Refilling takes about the same time, but adjustment of the fresh water to room temperature lasts approximately half a day. Experiments were always performed at room temperature to avoid thermal influences. The channel is closed at both ends with vertical PVC sheets. About $1m$ at the left end was reserved for the installation of the wave generating machinery.

The waves are generated either by a piston (figure 13 shows a wedge-type form) which moves horizontally in a prescribed manner, or a plate that is held in a cylindrical pin at the bottom and can freely rotate as shown in figure 13. This rotation causes the water in front of the plate to be displaced. The plate thus acts as a wave generator. Its motion, too, can be accurately described. Piston and plate tightly seal the channel sides. However, to minimize friction, the piston was set on roller bearings; this required a small free slot underneath the piston of about $1mm$ width at the front, which, when under motion, caused a draft of water from the piston front to its back underneath the piston. This draft was so small that the waves of interest were essentially unaffected by it.

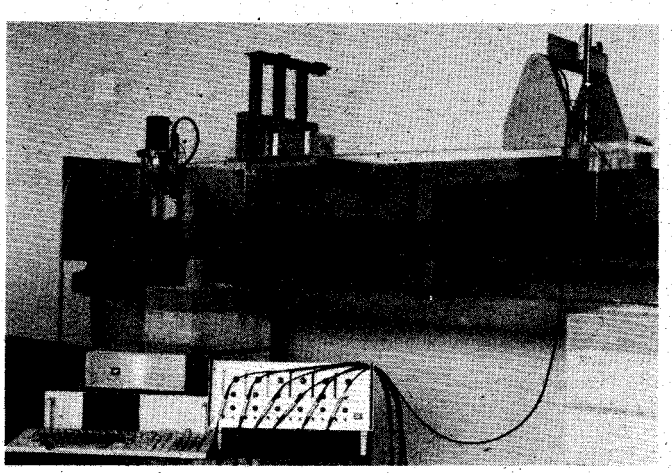

Figure 12: *General view of the experimental set-up.*

To obtain a horizontal motion of the piston the rotation of an electrical stepping-motor is transformed into the horizontal translation by means of a gearing with cross-like slot guides (see figure 14). The device was constructed so that two parallel bars, one on each side of the device, will simultaneously move forward. Pins connect the far ends of the bars with the piston and thus transfer their motion to a pure translation of the face of which the shape is still arbitrary.

The geometric arrangement of the bars and pins in the cross-slot gearing determines how the angular velocity of the motor is transferred to the translation of the piston. The mechanism consists essentially of two bars which are guided and pinned as shown in figure 15. Bar $\overline{AC}$ is set in rotation by the stepping motor and revolves about point A. At C a second bar $\overline{BD}$ is pinned to it. Relative to $\overline{AC}$, $\overline{BD}$ can rotate about point C while points B and D are guided in the cross slots as indicated. In order to let $\overline{AC}$ rotate and B (D) move horizontally (vertically), the lengths must be $\overline{AC} = \overline{DC} = \overline{CB} = a$. While bar $\overline{AC}$ performs one revolution point B moves horizontally from left to right and right to left, and D moves downward and upward, as indicated in figure 15. Let $\varphi(t)$ be the angle (BAC), $\dot{\varphi}(t)$ the angular velocity of bar $\overline{AC}$ and d the distance which B has moved from the centre of the cross. Then

$$\begin{aligned} d &= 2a\cos\varphi(t)\,, \\ \dot{d} &= -2a\dot{\varphi}(t)\sin\varphi(t)\,. \end{aligned} \tag{2.1}$$

It follows from (2.1) that, with $\dot{\varphi}(t) = const.$, the horizontal velocity of point B oscillates sinusoidally. On the other hand, for a prescribed $\varphi(t)$, eq. (2.1) gives the motion of the piston. In our actual set-up, there is a gear box between the stepping motor and the bar $\overline{AC}$ which slows the rotational speed of the bar $\overline{AC}$ relative to

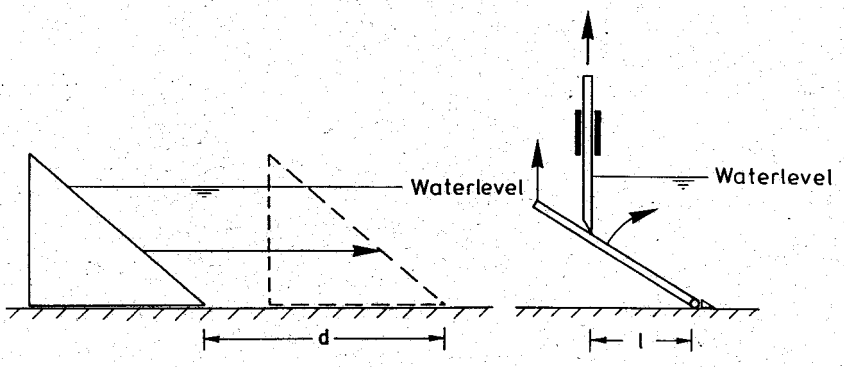

Figure 13: *Wave generating faces.Left: Moving wedge. Right: Rotating plate.*

that of the motor by a factor of five.

The stepping motor that drives the entire mechanism turns the motor's axle 0.36^0 per step. A commercial chip (HSMC20, of Rubran AG, Zürich) generates the step frequency at which the motor rotates. A constant frequency corresponds to a constant angular velocity $\dot{\varphi}(t)$ of the bar $\overline{AC}$ and generates a piston velocity which varies sinusoidally in time.

In our experiments we use the angular velocity profile shown in figure 16. As shown, the motor is linearly accelerated until the maximum angular velocity FM is reached. Thereafter, $\dot{\varphi}(t)$ is held constant at this maximum for some time, and then, over the same time scale as it accelerated, the motor decelerates linearly to a complete stop. This is done within a predefined number of steps, NP. 5000 steps turn the axle of the motor five times; because of the gear box this corresponds to a motion of the piston forth and back. Hence starting at its rear position, $NP = 2500$ steps are needed to move the piston forward to its maximum front position. With $a = 6.25cm$, the total displacement of the piston amounts to $25cm$. To guarantee no backward motion of the piston, the number of steps was reduced to 2350, corresponding to a total horizontal displacement of about $23cm$. The step frequency varied between 500 and $5000s^{-1}$, and in terms of figure 16 the acceleration was adjusted so that $N_R/FM = 1000$ is always constant. This means that the motor attains its maximum velocity after 1 to 5 steps (according to 0.5 to $5ms$) depending on the value of FM. The same time is also needed for deceleration. This is about 1% of the total time the face is moving. For further calculation we neglect this ramp part and assume that the motion of the piston is sinusoidal in time all the way. From eq. (2.1) the piston velocity is given by

$$v_{Piston} = \frac{\pi}{4}\frac{FM}{5000}\sin(2\pi\frac{FM}{5000}t)\ ,\quad [\frac{m}{s}]\ ,\quad 0 \le t \le t_{max} \tag{2.2}$$

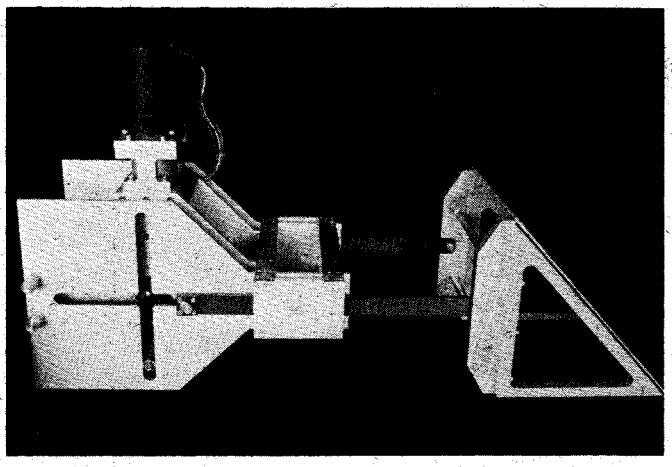

Figure 14: *Wave generating machinery with cross-like slot guided gearing.*

and the distance the piston moves becomes

$$d_{Piston} = 0.125(1 - \cos(2\pi \frac{FM}{5000} t)) \ , \quad [m] \ , \quad 0 \leq t \leq t_{max} \ . \tag{2.3}$$

These functions are graphically displayed in figure 17.

We now turn to the description of the piston geometry. It determines the manner in which the bottom of the channel or the left boundary is changed and, as a result, the water mass is displaced.

Three types of moving boundaries have been implemented:

- *The water is shifted over its entire depth.* To this end a vertical plate which covers the whole cross section of the channel is screwed onto the piston of the wave generator. The generator will push the piston just once from its rear position to the maximum front position where it comes to a full stop. In other experiments the vertical plates were replaced by wedges having inclination angles of 45^0, 30^0 and 15^0, respectively. By moving them forward they displace equal volumnes of liquid for equal travelled distances d. The displaced volume per unit width is

  $$V(t) = h \cdot dx(t) = h \int_0^t v(\tau)\, d\tau \ ,$$

  where h equals the water depth. This expression is linear in the time integral of the velocity.

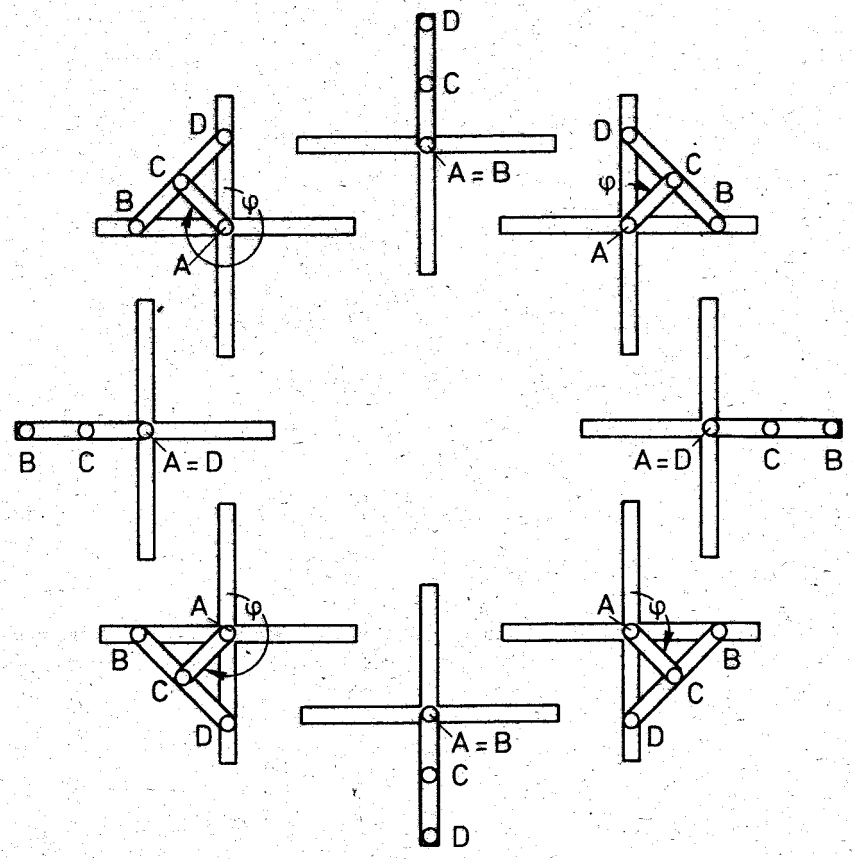

Figure 15: *Scheme of the cross slot guided gearing. Bar $\overline{AC}$ rotates about A. Bar $\overline{BD}$ is guided in the vertical and horizontal slots so that D moves downwards and upwards and B from left to right and back.*

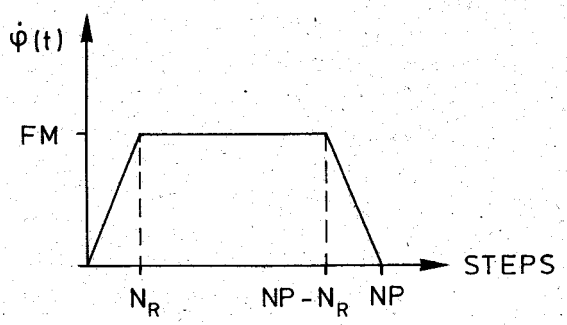

Figure 16: *Velocity profile of the stepping motor.*

- *The water is displaced by a fully submerged device.* These devices were constructed with the wedges described above, but in front of them a vertical plate spanning the channel was added (Fig. 18). The plate is mounted in bearings so that it can move in the vertical direction. As the wedge is pushed horizontally forward it lifts the plate according to the inclination angle of the wedge. The motor of the wave generator is stopped at a time before the base point of the vertical plate passes the water line. In this case the displaced volume per unit width of the device increases with the square of the time integral of the velocity:

$$V(t) = 0.5\, s \cdot (dx(t))^2 = 0.5\, s \,(\int_0^t v(\tau)\, d\tau)^2\,,$$

where s equals the slope of the wedge.

Another shape that was used is a box, about $1.25m$ long, $5cm$ high that spans the channel. This box moves through a slot of a fixed vertical wall that defines the left boundary. At the front of the box small wedges of 30^0 or 45^0 with the same height as the box can be attached. The box operates as a moving step and displaces a volume per unit width of

$$V(t) = b \cdot dx(t) = b \int_0^t v(\tau)\, d\tau\,,$$

where b is the height of the box (Fig. 18).

- *The water is displaced by a rotating plate.* This method of generating water waves has already been sketched in figure 13 on page 80. The plate, which is between $30cm$ to $50cm$ long, is hinged at the bottom in a cylindrical bearing and rotates according to the pull that is exerted at the end of the plate. A second, vertical, and freely moveable plate bounds the fluid from the left. The vertical plate is placed at a fixed position in the channel just above the rotating plate, and is lifted by its motion. In this configuration the displaced

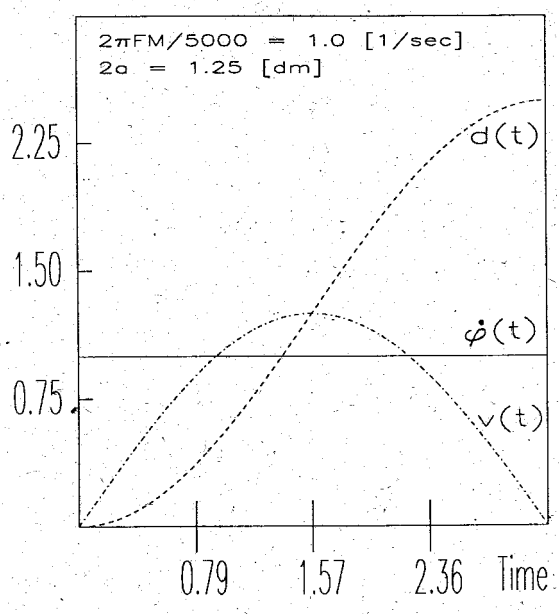

Figure 17: *Distance $d(t)$ and velocity $v(t)$ of the wave generating piston due to a constant angular velocity $\dot{\varphi}(t)$ of the generator's motor.*

volume per unit width is

$$V(t) = 0.5\, l \cdot \int_0^t v(\tau)\, d\tau\,,$$

where l is the horizontal distance of the wall from the pivot as shown in figure 13.

2.2 Wave-height-time series

Whatever the device that displaces a water mass, it generates a wave which is initiated essentially at the wave generator and runs to the right along the channel, is nearly perfectly reflected at the smooth right channel end and moves back to the wave generator, is reflected again etc. We are primarily interested in the onset and propagation of the wave train prior to any reflection. In particular, our aim is to record wave heights and velocity profiles of the waves as they pass positions at various distances from the wave generator.

Eight gauges by which wave heights can be measured were installed at equal distances along the channel. At each gauge, the passage of the wave produces a time dependent signal, recording the wave height at that gauge. Each gauge consists

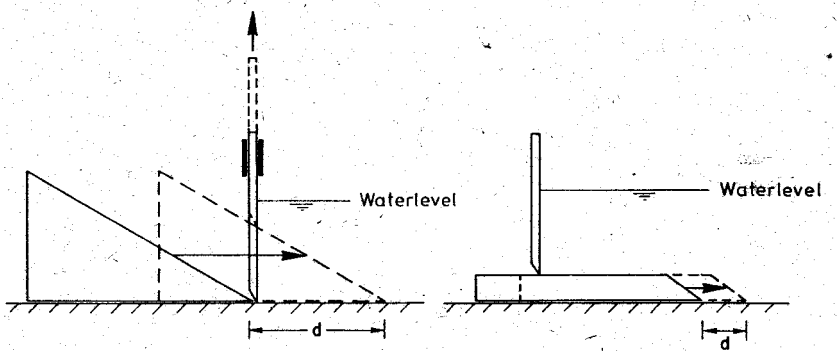

Figure 18: ***Fully submerged pistons.*** ***Left: moving wedge which lifts a vertical plate.*** ***Right: box moving below a vertical plate.***

of two parallel wires $0.15mm$ in diameter which are made of stainless steel. The wires are partly submerged in the water. In the motionless equilibrium state the submerged part of the wires constitutes a fixed portion of the total length. When a wave passes the gauge the length of the submerged portion of the wires is changed. The measuring technique is now based on the different electrical conductivties of the wires when being surrounded by water and air, respectively. A change in water level then changes the electrical conductivity σ. Because $\sigma \sim R^{-1}$ where R is the electrical resistivity, water level variations can be measured by means of an electrical bridge. An inverter, coupled with an amplifier, transforms the signal to a voltage U which is proportional to the water level (see figure 19). With a high frequency voltage electrolysis of the water is prevented.

The amplifier needs a warm-up time of about 15 minutes. Then the amplification is nearly linear for several hours. Its calibration is as follows: We lower the gauges until they touch the bottom of the channel. This corresponds to the maximum gain; a voltage reading can be taken. Then we lift the gauge a prescribed amount; with the vernier scale that is attached to the gauge the difference in position can be measured to within $\pm 0.05mm$ accuracy. We record the new voltage value. Repeating this procedure for several positions of the gauge, the difference in depth can be related to the corresponding voltage difference. This reference curve will serve as calibration curve of the height measurements for all experiments.

The voltage that leaves the amplifier is an analog signal which passes through a low pass filter of 3000 Hz and is digitized with a scanner frequency of 11025 Hz. Short periodic high frequency noise is thus filtered out and aliasing effects are prevented. The analog-digital converter has a 12 bit resolution. Parallel with the

digitized signal the actual time is also stored with a time step of $0.02s$. The digitized signals are stored on a magnetic tape for further analysis.

The measuring system, consisting of the gauges, converter, amplifier, digitizer and tape-recorder allows eight parallel measurements of wave-height-time series. The amplification of the individual gauges are not electrically separate but the mutual interaction is so small to be negligible. Furthermore the disturbances from other electrical fields like that of the stepping motor are observable but they merely contribute to the noise level.

2.3 Velocity profiles

Usual theoretical models of nonlinear shallow water waves make use of a uniform velocity profile. It is interesting to see to which degree such an assumption is justified.

Estimates for the vertical distribution of the horizontal velocity were obtained with the Hydrogen-Bubble-Method. This method is based on the electrolysis of H_2O. It works as follows: a stainless steel wire $0.15mm$ in diameter is stretched between the channel bottom and the free surface (or beyond). In order to have a minimum side wall effect this wire is placed in the middle between the channel walls approximately midway between the wave generator and the channel end. Onto the back wall of the same cross section a thin copper plate, $5cm$ wide and $30cm$ long is glued. A direct current of 30 to 70 Volts is established between the wire and the copper strip. The water is electrolysed by an electric current according to the reaction $2H_2O + 2e^- \rightarrow H_2 + 2OH^-$. The H_2 gas is generated at the anode, which ought to be the wire. With the appropriate sign of the potential this can always be achieved. Small H_2 bubbles are formed. According to Schraub et al. [74] these bubbles are nearly spherical with a diameter of about one half of the wire diameter. Owing to the buoyancy effects they rise against gravity. The measuring method is as follows: The electric voltage is turned on for a short time. It generates along the wire a column of H_2 bubbles which are carried away by the fluid with essentially the local velocity of the carrier medium. Taking snapshots of the bubbles at later times will show them distorted and deformed from the vertical straight line. To first order the snapshots yield the horizontal displacements of individual H_2 bubbles which trace the fluid particle trajectories.

An estimate of the bubble rise velocity can be obtained on the assumption that the flow around the bubble is laminar, creeping and stationary, so that Stokes' law of drag resistance (which is accurate for $Re \leq 1$) is applicable,

$$F_D = 6\pi\mu r v\,, \tag{2.4}$$

where μ is the dynamic viscosity. This viscous drag F_D must be balanced by the buoyancy force F_B, where

$$F_B = \frac{4}{3} g\pi r^3 (\rho_{H_2O} - \rho_{H_2})\,, \tag{2.5}$$

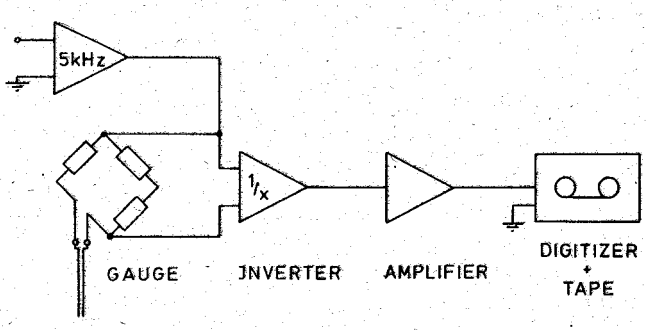

Figure 19: *Electrical set up of the wave height recorder.*

which yields for the rising velocity

$$v = gr^2 \frac{2(\rho_{H_2O} - \rho_{H_2})}{9\mu} . \tag{2.6}$$

With

$$\begin{array}{llll} \rho_{H_2O} = 1010 & kg\,m^{-3}, & g = 9.81 & m\,s^{-2}, \\ \rho_{H_2} = 0.09 & kg\,m^{-3}, & r = 7.5 \cdot 10^{-5} & m, \\ \mu = 1.002 \cdot 10^{-3} & N s\,m^{-2} & & \end{array}$$

(Data from Handbook of Chemistry and Physics [91]), this yields $v = 1.2 \cdot 10^{-2} m s^{-1}$, somewhat more than a centimeter per second. The Reynolds number Re for this rise-rate is $Re = 2vr\rho_{H_2O}\mu^{-1} = 1.8$, Oseen's correction (valid for $Re < 5$) will give a velocity of $v = 0.97 \cdot 10^{-2} m s^{-1}$ and $Re = 1.5$. Observations indicate that the growth of the bubbles is substantially increased if the carrier velocity decreases. However, in this case the bubbles tend to coalesce. Also, the bubbles formed are bigger and so rise much faster, making them less sensitive to the water velocity. Their trajectories may then no longer follow the fluid particle trajectories. To avoid ambiguous results we have adjusted the voltage according to the speed that was present. Prior to the passage of the wave the voltage was set to zero. As the wave approaches the wire the voltage is increased such that its maximum of about 70 Volts is reached when the wave maximum passes the position of the wire.

The trajectories of the bubbles are a superposition of the water velocity and the buoyancy velocity. To first order these velocities may be identified with the tangential velocities along the streamlines. To determine the velocity in the horizontal direction, consecutive snapshots of the bubble positions must be taken. The ratio between the horizontal distance Δx of corresponding bubbles and the time interval Δt between the shots yields an approximation for the horizontal velocity component at some depth, see figure 20.

A camera, taking 14 pictures per second with an exposure time not smaller than 1/250 seconds, yielded a series of photographs of bubble lines which very nearly

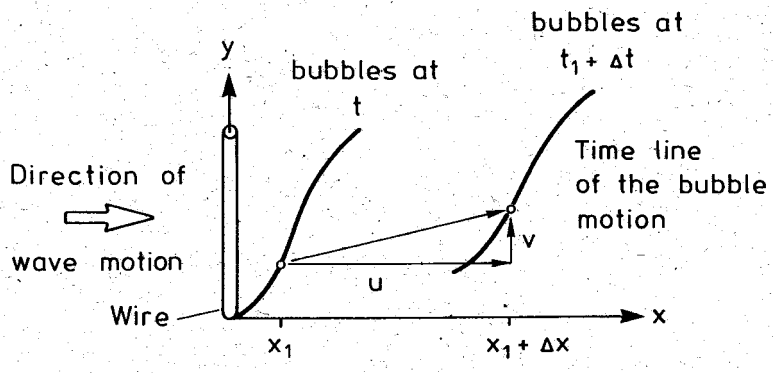

Figure 20: *Sketch how to determine the horizontal velocity u from successive time-lines. v is the horizontal velocity due to buoyancy.*

correspond to time lines of streamlines [15]. The velocity is determined by measuring the horizontal distance of successive time lines of the bubbles; this is independent of buoyancy effects, because the horizontal shift of the time lines is independent of buoyancy. A representative horizontal velocity is then obtained from

$$\overline{u}(y,\overline{t}) = \frac{\Delta x(y)}{\Delta t}\,, \tag{2.7}$$

where Δt is a time between the two snapshots. Clearly, the method is inappropriate for measurements of velocities at the bottom of the channel. In a non-stationary flow field such as ours, the accuracy of the velocity profile determined by eq. (2.7) depends upon the frequency of photographs that can be taken. With fourteen shots per second and a maximum wave speed of $0.3ms^{-1}$ this amounts to an estimated relative error of approximately 15%. This should be born in mind; results have therefore mainly qualitative significance.

The procedure to determine the averaged velocities according to eq. (2.7) is as follows: The part of the channel where water was electrolysed was illuminated by two head lights of 500 Watt each, such that reflection on the frontal plate of the channel was minimized. For proposes of improved contrast against the nearly white bubbles the back wall was painted black. Photos were taken from behind the positions of the headlights, using a normal $50mm$ objective. To fix the geometry in the plane of the wire and the channel axis, three points were marked: one on the wire $5cm$ above the bottom, the second at the bottom point of the wire and the third $10cm$ to $20cm$ downstream at the bottom along the channel axis. These points define a coordinate system against which the bubble positions on the photographs can be located. Photos were analysed with the aid of a digitizing table. The reference

[15] Here a timeline of streamlines is the line connecting bubbles that originate from the wire released at the same time.

points defined the length scales and thus permitted determination of the bubble positions; 40 to 60 points for each time line were digitized. The small anisotropic distortion at the boundaries of the prints due to the optical quality of the lenses had to be ignored. Better optical quality could have been obtained with a teleobjective, but this was not available.

The velocity profile according to eq. (2.7) was deduced from the digitized data using linear interpolation. Note that the upper most (lower most) points of two consecutive time lines were defined by the corresponding minimum (maximum) of the highest (lowest) bubble of the two time lines.

We now close the description of the general experimental set-up and turn our attention to the experimental features and their results.

3 Experimental Results

3.1 Velocity Profiles

The evolution of the velocity profiles was determined only for a selection of experiments, since it turned out that the general features were very simular in all experiments. Figure 21 shows a succession of eight snapshots with time lines of H_2 bubbles, the individual photos being $1/14s$ apart. For the experiments shown, waves were generated in $10cm$ deep water by a piston-plate configuration having the plate inclined at 45^0. The waves so generated were very close to solitary, however the wave height and speed were such that traces of wave breaking can be detected at the wave crests. As can be seen from the photographs, the nearly uniform velocity profile at the onset of the wave passage is altered to a non-uniform velocity profile with the highest velocity at the water surface and the lowest at the bottom. We emphasize that the time lines closely mimic the water particle displacements, even though time lines are not necessarily proportional to velocity profiles.

The outcome of the digitization and the analysis according to eq. (2.7) is summarized in the graphs of figures 22, 23, 24. They show the vertical velocity profiles and the water levels at consecutive times when the wave passes through the cross section of the velocity gauge. The plotted water level distribution corresponds to the time shown in each panel, and the velocity profile is representative for the time interval immediately before the time for which it is drawn. The following table lists some properties pertinent to each of the experiments.

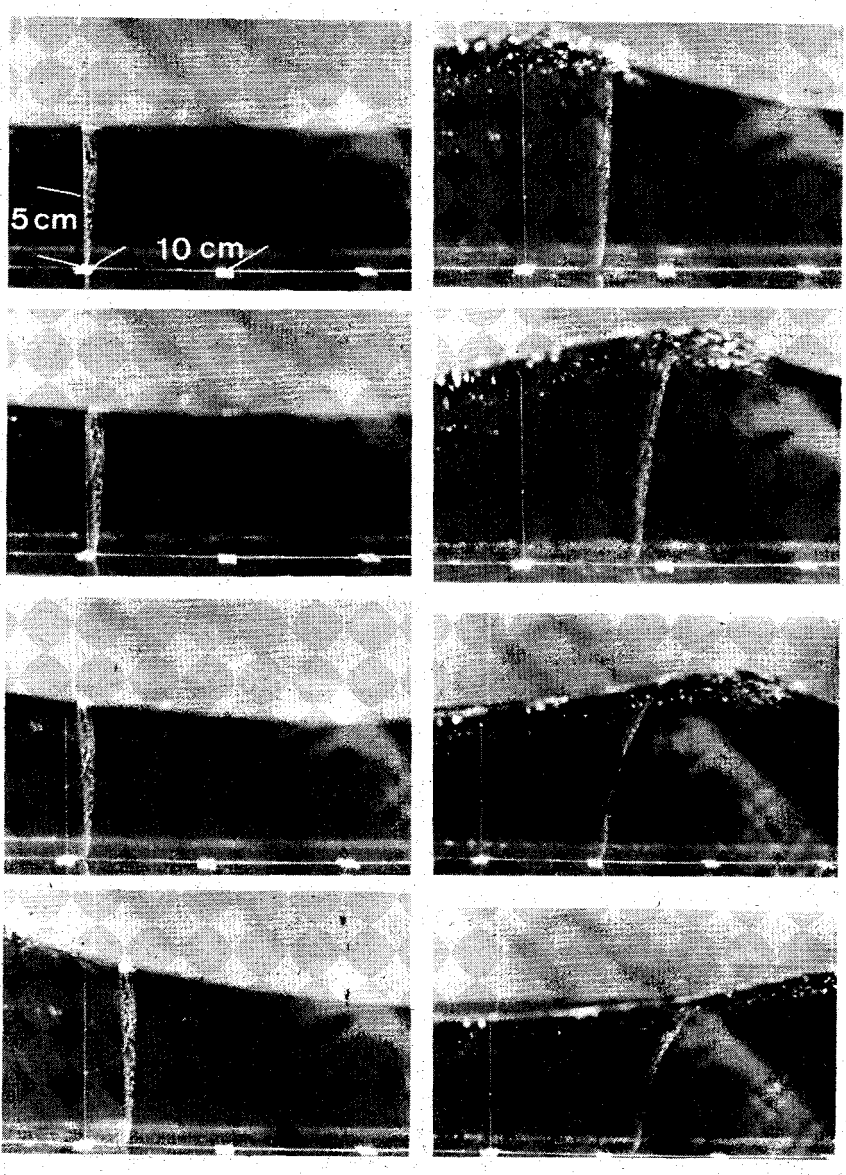

Figure 21: *Photographs of timelines generated with the Hydrogen Bubble Method. The photos are* 1/14*s apart. The distances from the bottom point of the wire to the points above it and to the right along the the channel are 5cm, 10cm, 20cm and 30cm, respectively.*

Figure	22	23	24
Wave generator	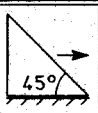		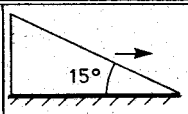
Wave form	solitary breaking at crest	solitary	solitary
Wave speed c	$1.3\,ms^{-1}$	$1.2\,ms^{-1}$	$1.1\,ms^{-1}$
$Fr_c = c(gh)^{-1/2}$	1.3	1.2	1.1

All waves were generated by a wedge type piston with inclination angle of either 45^0 or 15^0, respectively. The momentum transfer was such that solitary waves evolved with estimated wave speeds and corresponding Froude numbers as indicated in the table above. Froude numbers are referred to the undisturbed height and are all below 1.4. In the case of figure 22 a clear trace of wave breaking can be discerned in the photographs (see also fig. 21). This is just below $Fr_c = 1.4$. Whenever $Fr_c > 1.4$ it is known that waves break (see Hager & Hutter [31]).

Qualitatively, the following inferences can be drawn from figures 22, 23 and 24: Prior to any wave arrival the H_2 bubbles remain attached to the wire. The velocity must be zero or so small that the bubbles are not torn off the wire. When the wave arrives, the water level rises on the left and small velocities set in from left to right. As the wave moves through the cross section and the slope becomes steeper, the velocities increase and vertical profiles deviate more and more from uniformity. The maximum velocities are difficult to determine; they seem to be reached about at the instant when the wave crest passes the position of the wire. After the wave has passed, the velocity decreases, and seems to slow down to zero once the water level has returned to its original horizontal position. As a function of the vertical coordinate, the velocity profile is always nearly uniform in the lower third to half of the channel. Only in the upper half and during the wave passage do velocities slightly increase towards the surface.

3.2 Wave heights

The motion of the water surface is registered at eight fixed points along the channel. At each of these positions, wave height time series were recorded with the gauges described in section 2.2.

Waves were generated under various different conditions, such as different speeds of the wave generating piston, different geometries of the piston, different water depths, etc. In order to have a common basis for comparison of these waves, a dimensional analysis was performed that indicated how the registered data ought to be represented. More precisely, a dimensional analysis yielded dimensionless

Figure 22: *Velocity distribution over the water depth, deduced from the Hydrogen Bubble Method. Figure 21 shows the original wave.*

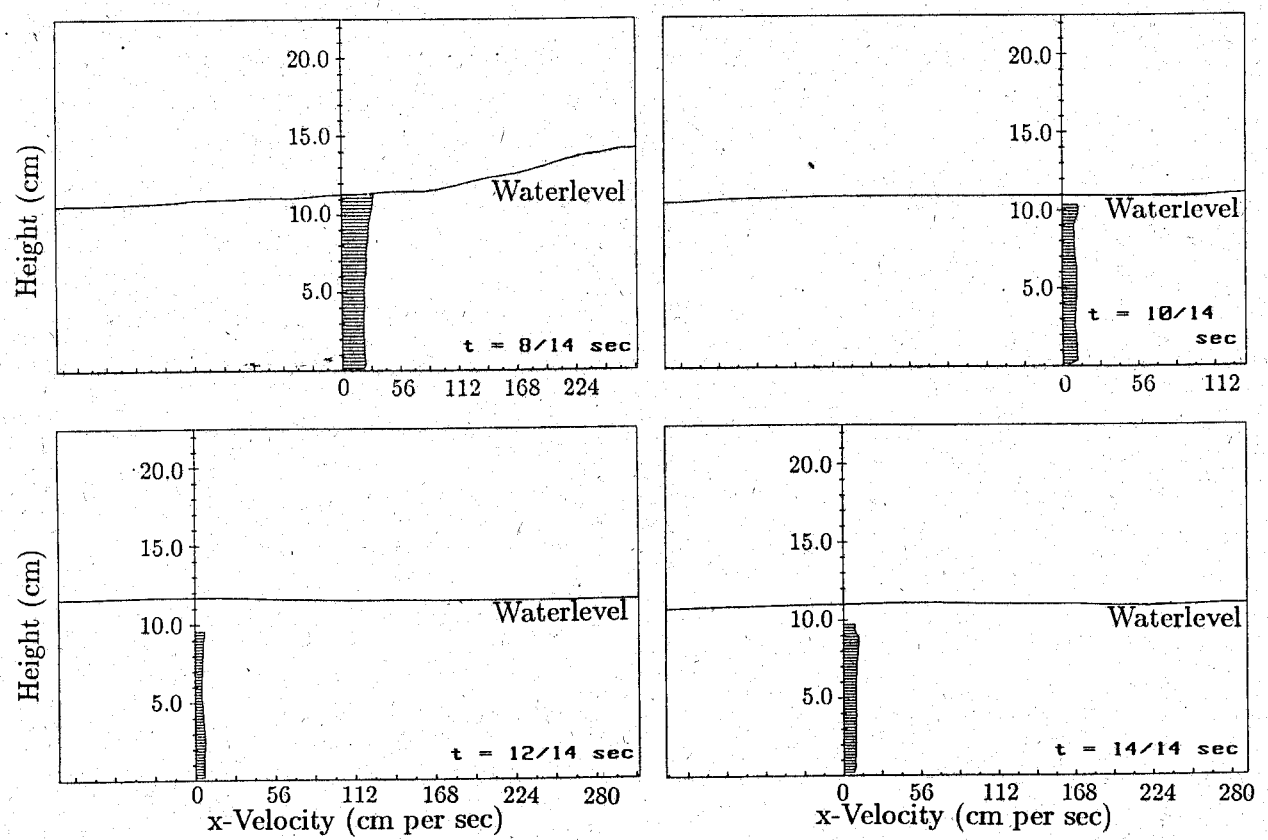
Height (cm)
20.0
15.0
10.0
5.0
Waterlevel
t = 8/14 sec
0 56 112 168 224
20.0
15.0
10.0
5.0
Waterlevel
t = 10/14 sec
0 56 112
Height (cm)
20.0
15.0
10.0
5.0
Waterlevel
t = 12/14 sec
0 56 112 168 224 280
x-Velocity (cm per sec)
20.0
15.0
10.0
5.0
Waterlevel
t = 14/14 sec
0 56 112 168 224 280
x-Velocity (cm per sec)

Figure 23: *Velocity distribution over the water depth, deduced from the Hydrogen Bubble Method.*

Note that the velocity scale can be identified with the vertical distance multiplied by $1/14s$.

Figure 24: *Velocity distribution over the water depth, deduced from the Hydrogen Bubble Method.*

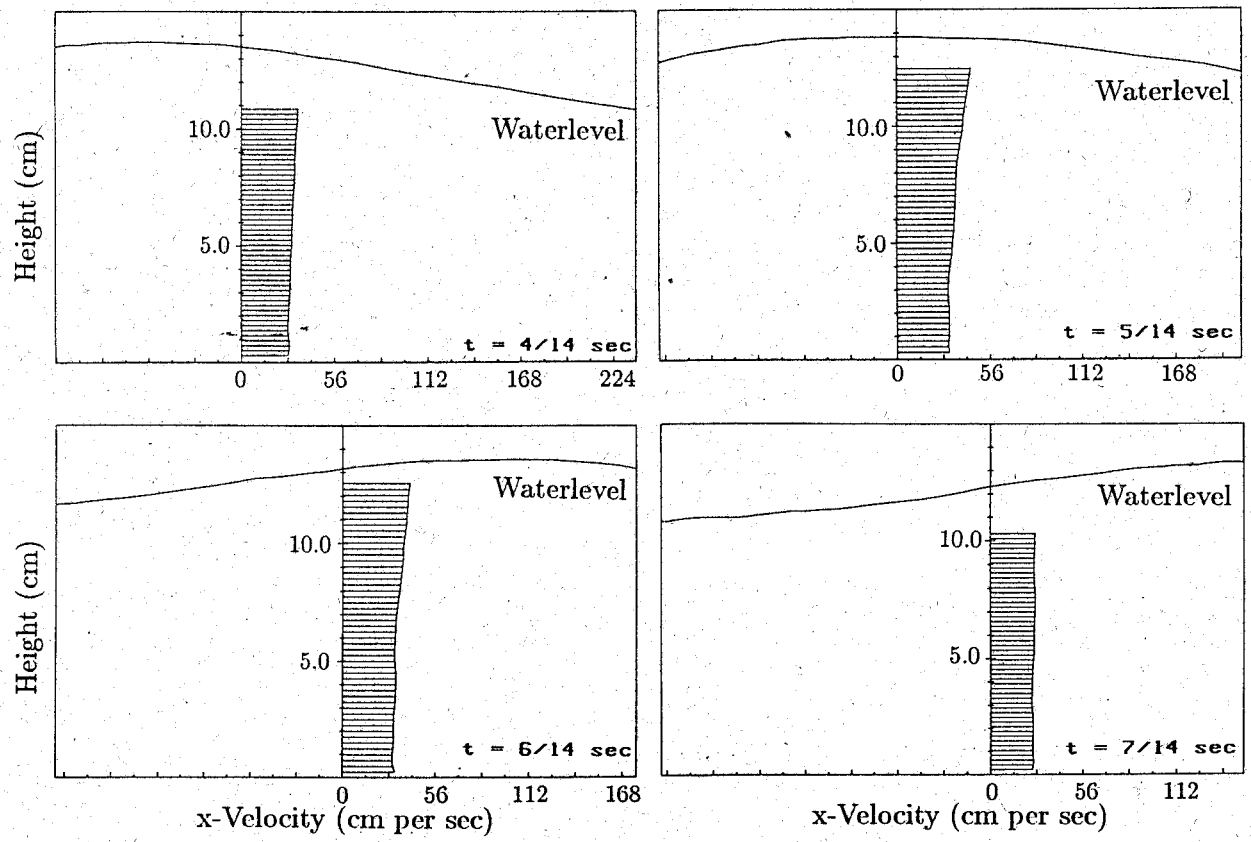
Height (cm)
Waterlevel
10.0
5.0
t = 4/14 sec
0
56
112
168
224
Waterlevel
10.0
5.0
t = 5/14 sec
0
56
112
168
Height (cm)
Waterlevel
10.0
5.0
t = 6/14 sec
0
56
112
168
x-Velocity (cm per sec)
Waterlevel
10.0
5.0
t = 7/14 sec
0
56
112
x-Velocity (cm per sec)

combinations of the physical parameters and observed variables which describe the wave properties *independent* of the individual conditions. Instead of representing the observables in terms of the absolute physical variables, their dimensionless counterparts are related to the dimensionless products.

The procedures of dimensional analysis are well known (Langhaar [47]). One first lists the variables that describe the phenomenon. Here, where the perturbed free surface of the water and the associated wave speeds are sought, this list is as follows:

h	undisturbed water depth,
η	wave amplitude,
μ	(dynamic) viscosity,
ρ	water density,
c	wave speed,
g	acceleration due to gravity.

From these variables, we then form the dimensional matrix:

variable / unit	h	c	η	μ	ρ	g
m	1	1	1	-1	-3	1
kg	0	0	0	1	1	0
s	0	-1	0	-1	0	-2

whose rank is three. Therefore, there exist three dimensionless products, i.e.,

$$\Pi_1 = \frac{\eta}{h}$$

$$\Pi_2 = \frac{c}{\sqrt{gh}} = Fr$$

$$\Pi_3 = \frac{\rho h^{3/2} g}{\mu} = \frac{h\sqrt{gh}}{\nu} = Re$$

in which $\nu = \rho^{-1}\mu$ is the kinematic viscosity, Fr the Froude number, and Re the Reynolds number of a wave with the velocity given by the linear wave theory: $c_0 = \sqrt{gh}$. Note that $\Pi_2 \cdot \Pi_3 = h\nu\mu^{-1}$ would also define a Reynolds number, but it would involve the unknown speed of the nonlinear wave. Buckingham's theorem allows the physical problem of nonlinear water waves to be expressed as a dimensionless homogeneous function of the Π_i:

$$F(\Pi_1, \Pi_2, \Pi_3) = 0 \ .$$

In ensuing developments, all diagrams that illustrate the shape will be drawn in terms of these nondimensional scales. The graphs will show how the waves evolve in time. In particular, our attention is focussed on the wave forms and their evolution immediately after initiation and on the dispersion into a certain number of solitons.

We shall first examine the waves that were generated by the rotating plate, and then turn to the waves which arise from the moving piston.

3.2.1 Waves generated by a rotating plate

For the rotating plate experiments we used a $30cm$ and a $50cm$ long plate. This plate was lifted at a rate such that its vertical velocity was within the interval $0.01 \leq v(gh)^{-1/2} \leq 0.2$, and its motion was stopped when the inclination was between 0.05 and 0.4. The undisturbed water depth was $5cm$, $10cm$ or $15cm$. It will be shown that the wave forms depend on all these parameters.

Figure 25, which shows time series of the free surface elevation at the first gauge (placed at $x/h = 9$), shows that even though the physical conditions are different in the illustrated cases the wave shapes agree with one another when the dimensionless parameters Froude number and dimensionless time $t\sqrt{g/h}$ have the same values. The plate rotates in 5, 10 and 15cm deep water and stops when an inclination of 3/15, 6/30 and 9/45 is reached (numerator: vertical distance in cm which the plate is lifted at $x = 0$, denominator: length of the plate in cm). At the Froude number of 0.01 the three wave forms differ slightly from each other, however. This seems to be due to small inaccuracies during the experiments as the vertical plate at $x = 0$ oscillated in the horizontal direction. By contrast the waves generated with $Fr = 0.08$ and $Fr = 0.1$ agree nearly perfectly.

The development of the emerging wave forms under various initial conditions was studied in greater detail by varying the rotation speed, the final slope s and the length of the wave generating plate. Figure 26 shows again time series of the water elevation at the first gauge. Initial conditions are expressed as a Froude number of the vertical component of the velocity of the rotating plate (which is held constant), and the slope s of its final position. Two different lengths of 50/15 and 30/15 are examined where 15 denotes the depth of the water in centimeters. Generally, the wave length and wave height depend on the final slope and Froude number. The Froude number is formed by the vertical velocity v of the plate at its rear end ($x = 0$) and the undisturbed water depth h: $Fr = v/\sqrt{gh}$. Higher slopes for the same length of the plate generate broader waves while increasing the Froude number results in higher amplitudes. Waves with low amplitudes, generated with a low Froude number, $Fr = 0.01$, and for slopes $s_i \geq 0.1$ are similar to a hydraulic jump. Longer plates generate higher waves, but the value of the wave height depends largely upon its form. Surprisingly, the wavelengths at Froude number 0.01 are of the same order when the final slope times the nondimensional length of the plate are identical.

These results pertain to the fixed gauge closest to the wave generator at the nondimensional distance of $x/h = 10.3$ for waves generated with the 50/15 long plate and $x/h = 9$ for the 30/15 long plate. As the waves travel along the channel, they will deform. Generally, the leading hump changes its height and splits up into several solitary waves. When they reach the end of the channel they may still be close to each other and weakly interacting; others may have completely separated.

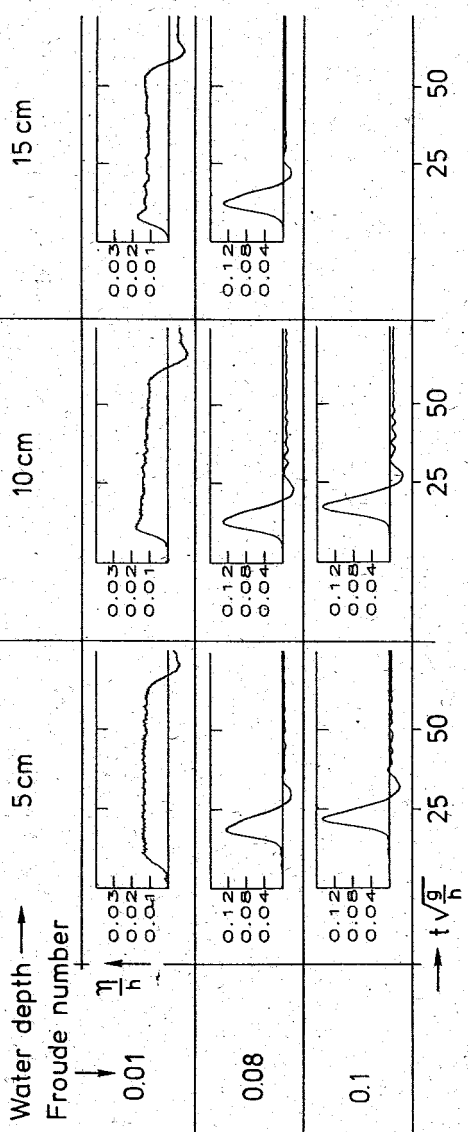

Figure 25: *Dimensionless water elevation at the first gauge plotted against time for different Froude numbers and water depths. The wave was generated by a rotating plate, which was stopped at the slope of 0.2. The gauge is located at $x/h = 9$.*

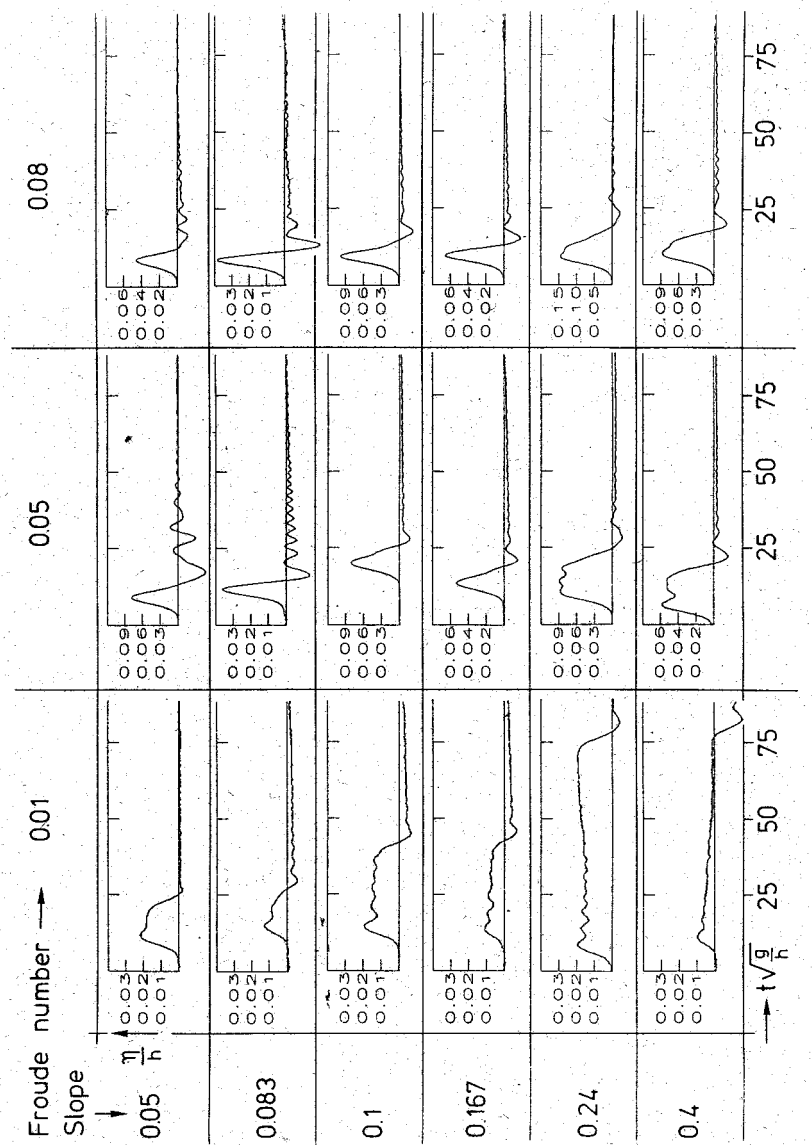

Figure 26: *Wave forms depending on slope and velocity of the rotating plate. All data are taken at the first gauge nearby the rotating plate. For the slopes 0.05, 0.1, 0.24 the dimensionless length of the plate is 1.3; when the slopes are 0.083, 0.167, 0.4 its length is 2.*

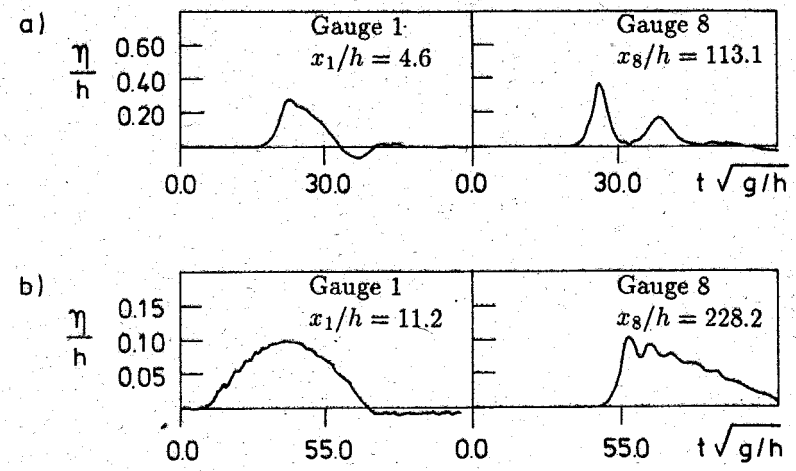

Figure 27: *Dispersion of an initial wave hump into a file of solitary waves,*
a) for a moving wedge with inclination angle of 15^0, $h = 10cm$ *deep water, and Froude number* $v/\sqrt{gh} = 0.4$.
b) for a moving wall in $h = 5cm$ *deep water and Froude number* $v/\sqrt{gh} = 0.11$.

These solitary wave behaviours are general features of large amplitude waves and will be described in the next section.

3.2.2 Waves generated by a moving piston

For all experiments, whatever the piston configuration, the piston velocity was constrained by $0.1 \leq v(gh)^{-1/2} \leq 1.1$. The Froude numbers of the waves Fr_c were always kept below $Fr_c = \sqrt{2}$, where waves begin to break. The observed shapes of the generated waves are essentially the same for all piston configurations: a steep front which extends to a first maximum followed by a slightly slower decay. The wave generator usually produced a wave train that begins with a compact wave form (a single hump or an N-form, see figure 27) that is quickly dispersed into a number of separate waves. Their succession is ordered according to their amplitudes with the larger ones being ahead of the smaller ones. The number of individual wave humps that develop depends on the initial wave form.

As was done for the waves generated by the rotating plate, we have studied the wave forms as they emerge from various initial conditions of the piston motion and several different water depths for the undisturbed water level. Figure 28, which is similar to figure 26, displays waves that were generated by a wedge with an inclination angle of 30^0. As with the previous case in figure 26, we see that the nondimensional distance the wedge is moved influences the scale of the wave

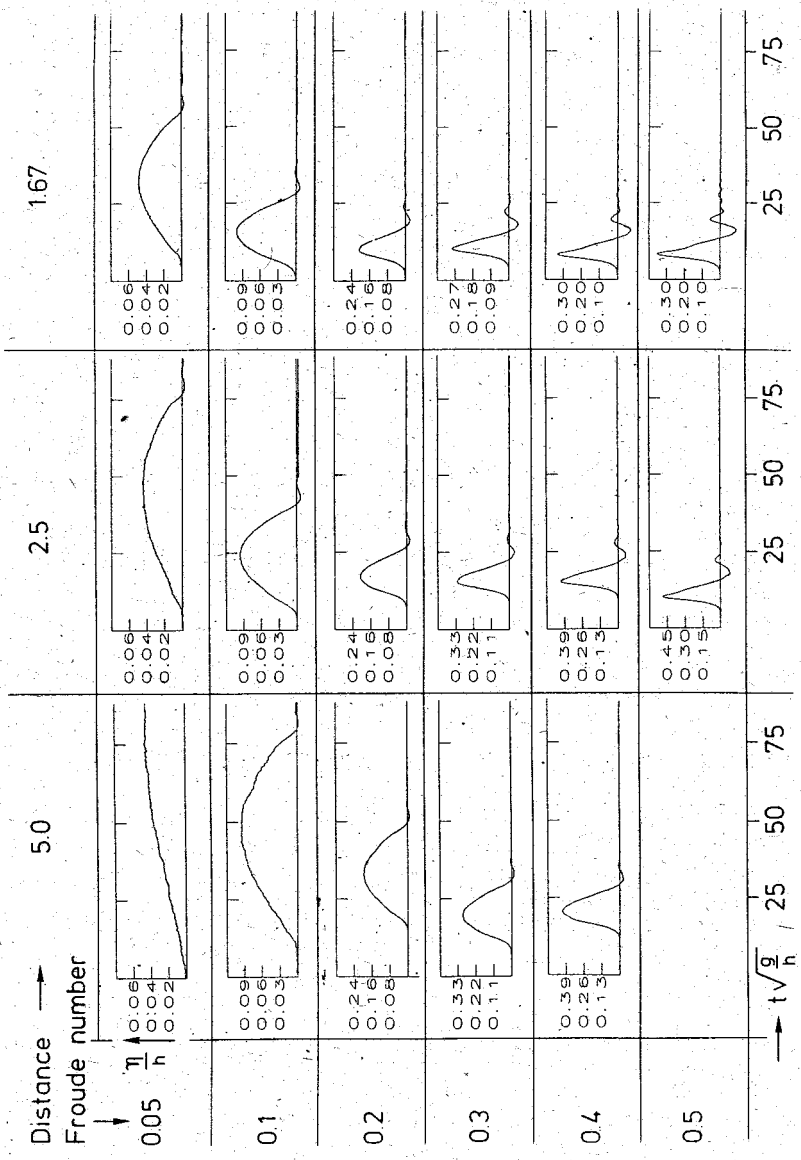

Figure 28: *Dimensionless time series of initial waves at the gauge nearest to the wave generator (wedge 30^0 inclined) for different Froude numbers of the piston velocity and different distances which the wedge was pushed forward.*

hump. Again, longer distances moved by the device result in broader wave forms. For a Froude number $Fr = 0.05$, the ratio of the length of the waves generated by different distances is 2 to 3, whereas for $Fr = 0.4$ it is reduced to about 1. This behaviour is maintained at all travel distances of the wedge and all listed Froude numbers. In summary: the longest waves are generated for low Froude numbers and long distances. The wavelengths decrease with increasing Froude number and decreasing travel distances of the moving device. On the other hand, the wave height depends mainly on the Froude number as was the case already for the rotating plate. Compared with previous experiments, the shorter the distance is that the piston travels the lower the wave amplitude will be. It should be noted that this distance is proportional to the volume of water that is pushed away by the device.

For all waves generated with the 30^0 inclined wedge one general form of the wave was obtained with differences mainly occuring in the wavelength and waveheight. This common form depends, however on the different geometries, such as the slope of the wedge. The three devices with different slopes we employed were moved forward a dimensionless distance of $x/h = 2.5$; the corresponding results are listed in fig. 29. The results were recorded by a gauge placed at $x/h = 6$. Initially the form of the wave is very similar for Froude numbers of $Fr = 0.05$ and $Fr = 0.01$. At higher Froude numbers the waves generated with a slope of 1.0 become more and more acute and solitary, while those of slope 0.268 begin to disperse.

So far a qualitative description was given for the behaviour of the wavelength and the waveheight in terms of different Froude numbers, distances the wedge was moved and slopes of the wedge. Now, let us turn to a quantitative characterization. Therefore a method of scaling is applied. The wavelengths and amplitudes of the wave will be scaled and from these a dimensionless number, closely related to the Ursell number will be deduced, which will only depend upon a Froude number.

For all experiments performed with the same slope of the wedge and the same distance the wedge is moved, we choose an upper bound η_∞ for the amplitude; it is selected to be slightly larger than any of all measured amplitudes at that slope. The maximum amplitude η_{max} of each of these experiments is scaled with η_∞. A similar length λ_∞ is determined for the maximum length of the individual waves λ_{max}. The two quantities λ_{max} and η_{max} may arise at different gauges and in different experiments.

A proper definition of the wavelength is, however, not so easy. It can be defined as the distance between two successive points with the same wave height (phase) that lie in the front and the rear of a wave hump, respectively, and possesses sufficiently small amplitude. The zero amplitude (still water level) could be chosen, but this is difficult owing to inherent uncertainties in the measuring system. We therefore choose as reference those points immediately in the front and in the back of a wave hump, of which the height is 3% of the maximum arising wave amplitude. With this definition the Ursell number $\sqrt{\lambda^2\eta/h^3}$ of a soliton profile $\eta\,\mathrm{sech}^2(\sqrt{\eta}\,x)$

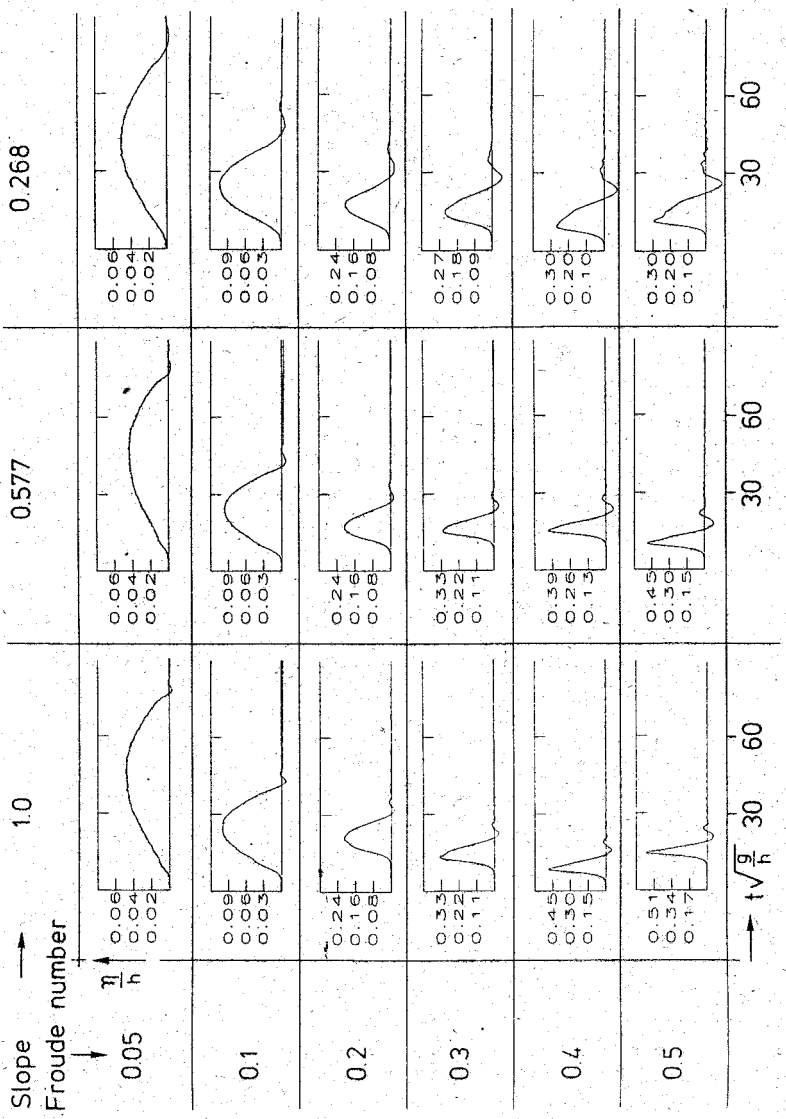

Figure 29: *Dimensionless time series of initial waves at the gauge nearest to the wave generator for different slopes of the wedges and different Froude numbers of the piston velocity.*

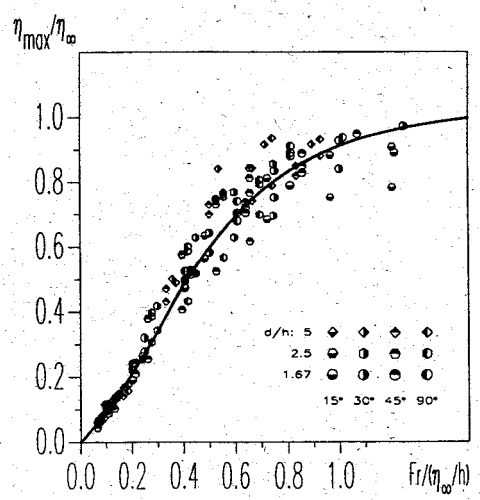

Figure 30: *Maximum amplitudes η_{max} scaled with the upper bound η_∞ of the amplitudes from all experiments plotted against a modified Froude numbers $Fr/(\eta_\infty/h)$. Shown are all experiments performed with a piston with angles and water depths as indicated.*

becomes $Ur = 24$ instead of $Ur \to \infty$ if the still water reference is chosen.

In figures 30 and 31 we have plotted η_{max}/η_∞ and $\lambda_{max}/\lambda_\infty$ against two modified Froude numbers, defined by $Fr/(\eta_\infty/h)$ and $Fr/(\lambda_\infty/h)$, respectively. By these stretchings of the classical Froude number the experimental points are clustered in fairly narrow bands which suggests a functional dependence of η_{max}/η_∞ and $\lambda_{max}/\lambda_\infty$ upon the modified Froude numbers. Despite the considerable scatter of approximately 15%, both graphs indicate a trend: The scaled waveheight grows with increasing modified Froude number $Fr/(\eta_\infty/h)$ and approaches the upper bound $\eta_{max}/\eta_\infty = 1$ as the modified Froude number becomes large. Clearly, η_{max}/η_∞ is vanishly small for $Fr/(\eta_\infty/h) = 0$. Alternatively, the scaled wavelength becomes smaller and smaller the larger the modified Froude number $Fr/(\lambda_\infty/h)$ is, and it grows with decreasing modified Froude number. It seems to approach unity as the modified Froude number becomes vanishly small. For decreasing slopes α one can expect that the waveheight equally decrease and the wavelength become infinitely large, so that $\alpha \downarrow 0$ implies $\eta_\infty/h \downarrow 0$ and $\lambda_\infty/h \uparrow \infty$. This is born out very clearly in figure 32, even though the number of experimental points to support this claim is not very large. Whereas the exact dependencies of the upper bounds η_∞/h and λ_∞/h on α cannot be inferred from the above figures, their variation with α cannot be doubted. It is thus worth recognizing that when the modified Ursell number

$$\widetilde{Ur} = \frac{\sqrt{\lambda^2\eta/h^3}}{d/h} \tag{3.8}$$

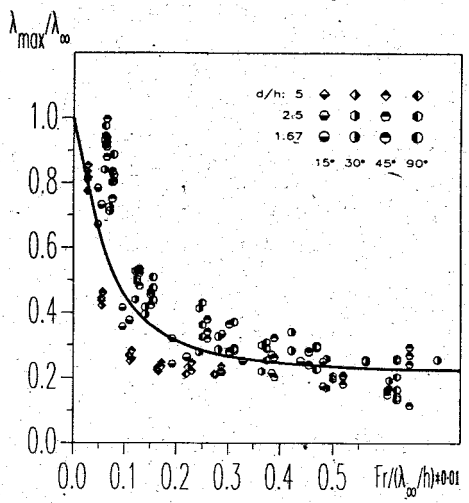

Figure 31: *Maximum length of the waves λ_{max} scaled with the upper bound λ_∞ of the wavelength from all experiments plotted against a modified Froude number $Fr/(\lambda_\infty/h)$. The inclination angles of the wedges and the water depths at which the experiments are performed are indicated.*

is plotted against α then it is seen from figure 33 that this Ursell number has the same constant value for all α and all distances the wedge is moved. In general, i. e. when $\widetilde{Ur}$ is defined with λ_{max} and η_{max} this Ursell number will depend on the Froude number as we shall see later on.

3.2.3 General characteristics of the waves

Dissipation and dispersion are two qualities of the wave which may be estimated from the observations. Dissipation influences the growth and decay history of the wave. Figure 34*a* shows the wave amplitudes which were generated by a wedge type piston with 15^0 inclination angle, moving in $10cm$ deep water. The wave height increases until dissipation and dispersion dominate the growth process. Evidently, the larger the Froude number (i.e. the faster the piston velocity) is, the higher is the amplitude and the more pronounced are the dispersion and dissipation mechanisms. Panel *b* in figure 34 indicates that waves flatten out more or less exponentially. Here the waves were generated by a moving box; gauge 1 is placed above the box and therefore represents a wave moving to the left, while the following gauges measure the waves travelling to the right. As before, faster piston velocities generate higher wave amplitudes. Dissipation appears to be due mainly to the water viscosity, rather than the roughness of the channel bottom, as was demonstrated by Göbel [25].

In figure 35, the shapes of the first hump of the wave train at gauge 1 and gauge

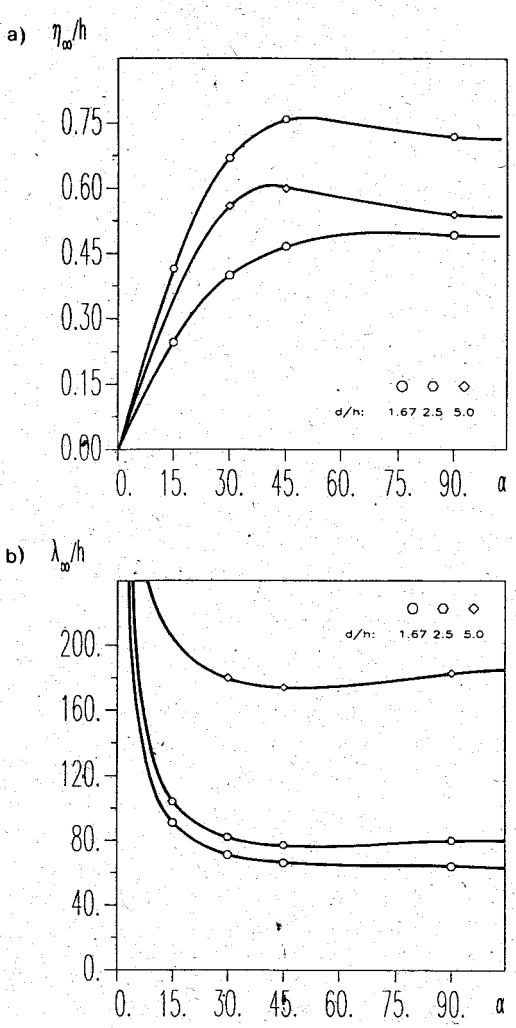

Figure 32: *a) Scaling factor η_∞/h plotted against the inclination angle α of the wedge for three different distances the wedge is moved.*
b) Scaling factor λ_∞/h plotted against the inclination angle α of the wedge for three different distances the wedge is moved.

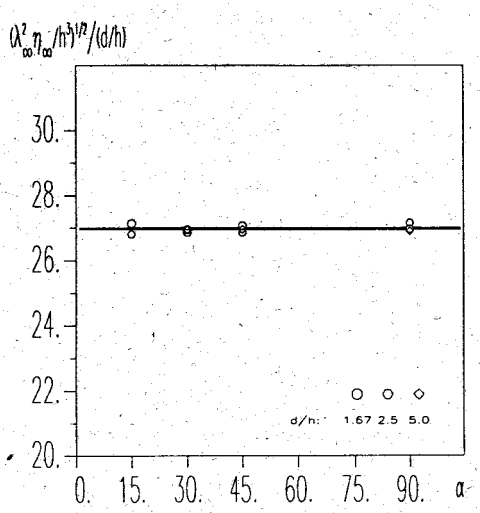

Figure 33: *Modified Ursell number plotted against the inclination angle α of the wedge for three different distances the wedge was moved.*

7 are compared with the solitary profile

$$\eta = \eta_{max}\,\mathrm{sech}^2(t\sqrt{0.75\eta_{max}\,h^{-3}})\,, \tag{3.9}$$

and a sinusoidal profile

$$\eta = \eta_{max}\sin(2\pi\lambda^{-1}t)\,, \tag{3.10}$$

in which λ is the wavelength representative of linear waves. Clearly, at the first gauge (see figure 35) the wave profile fits none of the theoretical profiles perfectly. Further away, at gauge 7, the wave front is identical to the solitary wave profile, and the rear end of the wave is very close to this profile, deviating only because of the complex tail. We have also observed that the largest amplitudes are closest to the solitary profile. Figure 36 shows a small amplitude wave which initially fits the sinusoidal shape quite well, but after propagating one length of the channel, its profile fits neither a linear nor a solitary wave [1]. This shows that our wave generating device may produce wave forms that travel reasonably large distances before these waves disperse into a number of solitons.

The mean wave velocity between successive gauges was also calculated. With the known distance between the gauges and the time which the maximum of the leading wave needs to travel this distance yields the mean velocity of the wave in this section of the channel. For all experiments done with a piston, the velocity c so calculated was normalized by the velocity $\sqrt{gh}$, and plotted against the normalized

[1]The parameters in equations (3.9) and (3.10) are determined once and for all once the scales of the wave are fixed. Hence one has no freedom in adjusting the width of the theoretical profiles.

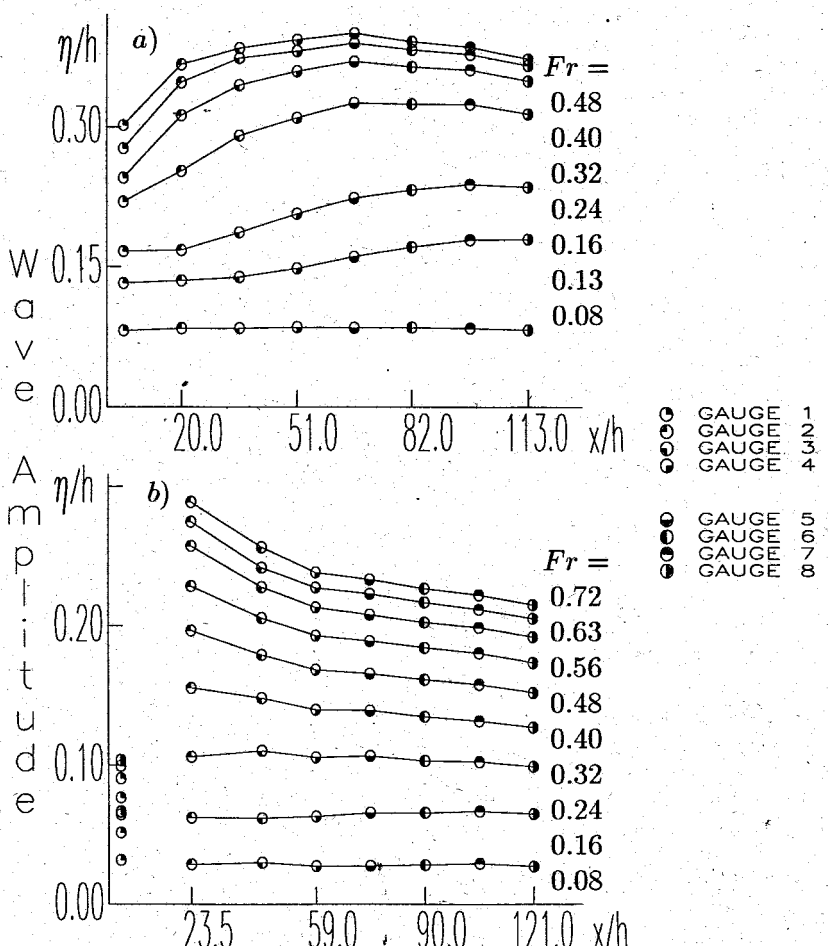

Figure 34: *Maximum dimensionless wave heights plotted against dimensionless distance from the wave generator. Connected by lines are the amplitudes of a travelling wave generated with a certain velocity of the piston.*
a) Waves generated by a 15^0 *inclined wedge in* $h = 10cm$ *deep water.*
b) Waves generated by a moving box of $5cm$ *height in* $h = 10cm$ *deep water.*

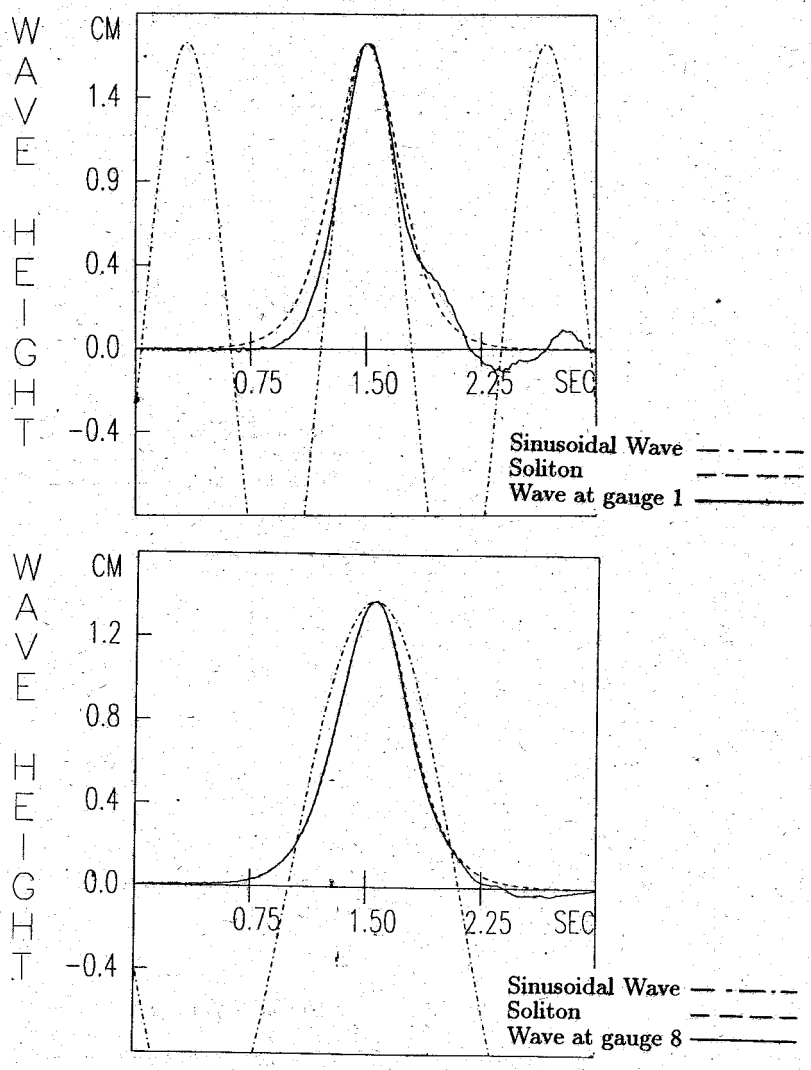

Figure 35: *Comparison of a wave with the solitary solution of the Boussinesq theory and the sinusoidal wave of the linear theory. Here the wave becomes solitary at the end of the channel. Gauge 1 is about* 0.5*m, gauge 7 about* 12*m away from the wave generator.*

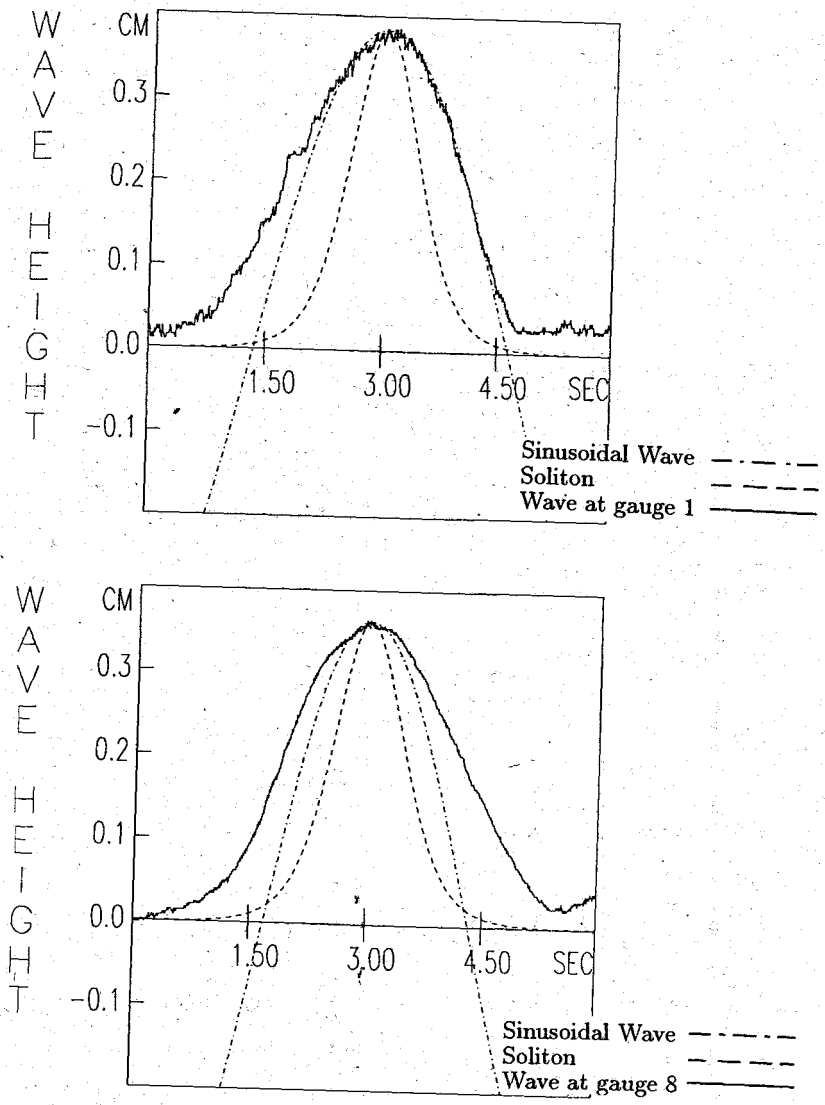

Figure 36: *Comparison of a wave at gauge 1 and 7 with the solitary and sinusoidal waves. The wave fits neither the linear nor the solitary profile.*

wave height ηh^{-1}. Near the wave generator (gauge 2 in fig. 37) the wave velocity-amplitude distribution is scattered, but as the distance travelled increases, waves of all but the smallest amplitudes converge on a line representing a normalized velocity that depends on the square root of the water depth (gauge 7). This is in agreement with the evolution of the wave shapes that was discussed earlier. Here again, the larger their amplitudes are, the more solitary-like the waves will be. A linear regression of all the data within the interval $0.8 \leq c(g(h+\eta))^{-1/2} \leq 1.20$ results in $c^2/(gh) = 0.96 + 1.02\eta/h$ at gauge two with a residual of 0.83 and $c^2/(gh) = 1.00 + 0.99\eta/h$ with a residual of 0.94 at gauge seven, see figure 37.

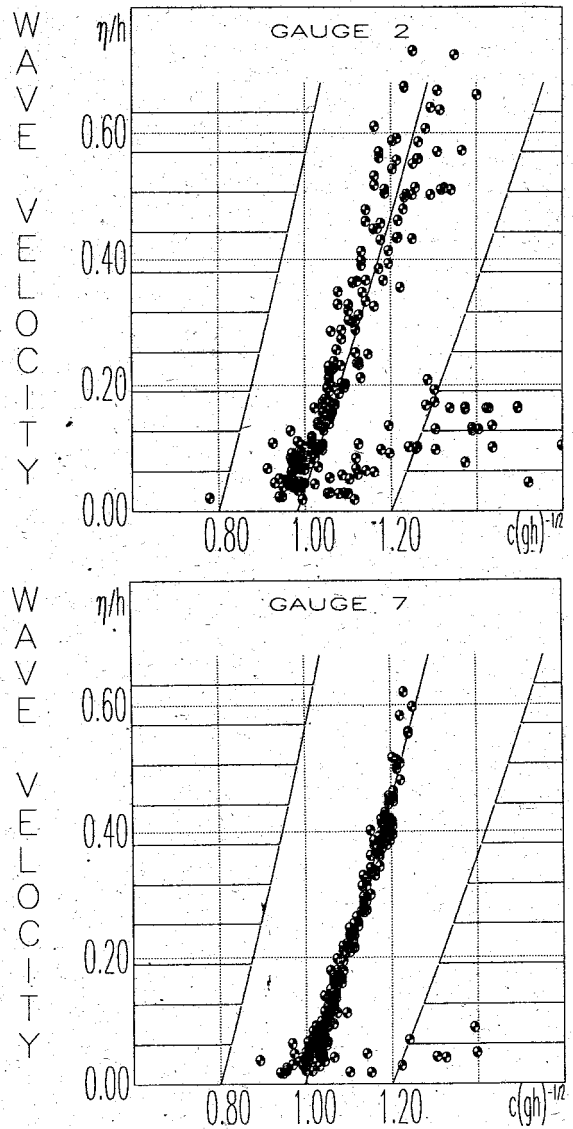

Figure 37: *Dimensionless wave height plotted against the ratio of the maximum velocity and a wave speed measured at gauge 2, closest to the wave generator, and gauge 7 at the end of the channel. The line drawn through the data is obtained from a linear regression of the data lying within the strip.*

4 Comparison of computational results with experiments

Having outlined in chapter 1 the governing equations of the motion of shallow water waves and measured in chapter 2 such channelized waves subject to clearly defined boundary and initial conditions, we shall in this chapter merge the two and test how well the theory matches observational data. As was mentioned before such comparisons do exist and it was found that the Korteweg-de Vries equation is a suitable model for the description of the motion of shallow water waves in a channel with constant water depth. Our goal here is not so much in corroborating this fact, even though this will be done, but to see whether the equations of Wu [96] and Villeneuve [89] are suitable when the water depth may be slowly varying in space and may also vary with time. We further aim for a computational scheme that accurately predicts the wave motion from initiation through time and may serve as a candidate for prognostic purposes. This scheme is that developed by Villeneuve [89], as will be demonstrated below.

The numerical solution of a differential equation which itself forms a description of a physical phenomenon is always fraught with errors. Apart from the limitations brought by the mathematical formulation, the discretization of the equations introduces further errors into or limitations of the solution, which can be detected by comparison of observational data with computational results.

In our problem of the propagation of shallow water waves the following comparisons are suggested and answers will be given:

- Does the inverse scattering technique applied to the Korteweg-de Vries equation appropriately describe the number of asymptotic solitary waves to given experimental initial conditions?

- Does the finite difference scheme, developed by Villeneuve and Savage [90] accurately reproduce the travelling wave forms of the experiments?

The first question will give indications as to whether initial conditions from the experiments will permit application of the inverse scattering method; the second will provide information as to whether the model equations are capable of reproducing both, waveforms and phase.

4.1 Inverse Scattering Considerations

Because the moving and deforming profile is limited in our experiments to the location of the wave generator, and since the channel possesses constant water depth except at the wave maker, the Boussinesq equation is a suitable model for the description of channelized shallow water waves throughout most of the channel.

Therefore, when we restrict considerations to forward moving waves the Korteweg-de Vries equation is the appropriate equivalent model. Provided then, that 'theoretical' initial conditions in the portion of the channel with constant depth can be deduced from the experiments, the entire apparatus of inverse scattering techniques of the Korteweg-de Vries equation may be employed to construct a solution to the latter to arbitrary smooth initial data. We shall outline the basic theory from which the main features of the solution will be visible. However, the construction of the solution is much too complicated to be useful for engineering purposes, but the asymptotic features, namely the number of solitons which will asymptotically evolve are easy to obtain. Therefore the number of evolving solitons can serve as a basis for the comparison of experimental and numerical data.

The following description of the inverse scattering method will essentially follow Segur [76] and Miura [60].

4.1.1 The inverse scattering method

In 1967 Gardner et al. [23] described a method of solution of the Korteweg-de Vries equation. Instead of solving this nonlinear equation they could reduce the problem to the linear Gel'fand-Levitan integral equation which depends only on the initial data $\eta(x,0)$ of the unknown solution. Lateron the solution of the integral problem was shown to exist for those functions $\eta(x,t)$ whose initial data $\eta(x,0)$ satisfy two conditions. First,

$$\int_{-\infty}^{+\infty} [\eta^2 + (\eta_x)^2 + (\eta_{xx})^2 + (\eta_{xxx})^2]\, dx < \infty\,, \tag{4.1}$$

which is necessary for a function for which η_{xxx} exists [5] or in other words guarantees the solution for the Korteweg-de Vries equation. Uniqueness of the solution was proved by Lax [50]. The second condition,

$$\int_{-\infty}^{+\infty} (1 + |x|)\, |\eta|\, dx < \infty, \tag{4.2}$$

insures the solvability of the integral equation [19]. These conditions can be assumed to be satisfied for the experimental and numerical data described here.

The method of solution described by Gardner is a sequence of four steps. They are as follows:

1. Solve the ordinary scattering problem, using the initial data $\eta(x;0)$:

$$\frac{d^2\psi(x)}{dx^2} + (\lambda + \eta(x;0))\,\psi(x) = 0, \tag{4.3}$$

for positive and negative eigenvalues λ and appropriate boundary conditions.

2. For *positive* eigenvalues $\lambda = k^2$ the boundary conditions for $\psi(x)$ guaranteeing bound eigenfunctions are

$$\psi(x) \sim \begin{cases} b(k)\exp(ikx) + \exp(-ikx), & for \quad x \to +\infty, \\ a(k)\exp(-ikx), & for \quad x \to -\infty. \end{cases} \tag{4.4}$$

The spectrum of the eigenvalues is continuous.

The functions $\exp(ikx)$ and $\exp(-ikx)$ represent a right and a left-going wave. Still unknown are $b(k)$ and $a(k)$, the reflection and transmission coefficients. To explain these coefficients a plane left going wave $\exp(-ikx)$ is thought to be sent from $+\infty$ to interact with the potential $\eta(x;0)$. Thereby a part of the wave will be reflected at the potential and the remainder is transmitted through the potential and will be observed at the boundaries. The energy of the reflected and transmitted waves is conserved and retains the value of the energy initially sent out.

For *negative* eigenvalues $\lambda = -K_n^2$ equation (4.3) possesses a bounded solution only for a discrete set of eigenvalues. The number N of discrete eigenvalues is finite, and the eigenfunctions $\psi_n(x)$ can be normalized such that

$$\int_{-\infty}^{+\infty} \psi_n(x)dx = 1\,, \tag{4.5}$$

and their asymptotic behaviour as $x \to \infty$ is given by

$$\psi_n(x) \sim c_n \exp(-K_n x). \tag{4.6}$$

3. As the next step the Gel'fand-Levitan integral equation must be solved for $L(x,y)$:

$$L(x,y) + B(x+y) + \int_x^{\infty} L(x,z)B(x+z)dz = 0 \tag{4.7}$$

with

$$B(\xi;t) = \sum_{n=1}^{N} c_n^2(t)\exp(-K_n\xi) + \frac{1}{2\pi}\int_{-\infty}^{+\infty} b(k;t)\exp(ik\xi)dk \tag{4.8}$$

Note that the function $B(\xi;0)$ contains only the information given at $\eta(x;0)$. The contributions correspond to the discrete spectrum and the reflection part of the continuous spectrum. The coefficients $b(k;0)$, $c(0)$ and the discrete eigenvalues $K_n(0)$ are determined from $\eta(x;0)$. Gardner et al. [23] found that they satisfy

$$\begin{aligned} b(k;t) &= b(k;0)\exp(8ik^3t), \\ c_n(t) &= c_n(0)\exp(4K_n^3t), \\ K_n(t) &= K_n(0). \end{aligned} \tag{4.9}$$

This fundamental theorem includes the basic assumption that the eigenvalues λ are independent of the time t.

4. The solution of the Korteweg-de Vries equation is obtained by evaluating $L(x,y;t)$ at $x=y$,

$$\eta(x,t) = 2\frac{d}{dx}L(x,x;t). \tag{4.10}$$

Evidently, the solution $\eta(x,t)$ evolves from a discrete and a continuous spectrum of eigenvalues. For a purely discrete spectrum it consists of N solitons. This is related to the fact that the soliton is a nonreflecting potential, so that $b(k,t)=0$. The amplitudes of the solitons depend on the eigenvalue λ_n. In the case that the spectrum is purely continuous, only a dispersive oscillatory tail evolves as an asymptotic solution. The wave amplitudes of the tail decay in time. Longer waves will move to the front while short waves dominate the rear of the tail. A mixed spectrum contains both solitary waves and an oscillatory tail plus some interaction terms. Cnoidal waves, which are the uniform wave train solutions of the Korteweg-de Vries equation, play no part in the asymptotic solution.

It is clear from the above analysis and it was already mentioned before that the solution to the Korteweg-de Vries equation is constructed from an initial wave profile $\eta(x;t_0)$. The measurement technique used by us recorded waveheight time series at a fixed gauge, $\eta(x_0,t)$, which is not in conformity with the inverse scattering method. If, however, the wave speed does not depend on amplitude, so that $x=\sqrt{gh}\,t$ our Eulerian gauge measurements would permit to deduce from the data a Lagrangian initial profile. The simple relation $x=\sqrt{gh}\,t$ is only correct for small amplitude waves. So the application of the inverse scattering method to our data is fraught with error.

To test whether the measured amplitude allows a prediction of the number of emerging solitons according to the Korteweg-de Vries equation, different methods have been employed: 1.) Counting the number of eigenvalues of the discrete spectrum of $\eta(x_0,t)$; 2.) Determination of an upper and lower bound for the number of eigenvalues by using a square-well potential.

All above is valid for the nondimensional Korteweg-de Vries equation

$$\eta_x + 6\eta\eta_x + \eta_{xxx} = 0 \tag{4.11}$$

with nondimensional amplitude η. Its back transformation into dimensional form (indicated by $\star$) is achieved by

$$\begin{aligned} x &= (x^\star - \sqrt{gh}\,t^\star)/\,h, \\ t &= 1/6\sqrt{g/h}\,t^\star, \\ \eta &= 3/(2h)\,\eta^\star(x^\star,t^\star) \end{aligned} \tag{4.12}$$

and yields the dimensional form of the Korteweg-de Vries equation [40]

$$\eta^\star_{t^\star} + \sqrt{gh}\left(\eta^\star_{x^\star} + \frac{3}{2h}\eta^\star\eta^\star_{x^\star} + \frac{1}{6}h^2\eta^\star_{x^\star x^\star x^\star}\right) = 0; \tag{4.13}$$

h is the water depth, g the acceleration of the earth. This equation emerges from the Boussinesq equation if the waves are restricted to unidirectional motion, as already shown. We emphasize that the measured amplitudes in the channel, η^* must be non-dimensionalized by using the factor $3/(2h)$ to obtain $\eta(x;t)$; the following procedures require this dimensionless form $\eta(x;t)$.

4.1.2 The number of solitons

One of the main features of the Korteweg-de Vries equation is that its solution can be regarded as the unknown potential of the time independent Schrödinger equation. To see this we relate η to the new variable v via the Miura–transformation [60],

$$-\eta = v_x + v^2. \tag{4.14}$$

For prescribed η, this relation forms a Riccardi differential equation for v. It can be linearized by substituting

$$v = \frac{\psi_x}{\psi}, \tag{4.15}$$

yielding

$$\psi_{xx} + \eta\psi = 0. \tag{4.16}$$

Because the Korteweg-de Vries equation is invariant under a Galilean transformation, η can be shifted by a constant λ and remains a solution under such a transformation. Therefore we get

$$\psi_{xx}(x) + (\eta(x;t) + \lambda)\,\psi(x) = 0. \tag{4.17}$$

This is the Schrödinger equation. ψ is the wave function, η plays the role of the potential, and λ are energy levels. The equation is independent of time and t has to be regarded as a parameter. The usual problem is to find a bound state energy level for a given potential (scattering problem). Here we are looking for the unknown potential (inverse scattering problem).

Gardner et al. [23] stated that the number of solitons agrees with the number of negative eigenvalues λ of the Schrödinger equation with boundary conditions according to eq. (4.3)-(4.6). At least one negative eigenvalue and therefore at least one soliton is obtained for a positive but finite discharged volume

$$\infty > \int_{-\infty}^{+\infty} \eta(x;t_0)\,dx > 0. \tag{4.18}$$

Only positive eigenvalues and no emerging solitons are possible if

$$\eta(x;t_0) \leq 0\,, \tag{4.19}$$

for all x.

The number of eigenvalues of the boundary value problem corresponds to the number of zeros of Ψ of the initial value problem (see for example Sauer & Szabó [72])

$$\begin{aligned} \Psi_{xx} + \eta(x;t_0)\Psi &= 0, \\ \Psi(x_1) &= 1, \\ \Psi_x(x_1) &= 0. \end{aligned} \tag{4.20}$$

η must vanish outside the interval $|x| > x_1$. The experimental data always satisfy this constraint.

The interval in which a point of zero for Ψ can appear can be restricted: If $\eta \leq 0$ in $[a,b]$ then there exists at most one zero of Ψ in $[a,b]$. This may abbreviate the numerical solution of (4.20).

A Runge-Kutta method of 4th order was used to find the numerical solution for Ψ for most of the cases. Nevertheless some of the measured data had long parts with negative η. Therefore equation (4.20) becomes stiff in these cases and Ψ will grow exponentially. However a Gear algorithm (IMSL-Library [35]), suitable for stiff equations was able to solve the differential equation in this case.

To obtain the initial data $\eta(x;t_0)$ from the measured waveheight-time series $\eta(x_0,t)$ several different procedures can be followed. First, the measured time-series at a particular gauge is stretched according to the transformation $x = c \cdot t$, $c = \sqrt{gh}$ of the linear wave approximation, in dimensionless coordinates corresponding to $c = 1$. This means that in this linearized approach the waveheight time series at a gauge could directly be used as potential function in equation (4.20) by identifying $\eta(x;t_0) = \eta(t_0,x)$. This is method 1. Second, the computed waveheight corresponding to a particular experiment could be used to obtain data in the form $\eta(x;t_0)$ or $\eta(x_0,t)$ and either of these applied as potential function of the initial value problem (4.20). We shall present results to all of these and call this method 2.

4.1.3 Upper and lower bounds for the number of solitons

It was shown by Bargmann [4] for a central radial field and later extended by Segur [76] to the case considered here, that for a bound potential

$$q(x) = \begin{cases} \eta(x;t_0) & \eta \geq 0 \\ 0 & \eta < 0 \end{cases} \tag{4.21}$$

the number N of zeros of the equation

$$\Psi_{xx} + q(x)\Psi = 0 \tag{4.22}$$

is limited by

$$N \leq 1 + \int_{-\infty}^{+\infty} |x|\, q(x)\, dx. \tag{4.23}$$

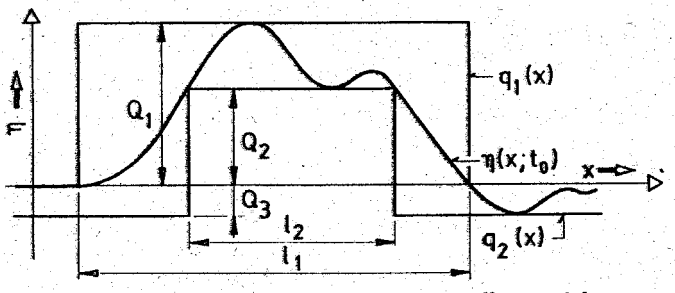

Figure 38: *Definition of the square-well potential.*

Instead of the original potential $\eta(x;t_0)$ of the measured wave amplitude Segur [76] suggested to choose a square-well potential as defined in fig. 38. From equation (4.23) it is obvious that the number of zeros of q_1 and q_2 is $N_1 \geq N \geq N_2$. The number of eigenvalues of the square well potential is well known (see for ex. Dodd et al. [15]) and given by

$$\begin{aligned} &\text{if } \tan(l_2 Q_2^{1/2}) \leq \frac{2Q_2^{1/2}}{Q_2 - Q_3} \quad : \quad \frac{l_2 Q_2^{1/2}}{\pi} - 1 < N < \frac{l_1 Q_1^{1/2}}{\pi} + 1 \quad , \\ &\text{if } \tan(l_2 Q_2^{1/2}) \geq \frac{2Q_2^{1/2}}{Q_2 - Q_3} \quad : \quad \frac{l_2 Q_2^{1/2}}{\pi} \leq N < \frac{l_1 Q_1^{1/2}}{\pi} + 1 \quad , \end{aligned} \tag{4.24}$$

where l_1, l_2, Q_1, Q_2, Q_3 are sketched in fig. 38.

These formulas are used to obtain upper and lower bounds for the number of solitons. Here $(lQ^{1/2})^2$ is an Ursell-number, l defines a characteristic length, Q a characteristic amplitude at a considerable distance away from the wave generating device. Upstream the wave begins to disperse and l becomes longer. At the beginning, during the wave generating process, the wave will grow in amplitude and redistribute its height as it travels along the channel. Dissipation and dispersion cause these processes. Thus, we can expect to obtain a reasonable approximation of the number of solitons if the initial profile for the estimates of l_1, l_2, Q_1 and Q_2 is chosen in a region where the wave height has reached its maximum and where the dissipation and dispersion processes have just started to develop. In most cases this is about when the wave has travelled half through the channel.

4.1.4 Number of solitons as obtained from experimental waveheight-time series

The above estimates will now be tested with our experimental findings. To this end the same graphical representation as in chapter 3.2.2 will be chosen. There it was demonstrated how a scaled waveheight and a scaled wavelength are related to accordingly modified Froude numbers. Moreover, it was shown that a modified Ursell number based on the same scaled variables is constant for all inclination angles of

the wedges that generated the waves.

As explained above with the aid of fig. 38 the number of asymptotically evolving solitons can be estimated from the known wavelength and waveheight at an initial time. This number of solitons is equivalent to an Ursell number. For waves generated by a wedge-type piston this Ursell number depends upon a modified Froude number, see chapter 3. It is therefore to be expected that the number of solitons, divided by the dimensionless distance d/h the wedge is moved, (this is the modified Ursell number) is uniquely related to the Froude number of the piston velocity multiplied by d/h.

In each experiment upper and lower bounds for the waveheight and wavelength are estimated, and with these the upper and lower bounds of the number of solitons are found via equation (4.24). These are shown in fig. 39 as open hexagons and open circles. Better estimates for the number of solitons are also constructed with the aid of the initial value problem (4.20) by counting the number of zeros of Ψ when the 'exact' potential $\eta(x;t_0)$ is used. In fig. 39 the corresponding points obtained according to method 1 in section 4.1.2 on page 120 are shown as full diamonds.

The results, of course, depend to a certain extent upon the location where the data are collected. If this is close to the wave generating device (in the experiments $x/h = 9$ and $x/h = 37$, respectively) the ranges of the upper and lower bounds of the number of solitons obtained for the square well potential are clearly separated, with the 'exact' number of solitons lying in the band between the two. The modified Ursell number $N^o/(d/h)$ (N^o = number of solitons) is seen to decrease monotonically with increasing modified Froude number $Fr(d/h)$. Also, the larger the distance becomes between the point where the data are taken and the wave generator, the more the data will scatter. At the point farthest from the wave generator (i. e. $x/h = 68$) the three domains overlap. Nontheless, to each number of solitons obtained with the 'exact' method there correspond upper and lower bounds, but the 'exact' number may be spread so that a clear separation is no longer possible. This can be explained with the dispersive behaviour of the wave. If a wave packet consists of a hump with two or more relative maxima, the portion with the highest maximum will travel fastest. Hence the extent of the hump increases, while its height will remain more or less the same and only slowly change by dissipation. In the experiment both, dispersion and dissipation are active but dissipation is ignored in the inverse scattering method of the Korteweg-de Vries equation. Therefore it is understandable that the data will deviate more and more from the ideal conditions of the theoretical model and thus yield larger scatter when evaluating the number of solitons by the different methods. Upper and lower bounds of the number of solitons will spread more and so will the average number of solitons obtained from the 'exact' method. The enhanced spread is clearly visible in fig. 40.

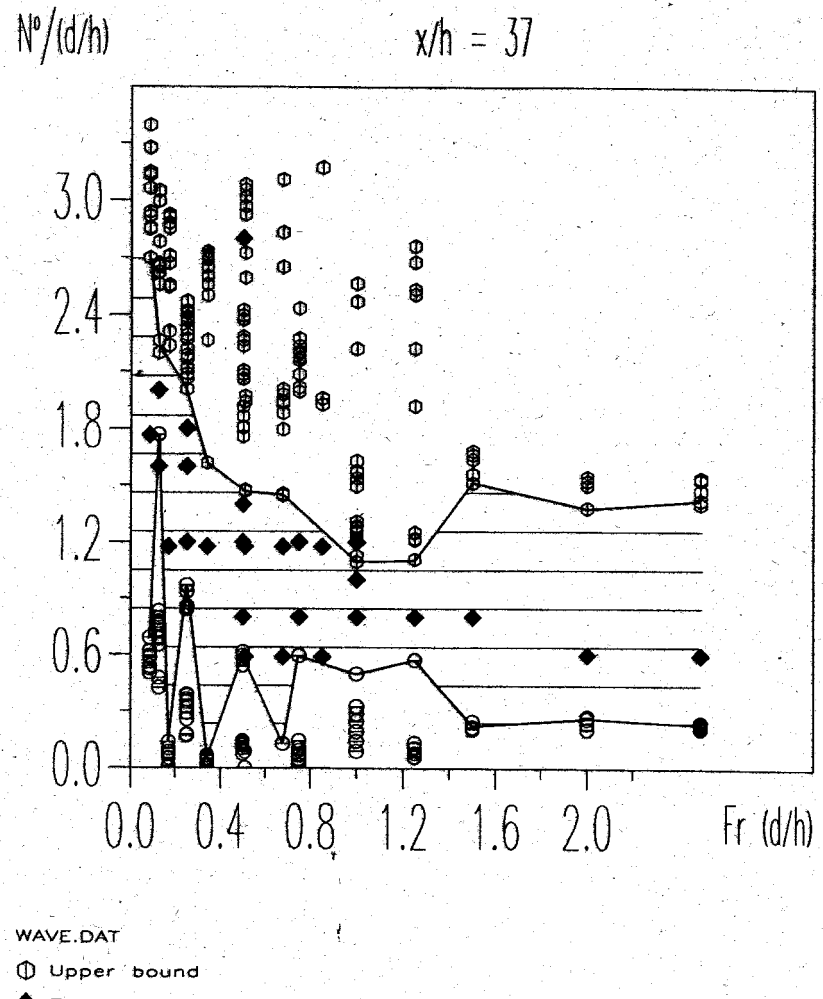

Figure 39: *Number of solitons: Upper bound, exact number and lower bound plotted against a modified Froude number. The wave is fully developed and its height nearly maximal. The region between upper and lower bound is lightly shaded.*

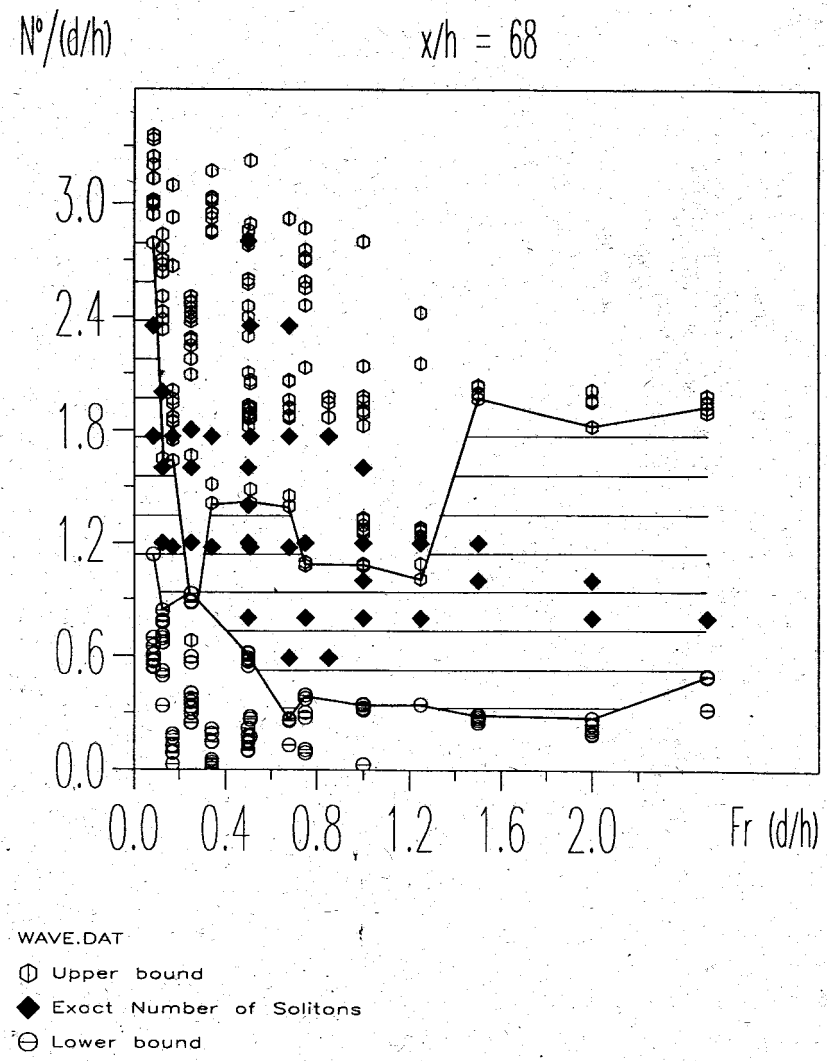

Figure 40: *Number of solitons: Upper bound, exact number and lower bound plotted against a modified Froude number. The wave has travelled through the whole length of the channel. The region between upper and lower bound is lightly shaded.*

4.1.5 Number of solitons as obtained from numerical waveheight distributions

We state again that the inverse scattering method applied to the Korteweg-de Vries equation requires data in the form $\eta(x;t_0)$ while the experiments provide them in the form $\eta(x_0,t)$ instead. Both forms are available from the numerical solution of the governing equations of Villeneuve & Savage [90] which are solved for the realistic boundary and initial conditions encountered in the experiments. The location x_0 and the initial time t_0 are chosen such that $x_0 = c\,t_0$, with c being the wave speed of the linear wave $c^* = \sqrt{gh}$, in dimensionless coordinates corresponding to $c = 1$. This corresponds to method 2 mentioned on page 120.

Figs. 41 - 49 show both forms. The data for $\eta(x_0,t)$ are called TIME.DAT and are displayed as solid lines; those for $\eta(x;t_0)$ are called LOCAL.DAT and are plotted as dotted lines.

The horizontal axes are a dimensionless distance x/h and a dimensionless time $t\sqrt{g/h}$, respectively, the origin of the coordinates of the former being at the left margin that of the latter at the right margin. In each panel we have chosen x_0 to correspond to the location of a measuring gauge in our real experiments and then computed $\eta(x_0,t)$ and $\eta(x;t_0)$ whereby $x_0 = c \cdot t_0$ and $c = 1$. The locations, where the maxima of the wave height occur are indicated as dotted and solid vertical dashes on the respective abscisses. Furthermore the LOCAL.DAT waveheight distributions are shifted in each panel such that the locations of the maxima of the plotted curves agree with one another. As can be seen from these figures the shift in each panel is different. This is, clearly, the result of the fact that x_0 and t_0 are connected to each other according to the linear wave theory. An adjustment due to nonlinearity can be made, but would have resulted in nonunique and implicit functions for the shift.

When using the computed profiles $\eta(x_0,t)$ and $\eta(x;t_0)$ as initial conditions for determining the likely asymptotic wave structure the two profiles should agree with one another over that part of the wave that is essential for the inverse scattering method, i. e. the portion where the wave packet exhibits essential amplitudes. Such conditions prevail provided the wave packet has moved a sufficiently large distance from the wave generator and / or a time span has elapsed long enough that the motion of the generator does no longer affect the wave packet. Glancing through figs. 41 - 49, it is seen that such is the case generally in panel 2, and more often, in panel 3. In panel 1, corresponding to gauge 1, the wedge is still moving when the wave hump passes, in panel 2 the motion of the wave generator may not have ceased (fig. 42), and often the first reflections are visible in panel 8, sometimes in panel 7 (see fig. 42).

It is clear from the above that the number of solitons that are obtained with the inverse scattering method will depend upon the selection of the initial conditions ($\eta(x;t_0)$ or $\eta(x_0,t)$, at a certain gauge). Again, upper and lower bounds and 'exact' estimates of the number of solitons can be determined. It is expected that predic-

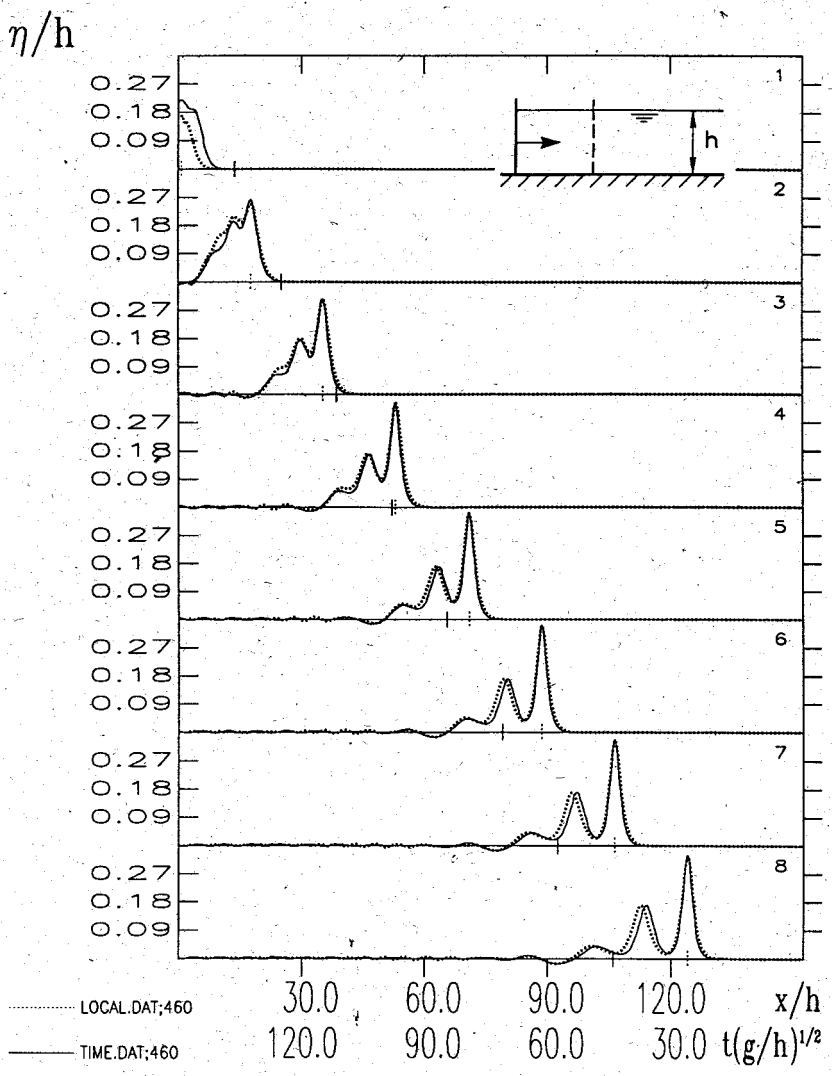

Figure 41: *Waves obtained from numerical calculations in different reference systems.* TIME.DAT *refers to a fixed location,* LOCAL.DAT *to a fixed time. The wave is generated with a vertical plate moving a distance* $d/h = 2.5$ *with a velocity of* $Fr = 0.2$.

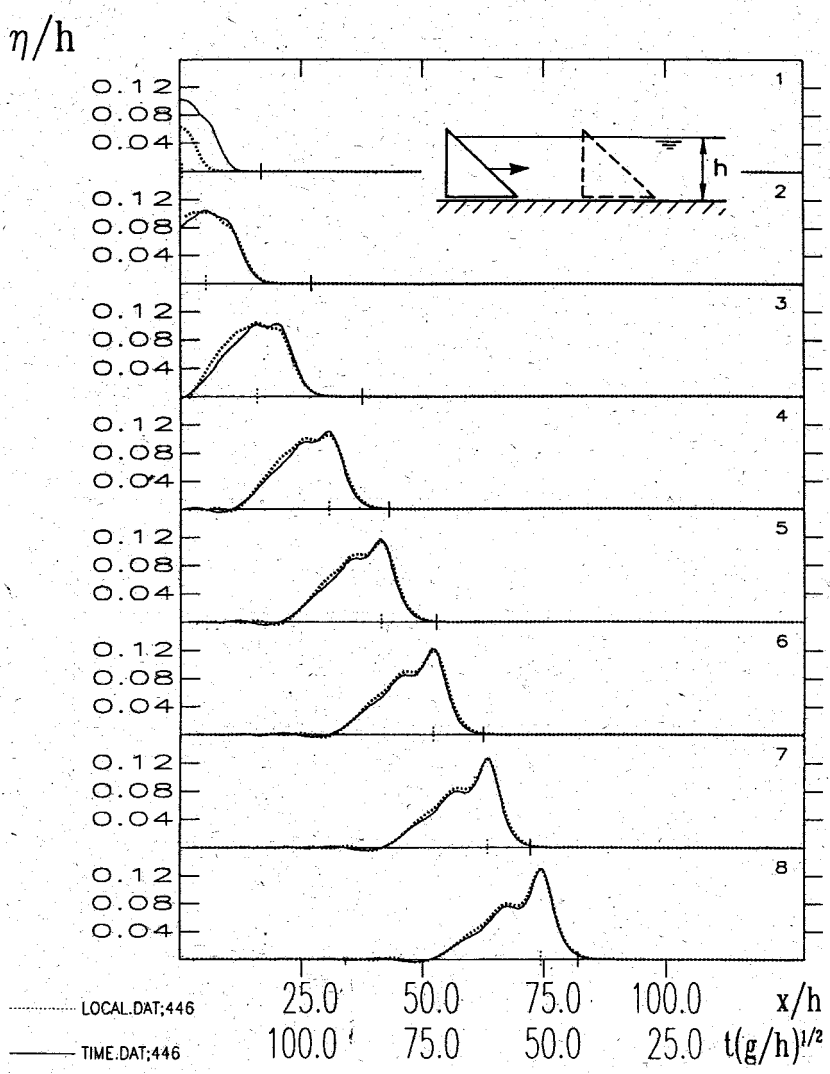

Figure 42: *Waves obtained from numerical calculations in different reference systems.* TIME.DAT *refers to a fixed location,* LOCAL.DAT *to a fixed time. The wave is generated with a wedge with slope* 1, *moving a distance* $d/h = 1.67$ *with a Froude number of* $Fr = 0.1$.

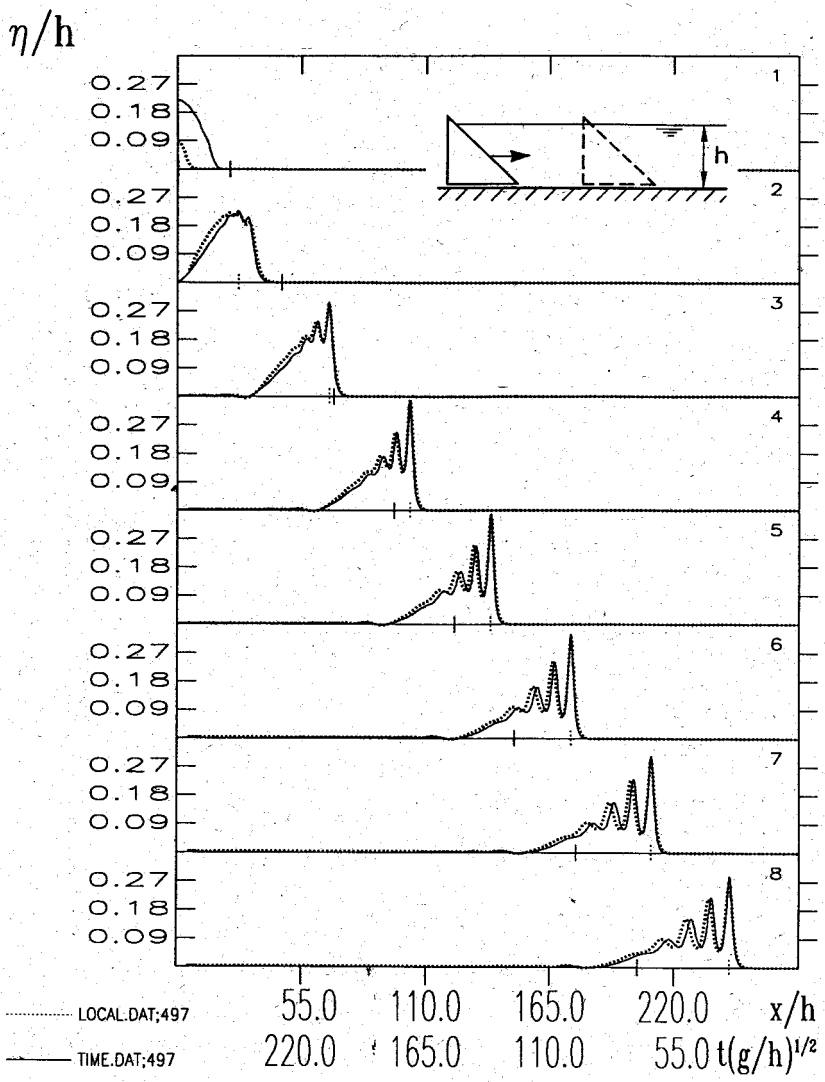

Figure 43: *Waves obtained from numerical calculations in different reference systems.* TIME.DAT *refers to a fixed location,* LOCAL.DAT *to a fixed time. The wave is generated with a wedge with slope* 1*, moving a distance* $d/h = 5$ *with a Froude number of* $Fr = 0.2$.

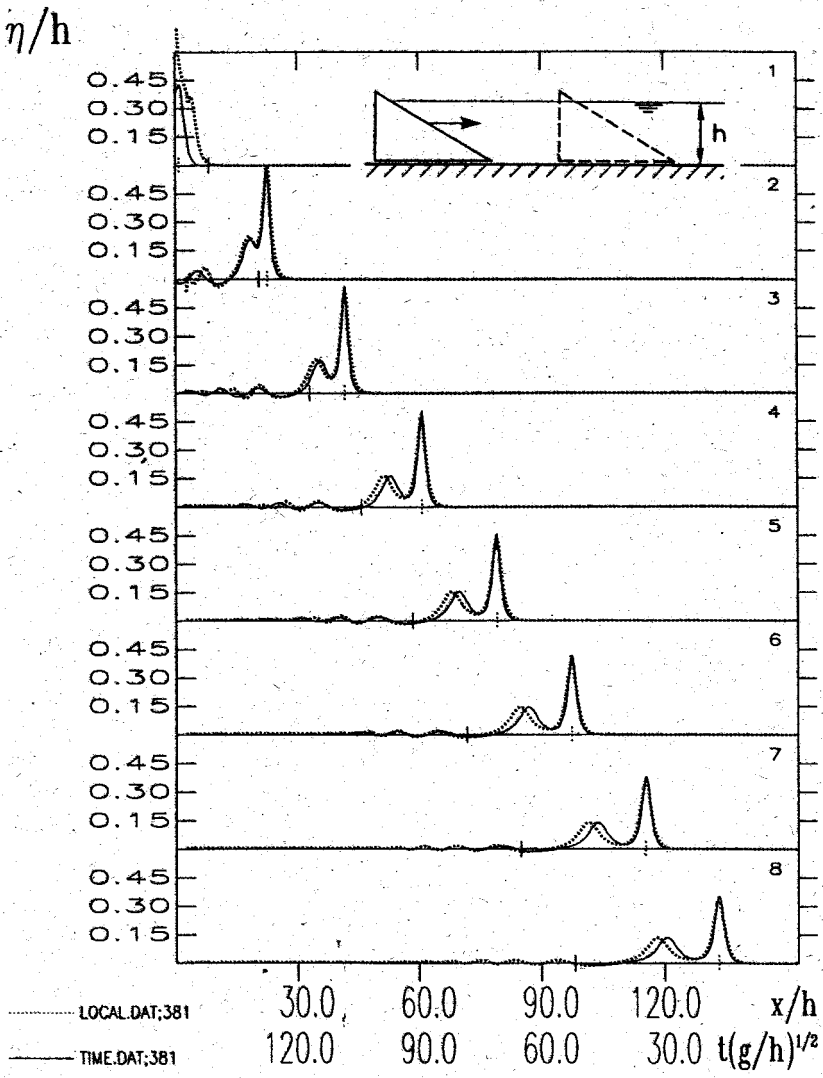

Figure 44: *Waves obtained from numerical calculations in different reference systems.* TIME.DAT *refers to a fixed location,* LOCAL.DAT *to a fixed time. The wave is generated with a wedge with slope* 0.577, *moving a distance* $d/h = 2.5$ *with a Froude number of* $Fr = 0.4$.

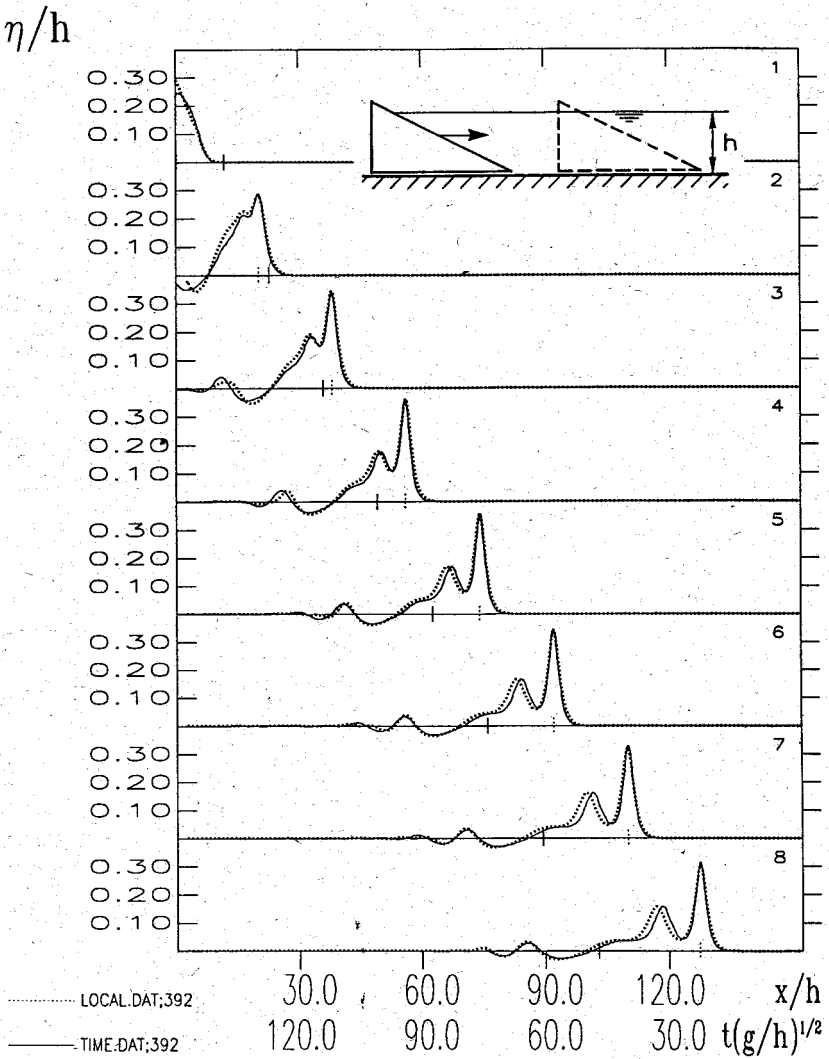

Figure 45: *Waves obtained from numerical calculations in different reference systems.* TIME.DAT *refers to a fixed location,* LOCAL.DAT *to a fixed time. The wave is generated with a wedge with slope* 0.268*, moving a distance* $d/h = 2.5$ *with a Froude number of* $Fr = 0.3$.

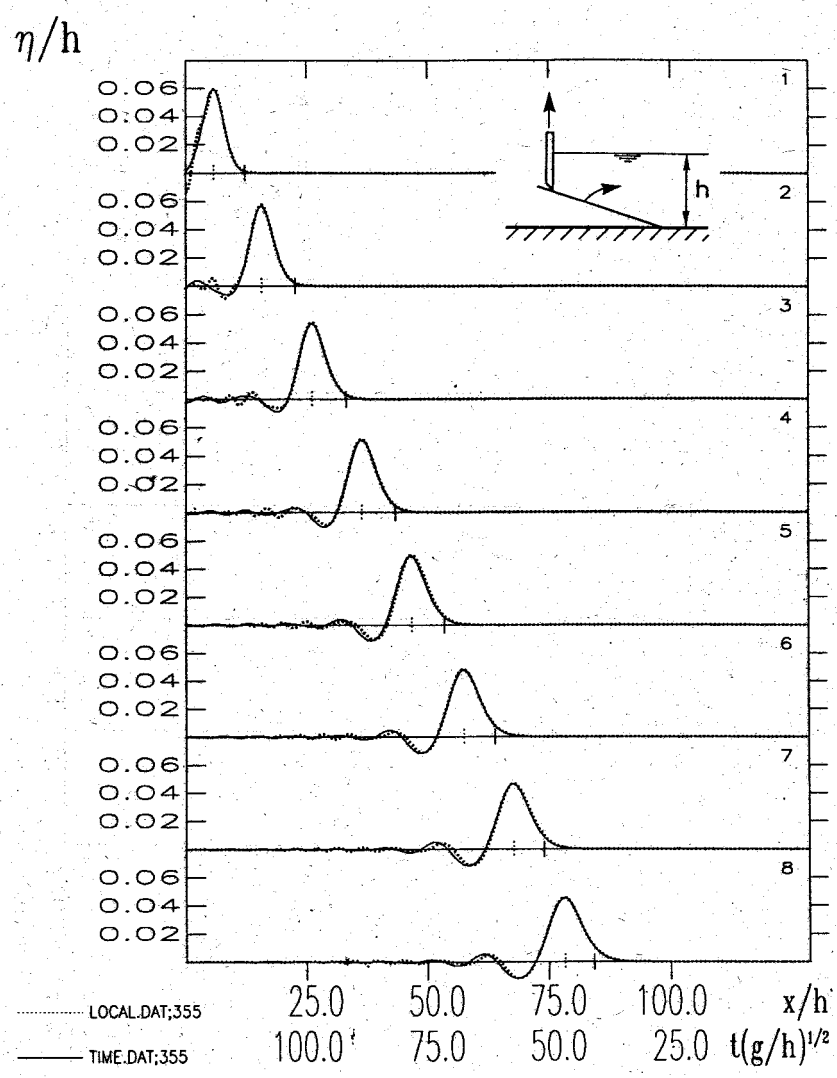

Figure 46: *Waves obtained from numerical calculations in different reference systems.* TIME.DAT *refers to a fixed location,* LOCAL.DAT *to a fixed time. The wave is generated with a rotating plate which is lifted up to a slope of* 5/30 *with a Froude number of* $Fr = 0.05$.

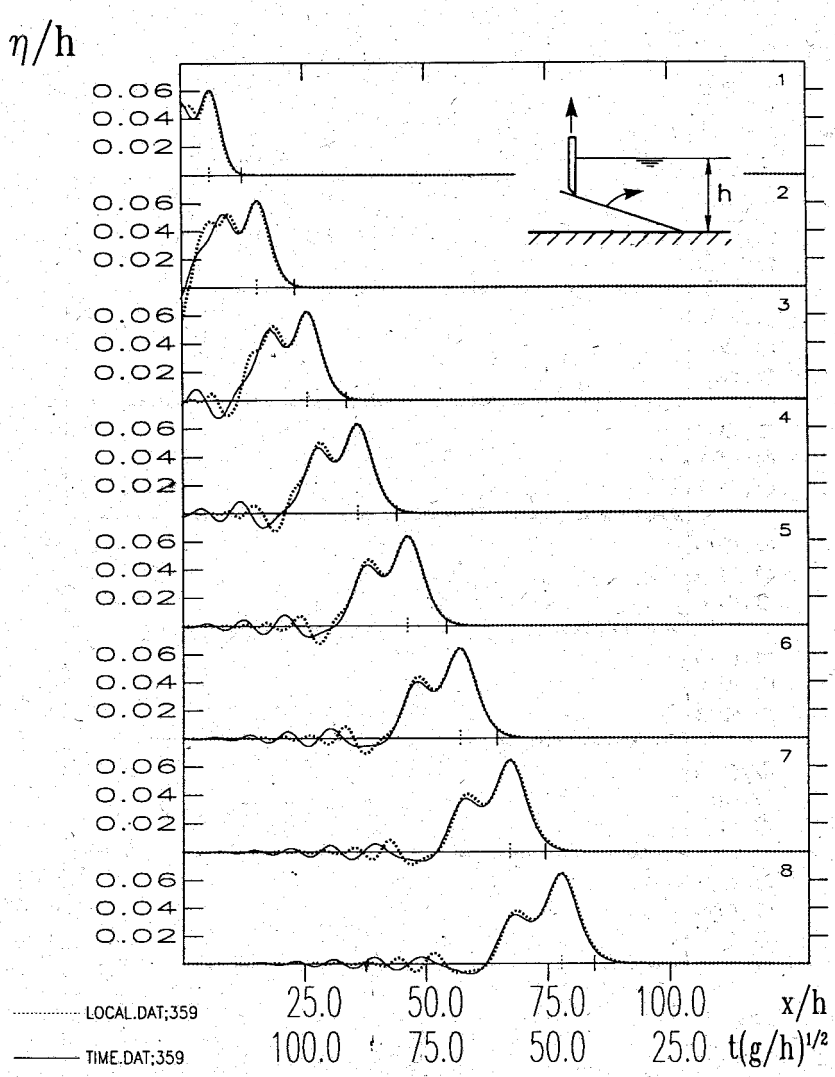

Figure 47: *Waves obtained from numerical calculations in different reference systems.* TIME.DAT *refers to a fixed location,* LOCAL.DAT *to a fixed time. The wave is generated with a rotating plate which is lifted up to a slope of* 12/30 *with a Froude number of* $Fr = 0.05$.

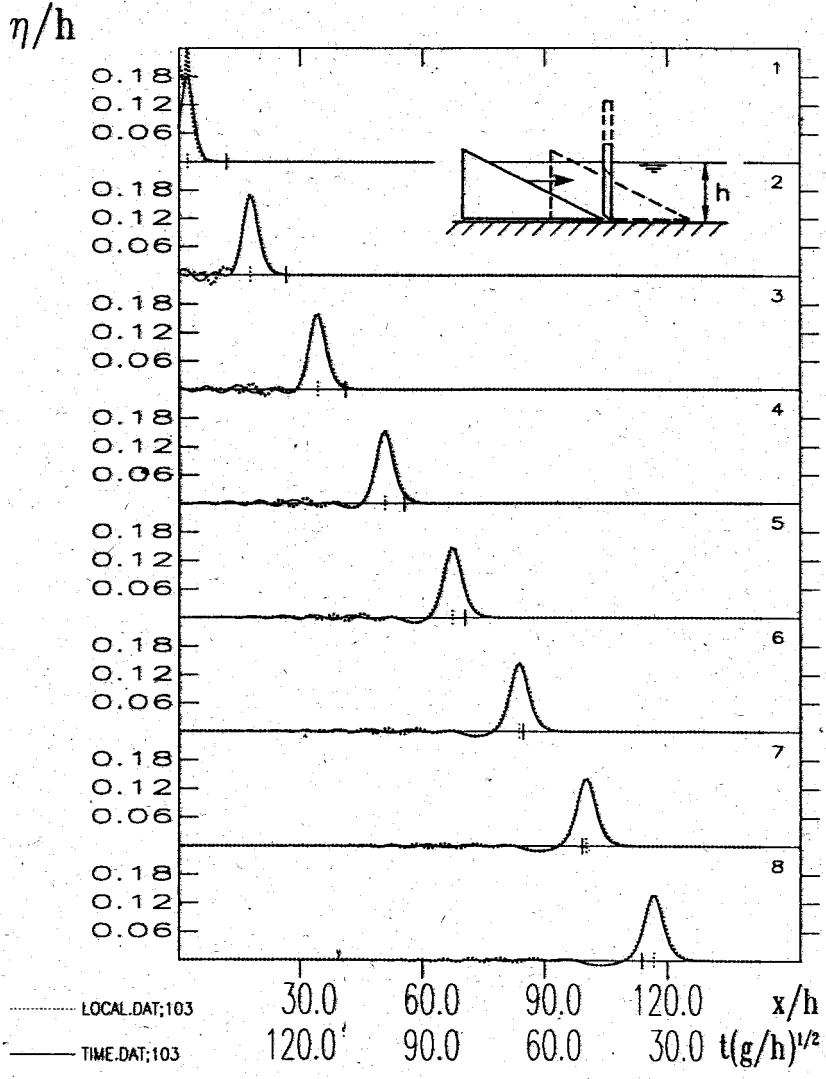

Figure 48: *Waves obtained from numerical calculations in different reference systems.* TIME.DAT *refers to a fixed location,* LOCAL.DAT *to a fixed time. The wave is generated with a submerged wedge with slope of* 0.268, *moving a distance* $d/h = 2.5$ *with a Froude number of* $Fr = 0.48$.

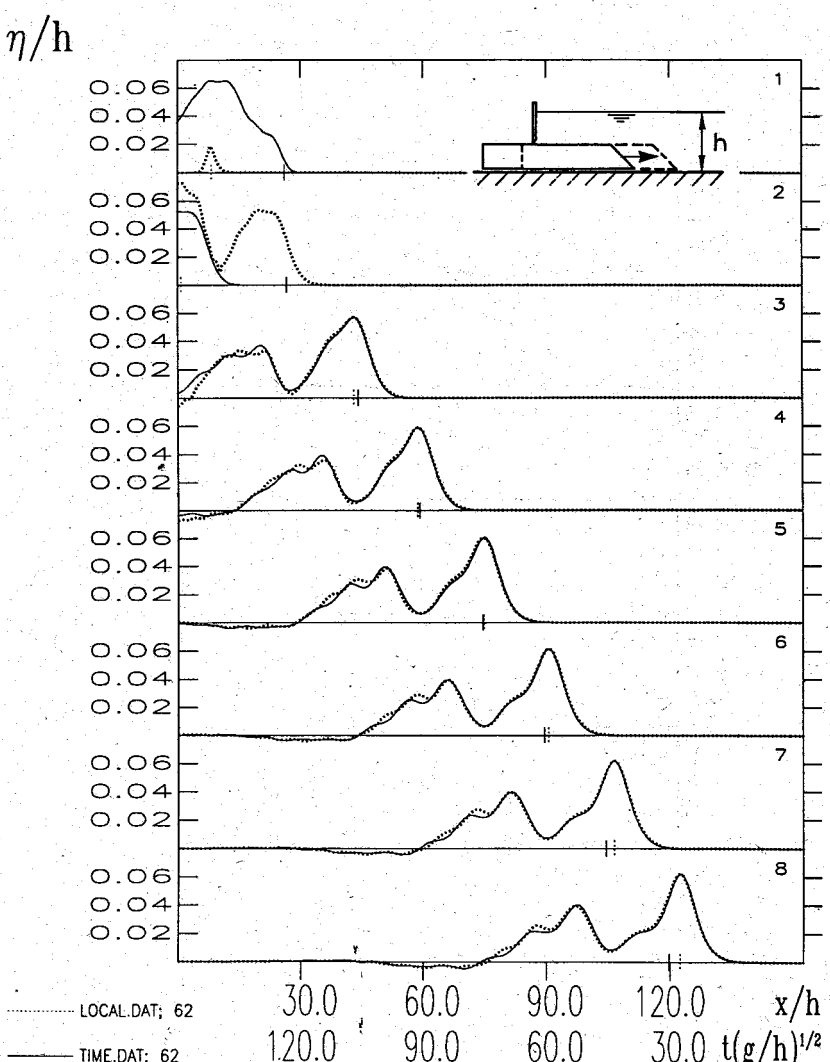

Figure 49: *Waves obtained from numerical calculations in different reference systems.* TIME.DAT *refers to a fixed location,* LOCAL.DAT *to a fixed time. The wave is generated with a step with height $h/2$, moving a distance $d/h = 2.5$ with a Froude number of $Fr = 0.16$.*

tions are likely to be unreliable when gauge 1 (panel 1) or gauges 6, 7 or 8 are chosen and should be best when profiles of gauge 3 or gauge 4 are selected as potentials for the inverse scattering method. Moreover, the inverse scattering method requires profiles $\eta(x;t_0)$. This mere fact is reason for us to suppose that results obtained with $\eta(x_0,t)$ will be less reliable than with $\eta(x;t_0)$.

Figs. 50 - 52 illustrate that these suppositions are essentially correct. Fig. 50 shows the results obtained for all experiments performed with moving wedges when profiles of gauge 1 are chosen. Most 'exact' numbers of solitons $N°/(d/h)$ lie above the lower limit of the upper bounds. Only at small modified Froude numbers do the 'exact' numbers of solitons lie within the shaded area between the upper and lower bounds.

Fig. 51 shows the corresponding results obtained for gauge 4, at a dimensionless distance $x/h = 37$, in panel *a* when $\eta(x;t_0)$ - profiles are selected, in panel *b* for $\eta(x_0,t)$ - profiles. Most points, representing the number of solitons $N°/(d/h)$ lie in the band between the upper and lower bounds, and the results in panel *a* are better than those in panel *b*, as expected. In fig. 52 the results are shown for gauge 6 ($x/h = 68$). They are less reliable than those in fig. 51, but panel *a* shows more reliable results than panel *b* in conformity of what was suspected above.

4.2 Comparison of the wave heighttime series

There still remains the verification that the evolution of the wave motion from initiation at the wave generator to the reflection at the opposite channel end can properly be modelled by the governing equations and its finite difference discretization of Villeneuve [89]. To this end, the surface-elevation time $\eta(x_0,t)$ series at the position x_0 of the gauges obtained from the measurements will be compared with those deduced from the computations. We shall plot the dimensionless height against dimensionless time at each gauge for the measured (solid lines) and computed (dotted lines) time series in the same graph and shall show results for the eight gauges that were installed for each experiment in one figure, see figs. 53 - 72. Such a representation permits a fair estimation of the agreement between theory and experiments. Because the starting time of the wedge was not recorded during the experiments, the experimental and computational waves can be compared with one another except for a shift in time. We chose this shift such that the times when the maximum wave heights occurred coincided at gauge 1 or 2 for the experimental and computational curves. We shall show results for a large variety of experiments with all kinds of wave generators and will *not* withhold the negative results that were obtained. In fact, the study of the behaviour of the numerical code in the vicinity of conditions for which agreement with experiments fails to be satisfactory, indicates the limitations of the governing equations and may point at directions of improvement.

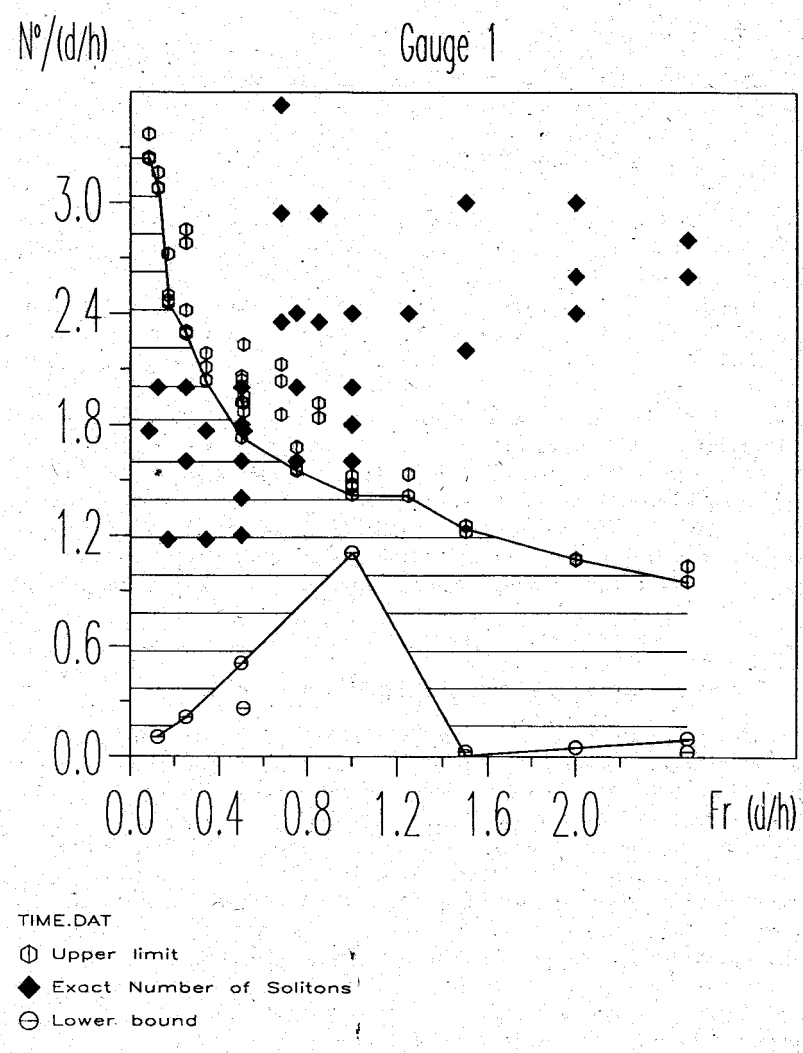

Figure 50: *Modified number of solitons for all experiments performed with a moving wedge as wave generator when computed profiles $\eta(x_0, t)$ at the first gauge were used. The profiles were obtained by solving the equations of Villeneuve & Savage [90] for initial and boundary conditions of the moving wedge experiments. Corresponding numbers of solitons are shown as full diamonds and denoted as 'exact'. Open hexagons show upper bounds and open circles lower bounds, obtained for the square well potential corresponding to the 'exact' computed profile. Shaded is the area where the 'exact' number of solitons should lie.*

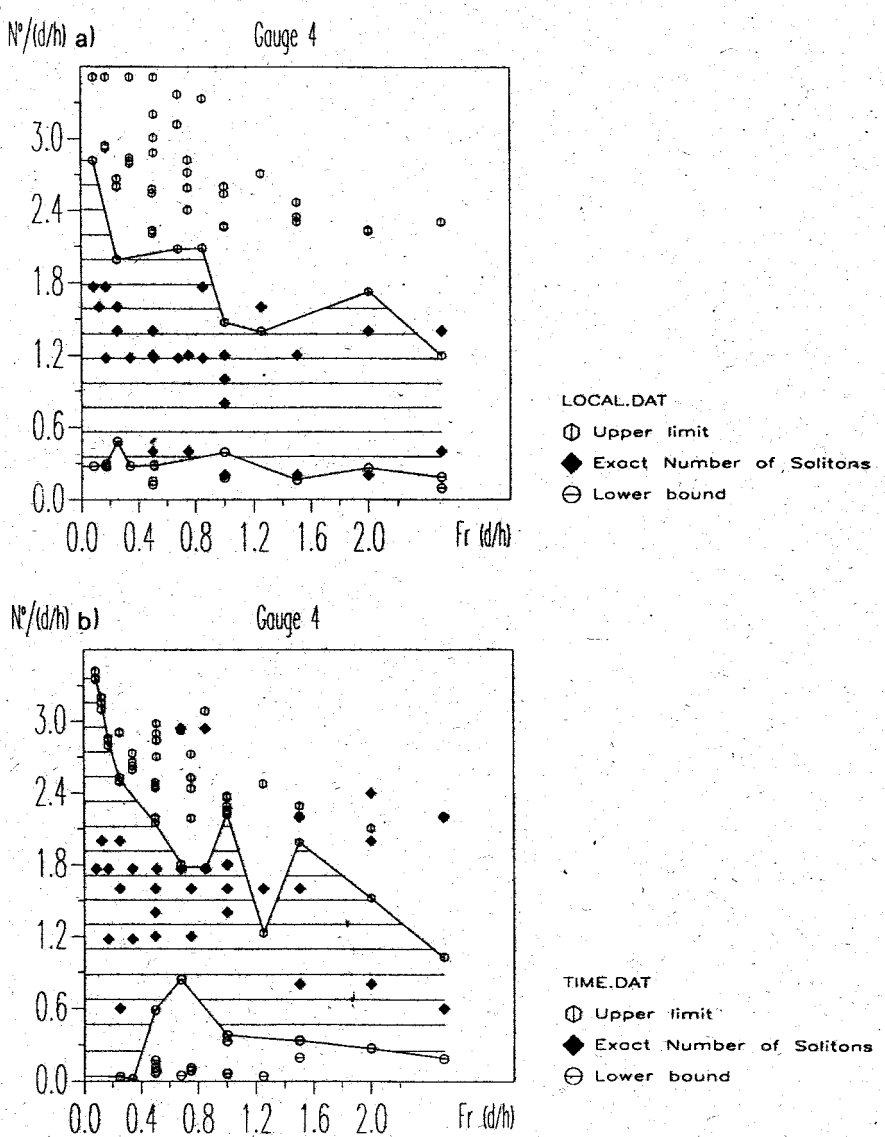

Figure 51: *Same as in fig. 50 but now when using the profiles* LOCAL.DAT *(panel a) and* TIME.DAT *(panel b) at gauge four. Note that results are slightly better in panel a than in panel b.*

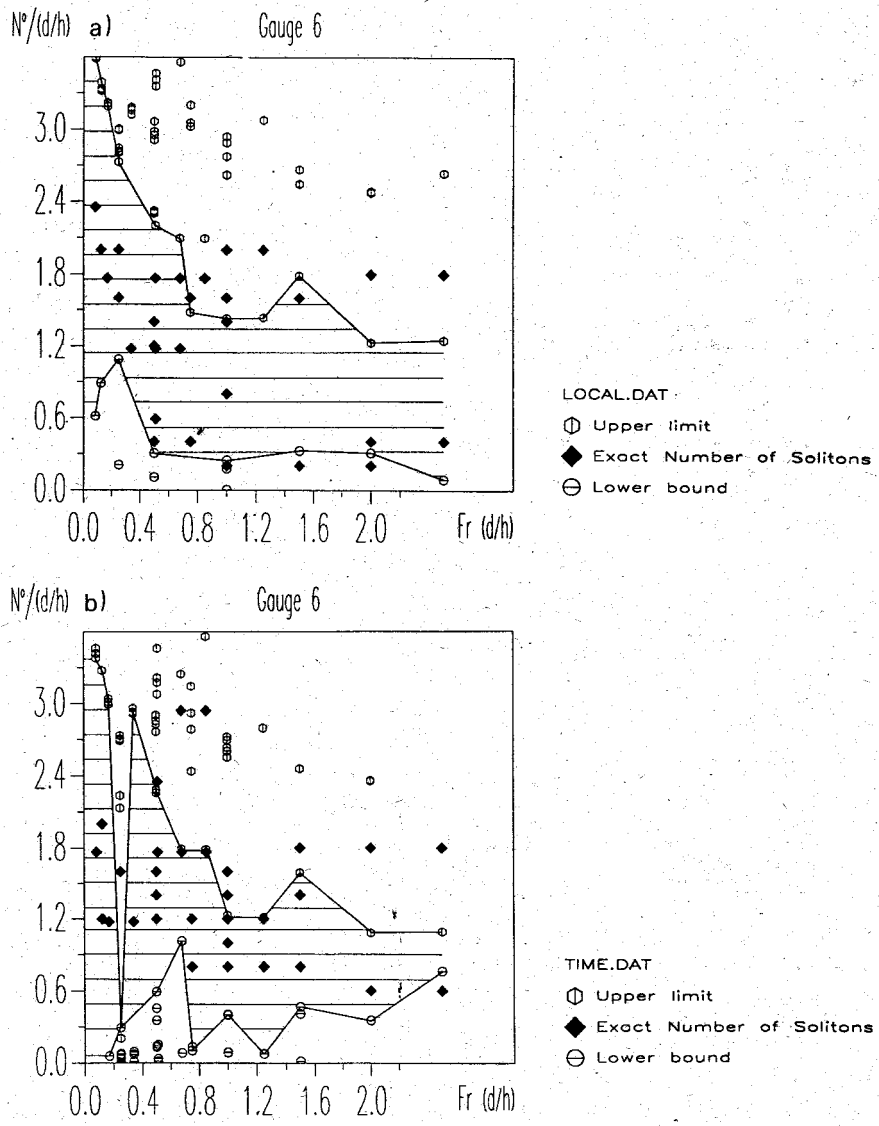

Figure 52: *Same as in fig. 50 and 51 but now when using the profiles* LOCAL.DAT *(panel a) and* TIME.DAT *(panel b) at gauge six. Note that results are less convincing than in fig. 51, but those in panel a are still better than in panel b.*

4.2.1 Moving wedge

A sensitivity analysis of the finite difference scheme of Villeneuve [89] to the Froude number of the velocity of the wedge will be given later. Here it may suffice to mention that the experimental and computational results only agree sufficiently well with one another when the piston Froude number is small, say roughly $Fr \leq 0.3$. With growing Froude number the waveheight close to the wave generator is increasingly overestimated and was becoming so large that computations became unstable.

Description of results. Table 3 summarizes the experimental conditions for which satisfactory results were obtained, figs. 53 - 59 display some of them graphically. Fig. 53 shows the results for a piston with vertical frontal wall moved forward with a Froude number of 0.2. A compact bell-shaped hump with a very small and rapidly attenuated tail at gauge 1 develops into what probably are two solitons and a small amplitude wave tail at gauge 8. This result was anticipated in our inverse scattering analysis. The agreement between measured and computed wave forms is initially excellent, but becomes poorer as the wave splits up into individual solitons. The amplitudes of the solitons are overestimated and the measured wave lags slightly behind the computed wave with growing phase shift as time increases. Moreover, the numerically determined tail is shorter than the experimental one, the likely reason being numerical diffusion, which causes the small amplitude wavelets to damp out quicker than their experimental counterparts. It appears that the numerical algorithm entails numerical dissipation which depends upon the amplitude and is more effective when amplitudes are small.

Fig. 54 shows results for a moving piston which differs from that of fig. 53 only by its speed, which is four times smaller. The evolving wave hump is now very long, and waveheights are correspondingly smaller. The measured and computed wave forms agree well with each other and no trace of phase shift is discernible. The likely reason is that linear behaviour is the prevailing mechanism here.

Additional examples of comparison are shown in figs. 55 - 58. They indicate an excellent agreement between theory and experiments when wave humps are compact and have not yet split into individual solitons (fig. 55). Initial conditions that favour an early breaking of the wave humps into individual solitons disclose the discrepancies between theoretical and experimental findings (figs. 53, 56, 57, 58): The computational waves have slightly different speeds than the experimental ones. Because of the different wave amplitudes the resulting time lag may arise for all individual wavehumps that develop (figs. 53, 56) or primarily for those with small amplitudes (figs. 57, 58). Also, the overestimated wave amplitudes of the individual solitons may or may not be attenuated as the wave travels through the channel (fig. 56 and 57).

For very slow piston motions and very long distances the wedge is moved, small elongated waves are generated (figs. 59, 54). In theses cases the predicted length

Experiment WAVE.DAT No.	Wedge slope	Distance moved d/h	Water depth [cm]	Froude number Fr	Remarks Fig.
Moving Wedge					
460	90^0	2.5	10	0.2	53
458	90^0	2.5	10	0.05	54
446	45^0	1.7	15	0.1	55
497	45^0	5.0	5	0.2	56
381	30^0	2.5	10	0.4	57
392	15^0	2.5	10	0.3	58
389	15^0	2.5	10	0.05	59
Rotating plate					
		Final slope			
355		5/30	15	0.05	63
359		12/30	15	0.05	64
342		2.5/50	15	0.01	65
348		12/50	15	0.01	66
Submerged Wedge					
	Wedge slope				
96	30^0	1.3	10	0.4	67
103	15^0	2.5	10	0.48	68
105	15^0	1.7	15	0.07	69
Submerged Box					
	Box height [cm]				
62	5	2.5	10	0.16	70
67	5	2.5	10	0.56	71
86	5	1.7	15	0.26	72

Table 3: *Conditions of the piston-type wave generators for which satisfactory agreement between theory and experiments was obtained.*

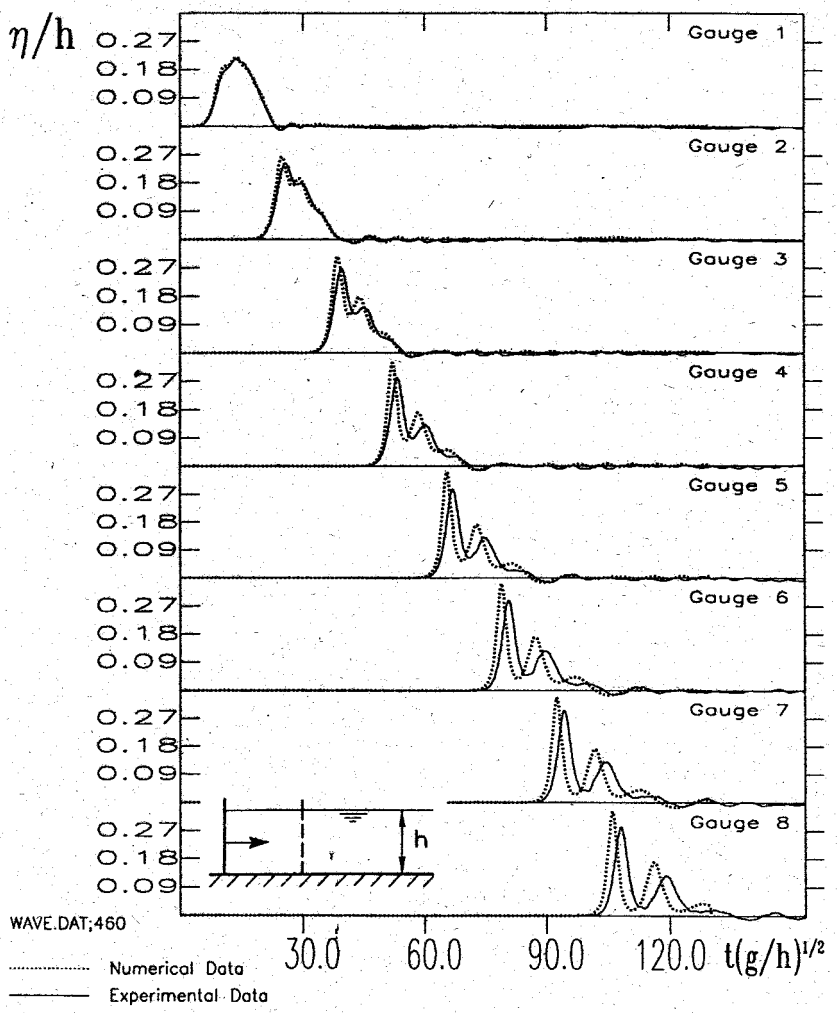

Figure 53: *Comparison of experimental and numerical data. The wave is generated with a vertical plate, moving a distance* $d/h = 2.5$ *with a Froude number of* $Fr = 0.2$.

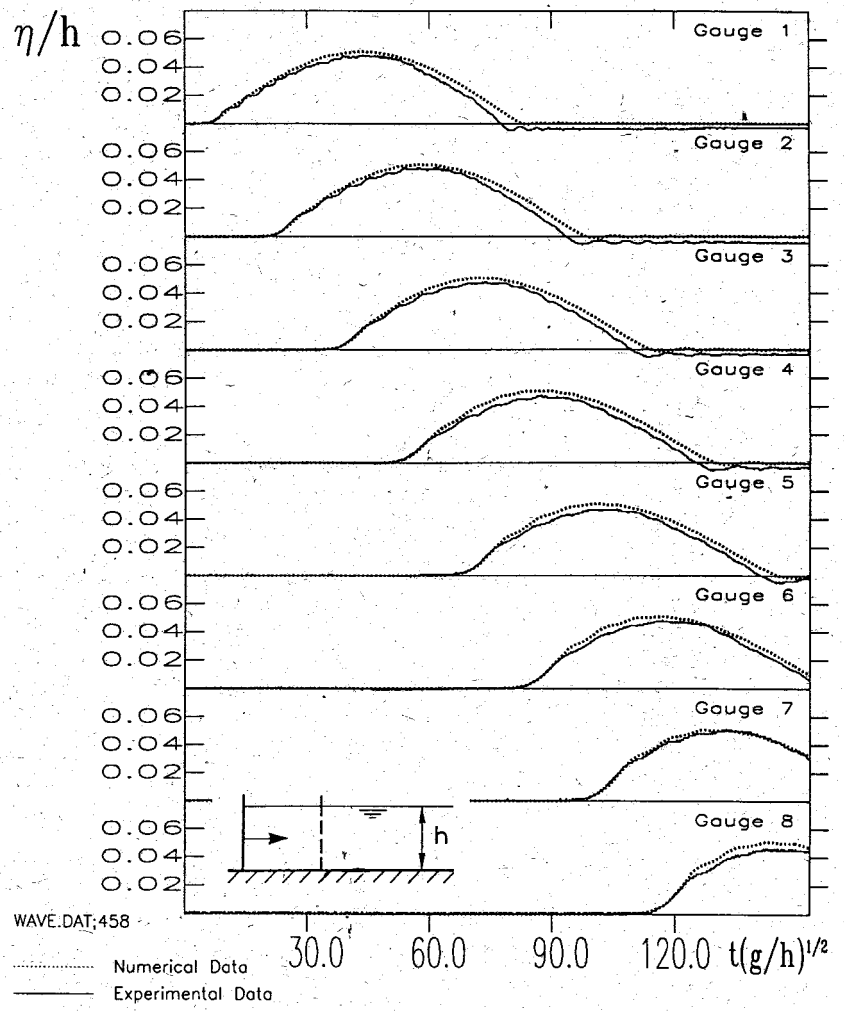

Figure 54: *Comparison of experimental and numerical data. The wave is generated with a vertical plate, moving a distance* $d/h = 2.5$ *with a Froude number of* $Fr = 0.05$.

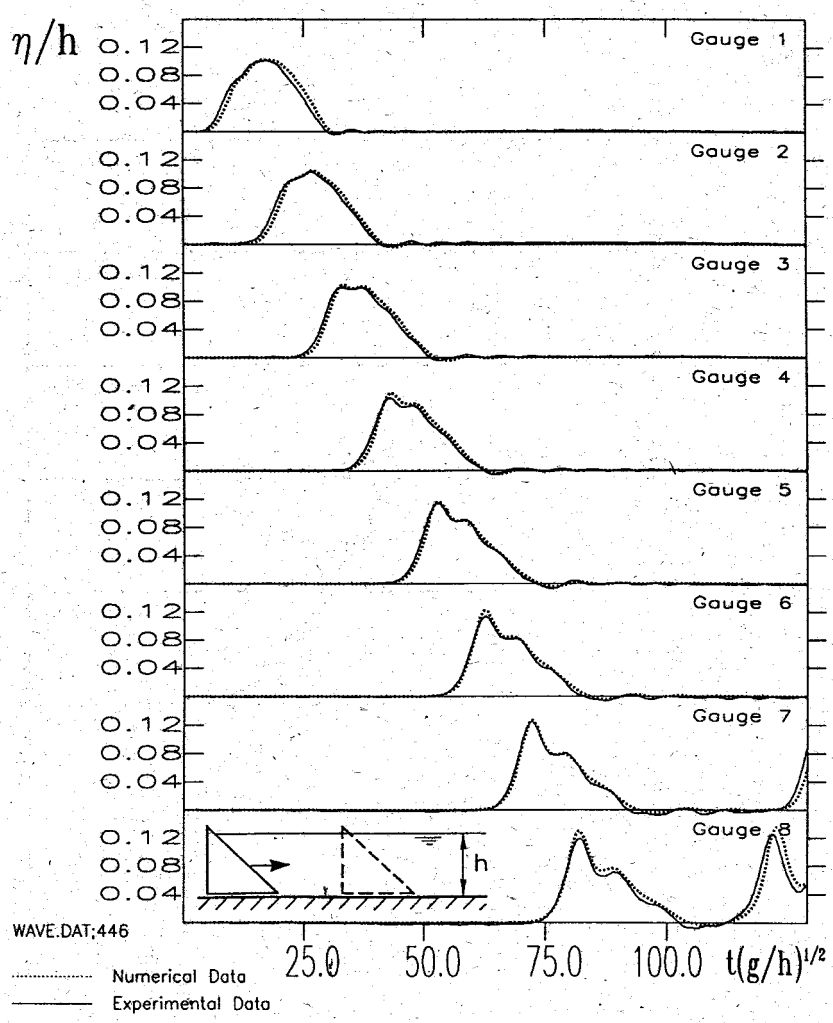

Figure 55: *Comparison of experimental and numerical data. The wave is generated with a wedge with slope of* 1, *moving a distance* $d/h = 1.67$ *with a Froude number of* $Fr = 0.1$.

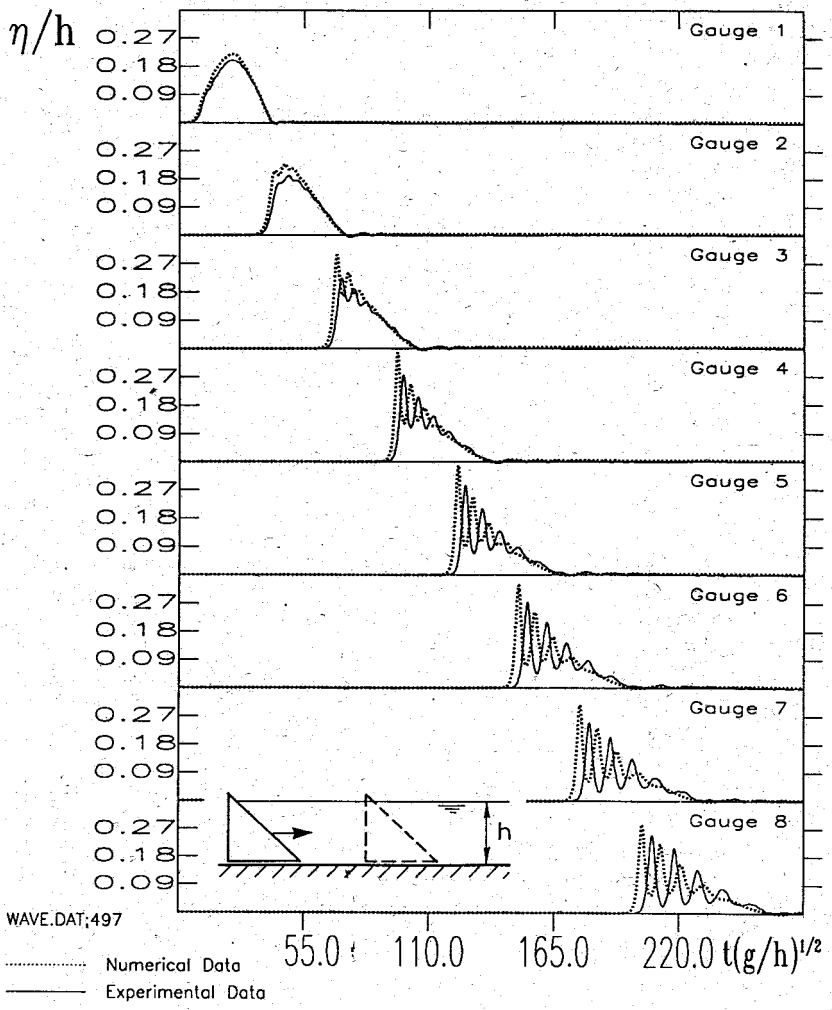

Figure 56: *Comparison of experimental and numerical data. The wave is generated with a wedge with slope of* 1, *moving a distance* $d/h = 5.0$ *with a Froude number of* $Fr = 0.2$.

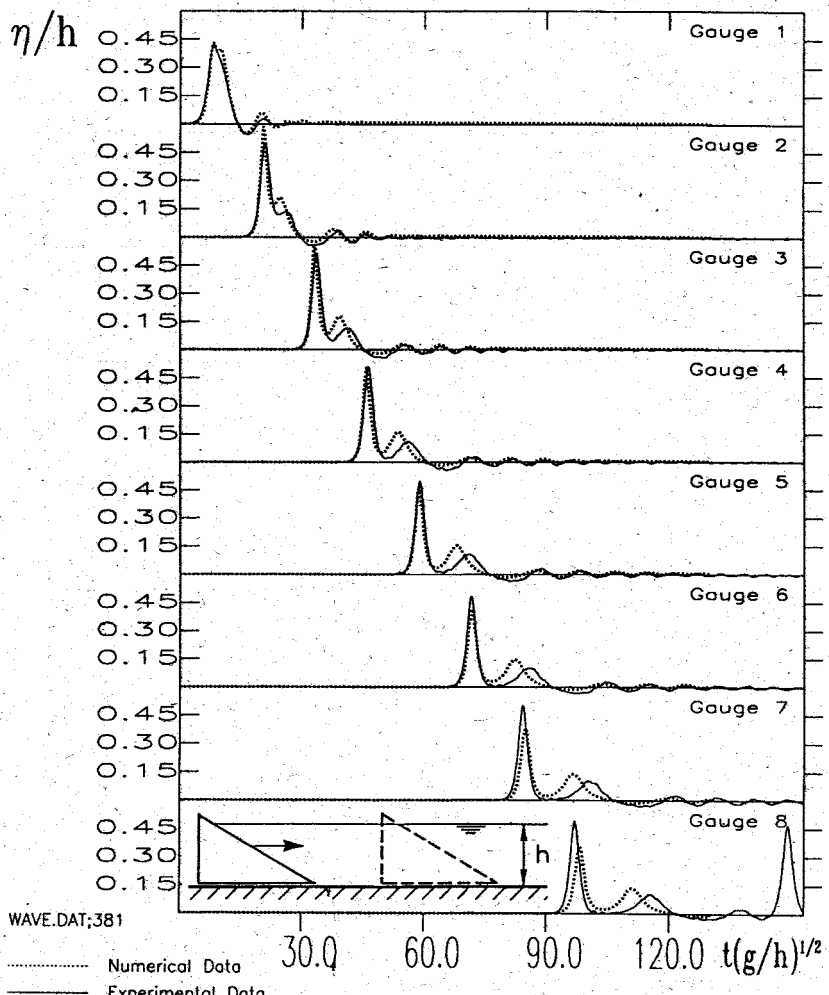

Figure 57: *Comparison of experimental and numerical data. The wave is generated with a wedge with slope of* 0.577, *moving a distance* $d/h = 2.5$ *with a Froude number of* $Fr = 0.4$.

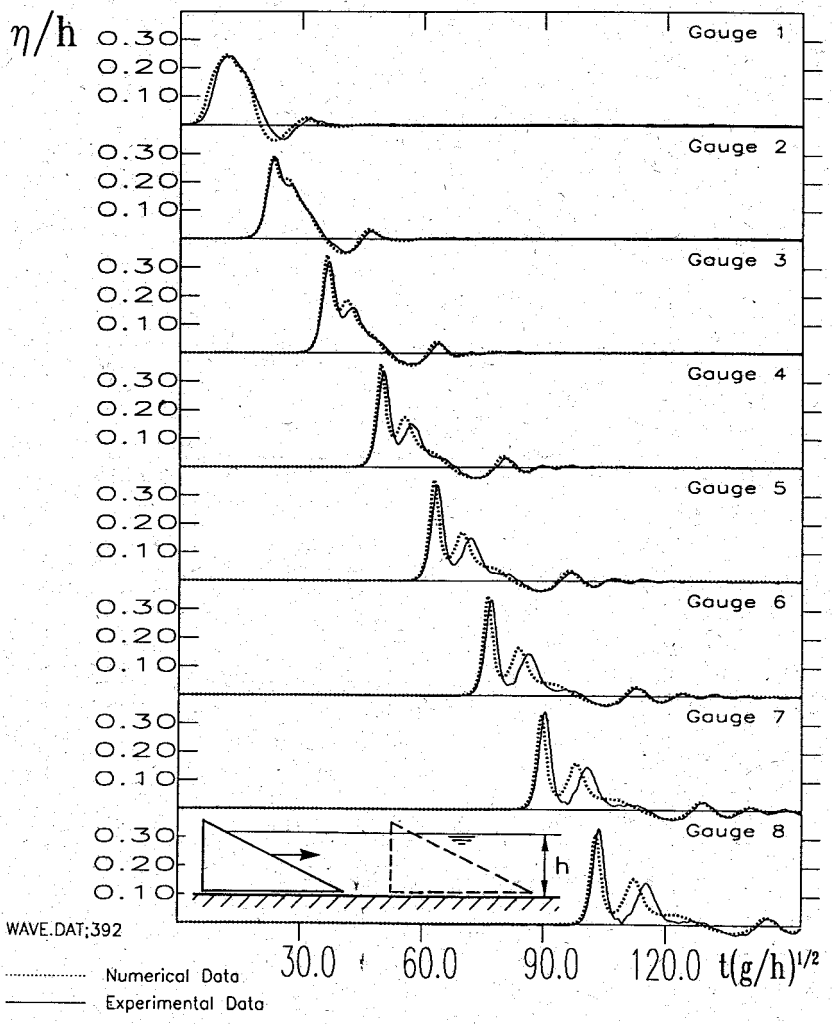

Figure 58: *Comparison of experimental and numerical data. The wave is generated with a wedge with slope of* 0.268, *moving a distance* $d/h = 2.5$ *with a Froude number of* $Fr = 0.3$.

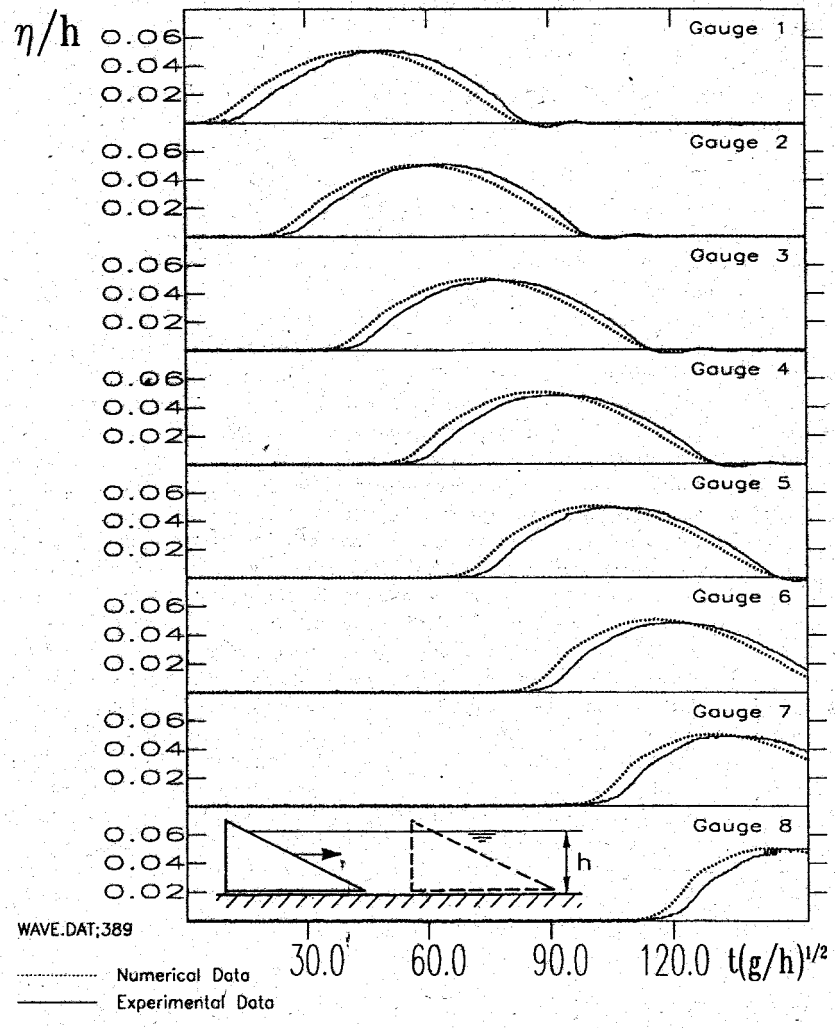

Figure 59: *Comparison of experimental and numerical data. The wave is generated with a wedge with slope of* 0.268, *moving a distance* $d/h = 2.5$ *with a Froude number of* $Fr = 0.05$.

of the wave is slightly overestimated but the height agrees fairly well. Here, the dispersive part of the equations dominates the nonlinear portion.

The sensitivity of the computational results to the piston speed. To study the sensitivity of the computational results upon the piston motion computations were performed for the piston with vertical front which was moved a nondimensional distance of d/h for different Froude numbers. For some of the configurations experimental results are available which permit identification of the range for the piston Froude number for which theoretical results adequately reproduce the experiments. Figs. 60 and 61 summarize the results. Each panel holds for a particular value of d/h, and each curve in an individual panel corresponds to a specific value of the Froude number, starting with $Fr = 0.1$ and increasing in steps of 0.1. The curves corresponding to the largest Froude number are the last ones (among those for which Fr is increased in steps of 0.1) for which the numerical scheme produced stable results. Plotted is the maximum dimensionless amplitude η/h that was registered for each time step at a dimensionless distance x/h. Where available, corresponding experimental points are also indicated (panel *b*, *c*, *d* in fig. 60). The general features are as follows: For small Froude numbers the maximum amplitudes grow with increasing distance from the wave generator. When Froude numbers are larger this monotonicity ceases and waveheights first grow, reach a maximum at a certain distance from the wave generator and then fall off with growing x/h. The behaviour of the solutions is similar to what was obtained by Gozali & Hunt [26] for nonlinear *nondispersive* waves. Their study differs from ours insofar as their dimensionless distance d/h which the piston was moved exceeded the value 10, $d/h \gg 10$, a fact that permitted them to scale the length coordinate with d rather than h, as we did. Typical of the solutions of Gozali & Hunt, as well as ours, is the fact that a maximum of the waveheight amplitude is reached at a certain distance followed by a strong attenuation. For large values of x/h it is likely that a limit value of η/h is reached. Comparing the individual panels it is seen that the range of Froude numbers for which computations are numerically stable increases with increasing d/h values. In no case, however, a value of $Fr = 1.30$ could be reached. It is not known to us whether this property is in any way connected with the fact that solitary waves with maximum amplitude only exist for $Fr_c < 1.35$ [53,20] or the physical wave instability (wave breaking) at $Fr_c = 1.41$ [31], but, of course, one is tempted to suppose so.

When comparing the numerically determined wave amplitudes with those obtained in the experiments (panels *b*, *c*, *d* in fig. 60) it is seen that agreement is only satisfactory for low Froude numbers. The steepening of the curves $\eta/h = f(x/h, Fr)$ that is increasing with growing Froude number and the formation of a conspicuous maximum that has developed is likely the trace of an onsetting numerical instability.

It should be mentioned that the experimental results are plotted as obtained from data in the form $\eta(x_0, t)$ rather than $\eta(x, t_0)$ as is done for the computed

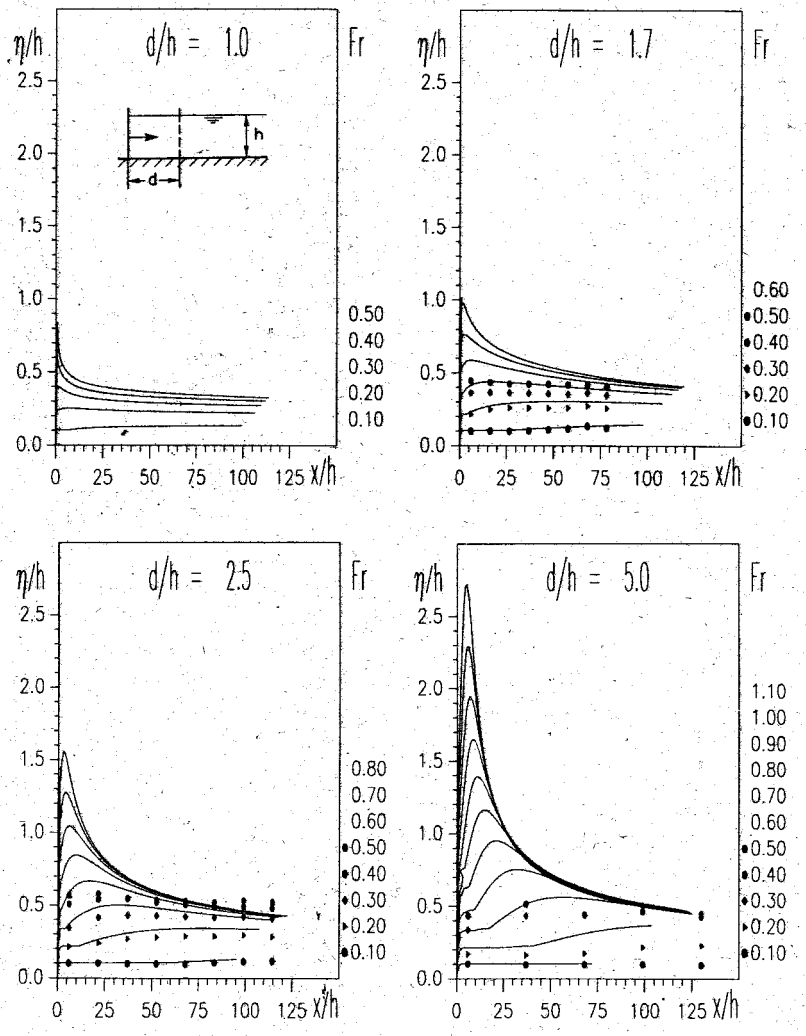

Figure 60: *Computed maximum dimensionless waveheight η/h arising at a distance x/h from the wave generator for a vertical wall that was moved with various different dimensionless speeds $Fr = v/\sqrt{gh}$. Each panel holds for a dimensionless distance d/h the wall was pushed forward. Shown are also experimental results, marked with filled symbols.*

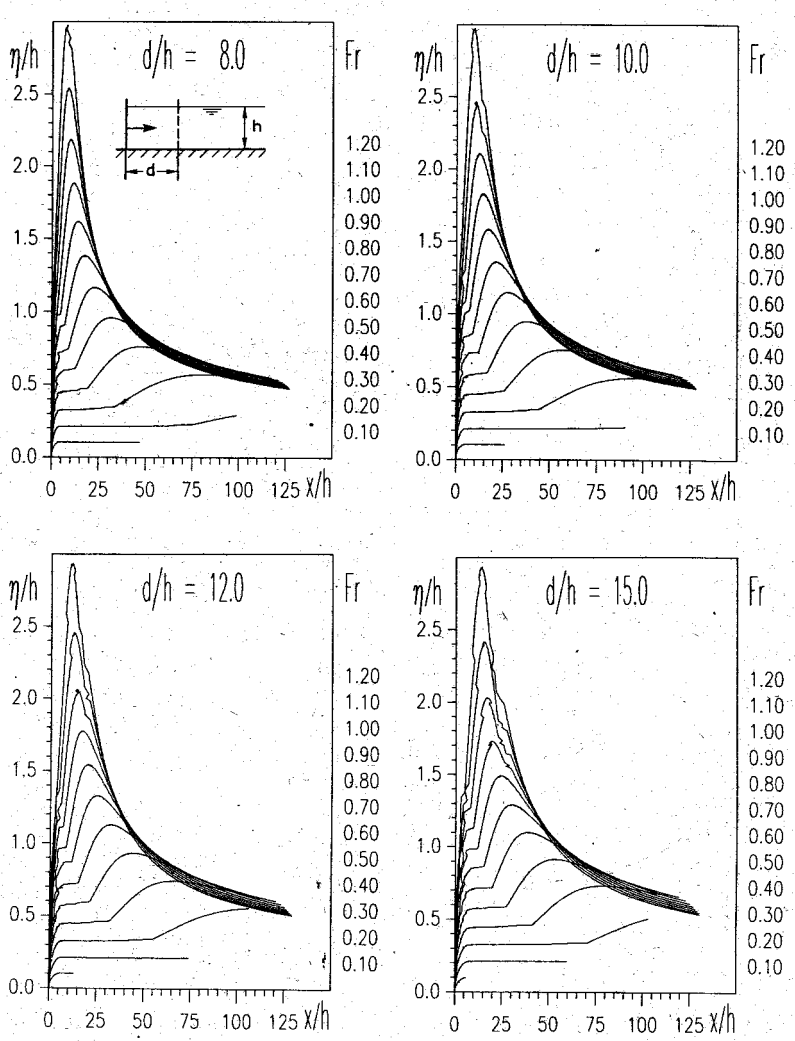

Figure 61: *Same as fig. 60 but for larger values of d/h. Experimental results are not available in these cases.*

curves; however, it was shown earlier that the errors associated with this are small and generally negligible.

A second examination was also performed for a wedge-type piston with a slope of 15^0. Due to a different boundary, the numerical scheme is based here upon Lagrangian coordinates. Fig. 62 shows that the calculations became unstable for lower Froude numbers than this was the case in the moving wall situation. Apart from this inconvenience, the agreement between experimental and computational results is within the same range as in the moving wall cases. As far as observations are possible, the steepening of the curves is the same as before. Why the calculation with the Lagrangian scheme became unstable earlier than in the case of the vertical wall were Eulerian coordinates were used is unknown.

The questionability of the numerical results at large piston velocities (or large piston Froude numbers) is founded upon two facts: First, both equation sets, that of Gozali & Hunt [26] as well as that of Villeneuve & Savage[90] are valid only for small values of $\eta/h < 1$. Second, the experimental results that are shown in fig. 60 where $d/h = 2.5$, 5 and 1.7 agree sufficiently accurately with computations as long as $Fr \leq 0.3$, say. For $Fr = 0.4$ and $Fr = 0.5$ the maximum wave height is always overestimated by the computational results. In light of the significance of the large Froude number when landslides or avalanches are impinging on lakes this problem warrants further study.

At this point we can only muse about the causes. The assumption of a inviscid fluid may be a too drastic idealization and dissipation may have to be incorporated. Most likely, however, strong basal friction may be active in the vicinity of the wave generator. Addition of a bottom friction term may help to overcome these difficulties.

4.2.2 Rotating plate

The displaced water masses in the rotating plate experiments are generally much smaller than for the piston experiments. As a result the wave amplitudes (scaled by water depth) are smaller, the waves therefore closer to the linear shallow water limit, and computational findings in better agreement with experiments than in the previous cases. The wave amplitude to water depth ratio hardly ever exceeds 6% (in comparison to up to 45% in the piston experiments). This does not seem to be a disadvantage as these ratios are generally in the vicinity of the lower value in lake applications.

The behaviour of the numerical algorithm is similar to the previous cases. Since the Froude numbers of the plate lifting velocities are in the range $0.05 \leq Fr \leq 0.1$ and displaced water masses are small no numerical instability was encountered. Computational and experimental waveheight-time series usually agree well with small time shifts developing as the wave proceeds (this is understandable because

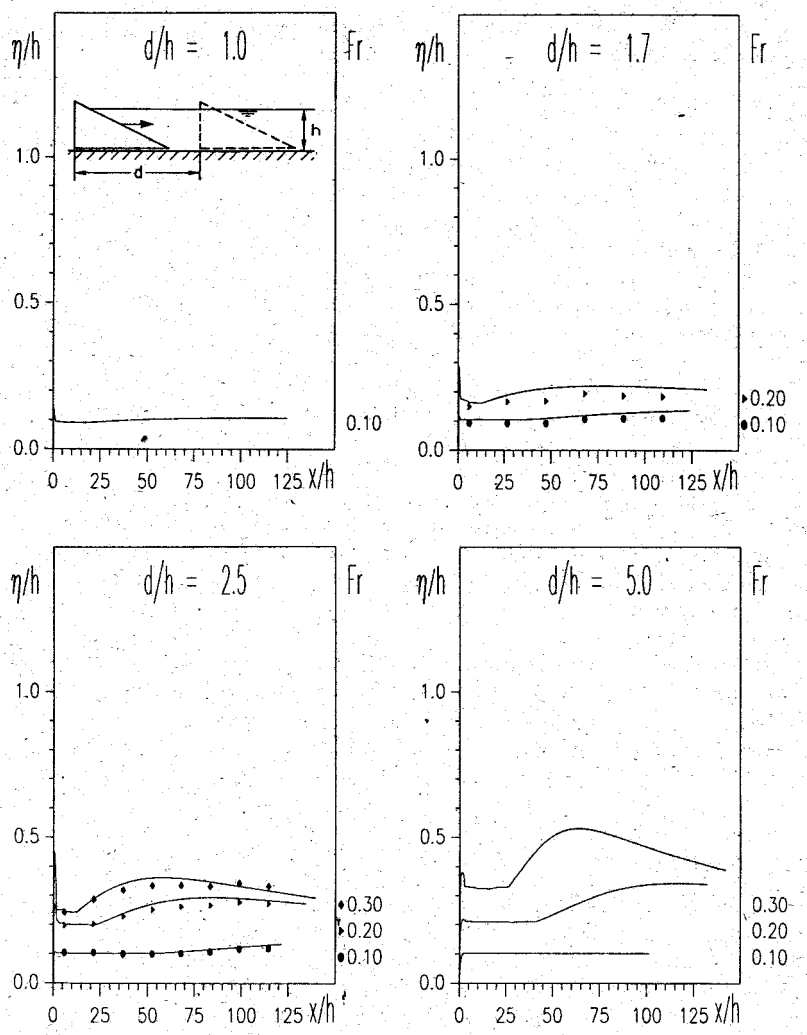

Figure 62: *Computed maximum dimensionless waveheight η/h arising at a distance x/h from the wave generator for a wedge with slope of 15^0 that was moved with various different dimensionless speeds $Fr = v/\sqrt{gh}$. Each panel holds for a dimensionless distance d/h the wedge was pushed forward. Shown are also experimental results, marked with filled symbols.*

nonlinearity affects the phase velocity less owing to the smaller amplitudes). However, the computational wave tailes are still attenuated much faster than the corresponding experimental ones.

One peculiarity, observed in all experiments performed with the rotating plate concerns the small amplitude wave tail. The experiments always show it to be below the zero level line (which marks the still water level of the entire channel) and slowly rising to this line. The likely reason is the fact of a drift of the zero point amplification during the measurements. Figs. 63 – 66 show the results and demonstrate that waveheight time series are in close proximity including the onsetting reflected wave parts.

4.2.3 Submerged wedge

As in the case of the rotating plate the governing equations are used in fixed Eulerian coordinates. The numerical results correspond better with the experiments than in the case of the simple wedges, where mesh changing Lagrangeian coordinates are used. The computations and experiments were performed for submerged wedges having slopes of $15^0, 30^0$ and 45^0 that were moved distances in the range $0.85 \leq d/h \leq 1.3$ at various speeds. Experiments and computations were performed for conditions listed in table 3 and figs. 67-69 which provide a cross section of comparisons between experiments and theory from best to worst.

4.2.4 Submerged box

Two different boxes are tested: A discontinuous change of the waterdepth (a step) and a continuous bottom $h(x)$ for which a small inclined plate is added at the front of the step. The submerged box generates both left going and right going waves. Therefore the Korteweg-de Vries equation is not valid and the complete Boussinesq-type equation has to be used.

For the discontinuous step no conditions were found for which computational results would come close to the experimental findings. The calculations produce large oscillating left going waves, the right going waves in the flat part of the channel agree in their wavelengths with the experiments but not in their height. Probably, the discontinuous change of the water depth causes this discrepancy, generating a strong wake behind the step and above the submerged box. Choosing the continuous step while keeping all other parameters fixed, computations reproduce experiments satisfactorily. Conditions for which comparisons were performed are listed in table 3 on page 140 and explicit comparisons are shown in figs. 70 - 72.

Because the submerged box experiments are physically closest to the kinematics of a landslide it is interesting to see how the numerical algorithm behaves in this case when the Froude number of the submerged box becomes larger. We have

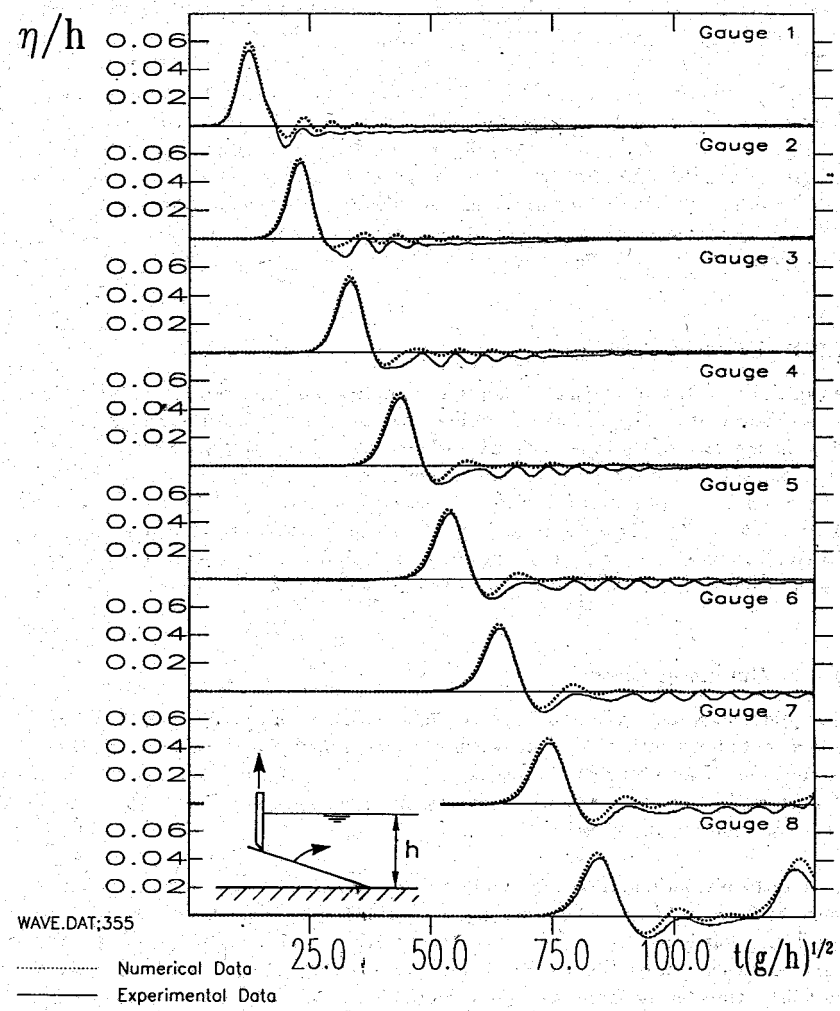

Figure 63: *Comparison of experimental and numerical data. The wave is generated with a rotating plate which is lifted up to a slope of* 5/30 *with a Froude number of* $Fr = 0.05$.

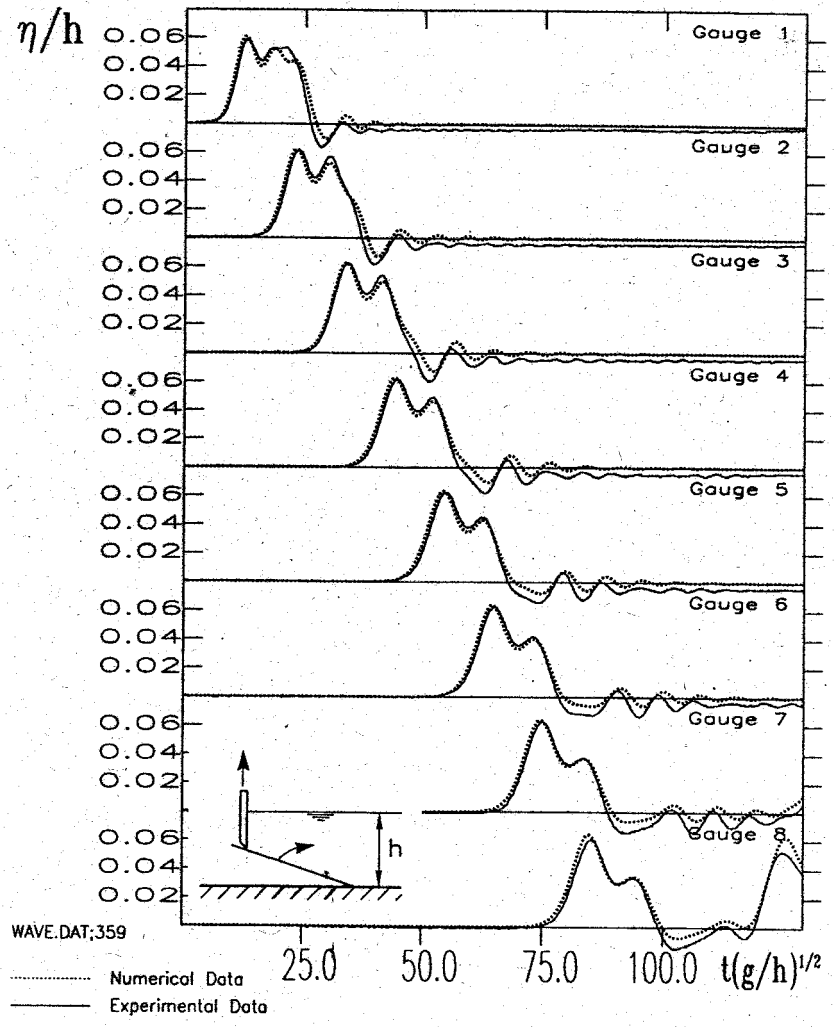

Figure 64: *Comparison of experimental and numerical data. The wave is generated with a rotating plate which is lifted up to a slope of* 12/30 *with a Froude number of* $Fr = 0.05$.

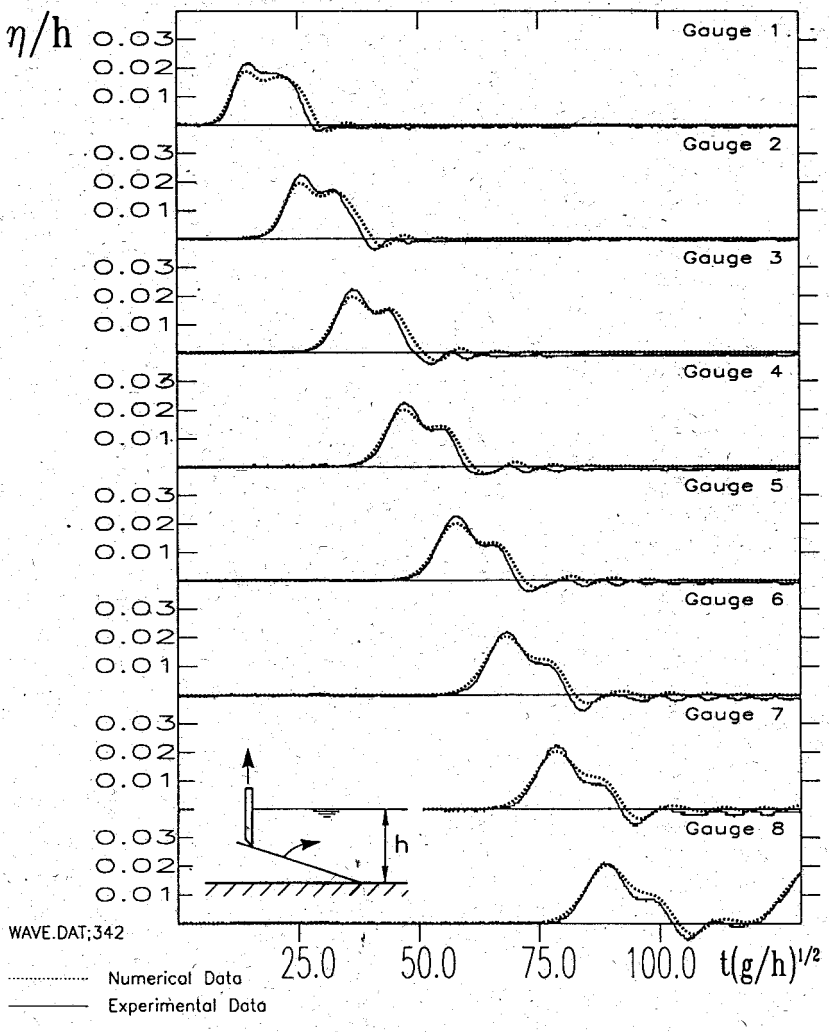

Figure 65: *Comparison of experimental and numerical data. The wave is generated with a rotating plate which is lifted up to a slope of* 2.5/50 *with a Froude number of* $Fr = 0.01$.

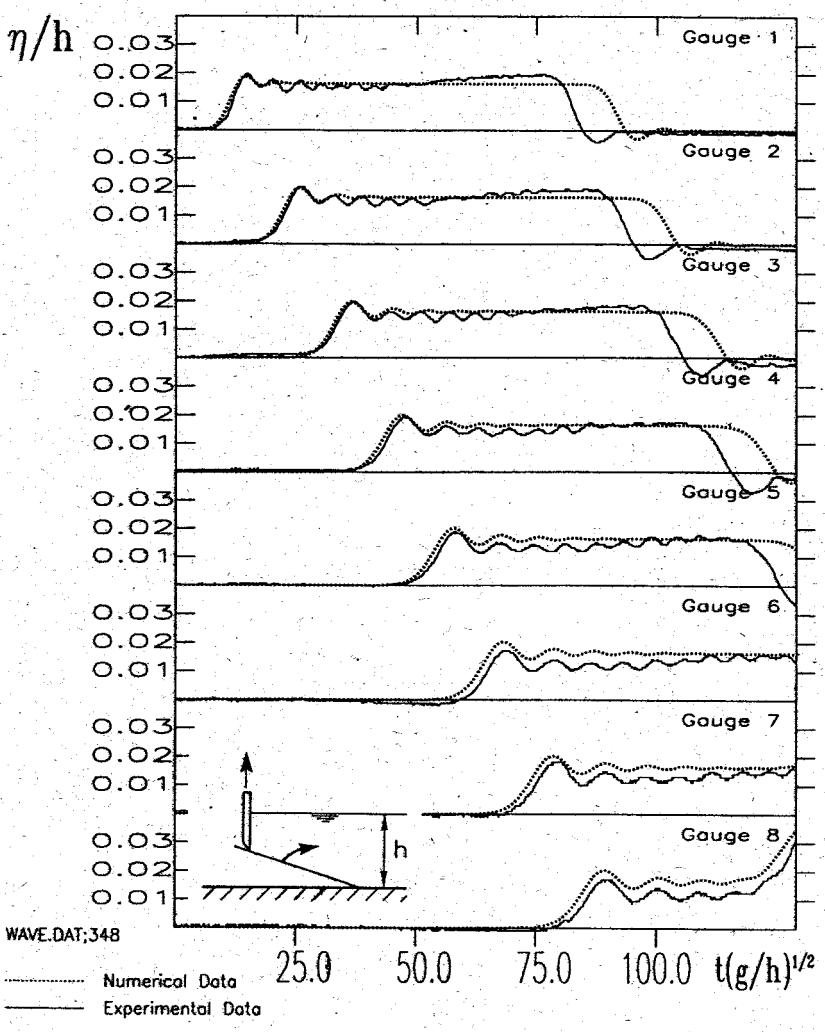

Figure 66: *Comparison of experimental and numerical data. The wave is generated with a rotating plate which is lifted up to a slope of* 12/50 *with a Froude number of* $Fr = 0.01$.

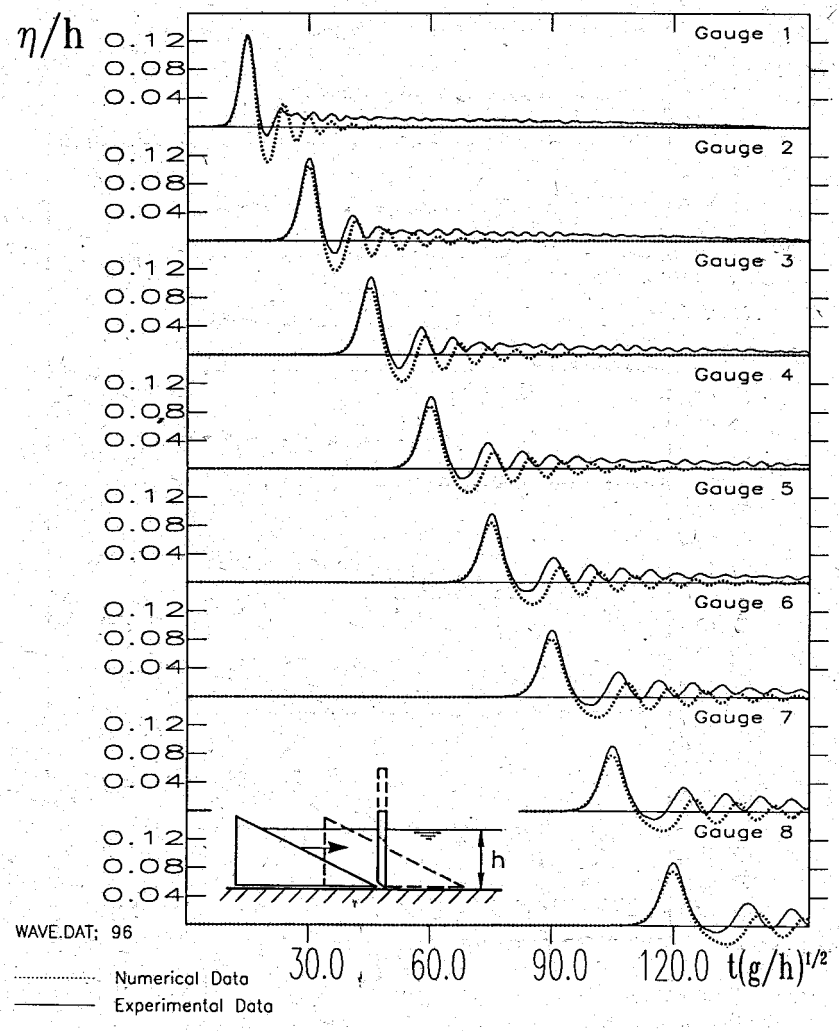

Figure 67: *Comparison of experimental and numerical data. The wave is generated with a submerged wedge with slope of* 0.577 *moving a distance of* $d/h = 1.3$ *with a Froude number of* $Fr = 0.4$.

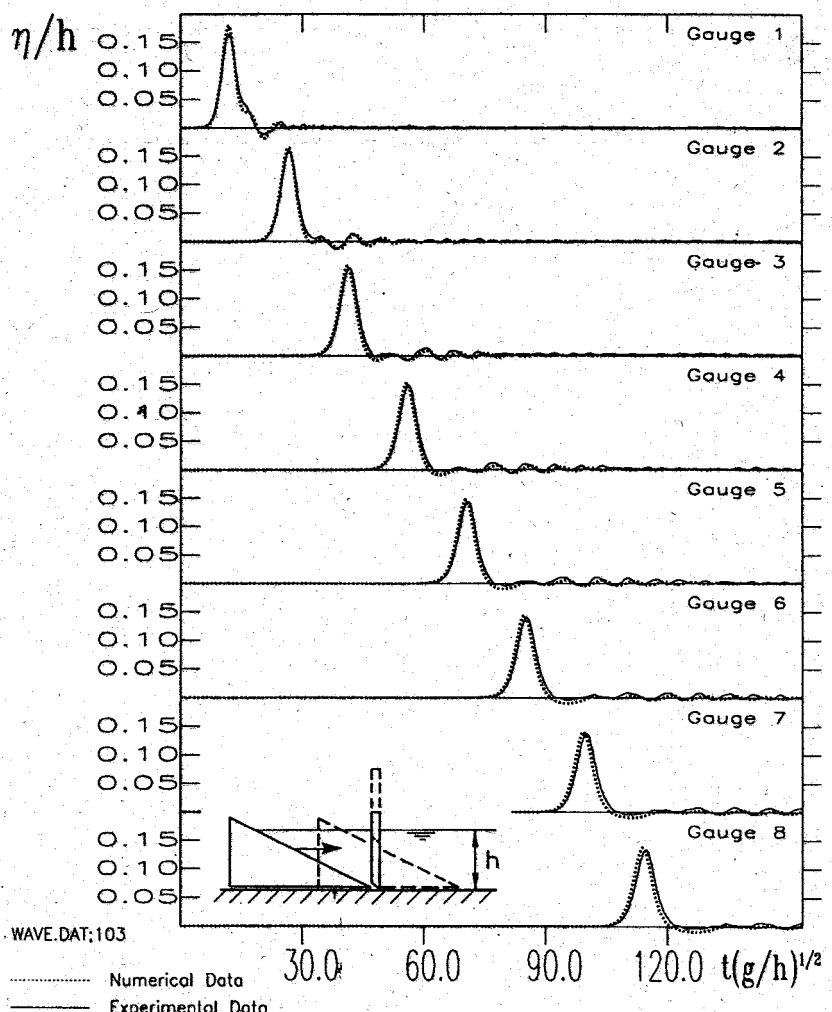

Figure 68: *Comparison of experimental and numerical data. The wave is generated with a submerged wedge with slope of* 0.268 *moving a distance of* $d/h = 2.5$ *with a Froude number of* $Fr = 0.48$.

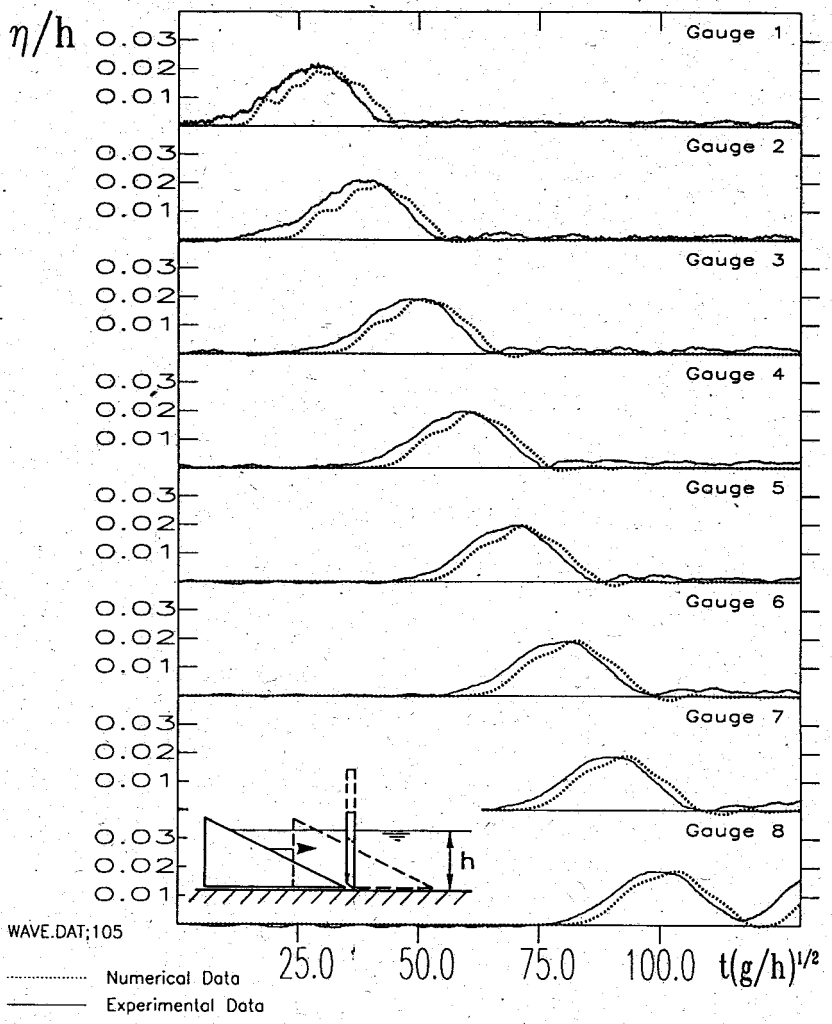

Figure 69: *Comparison of experimental and numerical data. The wave is generated with a submerged wedge with slope of* 0.268 *moving a distance of* $d/h = 1.7$ *with a Froude number of* $Fr = 0.07$.

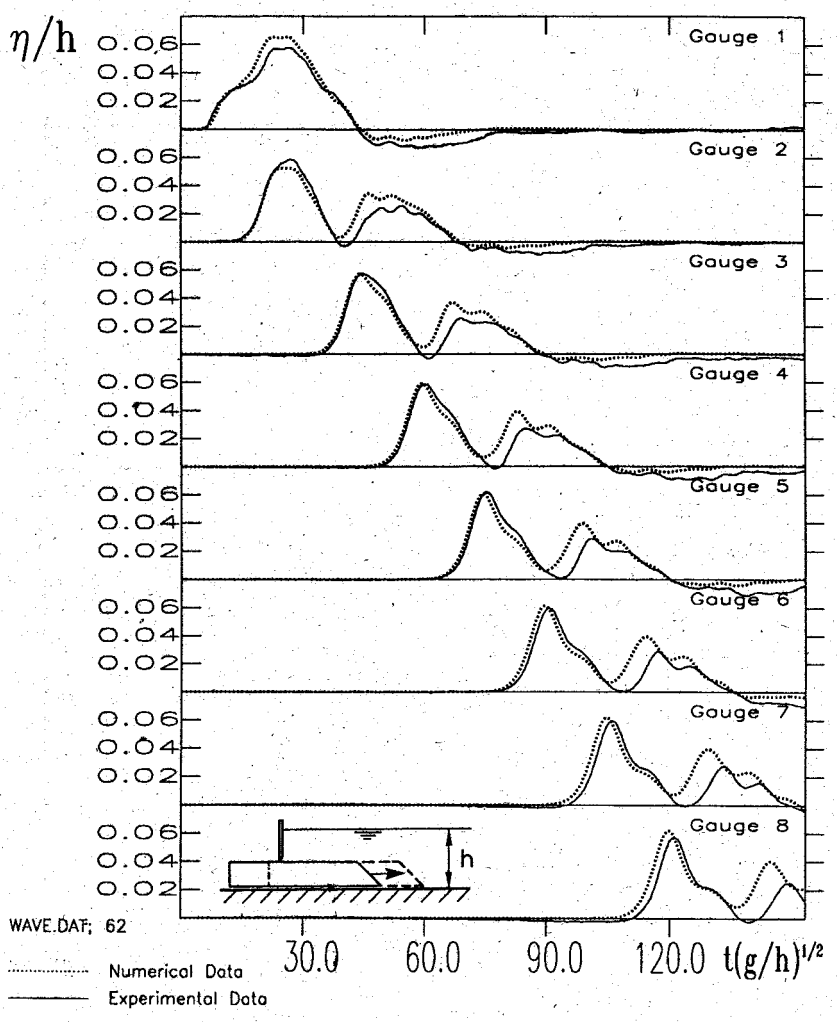

Figure 70: *Comparison of experimental and numerical data. The wave is generated with a submerged box with height $h/2$, moving a distance of $d/h = 2.5$ with a Froude number of $Fr = 0.16$.*

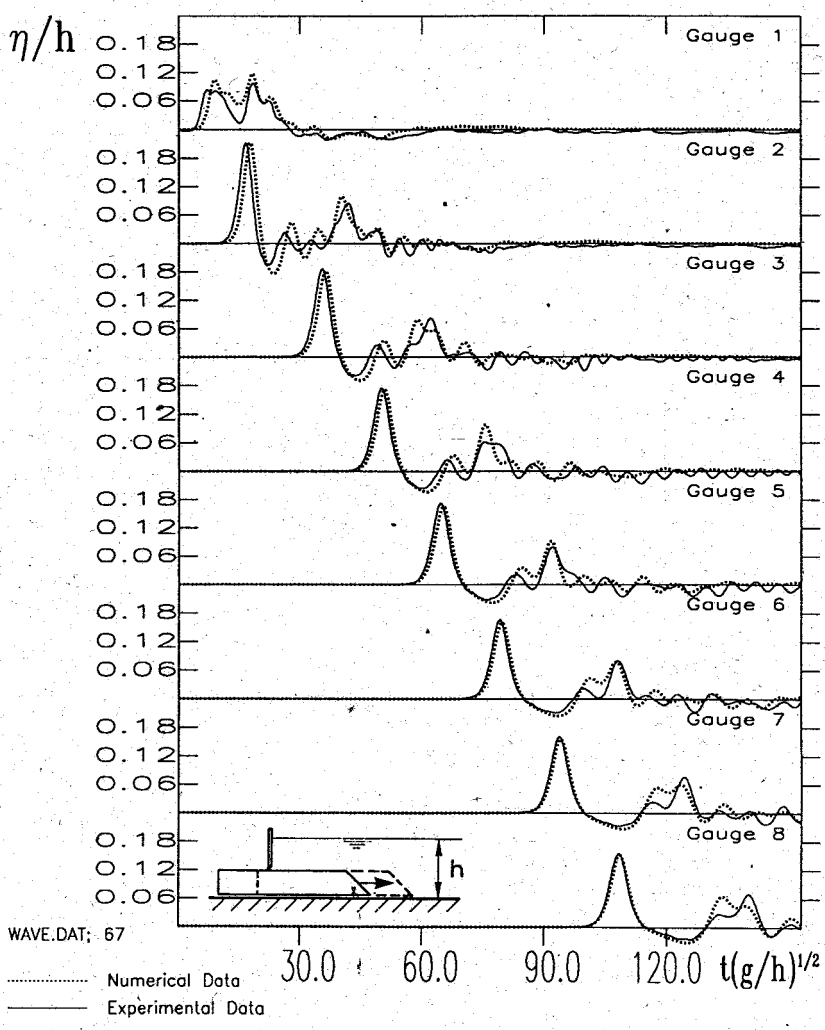

Figure 71: *Comparison of experimental and numerical data. The wave is generated with a submerged box with height $h/2$, moving a distance of $d/h = 2.5$ with a Froude number of $Fr = 0.56$.*

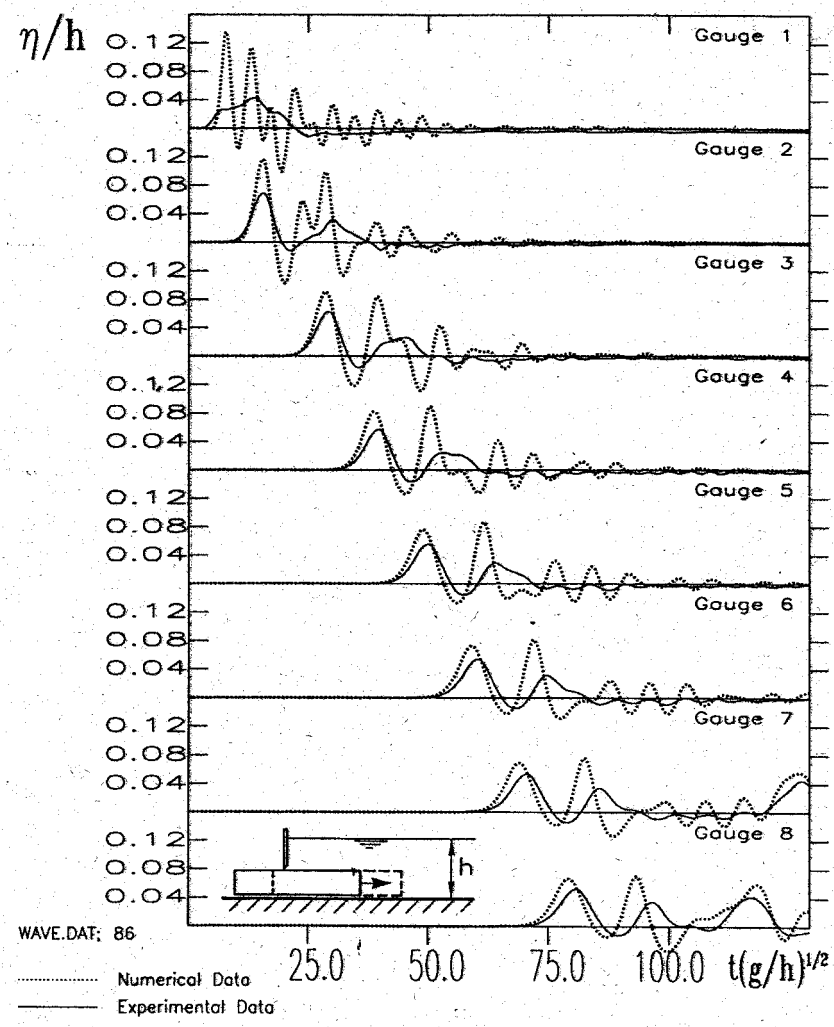

Figure 72: *Comparison of experimental and numerical data. The wave is generated with a submerged box with height $h/3$, moving a distance of $d/h = 1.7$ with a Froude number of $Fr = 0.26$.*

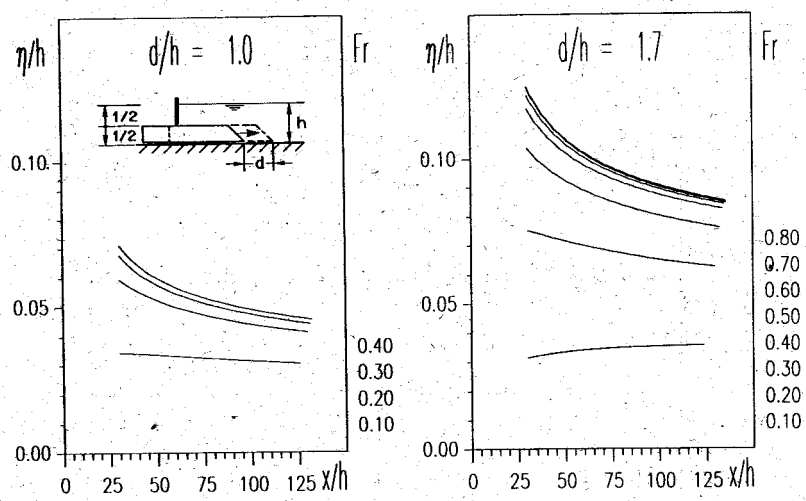

Figure 73: *Computed maximum dimensionless waveheight η/h arising at a distance x/h from the wave generator for a submerged step that was moved with various different dimensionless speeds $Fr = v/\sqrt{gh}$. Each panel holds for a dimensionless distance d/h the step was pushed forward.*

performed such a computational exercise and have summerized it in fig. 73. The maximum amplitude is plotted whenever it has reached a distance $x/h \geq 30$, to avoid difficulties above the box. The length of the box is $7.5\,h$, its height $h/2$. The amplitude increases with larger Froude number but seems to reach a maximum curve (see panel *b* for $d/h = 1.7$). It should be noted that the scale of the amplitude is about ten times smaller than in the corresponding figures of the piston types. When increasing the distance d/h the box is moved, no stable result was obtained.

4.3 Concluding remarks

In this chapter weakly nonlinear shallow water waves on a gently varying bottom which may move in time have been analysed both computationally and experimentally. Over most part of the $15m$ long channel the depth of the water was constant so that in this portion unidirectional wave theory could be employed. The wave generating device, however, required a theoretical concept with moving bottom. Two items comprise the main goals of this chapter, first, inverse scattering considerations in the constant depth portion of the channel and direct comparison of measured waveheight time series with corresponding computational results.

To verify whether the inverse scattering theory of the Korteweg-de Vries equation is applicable the measured data were brought into a form that was thought to

be suitabel for this comparison. One prerequisite for a comparison is that the initial data are such that influences from boundaries have sufficiently died out and all waves of a wave packet are moving in one direction only. Initial data are needed in the form $\eta(x;t_0)$, t_0 fixed, rather than $\eta(x_0,t)$, x_0 fixed, but it was interesting to see, how the two sets differ from one another and, therefore, how the number of evolving solitons is influenced by the application of the two different starting sets. It was found that for the experimentally generated waves the curves $\eta(x;t_0)$ and $\eta(x_0,t)$ differed only slightly; phase shifts were encountered and wave tails were differently obtained. It is, of course difficult to judge experimentally, when a wave hump will no longer be affected by boundaries. As a result of this it should be no surprise, that the number of solitons which was estimated with the inverse scattering method differed according to the phase and/or time from where or when the wave profile was taken. Nontheless the many experimental results provide a coherent and satisfactory corroboration of the inverse scattering method of the Korteweg-de Vries equation.

In the second portion of this chapter, the waveheight time series of the experiments and the computations were compared for four different wave generators, the moving wedge, the rotating plate, the submerged moving wedge and the submerged box. It was found that agreement between measured and computed water-elevation time series was good in general provided that characteristic Froude numbers of the wave generating device were small enough. If the motion of the wave generator is too large, then the computed wave amplitudes are overestimated. This phenomenon has always led to a computational instability. However, even in the range of Froude numbers where the main wave hump is adequately predicted are some persistent deviations of the computations from the experiments discernable. The computed wave speed differs slightly from that of the experiments and is often somewhat larger than that of the experiments. Moreover, small amplitude wave tails hardly ever agree; the reason is likely a combination of two effects: the drift properties of the measuring device and the large numerical diffusion that is incorporated in the numerical code. The waveheight time series of one experiment was never properly reproduced by the computations. It was the wave generated by the submerged step with vertical frontal wall. The exact reasons for the inadequacy of the model equations are difficult to evaluate but a likely cause is the fact that the shallow water equations are certainly inappropriate in the vicinity of the edge of the moving submerged piston. Adding a wedge to the front indeed substantially improved the perfomance of the model.

A major concern of the developed computational code is its inadequacy in the range of large Froude numbers of the wave generator. This is the range that arises when an avalanche or landslide plunges into a lake or reservoir. An initiating model in the neighbourhood of the wave generator is therefore needed which improves the perfomance of the model. At this stage of the knowledge we are only able to muse about what could contribute to a better performance. We believe that basal friction and perhaps turbulent friction mechanisms might be sufficient to achieve this goal.

Future work will have to concentrate on this problem.

5 Generation of waves by a porous piston

Most of the avalanches impinging on lakes do not consist of a single mass of rock rather a more or less dense assemblage of stones is moving down and will thus react differently with the water. Experiments done so far have ignored this. Therefore, two different experimental models will be examined with the aid of which a wave in a channel is generated by a moving porous body. As before a simple triangular geometry of the body is chosen. A numerical model is then developed which is able to simulate the experimental results.

5.1 Experimental set-up

The only difference in the set-up of the experiments described before and the experiments we want present now consists in a differently modelled wedge-type piston of the wave generator. Before we used a completely closed wedge where the masses of the water would climb up but not penetrate into. Now the body of the wedge is kept porous. Two different wedges are used. One is entirely open in the front and the rear, the other is closed by a vertical wall at its back side. In the first case, the water is free to move in a channel confined between two fixed vertical walls, one at the far end of the channel, the other just behind the piston, $10cm$ behind the porous wedge when the latter is in its back position. In the second layout the impervious wall of the moving wedge confines one end of the channel. This is, clearly, reminiscent of the impervious wave generator device. The other details of the experimental arrangements are the same as before. In particular, two bars that are moved by the gearbox of the wave generator now push the porous wedge.

As regards the numerical model we must avoid turbulence and also have to ensure the water motion to be as much parallel and along the channel as possible. Therefore, the skeleton or matrix of the porous body was built of voluminous elements, which would generate a water stream parallel to the channel. Between two triangular plates circular aluminium pipes are spanned. The pipes are mounted perpendicularly to the direction of the channel. On the inclined front and the rear side of the wedge solid cylinders where cut and polished according the inclination of the wedge (see fig 74). The length of this porous wedge is $30cm$ with an angle of inclination of 45^0. Its weight is about $10kg$ and rolls on ball bearings. The diameter of the pipes is $16mm$. Altogether about 120 cylinders were installed.

The porosity of a body is defined by

$$n = \frac{\text{Volume of the pores}}{\text{Total volume of the body}} = 1 - \frac{\text{Volume of the skeleton}}{\text{Total volume of the body}}. \qquad (5.1)$$

A base cell of the porous medium packed by cylinders and the distances between the pipes is sketched in fig. 75. The porosity of the wedge is then found to be

$$n = 1 - \frac{\pi R^2}{6R^2} = 1 - \frac{\pi}{6} = 0.48\,. \qquad (5.2)$$

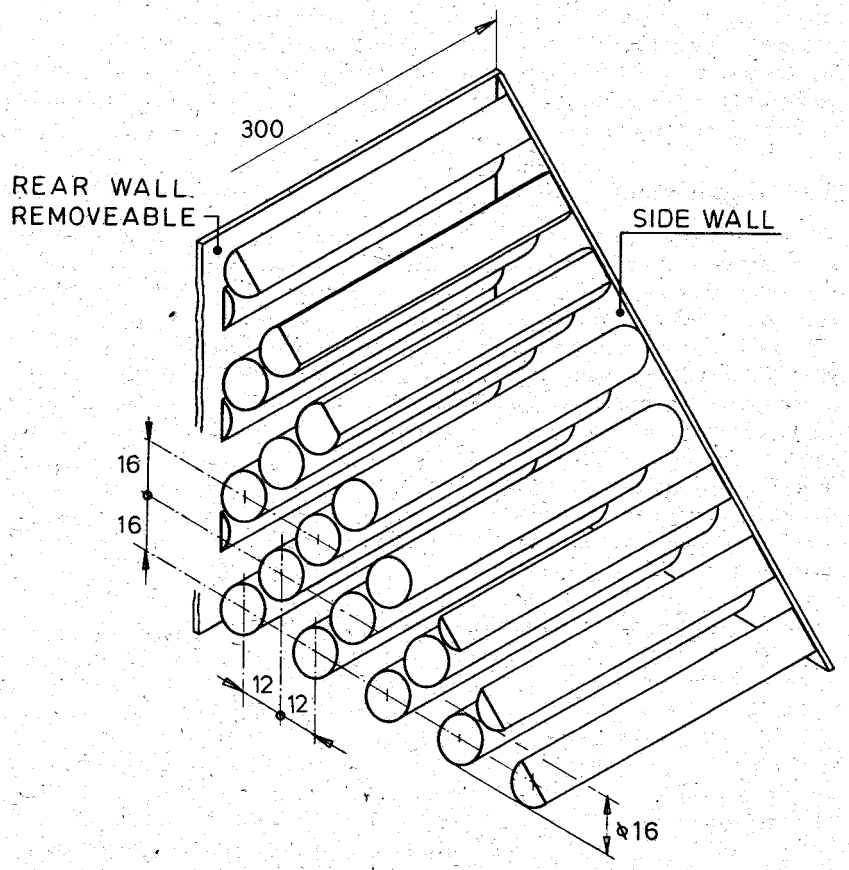

Figure 74: *Sketch of the porous wedge used as wave generator. The back side of the wedge is removeable. The wedge is* 45^0 *inclined. All distances are given in mm.*

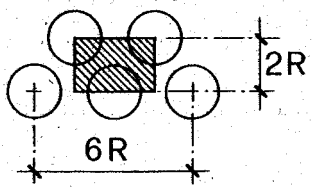

Figure 75: *Base cell (dashed) of the porous body used in the experiments. The radius of the pipes and the distance between the pipes is indicated.*

The porosity is independent of the radius R and the length of the pipes. How the radius influence the generated waves is examined indirectly in so far as three different water depths of $5cm$, $10cm$, and $15cm$ are used.

5.2 Experimental results

Waves which evolve during the motion of an entirely open porous wedge differ essentially from those which are generated by a porous wedge whose rear side is closed. In the case of the porous wedge closed at its back the waves are very similar to the waves generated by a vertical plate or a wedge type generator with inclination angle of 45^0 (both are piston type wave generators). Figures 76 - 78 compare the evolution of the waves generated with the piston and the closed porous wedge. The wave displayed in figure 76 is generated in water of depth $5cm$ and with a Froude number of the motion of the generation device $Fr = 0.4$, for the wave of figure 77 $h = 10cm$, $Fr = 0.2$ and for that of figure 78 $h = 5cm$ and $Fr = 0.05$. In all cases it seems that the skeleton of the porous body accounts very little for the resulting wave form. Only a slite difference in the waveheights occur while the wavelengths (i. e. the length of the first hump) are identical.

A substantially different form of the wave is obtained when an open porous body is used, so that the water is able to flow through the body. During the motion of this wedge the gap between the rear of the porous body and the left end of the channel increases. Because of this free flux the length of the channel is constant for all times. The volume the water mass occupied inside the channel *must* therefore be constant for all times. This did not prevail when the length of the channel was changed due to the motion of the wave generator. Figures 79, 80 and 81 show the time history of the wave amplitude at different stations along the channel. For each of the curves the integral of the wave amplitude vanishes after long time. In other words, the area underneath the wave elevations is the same as the area above the wave depressions. Three examples are given. One is obtained in water of depth $h = 5cm$ and a Froude number of $Fr = 0.4$ (fig. 79), one for $h = 10cm$, $Fr = 0.2$ (fig. 80) and another one for $h = 15cm$, $Fr = 0.05$ (fig. 81). From the drawings it can be seen that during the motion of the open wedge a depression of the water level occurs behind the first hump of the wave. The cause of this depression is the exchange of mass and

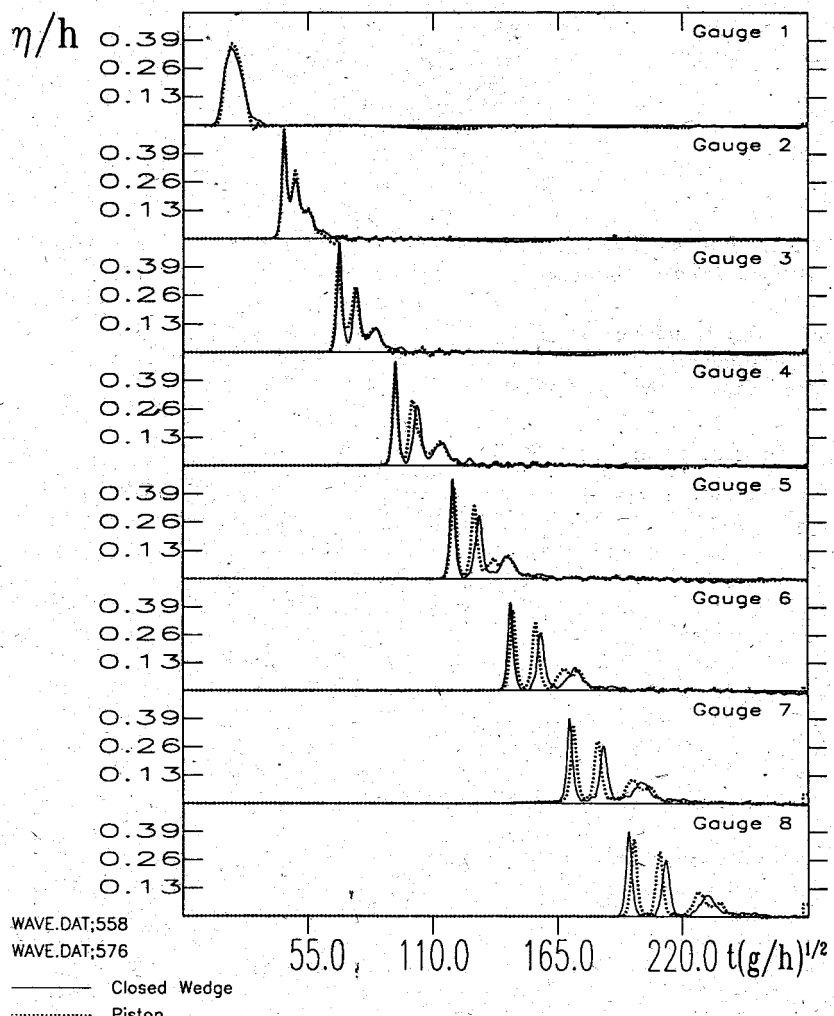

Figure 76: *Comparison of experimental data. The wave is generated either by a vertical plate (piston, dotted lines) or by a porous wedge (solid lines) which is closed at its rear side. Both generators are moving a distance* $d/h = 5.0$ *with a Froude number of* $Fr = 0.4$.

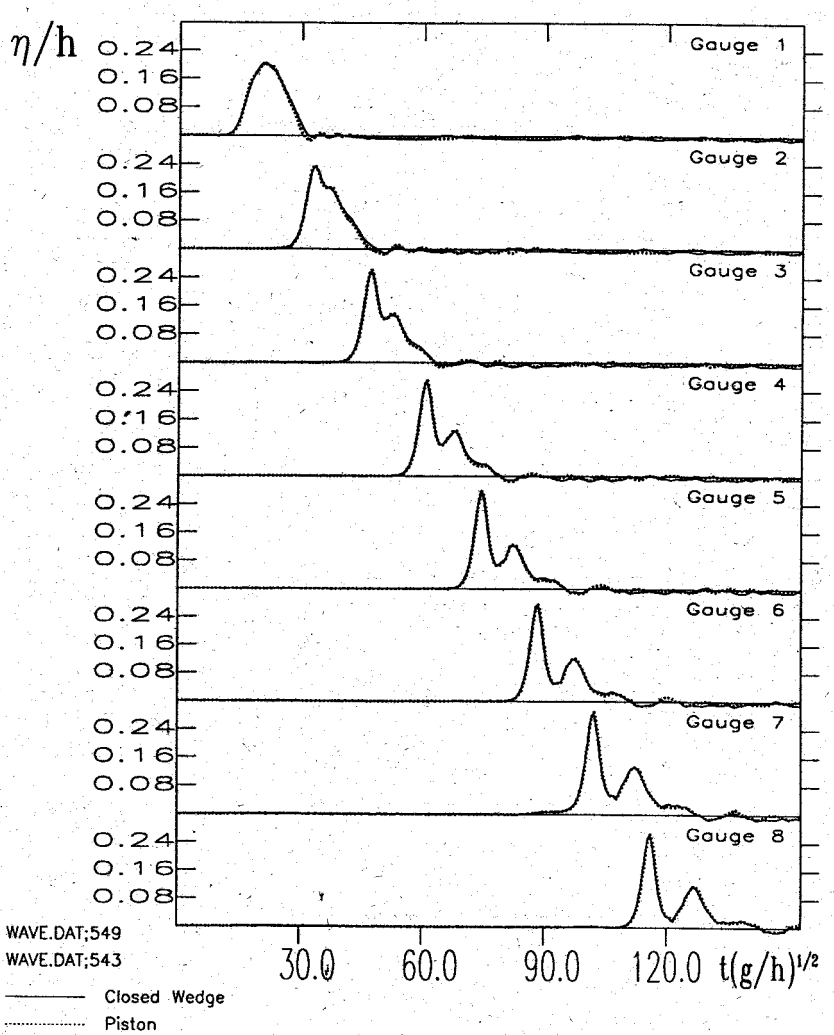

Figure 77: *Comparison of experimental data. The wave is generated either by a vertical plate (piston, dotted lines) or by a porous wedge (solid lines) which is closed at its rear side. Both generators are moving a distance $d/h = 2.5$ with a Froude number of $Fr = 0.2$.*

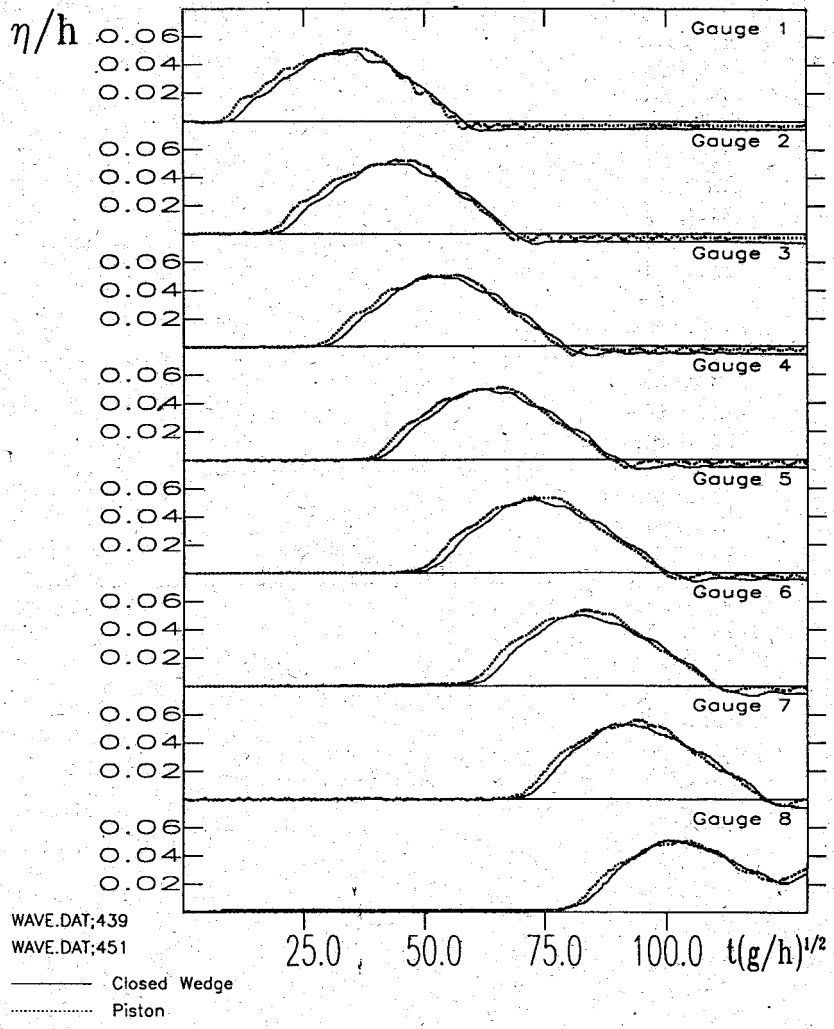

Figure 78: *Comparison of experimental data. The wave is generated either by a vertical plate (piston, dotted lines) or by a porous wedge (solid lines) which is closed at its rear side. Both generators are moving a distance* $d/h = 1.7$ *with a Froude number of* $Fr = 0.05$.

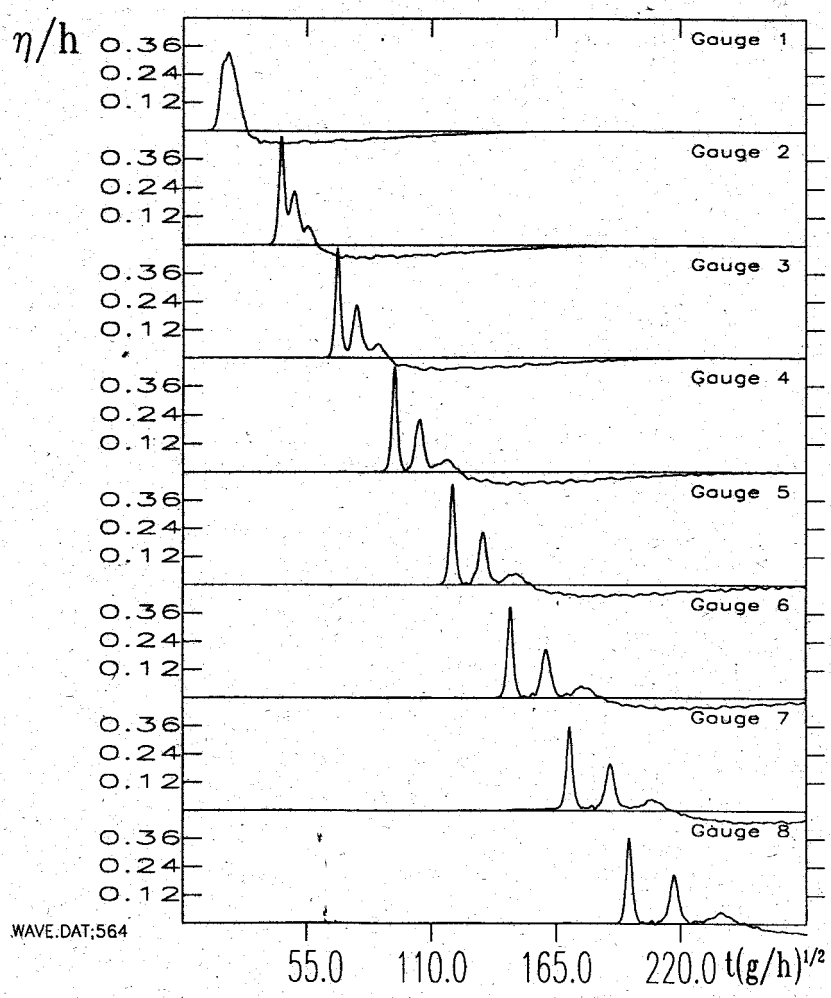

Figure 79: *Wave generated with a porous wedge. The wedge is entirely open, so that the water can flow through. The porous wedge is moving a distance* $d/h = 5.0$ *with a Froude number of* $Fr = 0.4$.

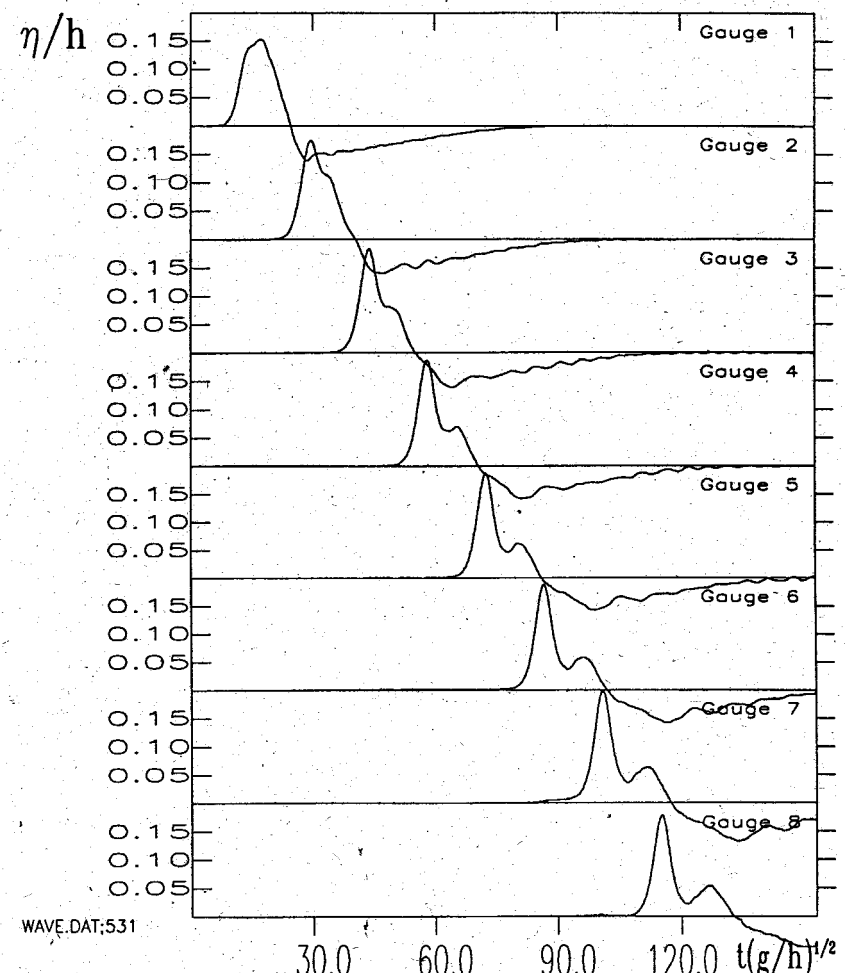

Figure 80: *Wave generated by a porous wedge. The wedge is entirely open, so that the water can flow through. The porous wedge is moving a distance* $d/h = 2.5$ *with a Froude number of* $Fr = 0.2$.

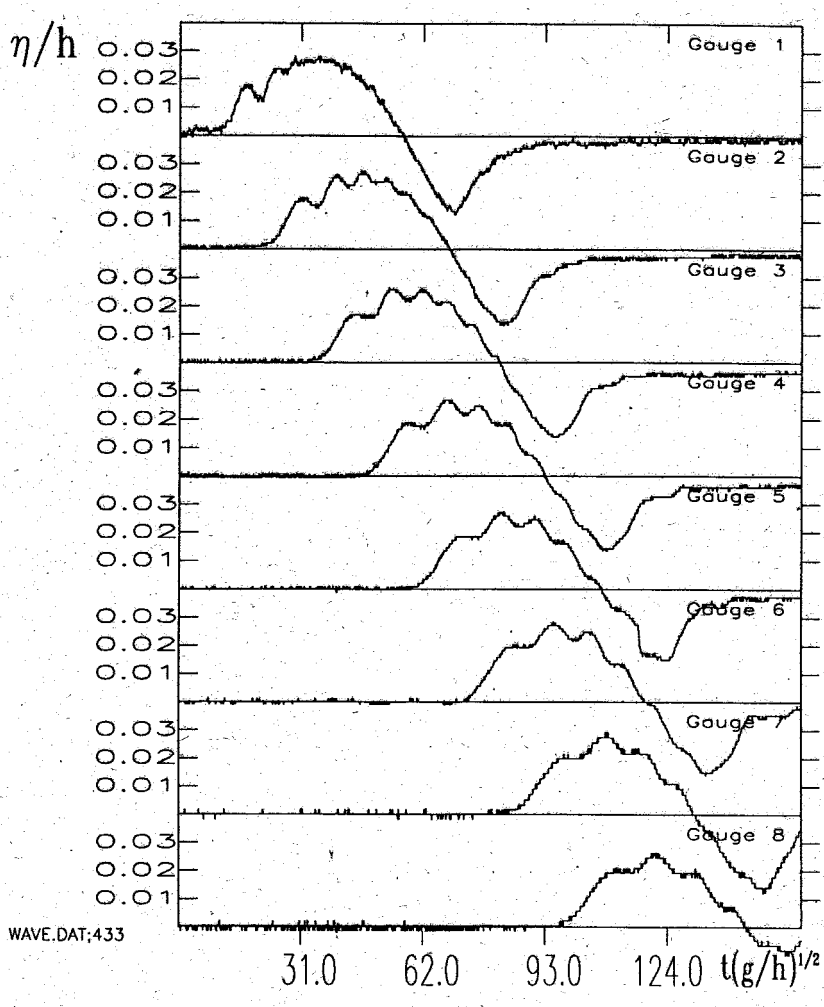

Figure 81: *Wave generated by a porous wedge. The wedge is entirely open, so that the water can flow through. The porous wedge is moving a distance* $d/h = 1.7$ *with a Froude number of* $Fr = 0.05$.

momentum between the water in front and behind the porous wedge. The sudden drop in water level behind the wedge as the latter moves forward is responded by a draft of water through the wedge due to the pressure difference before and behind it. This pressure difference is reduced by levelling out the water surface in front and at the back of the wedge. As can be seen from numerical calculations and is also physically evident, the average horizontal velocity of the water particles behind the wedge is first in the direction of the motion of the wedge. Therefore the water level is lowered behind the porous body and elevated in its front. After a while, but also when the wedge is still moving, the sign of the velocity of the water behind the body changes and the water level raises, while the depression moves through the porous body into the channel.

Small Froude numbers produce lower waveheights but deeper depressions whereas higher Froude numbers result in higher waves with less deep sunks. Compared to the experiments done with the closed porous wedge (figs. 76 - 78), the amplitudes in the open wedge case are less high and the wavelengths are shorter. But the form of the positive part of the first wave remains similar. As a consequence the number of visibly evolving solitons agrees for both porous bodies.

5.3 Numerical modelling of a porous wave generator

A numerical model able to describe the two dimensional motion of the free surface of an ideal fluid in a channel will now be developed. Thereby a small part of the channel will be completely filled with a porous medium under motion. Thus, within this part the free surface is *a priori* and always *within* the porous medium. In front of this domain a region follows in which the medium is porous over part of its depth, and consequently consisting of a two-component structure, and an upper part of pure water. A direct modelling of an inclined wedge type body is beyond our scope but an approximate simulation of the wedge is achieved by a special choice of flux conditions. The free surface is introduced into the equations of momentum by integrating them over depth. Further, the two coupled equations of momentum will be de-coupled, and an appropriate approximation, where terms of small order are neglected, will lead to an equation of the shallow water or Boussinesq type. The flow inside the porous medium is regarded as a two phase flow, where momentum transfer from the skeleton of the porous medium into the fluid is assumed to follow a law similar to a Darcy - Forchheimer law.

The flow of a fluid inside an isotropic porous medium can be regarded as a two component flow of the fluid and the skeleton of the porous medium. Neglecting terms involving mechanical dispersion of momentum on microscopical level (i. e. a velocity gradient due to the stick of the fluid on the surface of the skeleton) the dimensionless equations of momentum read (see Gray & O'Neill) [27]

$$\frac{1}{n}\frac{\partial u}{\partial t} + \frac{1}{n^2}\frac{\partial u^2}{\partial x} + \frac{1}{n^2}\frac{\partial uv}{\partial y} =$$

$$- F\frac{\partial p}{\partial x} + An\left(\frac{1}{1-n}u_{sk} - \frac{1}{n}u\right) + Bn\left(\frac{1}{1-n}u_{sk} - \frac{1}{n}u\right)\left|\frac{1}{1-n}u_{sk} - \frac{1}{n}u\right|, \tag{5.3}$$

$$\frac{1}{n}\frac{\partial v}{\partial t} + \frac{1}{n^2}u\frac{\partial v}{\partial y} + \frac{1}{n^2}v\frac{\partial v}{\partial y} = - F\frac{\partial p}{\partial y} - \frac{1}{n} + An\left(\frac{1}{1-n}v_{sk} - \frac{1}{n}v\right) + Bn\left(\frac{1}{1-n}v_{sk} - \frac{1}{n}v\right)\left|\frac{1}{1-n}v_{sk} - \frac{1}{n}v\right|. \tag{5.4}$$

Here, A, B and F are constants. They are described by the properties of the porous medium and the properties of the fluid and must be determined by experimental investigations. The horizontal and vertical velocity of the porous body is denoted by u_{sk} and v_{sk} respectively. We further assume that the body is rigid, implying that u_{sk} and v_{sk} are independent of x and y. Integration of (5.3) over the depth of the water $H = h + \eta$ leads to

$$\frac{\partial}{\partial t}\left(\frac{H}{n}\overline{u}\right) + \frac{\partial}{\partial x}\left(\frac{H}{n^2}\overline{u}^2\right) - \frac{1}{n}\frac{\partial \eta}{\partial t}u_\eta - \frac{1}{n^2}\frac{\partial \eta}{\partial x}u_\eta^2 + \frac{1}{n^2}u_\eta v_\eta - \frac{1}{n}\frac{\partial h}{\partial t}u_{-h} - \frac{1}{n^2}\frac{\partial h}{\partial x}u_{-h}^2 - \frac{1}{n^2}u_{-h}v_{-h} = - \frac{\partial}{\partial x}(FH\overline{p}) + F\frac{\partial \eta}{\partial x}p_\eta + F\frac{\partial h}{\partial x}p_{-h} + AnH\overline{\omega} + BnH\overline{\omega|\omega|}, \tag{5.5}$$

with a bed $-h(x,t)$ variable in time and space and the free surface $\eta(x,t)$. The average velocity $\overline{u}$ and similarly the average pressure $\overline{p}$ is given by

$$\overline{u} = \frac{1}{H}\int_{-h}^{\eta} u\,dy, \tag{5.6}$$

$$\overline{p} = \frac{1}{H}\int_{-h}^{\eta} p\,dy, \tag{5.7}$$

and the horizontal velocity relative to the porous body is

$$\omega = \frac{1}{1-n}u_{sk} - \frac{1}{n}u. \tag{5.8}$$

Later we also will need the vertical velocity relative to the porous body, denoted by

$$\nu = \frac{1}{1-n}v_{sk} - \frac{1}{n}v. \tag{5.9}$$

The velocity components of the fluid on the free surface are denoted by u_η and v_η, those at the bed as u_{-h} and v_{-h}. The derivation of equation (5.5) also includes the approximation

$$\overline{u^2} \simeq \overline{u}^2. \tag{5.10}$$

Villeneuve [89] showed, that this is exact for a flat bottom; its use thus incorporates some restraints on the scale of the motion for a variable bed. The kinematic

boundary conditions at the free surface and the bed are given by

$$\frac{\partial h}{\partial t} + \frac{1}{n} u_{-h} \frac{\partial h}{\partial x} = -\frac{1}{n} v_{-h}, \tag{5.11}$$

$$\frac{\partial \eta}{\partial t} + D\left(u_\eta \frac{\partial \eta}{\partial x} - v_\eta\right) = D\frac{n}{1-n}\left(u_{sk}\frac{\partial \eta}{\partial x} - v_{sk}\right), \tag{5.12}$$

in which is $1 \leq D \leq 1/n$. Equation (5.12) expresses the fact that only particles whose velocity differs from the velocity of the porous body can leave the surface of the body (which is identical to the free surface). The equation assumes that the velocity of a fluid particle inside the porous body is $(1/n)(u,v)$. In general we find inside the porous medium

$$D = \frac{1}{n}; \tag{5.13}$$

anywhere outside we have instead

$$\begin{aligned} n &= 1, \\ D &= 1, \\ A = B &= 0, \\ u_{sk} = v_{sk} &= 0. \end{aligned} \tag{5.14}$$

The above is reasonable when the free surface lies completely inside the porous body. To model the processes in the domain of the fully submerged portion of the wedge, we pretend that the porous body and the free portion can be replaced by a (virtual) mathematical porous body that covers the entire water depth (fig. 82). The porous equations are taken over in this case from above and adjustments will be made by changing the flux through the boundary and choosing appropriate values for D: $1 \leq D \leq 1/n$.

Integration of the continuity condition

$$\frac{\partial u}{\partial x} + \frac{\partial v}{\partial y} = 0 \tag{5.15}$$

leads to an equation for the flux $\overline{u}$

$$\frac{\partial}{\partial x}(H\overline{u}) - u_\eta \frac{\partial \eta}{\partial x} - u_{-h}\frac{\partial h}{\partial x} + v_\eta - v_{-h} = 0. \tag{5.16}$$

By including the boundary conditions (5.11) and (5.12) we obtain

$$\frac{1}{n}\frac{\partial}{\partial x}(H\overline{u}) + \frac{\partial h}{\partial t} + \frac{1}{Dn}\frac{\partial \eta}{\partial t} - \frac{1}{1-n}\left(u_{sk}\frac{\partial \eta}{\partial x} - v_{sk}\right) = 0. \tag{5.17}$$

This equation is exact. The pressure at the bottom p_{-h} is obtained from the momentum equation (5.4) with the assumption that the pressure at the free surface vanishes:

$$p_\eta = 0, \tag{5.18}$$

$$\begin{aligned} p_{-h} = {} & \frac{H}{Fn} + \frac{1}{F}\int_{-h}^{\eta}\left\langle \frac{1}{n}\frac{Dv}{Dt}\right\rangle dy \\ & - A\frac{n}{F}\int_{-h}^{\eta}\nu\, dy - B\frac{n}{F}\int_{-h}^{\eta}\nu\,|\omega|\, dy, \end{aligned} \tag{5.19}$$

where the total derivative is abbreviated by

$$\left\langle \frac{1}{n}\frac{Dv}{Dt} \right\rangle = \frac{1}{n}\frac{\partial v}{\partial t} + \frac{1}{n^2}u\frac{\partial v}{\partial x} + \frac{1}{n^2}v\frac{\partial v}{\partial y}. \tag{5.20}$$

In the same way we obtain the pressure distribution, which is non-hydrostatic

$$\begin{aligned} p &= \frac{1}{Fn}(\eta - y) + \frac{1}{F}\int_y^\eta \left\langle \frac{1}{n}\frac{Dv}{Dt} \right\rangle dy \\ &\quad - A\frac{n}{F}\int_y^\eta \nu\, dy - B\frac{n}{F}\int_y^\eta \nu\,|\omega|\, dy. \end{aligned} \tag{5.21}$$

Next the momentum equation (5.5) is reduced to simpler form by incorporating the integrated mass balance equation (5.17) and the pressure condition (5.21), the result being

$$\begin{aligned} & H\left(\frac{1}{n}\frac{\partial \overline{u}}{\partial t} + \frac{1}{n^2}\overline{u}\frac{\partial \overline{u}}{\partial x} + \frac{1}{n}\frac{\partial \eta}{\partial x}\right) = \\ & \quad - h\frac{\partial}{\partial x}\left(H\,\overline{\left\langle \frac{1}{n}\frac{Dv}{Dt} \right\rangle} - AnH\,\overline{\nu} - BnH\,\overline{\nu\,|\omega|}\right) \\ & \quad - \frac{\partial}{\partial x}\left(H\,\overline{y\left\langle \frac{1}{n}\frac{Dv}{Dt} \right\rangle} - AnH\overline{y\nu} - BnH\,\overline{y\nu\,|\omega|}\right) \\ & \quad + AnH\overline{\omega} + BnH\overline{\omega\,|\omega|}. \end{aligned} \tag{5.22}$$

This equation does not explicitly include the pressure p, and the pressure distribution factor F has disappeared. To eliminate the vertical velocity, we make use of the shallow water assumption

$$u(x,y,t) \simeq \overline{u}(x,t). \tag{5.23}$$

From continuity we obtain

$$v(x,y,t) = v_{-h} - \int_{-h}^{y}\frac{\partial u}{\partial x}\,dy, \tag{5.24}$$

which can be approximated by

$$v(x,y,t) \simeq v_{-h} - (y+h)\frac{\partial \overline{u}}{\partial x}. \tag{5.25}$$

Invoking the boundary condition at the bottom (5.11) we obtain

$$v = -n\frac{\partial h}{\partial t} - u_{-h}\frac{\partial h}{\partial x} - (y+h)\frac{\partial \overline{u}}{\partial x}, \tag{5.26}$$

and again, with the shallow water assumption we get

$$v = -n\frac{\partial h}{\partial t} - \overline{u}\frac{\partial h}{\partial x} - (y+h)\frac{\partial \overline{u}}{\partial x}. \tag{5.27}$$

In a similar fashion the total derivative (see (5.20)) of the velocity components u and v can be approximated:

$$\left\langle \frac{1}{n}\frac{D}{Dt} \right\rangle [u,v] \simeq \left(\frac{1}{n}\frac{\partial}{\partial t} + \frac{1}{n^2}\overline{u}\frac{\partial}{\partial x} + \frac{1}{n^2}v\frac{\partial}{\partial y} \right)[u,v]\,. \tag{5.28}$$

Finally, equation (5.22) includes only terms involving the unknown flux $\overline{u}$ and the unknown surface η:

$$\begin{aligned}
&\frac{1}{n}\frac{\partial \overline{u}}{\partial t} + \frac{1}{n^2}\overline{u}\frac{\partial \overline{u}}{\partial x} + \frac{1}{n}\frac{\partial \eta}{\partial x} = \\
&\quad \frac{\partial \eta}{\partial x}\Gamma + \frac{H}{2}\frac{\partial \Gamma}{\partial x} + H\left(\frac{\partial \eta}{\partial x} + \frac{1}{2}\frac{\partial h}{\partial x}\right)\Theta + \frac{H^2}{3}\frac{\partial \Theta}{\partial x} \\
&\quad + An\left(\frac{\partial \eta}{\partial x}\Omega + \frac{H}{2}\frac{\partial \Omega}{\partial x} + H\left(\frac{\partial \eta}{\partial x} + \frac{1}{2}\frac{\partial h}{\partial x}\right)\Psi + \frac{H^2}{3}\frac{\partial \Psi}{\partial x}\right) \\
&\quad + Bn\left(\frac{\partial \eta}{\partial x}\Omega|\overline{\omega}| + \frac{H}{2}\frac{\partial \Omega|\overline{\omega}|}{\partial x} + H\left(\frac{\partial \eta}{\partial x} + \frac{1}{2}\frac{\partial h}{\partial x}\right)\Psi|\overline{\omega}| + \frac{H^2}{3}\frac{\partial \Psi|\overline{\omega}|}{\partial x}\right) \\
&\quad + An\overline{\omega} + Bn\overline{\omega|\omega|}\,,
\end{aligned} \tag{5.29}$$

with

$$\Gamma = \frac{\partial^2 h}{\partial t^2} + \frac{1}{n}\frac{\partial h}{\partial x}\frac{\partial \overline{u}}{\partial t} + \frac{2}{n}\overline{u}\frac{\partial^2 h}{\partial x \partial t} + \frac{1}{n^2}\frac{\partial h}{\partial x}\frac{\partial \overline{u}}{\partial x}\overline{u} + \frac{1}{n^2}\frac{\partial^2 h}{\partial x^2}\overline{u}^2\,, \tag{5.30}$$

$$\Theta = \frac{1}{n}\frac{\partial^2 \overline{u}}{\partial x \partial t} + \frac{1}{n^2}\overline{u}\frac{\partial^2 \overline{u}}{\partial x^2} - \frac{1}{n}\frac{\partial \overline{u}^2}{\partial x}\,, \tag{5.31}$$

$$\Omega = \frac{\partial h}{\partial t} + \frac{1}{n}\overline{u}\frac{\partial h}{\partial x} + \frac{1}{1-n}v_{sk}\,, \tag{5.32}$$

$$\Psi = \frac{1}{n}\frac{\partial \overline{u}}{\partial x}\,, \tag{5.33}$$

According to the shallow water approximations, we introduce the scaling factors already used in chapter 1

$$\sigma = \frac{h}{\lambda}\,, \tag{5.34}$$

$$\epsilon = \frac{\eta_0}{h}\,, \tag{5.35}$$

where λ denotes the wavelength (or any other typical horizontal length) and η_0 the waveheight (or any other typical vertical length), and h is the undisturbed water depth. For long waves it is assumed that

$$(x,t) = \frac{1}{\sigma}(\hat{x},\hat{t})\,, \tag{5.36}$$

$$(\eta,u) = \epsilon(\hat{\eta},\hat{u})\,, \tag{5.37}$$

where $\hat{\eta}$ and $\hat{u}$ denotes scaled variables. To obtain a Boussinesq type equation, we now scale equation (5.29). All terms which are larger than $O(\epsilon^2\sigma^3)$ will be kept,

the others are assumed to be so small that they can be omitted. After lengthy manipulations the scaled equation (for simplicity hats are omitted) is obtained:

$$\begin{aligned}
&\frac{1}{n}\frac{\partial \overline{u}}{\partial t}+\frac{1}{n^2}\overline{u}\frac{\partial \overline{u}}{\partial x}+\frac{1}{n}\frac{\partial \eta}{\partial x}= \\
&\quad \frac{\partial \eta}{\partial x}\frac{\partial^2 h}{\partial t^2}+\frac{H}{2}\frac{\partial^3 h}{\partial x \partial t^2}+\frac{h}{2n}\frac{\partial h}{\partial x}\frac{\partial^2 \overline{u}}{\partial t \partial x}+\frac{h}{2n}\frac{\partial^2 h}{\partial x^2}\frac{\partial \overline{u}}{\partial t} \\
&\quad +\frac{h}{n}\frac{\partial^2 h}{\partial x \partial t}\frac{\partial \overline{u}}{\partial x}+\frac{h}{n}\frac{\partial^3 h}{\partial x^2 \partial t}\overline{u}+\frac{h}{2n}\frac{\partial h}{\partial x}\frac{\partial^2 \overline{u}}{\partial x \partial t}+\frac{h^2}{3n}\frac{\partial^3 \overline{u}}{\partial x^2 \partial t} \\
&\quad +An\left(\frac{\partial \eta}{\partial x}\Omega+\frac{H}{2}\frac{\partial \Omega}{\partial x}+\left(h\frac{\partial \eta}{\partial x}+\frac{H}{2}\frac{\partial h}{\partial x}\right)\Psi+\frac{2h\eta+h^2}{3}\frac{\partial \Psi}{\partial x}\right) \\
&\quad +Bn\left(\frac{\partial \eta}{\partial x}\Omega|\omega|+\frac{H}{2}\frac{\partial \Omega|\omega|}{\partial x}+\left(h\frac{\partial \eta}{\partial x}+\frac{H}{2}\frac{\partial h}{\partial x}\right)\Psi|\omega|+\frac{2h\eta+h^2}{3}\frac{\partial \Psi|\omega|}{\partial x}\right) \\
&\quad +An\overline{\omega}+Bn\overline{\omega|\omega|}\,. \qquad (5.38)
\end{aligned}$$

Within a non-porous medium this equation reduces to the equation of Villeneuve & Savage [90] and can be transformed with an error of $O(\epsilon^2\sigma^3)$ into the equation of Wu [96]. For a constant bed $h=1$ and a vanishing vertical velocity of the porous skeleton $v_{sk}=0$ we finally obtain as momentum equation

$$\begin{aligned}
&\frac{\partial \overline{u}}{\partial t}+\frac{1}{n}\overline{u}\frac{\partial \overline{u}}{\partial x}+\frac{\partial \eta}{\partial x}= \\
&\quad \frac{1}{3}\frac{\partial^3 \overline{u}}{\partial x^2 \partial t}-An\left(\frac{\partial \eta}{\partial x}\frac{\partial \overline{u}}{\partial x}+\frac{1}{3}(1+2\eta)\frac{\partial^2 \overline{u}}{\partial x^2}\right) \\
&\quad -Bn\left(\left(\frac{\partial \eta}{\partial x}\frac{\partial \overline{u}}{\partial x}+\frac{1}{3}(1+2\eta)\frac{\partial^2 \overline{u}}{\partial x^2}\right)\left|\frac{n}{1-n}u_{sk}-\overline{u}\right|-\frac{1}{3}(1+2\eta)\frac{\partial \overline{u}}{\partial x}\left|\frac{1}{n}\frac{\partial \overline{u}}{\partial x}\right|\right) \\
&\quad +An\left(\frac{n}{1-n}u_{sk}-\overline{u}\right) \\
&\quad +B\left(\frac{n}{1-n}u_{sk}-\overline{u}\right)\left|\frac{n}{1-n}u_{sk}-\overline{u}\right|\,, \qquad (5.39)
\end{aligned}$$

and as continuity equation

$$(1+\eta)\frac{\partial \overline{u}}{\partial x}+\frac{\partial \eta}{\partial x}\left(\overline{u}-\frac{n}{1-n}u_{sk}\right)+\frac{1}{D}\frac{\partial \eta}{\partial t}=0\,. \qquad (5.40)$$

A numerical solution of the equations was achieved with the technique used by Villeneuve [89]. He used a central finite difference scheme in lieu of the partial derivatives. Within a first step (predictor) the continuity equation is solved to obtain a prediction at an intermediate time level for the free surface. With this the momentum equation is solved for the velocity field. In a second step (corrector) the free surface is calculated from the continuity equation for the advanced time level. Afterwards a smoothing technique (Flux Corrected Transport, FCT) filters high order frequencies without loss of accuracy. Whenever the velocity gradients are steep dispersive ripples are introduced by a high order numerical finite difference scheme. These ripples are diffused with the aid of a low order scheme.

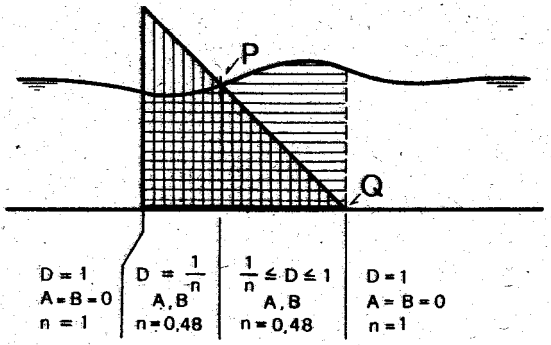

Figure 82: *Definition of the flux parameter to model a wedge type porous body. The experimental wedge shaped porous body is simulated in the numerical model by changing the flux parameter D within the numerical porous box.*

5.4 Comparison of experimental and numerical results

As described above the experimental set-up could not directly be modeled by the equations deduced before. Therefore the flux inside the numerical porous 'box' was manipulated according to fig. 82 by changing the flux parameter D at each time step. The parameter is changed linearly between points P and Q in fig. 82 from $d = 1/n$ at P to $D = 1$ at Q. As was mentioned before, the parameters A and B have to be determined from the experiments. Therefore the equations were solved with different values of A and B. The maximum wave heights at a gauge nearby the wave generator are obtained from a set of numerical experiments and are shown in fig. 83 for the open wedge case and in fig. 84 for the wedge closed at its rear side with a vertical wall. In both cases the wave generator moves a distance of $d/h = 2.5$. Results are shown for $Fr = 0.2$. For this (and other Froude numbers) the following typical results were obtained.

- In the case of the open porous wedge no wave is generated whenever $A = B = 0$. Increasing the parameter A or B increases the wave height.
- In the case of the closed porous wedge the highest wave amplitude is recorded when $A = B = 0$. (Identical with a moving vertical wall.) Increasing A or B will decrease the wave height.
- The variation of the amplitudes is much more narrow in the closed wedge case than for the open wedge.

A small band of values of A and B exists where the computed wave fits the experimentally obtained waves. Comparison of experiments with numerical results are given in figures 85, 86 and 87 for an open wedge moving a distance of $d/h = 2.5$ with a Froude number of $Fr = 0.4$, and the values $A = 3.5$, $B = 4.5$, for $Fr = 0.2$, $A = 5.5$, $B = 3.5$ was chosen and for $Fr = 0.05$, $A = 14.5$, $B = 0.5$. With the

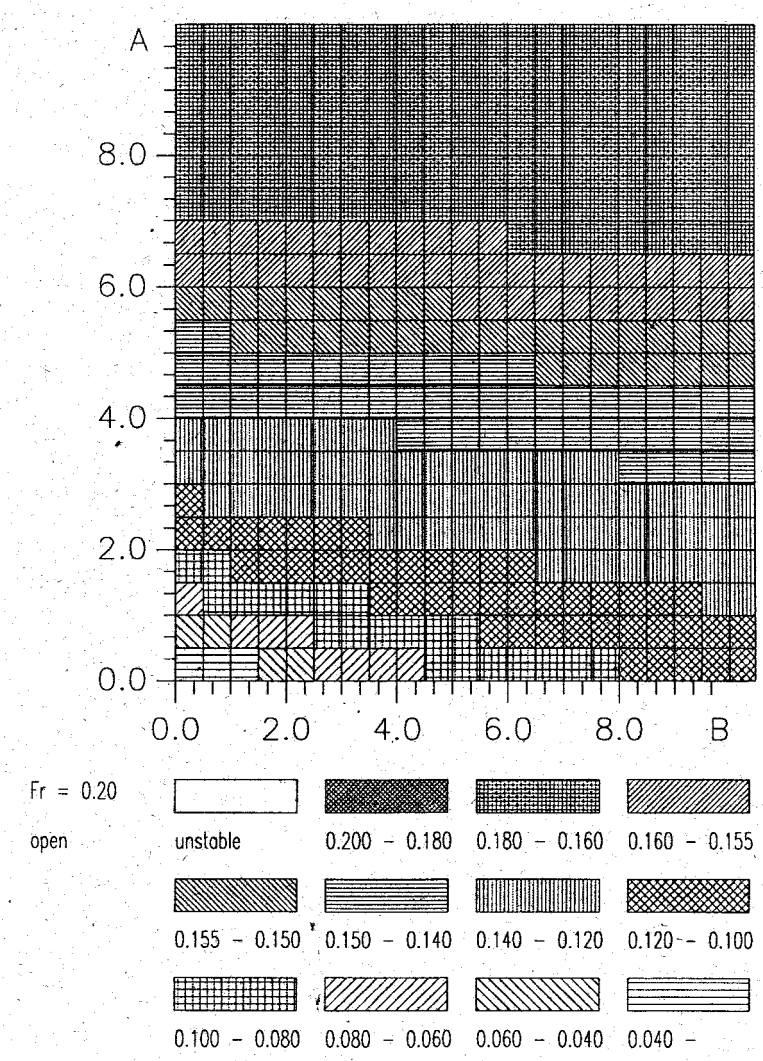

Figure 83: *Wave amplitude at a gauge in front of the entirely open porous wedge. The numerical solutions are obtained for different values of the parameters A and B which determine the transfer of momentum. The porous body moves a distance of $d/h = 2.5$ with a Froude number $Fr = 0.2$. The various shadings indicate the ranges of values of a dimensionless wave amplitude.*

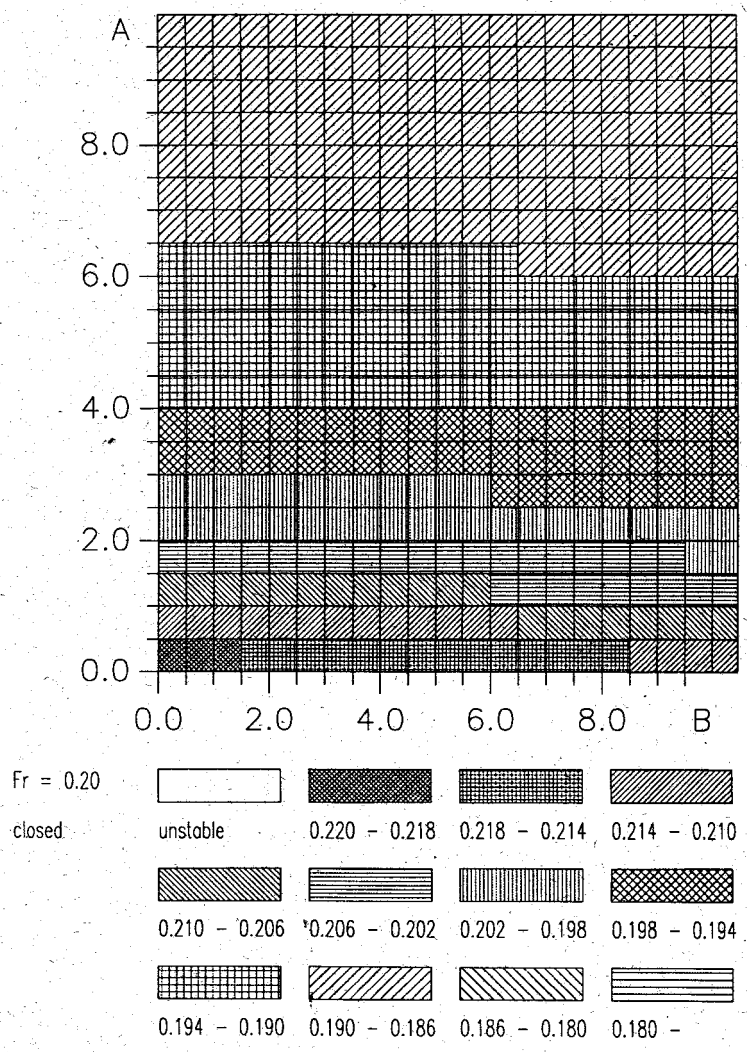

Figure 84: *Wave amplitude at a gauge in front of the porous wedge closed at its rear side. The numerical solutions are obtained for different values of the parameters A and B which determine the transfer of momentum. The porous body moves a distance of* $d/h = 2.5$ *with a Froude number* $Fr = 0.2$. *The various shadings indicate the ranges of values of a dimensionless wave amplitude.*

same distances and Froude numbers the time history of a wave generated with the closed wedge is obtained and displayed in figures 88 with $A = 4.5$, $B = 3.5$, 89 with $A = 1.5$, $B = 0.5$ and 90 with $A = 10.0$, $B = 4.5$. Thereby the values of A and B are chosen so that the wave amplitude of the experimental and numerical results fit best.

In summary. The results suggest that the form of the porous body plays a minor part in the generation of the wave. The wedge form used in the experiments is successfully simulated with an appropriate choice of the flux between the porous material and the full fluid. For an open body through which the water is able to flow it is more important to know how the transfer of momentum is achieved i. e. how the values of the parameters A and B must be chosen. Alternatively the waves generated with a porous body whose back side is impervious the wave characteristics are primarily controlled by the simple wall geometry.

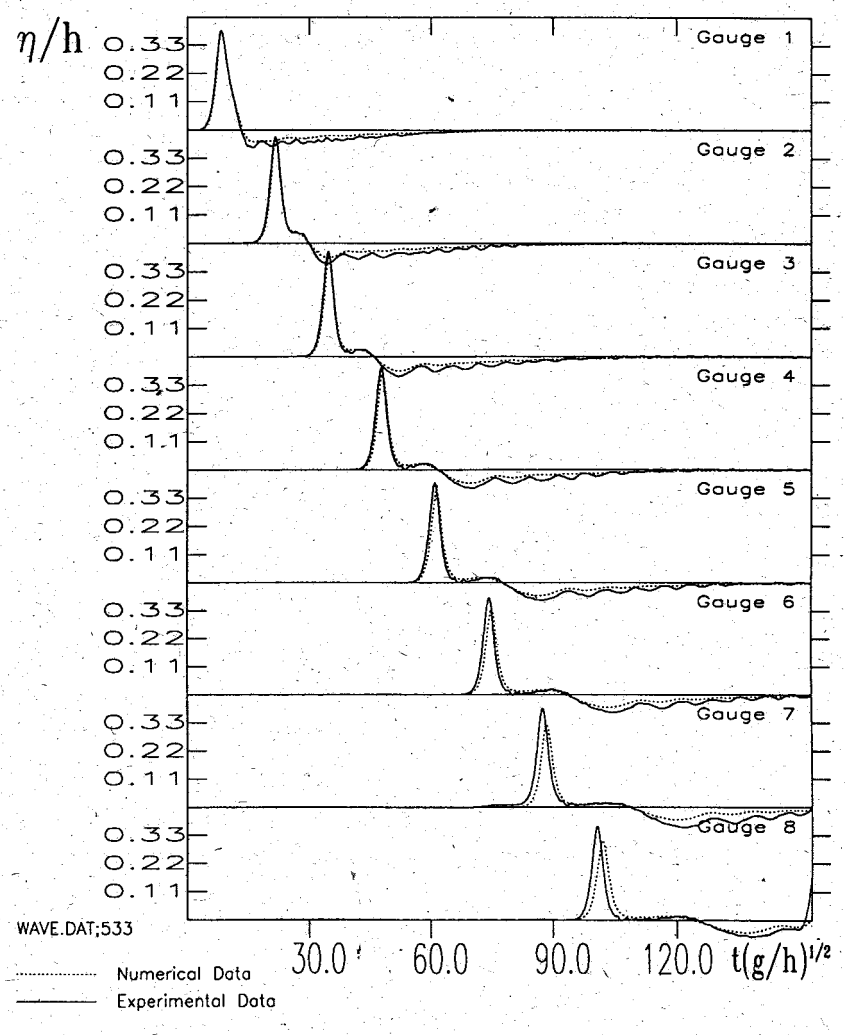

Figure 85: *Comparison of experimental and numerical data. The wave is generated by an entirely open porous wedge with slope* 1, *moving a distance* $d/h = 2.5$ *with a Froude number of* $Fr = 0.4$.

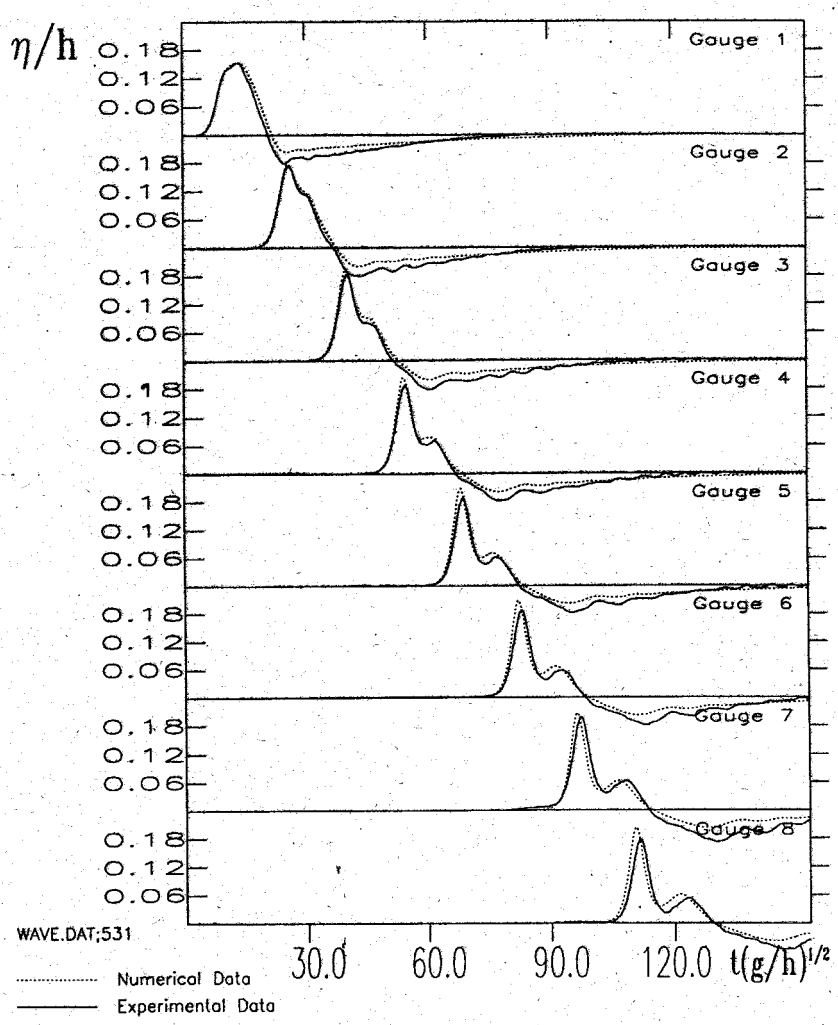

Figure 86: *Comparison of experimental and numerical data. The wave is generated with an entirely open porous wedge with slope* 1, *moving a distance* $d/h = 2.5$ *with a Froude number of* $Fr = 0.2$.

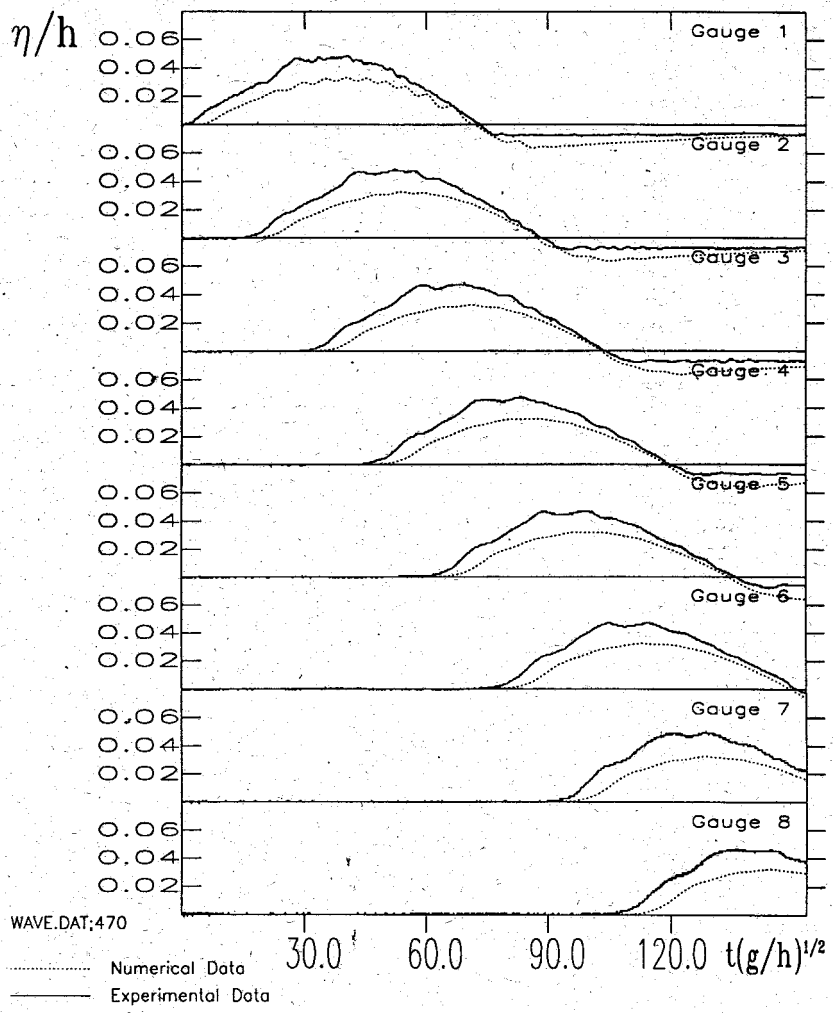

Figure 87: *Comparison of experimental and numerical data. The wave is generated with an entirely open porous wedge with slope* 1, *moving a distance* $d/h = 2.5$ *with a Froude number of* $Fr = 0.05$.

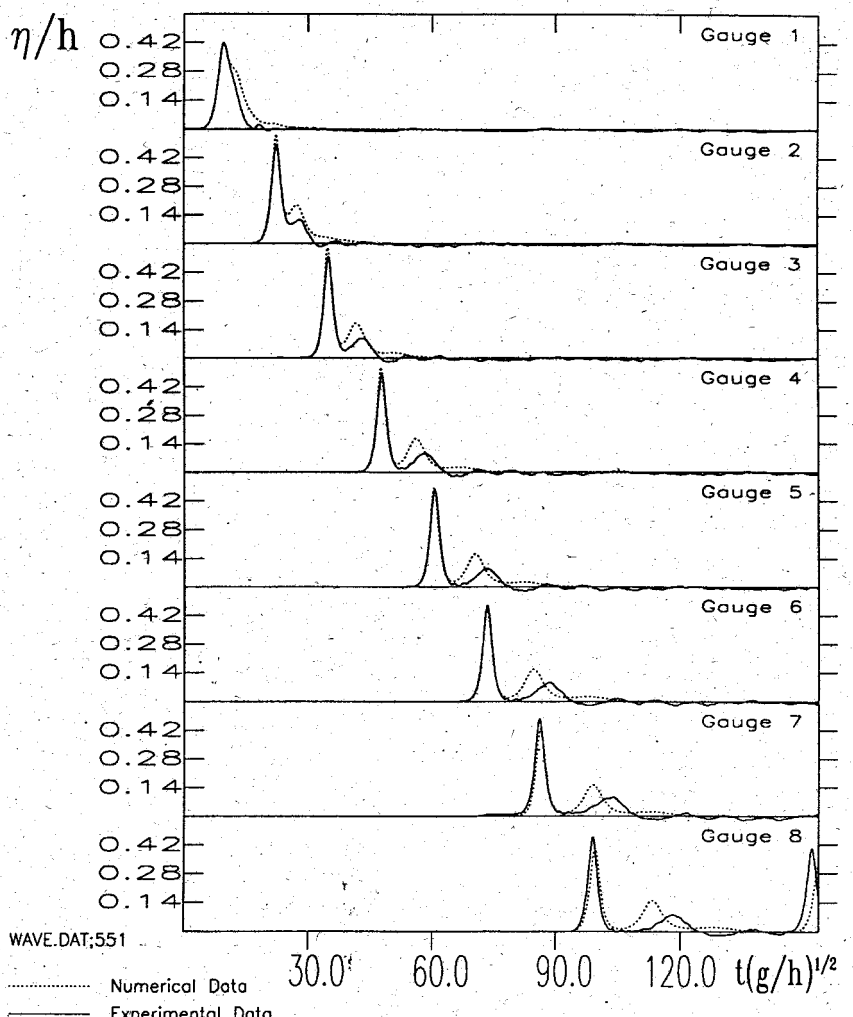

Figure 88: *Comparison of experimental and numerical data. The wave is generated with a porous wedge with slope* 1 *closed at its rear side with a vertical wall. The wedge is moving a distance* $d/h = 2.5$ *with a Froude number of* $Fr = 0.4$.

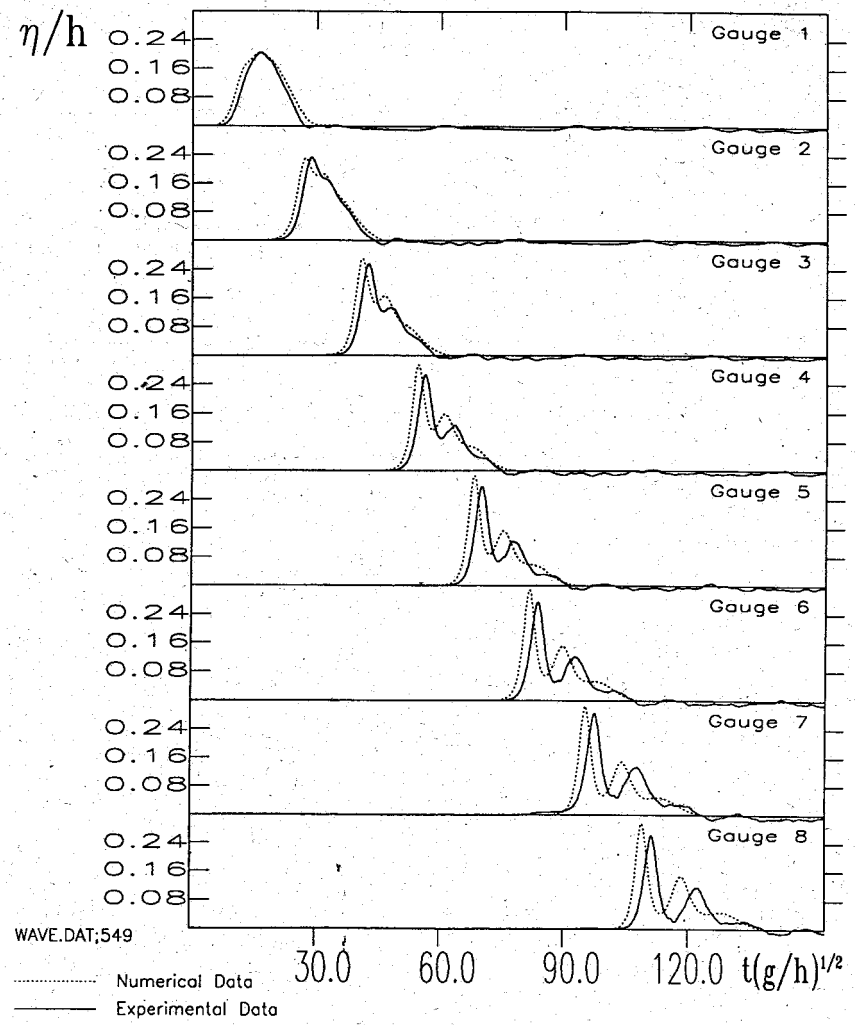

Figure 89: *Comparison of experimental and numerical data. The wave is generated with a porous wedge with slope* 1 *closed at its rear side with a vertical wall. The wedge is moving a distance* $d/h = 2.5$ *with a Froude number of* $Fr = 0.2$.

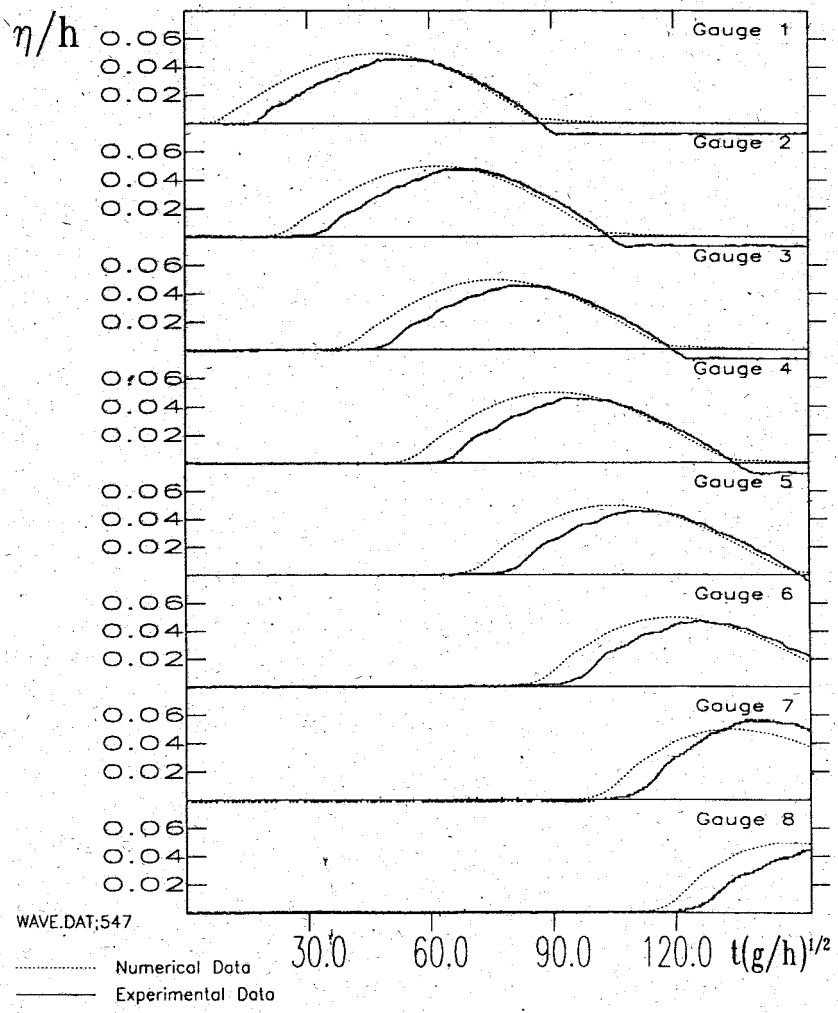

Figure 90: *Comparison of experimental and numerical data. The wave is generated with a porous wedge with slope* 1 *closed at its rear side with a vertical wall. The wedge is moving a distance* $d/h = 2.5$ *with a Froude number of* $Fr = 0.05$.

Acknowledgements

This work was made possible by Prof. Dr. D. Vischer, director of the Laboratory. He provided all facilities and equipment. His continuous support and generosity is gratefully acknowledged. Prof. Dr. K. Hutter guided and advised my first steps into the world of sciences. His engagement and personality were essential basis. I am very much indebted to him.

I thank Dr. W. H. Hager, whose open mind made a variety of fruitfull discussions possible. I also wish to thank Prof. Dr. S. B. Savage and M. Villeneuve of McGill University in Montreal for their cooperation and kind help.

C. Bucher constructed the gear box of the wave generator and was able to convert many ideas into a technical reality. He and Mrs. I. Wiederkehr and Mrs. A. Krätzer prepared skilfully the drawings. Their help is gratefully thanked. The construction of the experimental set-up was done in the workshop of the Laboratory. I thank the labourer for their excellent work.

References

[1] Abramowitz M., Stegun A., editor. *Handbook of Mathematical Functions with Formulas, Graphs and Mathematical Tables.* United States Department of Commerce, National Bureau of Standards, 3. edition, 1965.

[2] Airy G. B. Tides and waves. *Encyclopaedia Metropolitana*, 5, Sect. 392, London:241–392, 1845.

[3] Aiton E. J. The contribution of Newton, Bernoulli and Euler to the theory of the tides. *Annals of Science*, 11:206–223, March 1955.

[4] Bargmann V. On the number of bound states in a central field of force. *Proceedings of the National Academy of Sciences of the United States of America*, 38:961–966, 1952.

[5] Bona J., Smith R. The Korteweg-de Vries equation in an unbounded domain. *Philosophical Transactions of the Royal Society of London. Ser. A, Mathematical and Physical Sciences*, 278:555–604, 1975.

[6] Boussinesq J. Théorie génénerale des mouvements qui sont progagés dans un canal rectangulaire horizontal. *Comptes Rendus Hebdomadaires des Séance de l'Académie des Sciences*, 73:256–260, 1871.

[7] Boussinesq J. Théorie de l'itumescence liquide appelée onde solitaire ou de translation, se propageant dans un canal rectangulaire. *Comptes Rendus Hebdomadaires des Séance de l'Académie des Sciences*, 72:755–759, 1871.

[8] Boussinesq J. Théorie des ondes et des remous qui se propagent le long d'un canal rectangulaire horizontal, en communiquant au liquide contenu dans ce canal des vitesses sensiblement pareilles de la surface au fond. *Journal de Mathématiques Pures et Appliquées*, 17:55–108, 1872.

[9] Chaudhry M. H., Mercer A. G., Cass D. Modeling of slide-generated waves in a reservoir. *Journal of Hydraulic Engineering*, 109, No. 11:1505–1520, 1983.

[10] Colladon D., Sturm C. Mémoires sur la Compression des Liquides. *Mémoires Presésentés par Divers Savants a l'Academie Royale des Sciences de l'Institut de France*, 5:267–347, (1827), 1838.

[11] Craig W. An existence theory for water waves and the Boussinesq and Korteweg-de Vries scaling limits. *Communication in Partial Differential Equations*, 10, No. 8:787–1003, 1985.

[12] Das M. M., Wiegel R. L. Waves generated by horizontal motion of a wall. *Journal of Waterways, Harbours and Coastal Engineering divison, Proceedings of the American Society of Civil Engineers*, 98, No. WW1:49–65, 1972.

[13] Davidson D. D., McCartney B. L. Water waves generated by landslides in reservoirs. *Journal of the Hydraulics Divison, Proceedings of the American Society of Civil Engineers*, 101, No. Hy12:1489–1501, 1975.

[14] de Saint-Venant J.-C. Movements des molécules de l'onde dite solitaire, propagée à la surface de l'eau d'un canal. *Comptes Rendus Hebdomadaires des Séances de l'Academie des Sciences, Paris*, 101:1101–1105, 1215–1218, 1885.

[15] Dodd R. K., Eilbeck J. C., Gibbon J. D., Morris H. C. *Solitons and Nonlinear Wave Equations*. Academic Press Inc. London, 1982.

[16] Earnshaw S. The mathematical theory of the two great solitary waves of first order. *Transactions of the Cambridge Philosophical Society*, 8:326–341, 1849.

[17] Euler L. Dècouverte d'un nouveau principe de mécanique. *Mémoires de l'Academie des Sciences de Berlin*, 6:185–217, (1750), 1752. Reprinted in: Leonhardi Euleri Opera Omnia, ed. Fleckenstein J. O., auctoritate et impensis Societatis Scientiarum Naturalium Helveticae, (Schweizerische Naturforschende Gesellschaft), Lausanne, 1957, Ser. II, Vol. 5, pp.81–108, Orell Füssli, Zürich.

[18] Euler L. De la propagation du son. *Mémoires de l'Academie des sciences de Berlin*, 15:185–209, (1759), 1766. Reprinted in: Leonhardi Euleri Opera Omnia, ed. Bernoulli E., Bernoulli R., Rudio F., Speiser A., sub auspiciis Societatis Scientiarum Naturalium Helveticae (Schweizerische Naturforschende Gesellschaft), Lausanne, 1926, Ser. III, Vol. 1, 428 – 451, Teubner Verlag, Leipzig und Berlin.

[19] Faddeev L. D. On the relation between the S–matrix and potential for the one–dimensional Schrödinger operator. *Soviet Physics Dokl.*, 3:747–751, 1958.

[20] Fenton J. A ninth-order solution for the solitary wave. *Journal of Fluid Mechanics*, 53, part 2:257–271, 1972.

[21] Friedrichs K. O. On the derivation of the shallow water theory. *Communications on Pure and Applied Mathematics and Mechanics*, 1, No. 1:81–87, 1948. Appendix to: The Formations of Breakers and Bores, by J. J. Stoker.

[22] Friedrichs K. O., Hyers D. H. The existence of solitary waves. *Communications on Pure and Applied Mathematics and Mechanics*, 7, No. 3:517–551, 1954.

[23] Gardner C. S., Greene S. M., Kruskal M. P., Miura R. M. Method for solving the Korteweg-de Vries equation. *Physical Review Letters*, 19:1095–1097, 1967. published by the American Physical Society.

[24] Gerstner F. Theorie der Wellen. *Annalen der Physik*, 32:412–445, 1809. id. Annalen der Physik, Neue Folge, Vol. 2. Reprinted from: Abhandlungen der königlichen Gesellschaft der Wissenschaften zu Prag für das Jahr 1802.

[25] Göbel N. Beitrag zur Hydromechanik von Schwall- und Sunkwellen. Mitteilung aus dem Institut für Wasserbau und Kulturtechnik No. 171, Karlsruhe 1984.

[26] Gozali S., Hunt B. Water waves generated by close landslides. *Journal of Hydraulic Research*, 27, No. 1:49–60, 1989.

[27] Gray W. G., O'Neill K. On the general equations for flow in porous media and their reduction to Darcy's law. *Water Resources Research, publ. American Geophysical Union*, 12, No. 2:148–154, 1976.

[28] Green A. E., Naghdi P. M. A derivation of equations for wave propagation in water of variable depth. *Journal of Fluid Motion*, 78, part 2:237–246, 1976.

[29] Grimshaw R. The solitary wave in water of variable depth. Part 2. *Journal of Fluid Mechanics*, 46, part 3:611–622, 1971.

[30] Grimshaw R. Theory of solitary waves in shallow fluids. In Cheremisinoff N. P., editor, *Encyclopedia of Fluid Mechanics*, pages 3–25, Gulf Publishing Company, Houston, 1986. Vol. 2.

[31] Hager W. H., Hutter K. On pseudo uniform flow in open channel hydraulics. *Acta Mechanica*, 53:183–200, 1984.

[32] Huber A. Schwallwellen in Seen als Folge von Felsstürzen. Mitteilungen der Versuchsanstalt für Wasserbau, Hydrologie und Glaziologie No. 47, Zürich, 1980.

[33] Hutter, K., editor. *Die Anfänge der Mechanik*. Springer Verlag, Berlin, 1989.

[34] Huygens C. *Horologium Oscillatorium sive de motu pendulorum ad horologio aptato, Demonstrationes geometricae*. Paris, 1673.

[35] *IMSL Library, Problem-solving Software system for mathematical and statistical FORTRAN programming*. Edition 9.2, 1984.

[36] Johnson J. W., Bermel K. J. Impulse waves in shallow water as generated by falling weights. *Transactions of the American Geophysical Union*, 30, No. 2:223–230, 1949.

[37] Kamphuis J. W., Bowering R. J. Impulse waves generated by landslides. In *Proceedings 12th Coastal Engineering Conference, American Society of Civil Engineers*, pages 575–588, Washington D. C., 1970.

[38] Keller J. B. The solitary wave and periodic waves in shallow water. *Communications on Pure and Applied Mathematics and Mechanics*, 1:323–339, 1948.

[39] Kennard E. H. Generation of surface waves by a moving partition. *Quarterly of Applied Mathematics*, 7, No. 3:303–312, 1949.

[40] Korteweg D. J., de Vries G. On the change of form of long waves advancing in a rectangular canal, and on a new type of long stationary waves. *London, Edingbugh and Dublin Philosophical Magazine and Journal of Science*, Ser.5, 39:422–443, Jan.–June 1895.

[41] Kouitas C. G. Finite element approach to waves due to landslides. *Journal of the Hydraulics Divison, Proceedings of the American Society of Civil Engineers*, 103, No.HY9:1021–1029, 1977.

[42] Kranzer H. C., Keller J. B. Water waves produced by explosions. *Journal of Applied Physics*, 30, No. 3:398–407, 1959.

[43] Lagrange J. L. Recherches sur la nature, et la propagation du son. *Miscellanea Taurinensia (Turiner Akademieberichte)*, I:1–112, 1759.

[44] Lagrange J. L. *Mécanique analytique.* Paris, 1788.

[45] Laitone E. V. The second approximation to cnoidal and solitary waves. *Journal of Fluid Mechanics*, 9, part 3:430–444, 1960.

[46] Lamb H. *Hydrodynamics.* Dover Publications, New York, 6 edition, 1945.

[47] Langhaar H. L. *Dimensional Analysis and Theory of Models.* John Wiley & Sons, Inc., 1951.

[48] Laplace P. S. Recherches sur quelques points du Système du monde. *Mémoires de l'Académie des Sciences*, (1775), 1778.

[49] Lavrent'ev M. A. (Lavrentieff). On the theory of long waves. *American Mathematical Society Translations*, 102:51–53, 1954.

[50] Lax P. D. Integrals of nonlinear equation and solitary waves. *Communications on Pure and Applied Mathematics and Mechanics*, 21:467–490, 1968.

[51] Longuet-Higgins M. S., Fenton J. D. On the mass, momentum, energy and circulation of a solitary wave. II. *Proceedings of the Royal Society of London. Ser. A, Mathematical and Physical Sciences*, 340:1–28, 1974.

[52] Lord Rayleigh. On waves. *London, Edingburgh and Dublin Philosophical Magazine and Journal of Science*, Ser. 5, Vol. 1, No. 4:257–279, April, 1876.

[53] McCowan J. On the solitary wave. *London, Edingburgh and Dublin Philosophical Magazine and Journal of Science*, Ser. 5, Vol. 32:45–58, July 1891.

[54] McCowan J. On the highest wave of permanent type. *London, Edingburgh and Dublin Philosophical Magazine and Journal of Science*, Ser. 5, Vol. 38:351–358, Oct. 1894.

[55] Mei C. C., Le Méhauté B. Note on the equation of long waves over an uneven bottom. *Journal of Geophysical Research*, 71, No. 2:393–400, 1966.

[56] Miles J. W. Solitary waves. *Annual Review of Fluid Mechanics*, 12:11–43, 1980.

[57] Miles J. W. The Korteweg-de Vries equation: a historical essay. *Journal of Fluid Mechanics*, 106:131–147, 1981.

[58] Miller R. L. An experimental study of form and transitions in impulse waves. In *Proceedings of the Symposium on long Waves*, pages 33–61, Delaware, Sept. 1970.

[59] Miller R. L. Prediction curves for waves near the source of an impulse. In *Proceedings 12th Coastal Engineering Conference, American Society of Civil Engineers*, pages 609–624, Washington, D. C., 1970.

[60] Miura R. M. The Korteweg-de Vries equation: A survey of results. *SIAM Review*, 18(3):412–459, July 1976. published by the Society for Industrial and Applied Mathematics.

[61] Newton I. *Philosophiae Naturalis Principia Mathematica.* London, 1687.

[62] Noda E. K. Water waves generated by landslides. *Journal of Waterways, Harbors and Coastal Engineering divison, Proceedings of the American Society of Civil Engineers*, 96, No. WW4:835–855, 1970.

[63] Noda E. K. Water waves generated by a local surface disturbance. *Journal of Geophysical Research*, 76 No. 30:7389–7400, 1971.

[64] Peregrine D. H. Long waves on a beach. *Journal of Fluid Mechanics*, 27, part4:815–827, 1967.

[65] Poisson S.-D. Sur la Vitess du son. *Annales de Chimie et de Physique*, 23:5–16, 1823.

[66] Prins J. E. Water waves due to a local disturbance. In *Proceedings 6th Coastal Engineering Conference, American Society of Civil Engineers*, pages 147–162, Gainesville, 1957.

[67] Prins J. E. Characteristics of waves generated by a local disturbance. *Transactions of the American Geophysical Union*, 39, No. 5:865–874, 1958.

[68] Pugh C. A., Chiang W.-L. Landslide-generated wave studies. In *Water Forum '86: World Water Issues in Evolution*, pages 27–34, American Society of Civil Engineers, Long Beach, California, 1986.

[69] Raney D. C., Butler H. L. Landslide generated water wave model. *Journal of the Hydraulics Divison, Proceedings of the American Society of Civil Engineers*, 102, No. HY9:1269–1282, 1976.

[70] Russell J. S. Report of the Committee on Waves. *Report of the 7th Meeting of the British Association for the Advancement of Science, Liverpool*, 417–496, 1838.

[71] Russell J. S. On waves. *Report of the 14th Meeting of the British Association for the Advancement of Science, York*, 311–390, 1845.

[72] Sauer R., Szabó I., editor. *Mathematische Hilfsmittel des Ingenieurs*. Springer Verlage Berlin, 1969.

[73] Scheidegger A. E. On the prediction of the reach and velocity of catastrophic landslides. *Rock Mechanics*, 5:231–236, 1973.

[74] Schraub F. A., Kline S. J., Henry J., Runstadler P.W. Jr., Littell A. Use of hydrogen bubbles for quantitative determination of time-dependent velocity fields in low-speed water flows. *Journal of Basic Engineering, Proceedings of the American Society of Mechanical Engineers*, 429–444, June 1965.

[75] Schwartz L. W., Fenton J. D. Strongly nonlinear waves. *Annual Review of Fluid Mechanics*, 14:39–60, 1982.

[76] Segur H. The Kortewég-de Vries equation and water waves. Solution of the equation. Part 1. *Journal of Fluid Mechanics*, 59, part 4:721–736, 1973.

[77] Shields J. J., Webster W. C. On direct methods in water-wave theory. *Journal of Fluid Mechanics*, 197:171–199, 1988.

[78] Slingerland R., Voight B. Evaluating hazard of landslide-induced water waves. *Journal of Waterways, Port, Coastal and Ocean Division, Proceedings of the American Society of Civil Engineers*, 108, No. WW4:508–512, Nov. 1982.

[79] Stoker J. J. *Water Waves*. Interscience, New York, 1957.

[80] Stokes G. G. On the theory of oscillatory waves. *Transactions of the Cambridge Philosophical Society*, 8:441–455, 1849.

[81] Stokes G. G. On the theory of oscillatory waves. In *Mathematical and Physical Papers*, Vol. 1, pages 197–229, Cambridge, University Press, 1880. Appendix B.: Considerations relative to the greatest height of oscillatory irrotational waves which can be propagated without change of form.

[82] Stokes G. G. The outskirts of the solitary wave. In *Mathematical and Physical Papers*, Vol. 5, page 163, Cambridge, University Press, 1905.

[83] Struik D. J. Détermination rigoureuse des ondes irrotationnelles permanentes dans un canal à profondeur finie. *Mathematische Annalen*, 95:595–634, 1926.

[84] Takahasi R. A model experiment on the mechanism of seismic sea wave generation. Part 1. *Bulletin of the Earthquake Research Institute. Tokyo Imperial University*, 1, Supplementary:152–181, 1934.

[85] Thacker W. C. Some exact solutions to the nonlinear shallow water wave equations. *Journal of Fluid Mechanics*, 107:499–508, 1981.

[86] Townson J. M., Kaya Y. Simulations of the waves in Lake Botnen created by the Rissa landslide. *Proceedings of the Institution of Civil Engineers*, 85, part 2:145–160, 1988.

[87] Truesdell C. A., editor. *Leonhardi Euleri Opera Omnia.* Volume 12, Ser. II, auctoritate et impensis Societatis Scientiarum Naturalium Helveticae (Schweizerische Naturforschende Gesellschaft), Lausanne, 1954.

[88] Ursell F. The long wave paradox in the theory of gravity waves. *Proceedings of the Cambridge Philosophical Society*, 49:685–694, 1953.

[89] Villeneuve M. *Nonlinear, dispersive, shallow-water waves developed by a moving bed.* Master's thesis, McGill University, Montreal, July 1989.

[90] Villeneuve M., Savage S. B. Nonlinear, dispersive, shallow water waves developed by a moving bed. *Proceedings of the 12th Canadian Congress of Applied Mechanics, Ottawa*, 1989.

[91] Weast R. C., editor. *CRC Handbook of Chemistry and Physics.* CRC Press Inc., 61 edition, 1980 - 1981.

[92] Weber E. H., Weber W. *Wellenlehre auf Experimente gegründet.* Leipzig, 1825.

[93] Wehausen J. V., Laitone E. V. Surface Waves. In Flügge S., editor, *Handbuch der Physik*, Springer Verlag, Berlin, 1960. Vol. 9, Strömungsmechanik III.

[94] Wiegel R. L. Laboratory studies of gravity waves generated by the movement of a submerged body. *Transactions of the American Geophysical Union*, 36, No. 5:759–774, 1955.

[95] Wiegel R. L., Noda E. K., Kuba E. M., Gee D. M., Tornberg G. F. Water waves generated by landslides in reservoirs. *Journal of Waterways and Harbour Division, Proceedings of the American Society of Civil Engineers*, 96, No. WW2:307–333, 1970.

[96] Wu T. Y. Long waves in ocean and coastal waters. *Journal of the Engineering Mechanics Division, Proceedings of the American Society of Civil Engineers*, 107:501–522, June 1981.